Molecular mechanisms of nociception and pain

Donald Iain MacDonald

A thesis submitted for the degree of Doctor of Philosophy to University College London

Wolfson Institute for Biomedical Research

University College London 2020

Declaration

I, Donald Iain MacDonald, confirm that the work presented in this thesis is my own. Where information has been derived from other sources, I confirm that this has been indicated in the thesis.

Abstract

My thesis uses *in vivo* calcium imaging to investigate the cell and molecular mechanisms of two unusual pain states: congenital analgesia and cold allodynia.

Genetic deletion of voltage-gated sodium channel $Na_V1.7$ in mice and humans leads to profound pain insensitivity. Paradoxically, peripherally-targeted pharmacological antagonists of $Na_V1.7$ fail to relieve pain in the clinic. To determine the mechanism of analgesia in $Na_V1.7$ null mutants, I used optical, electrophysiological and behavioural methods to investigate the effect of peripheral $Na_V1.7$ deletion on nociceptor function. Surprisingly, both calcium imaging and extracellular recording of $Na_V1.7$-deficient sensory neurons *in vivo* found limited deficits in the response to noxious stimuli. Synaptic transmission from nociceptor central terminals in the spinal cord was however compromised following $Na_V1.7$ deletion. Importantly, both synaptic deficits and behavioural analgesia were reversed by blocking central opioid receptors. Collectively, these data account for the failure of peripherally-targeted $Na_V1.7$ blockers and point to a central mechanism of analgesia in $Na_V1.7$ null mutants that requires opioid receptors.

Chronic pain patients suffering from cold allodynia experience normally innocuous cooling as excruciating pain, but the cells and molecules driving cold allodynia remain elusive. I used *in vivo* calcium imaging to investigate how the activity of cold-sensing neurons was altered in three mouse models of neuropathic pain: oxaliplatin-induced neuropathy, peripheral nerve injury and ciguatera poisoning. In neuropathic mice exhibiting cold allodynia, a subset of cold-insensitive, large-diameter, peptidergic nociceptors became responsive to cooling. Diptheria toxin-mediated ablation of these silent cold-sensing neurons decreased neuropathic cold hypersensitivity. Voltage-gated potassium channels $K_V1.1$ and $K_V1.2$ were highly expressed in silent cold-sensing neurons and pharmacological inhibition of these channels rapidly induced cold responsiveness in cold-insensitive neurons. Taken together, I reveal that silent-cold sensing neurons contribute to cold allodynia in neuropathic pain and identify K_V1 channel downregulation as a driver of *de novo* cold sensitivity, *in vivo.*

Impact Statement

We live in a world of too much pain – a world of chronic disease and complex chronic pain syndromes. Of arthritis pain, and diabetic pain, and cancer pain, and chemotherapy pain, and fibromyalgia pain. Of opioid epidemics and opioid-induced pain. Pain that serves no useful purpose, that persists long after injury and that is poorly treated by analgesics.

One in every five of us will suffer from deeply debilitating and excruciating chronic pain in our lifetimes. My thesis makes a small, but important, contribution to tackling this clinical problem. Billions of dollars have been invested in $Na_V1.7$ antagonists as analgesics, but they fail to relieve pain in the clinic. By revealing how loss of the gene *SCN9A* encoding $Na_V1.7$ abolishes pain, my work explains the failure of $Na_V1.7$ blockers and thus provides a mechanistic rationale for new gene therapies targeting $Na_V1.7$ and associated endogenous opioid systems. By defining the underlying pathophysiology of cold allodynia in neuropathic pain, I have identified new cellular and molecular targets for treating this previously mysterious symptom of chronic pain. These discoveries will make an impact both in the academic study of pain, while also providing useful information for clinical studies. The development of novel methodologies such as glutamate imaging gives new opportunities for studying pain pathways. My work has also formed the basis of further translational studies by others in the lab, aimed at treating cold allodynia.

The results of this thesis have been disseminated at several international conferences, through five poster presentations and four talks. The initial work on cold sensation was published in PNAS in 2019, while both the $Na_V1.7$ paper and cold allodynia study are currently being revised for re-submission in response to peer reviewers' comments. A review article on the molecular mechanisms of cold pain has also been published in Neurobiology of Pain.

My work has also been communicated to the public through various channels. I designed and taught a course called 'Aches and Brains: the neuroscience of pain' to under-represented students at secondary schools in London. I have also written a number of articles for Pain Research Forum on pain science. Lastly, I have organized a monthly public engagement event called PubhD in London, with the goal of sharing academic research with the public, where I presented my work three times.

Dedication

Tha an obair seo na chuimhneachan air mo sheanmhair Ceit Dòmhnallach.

Fois siorruidh.

This work is dedicated to the memory of my grandmother Kate MacDonald.

Acknowledgements

I would like to thank my primary supervisor Professor John Wood for giving me the opportunity to pursue a PhD in the Molecular Nociception Group. I am very grateful for all his guidance, encouragement and good ideas.

I would also like to thank my secondary supervisor Professor Robert Brownstone for all his support and advice, and for giving me the chance to work in his laboratory.

I wish to thank all members of the Molecular Nociception Group, past and present, for their support and encouragement. This has been a fantastic environment to pursue a PhD – I am grateful for the good humour, great cakes and even better science. I would also like to thank members of the Brownstone Group for welcoming me into their lab.

I would like to thank Dr Edward Emery for his guidance and intellectual support over the past four years. I also want to thank Dr Ana Luiz for teaching me (almost) everything I know about experimental pain research, as well as her patience, generosity and thoughtful ideas. I am very grateful to both of you for helping me learn to be a good scientist and for much else besides.

Thank you to Queensta Millet for working with me on Substance P and on numerous behavioural experiments, her good humour and positivity got us through some difficult times. And to Sonia Santana and Sam Gossage for sorting out all problems, helping me in countless ways and keeping the fun office fun. Thank you to my fellow PhD students and postdocs, especially Alice Fuller, Dr Alex Kanellopoulos, Dr Larissa de Clauser, Dr Sascha Alles and Dr Shafaq Sikandar, for insightful discussions and moral support at various points throughout this PhD. I would also like to thank Dr James Cox, Dr Jing Zhao and Dr Andrei Okorokov for always being happy to answer questions and giving great advice. Thank you also to Aida Marcotti for teaching me the unilateral cold plate test.

I wish to thank all the other colleagues and collaborators whose data contributed to the work presented in this thesis: Prof. Marco Beato, Dr. Filipe Nascimento, Dr. Jan Weiss, Dr. Martina Pyrski, Prof. Frank Zufall, Dr. Flavia Mancini and Prof. Gian D. Iannetti.

I would like to acknowledge Professor Richard Lewis for the generous gift of ciguatoxin-2.

Thank you to all the excellent BSU staff for their hard work and professionalism in taking care of the animals used in this study.

Many thanks to all the students of the Wolfson PhD programme, who created an incredibly friendly and supportive community here at UCL. I would especially like to thank Elizabeth Halton, who helped me out in numerous ways these past four years, and whose care and dedication made the Wolfson programme such a positive experience for us all.

I would like to thank all those who taught or supervised me at UCL, Calgary, Oxford, and, before then, Sgoil Lionacleit and Sgoil Eirisgeidh for their support in getting me to this point.

Thank you to my friends for making these four years in London such a fun and happy time.

And finally thank you to my parents and family for everything.

Mìle taing dhuibh uile.

Funding

I would like to thank the Wolfson Foundation for funding my PhD studies.

Publications

Luiz, A. P. *et al.* Cold sensing by NaV1.8-positive and NaV1.8-negative sensory neurons. *Proc. Natl. Acad. Sci. U. S. A.* **116**, 3811–3816 (2019).

MacDonald, D. I., Wood, J. N. & Emery, E. C. Molecular mechanisms of cold pain. *Neurobiology of Pain* **7**, 100044 (2020).

Table of contents

List of figures

List of tables

List of abbreviations

4-AP	4-aminopyridine
AAV	Adeno-associated virus
AC	Adenylate cyclase
ACSF	Artificial cerebrospinal fluid
ADP	Adenosine di-phosphate
AITC	Allyl isothiocyanate
α-DTx	alpha-dendrotoxin
ANOVA	Analysis of variance
ASIC	Acid sensing ion channel
ATP	Adenosine tri-phosphate
BAC	Bacterial artificial chromosome
BDNF	Brain-derived neurotrophic factor
BSA	Bovine serum albumin
cAMP	Cyclic adenosine monophosphate
CB1	Cannabinoid receptor 1
CCI	Chronic constriction injury
CFA	Complete Freud's Adjuvant
CGRP	Calcitonin gene-related peptide
CHRNA1	Cholinergic receptor nicotinic alpha 1 subunit
CIP	Congenital insensitivity to pain
CNS	Central nervous system
COX2	Cyclooxygenase-2
CRISPR	Clustered regularly interspaced short palindromic repeats
CRPM2	Collapsin Response Mediator Protein-2
CSF	Cerebrospinal fluid
DMEM	Dulbecco's Modified Eagle Medium
dNTP	Deoxynucleoside triphosphate
DRG	Dorsal root ganglion
DTA	Diphtheria toxin fragment A
DTR	Diphtheria toxin receptor
eEPSC	Evoked excitatory post-synaptic current
eGFP	Enhanced green fluorescence protein
ELISA	Enzyme-linked immunosorbent assay

ENaC	Epithelial sodium channel
EPL	External plexiform layer
EPP	Excitatory post-synaptic potential
ESC	Embryonic stem cell
FAAH	Fatty acid amide hydrolase
FACS	Fluorescence activated cell sorting
FBS	Fetal bovine serum
FIJI	Fiji is just ImageJ
GABA	Gamma aminobutyric acid
GCaMP	GFP Calmodulin M13 protein
GIRK	G-protein-coupled inwardly-rectifying potassium channel
GLR-3	Glutamate-like receptor 3
GPCR	G-protein-coupled receptor
GrL	Granule cell layer
HCN	Hyperpolarization-activated cyclic nucleotide–gated channel
HEK	Human embryonic kidney cell
HPA	Hypothalamic-pituitary-adrenal axis
HSAN	Hereditary sensory autonomic neuropathy
IASP	International Association for the Study of Pain
IB4	Isolectin B4
IEFD	Intra-epidermal fibre density
IEM	Inherited erythromelalgia
iGluSnFR	Intensity-based glutamate sensing fluorescent reporter
IKD	Excitability brake current
IPI	Inter pulse interval
K2P	Two-pore domain potassium channel
k-DTx	k-dendrotoxin
KO	Knockout
KRAB	Kruppel associated box
K_V	Voltage-gated potassium channel
Mrgpr	Mas-related G-protein-coupled receptor
Na_V	Voltage-gated sodium channel
NFAT5	Nuclear factor of activated T cells-5
NGF	Nerve growth factor
NMDA	N-methyl-D-aspartate receptor

NSAID	Non-steroidal anti-inflammatory drug
ONL	Olfactory nerve layer
OSN	Olfactory sensory neuron
Oxa.	Oxaliplatin
PCR	Polymerase chain reaction
P-CTX-2	Ciguatoxin-2
PENK	Preproenkephalin
PEPD	Paroxysmal extreme pain disorder
PF-771	PF 05089771
PGE2	Prostaglandin E2
PKA	Protein kinase A
PLAP	Placental alkaline phosphatase
PMT	Photomultiplier tube
PNL	Partial sciatic nerve ligation
PNS	Peripheral nervous system
PPR	Paired pulse ratio
RIIIJ	Conotoxin kM RIIJ
ROI	Region of interest
SEM	Standard error of the mean
sEPSC	Spontaneous excitatory post-synaptic current
SFN	Small fibre neuropathy
siRNA	Small interfering RNA
SNARE	SNAP Receptor protein
SNI	Spared nerve injury
SNP	Single nucleotide polymorphism
SNR	Signal to noise ratio
SUMO	Small Ubiquitin-like Modifier protein
TEA	Tetraethylammonium
TG	Trigeminal ganglion
TH	Tyrosine hydroxylase
Trk	Tropomyosin receptor kinase
TRP	Transient receptor potential channel
TTX	Tetrodotoxin
WDR	Wide dynamic range neuron
WT	Wild-type

1 General Introduction

1.1 The problem of pain

1.1.1 Pain and nociception

What is pain? The word pain derives from Poinê, the Greek goddess of vengeance.[1] Across different cultures and ages, pain has been associated with heavenly punishment. In the Book of Genesis, for her disobedience, Eve and her descendants are cursed to painful childbirth.[2] Throughout medieval Europe, pain was understood in religious terms, with fortitude in the face of pain valorised. The Judeo-Christian moralization of pain as punishment gave way in the modern era to a more naturalistic perspective rooted in the physiological functioning of the nervous system. Under the stewardship of John Bonica, in 1979 the International Association for the Study of Pain (IASP) defined pain in psychological terms as an "an unpleasant sensory and emotional experience associated with actual or potential tissue damage, or described in terms of such damage."[3] This description differs markedly from the vernacular understanding of pain, which denotes trial and suffering in the broader sense. By emphasizing the subjective nature of pain, the IASP definition centres the feelings of the patient, while creating a precise, circumscribed definition amenable to scientific enquiry.

This definition of pain is not without criticism. Alternatives focus on function: "pain is the unpleasant sensation that has evolved to motivate behaviour which avoids or minimizes tissue damage, or promotes recovery."[4] Consider this description of a ten year old Pakistani boy born unable to feel pain due to a loss-of-function mutation in the gene *SCN9A* encoding voltage-gated sodium $Na_V1.7$:

"[He was] well known to the medical service after regularly performing 'street theatre'. He placed knives through his arms and walked on burning coals, but experienced no pain. He died before being seen on his fourteenth birthday, after jumping off a house roof."[5]

Why do we feel pain? First, pain acts as an early-warning system that drives immediate withdrawal from potentially harmful stimuli. The boy was able to stab himself and walk on hot coals because he lacked the acute pain response that would normally stop him doing this. Second, pain from injured tissue forces you to act carefully, promoting healing by preventing further damage of the wound. This boy performed street theatre

'regularly' in spite of the resultant injuries because his wounds never hurt him. Third, the unpleasant experience of pain is a negative reinforcer that teaches you not to repeat the behaviour that initially triggered the pain. Sadly, the boy passed away after jumping off a roof. His lack of pain ensured he never learnt to avoid dangerous or damaging actions. Evidently, pain is crucial to survival.

Pain is not the same as nociception. The term nociception was coined by Charles Sherrington to distinguish the physiological processes occurring in the nervous system from the subjective experience of pain.[6] For IASP, nociception is strictly limited to "the neural process of encoding noxious stimuli."[7] Nociception can drive behavioural and homeostatic changes, without any attendant experience of pain. Conversely, in the case of patients with brain lesions or stroke, pain can be experienced in the absence of activity in peripheral nociceptors.[8] In principle, we are limited to studying nociception when working with animals as they can never self-report pain.[9] In her influential book 'The Body in Pain,' Elaine Scarry argues that pain is similarly inexpressible by humans – pain is a private, subjective experience which, when communicated, destroys language with patients resorting to pre-linguistic cries and groans.[10] In practice, then, we can consider nocifensive behaviours as pain-like behaviours that read-out the probable pain state of the animal. Although we can never access the subjective pain experience of other humans or animals, when studying pain, the guiding value should be to assume the worst.

Nociception and pain-like behaviours are widespread throughout the natural world, indicative of their value for survival. There is a gradation. Even bacteria withdraw from noxious pressure.[11] However, true nociception requires a nervous system – searching for specialized nociceptors and nociceptive reflexes that drive avoidance behaviour yields a more selective list. Cnidarians and ctenophores, with their primitive nerve nets, do not seem to have nociceptors and do not respond to noxious heat.[12] Among invertebrates, nociceptors are found in nematodes, annelids, arthropods and molluscs, including common lab animals like *D. melanogaster* and *C. elegans*. Of culinary interest, crustaceans show nociceptive behaviours in response to noxious heating.[13] Among vertebrates, nociceptors have been found in mammals, amphibians, reptiles, birds and fish, although cartilaginous fish lack the unmyelinated afferents that subserve nociception in most species.[14] Intriguingly, evolution has given rise to species with diminished nociception. The naked mole rat is insensitive to acid thanks to a variant of $Na_V1.7$ that is potently blocked by protons to prevent acid-evoked action potential firing – adaptive in this animal's CO_2-choked communal burrows.[15]

A cardinal feature of nociception is sensitization. While our visual and tactile systems adapt to prolonged stimulation, nociceptors ramp up their responses. Sensitization can be maladaptive, triggering prolonged and purposeless pain.[16] Why did this unusual sensitization evolve? Squid have nociceptors that sensitize after injury and become spontaneously active. When this sensitization is blocked using an anaesthetic, injured squid show decreased long-term survival due to slower escape responses when exposed to predators compared to both uninjured squid and injured squid with intact sensitization.[17] Cold, Darwinian logic thus demonstrates that pain plasticity is adaptive, conferring a survival advantage, but can, in time, go awry, driving persistent pathological pain.

1.1.2 Chronic pain

Chronic pain afflicts a fifth of people worldwide, with many patients refractory to treatment.[18] Aberrant plasticity in the pain pathway drives pain that is without purpose, lasting long after the resolution of injury, and dealing out immense suffering. Three observations stand out. First, the absolute number and proportion of people in pain is increasing with our ageing population.[19] Second, poorly managed pain has a ruinous effect on quality of life and is the most common reason people seek out medical treatment.[20] Third, currently available analgesic drugs do not provide adequate pain relief for a large number of patients.[21] Both quantitatively and qualitatively, the problem of pain represents arguably the greatest clinical challenge of the 21st century.

For IASP, chronic pain is standardized as pain that continues for more than three months.[22] Chronic pain is a feature of numerous chronic and age-related diseases, including arthritis, diabetes, fibromyalgia and cancer. In the UK, a recent meta-analysis showed up to 14.3% of the general UK population suffers from chronic pain categorized as moderate to severe.[23] Risk factors for chronic pain include age and weight – with an ageing and increasingly obese population, the preponderance of pain will likely increase.[24] A puzzling statistic is that women experience chronic pain at rates higher than men; in the US, the figures are 34% and 27%, respectively.[25] Unsurprisingly, chronic pain negatively impacts quality of life, putting patients out of work and affecting their mental health. On the individual level, chronic pain is often co-morbid with anxiety and depression, with untreated pain a major driver of suicide.[26] Collectively, chronic pain is a significant burden on the medical system, and comes at an enormous economic cost, to the tune of $300 billion in the US.[27]

Compounding the problem, chronic pain is poorly- or under-treated. Current therapies successfully manage short-lasting pains like post-surgical pain, however persistent pain states are more challenging to treat. Pregabalin reduces pain in only a third of patients with chronic neuropathic pain such as shingles or diabetic neuropathy.[28] For lower back pain, paracetamol, the most widely prescribed painkiller, was shown to be completely ineffective in a systematic review.[29] In the US, opioids – which are highly effective for acute or end-of-life pain treatment – have been heavily prescribed for long-term pain, despite flimsy evidence to support their use.[30] Inappropriate opioid prescribing has resulted in the widespread availability of prescription opioids, triggering an epidemic of opioid addiction. In 2017, ~50,000 people died of opioid overdose in the US alone, a humanitarian crisis of vast proportions (**Figure 1.1**).[31] Chronic NSAID use, common among older generations, is also associated with significant mortality. Gastric bleeding, renal failure and increased cardiovascular effects are all likely causes.[32] Consequently, there is a pressing and unmet need for analgesics with improved efficacy, fewer side effects and reduced risk of addiction.

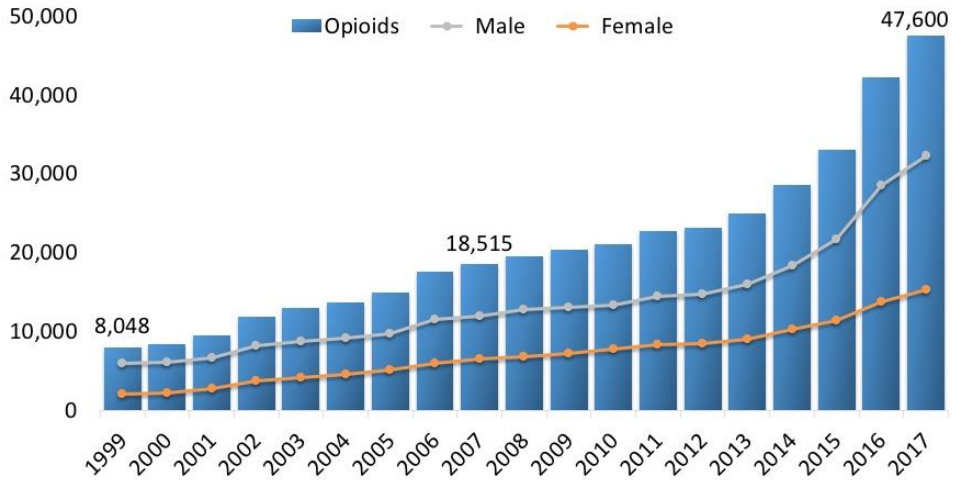

Figure 1.1 (*adapted from ref. 31).* Annual opioid overdose deaths in the USA, for both men and women

Graph plotting the number of deaths resulting from opioid overdose in the USA over time from 1999 to 2017, both overall (bars) and by gender (lines). Here opioid refers to any prescription opioid, as well as methadone, illicit opioids (e.g. heroin), and synthetic opioids (e.g. fentanyl). Note the striking increase in the number of overdose deaths from 18,515 in 2007 to 47,600 in 2017.

In 2010, IASP published the Declaration of Montréal which declared that access to adequate pain treatment is a fundamental human right.[33] Few would disagree that the alleviation of suffering is a moral imperative for science and society. When choosing to study the biological mechanisms of chronic pain, Patrick Wall – the father of the pain

field – said his instinct was to follow his "socialist thinking and to opt for fields with social relevance."[34] To solve the problem of pain, we must develop new therapeutic strategies for pain relief. New biological targets must be identified and validated in a rational manner. To this end, we need a mechanistic understanding of physiology and pathology that can only be gained by basic experimental research.

1.1.3 Theories of pain

The first person to study pain experimentally was the Greek physician Galen. Galen and his students saw pain as driven by dysfunction in the four humours resulting in irritation of the nerves. He showed that severing the spinal cord of piglets caused sensory deficits below the cut, hinting at an ascending somatosensory pathway.[35,36] In the 11th century, the Iranian polymath Avicenna's clinical observations led him to conclude pain could be dissociated from touch and temperature as an independent sensation.[37] Anatomical studies of the nervous system were made throughout the medieval era, flourishing with the Renaissance, when Vesalius extended the findings of Galen.[38] But it is Descartes who is usually credited with originating the scientific study of pain. In his *Treatise of Man*, Descartes likened the nervous system to a machine, where particles of fire caused animal spirits to flow down specific filaments to the brain where pain was experienced. La Forge's famous drawing, incorporating Descartes' theory and the contemporary cutting-edge of anatomy, might therefore be regarded as the first scientific model of pain (**Figure 1.2**).[36]

Descartes' model anticipated what we now call the Specificity Theory of pain, whose modern conception is attributed to Scottish physician Charles Bell:

"Each organ of sense is provided with a capacity of receiving certain changes […] yet each is utterly incapable of receiving the impressions destined for another organ of sensation. It is also very remarkable that an impression made on two different nerves of sense, though with the same instrument, will produce two distinct sensations; and the ideas resulting will only have relation to the organ affected."[39]

In Specificity Theory, pain is a distinct sensation conveyed along specific channels from periphery to perception, where the amount of pain experienced is directly proportional to the strength of stimulus. Lesion studies supported the existence of a separate pain pathway. In the 19th century, cutting different levels of the spinal cord revealed an anterolateral pathway for pain and temperature, while the posterior bundles were specialized for innocuous mechano-sensation.[38] Gowers, a doctor in London, described a patient with a bullet wound to the grey matter who lost the sense of pain and

temperature but not touch.[38] Charles Sherrington, the great physiologist, postulated the existence of nociceptors – specific nerves dedicated to detecting damaging stimuli and whose activation led to pain – that were finally found half a century later by Ed Perl and colleagues.[6,40,41]

Figure 1.2. La Forge's famous drawing, published in Descartes' Treatise of Man.

This drawing summarizes Descartes' understanding of the acute pain response. The man's foot (B) is close to the fire (A). The flames press the skin and pull on the filamentous tube, or fibril (C). This opens the pore (D and E) in the brain where the fibril terminates. Opening of the pore ensures animal spirits can flow from the cavity in the brain (F) into the fibril. The animal spirits then activate muscles to retract the foot from the fire – what we would now call a nocifensive reflex or behaviour.

But Specificity Theory leaves little room for the cognitive and affective domains of pain. Competing theories therefore tried to reconcile the physiological and anatomical data with the complexity of the pain experience apparent in the clinic. In the late 19th century, William Erb observed that intense sensations are normally unpleasant and caused by strong stimuli, suggesting that pain was the emotional outcome of the excessive activation of unspecialized sensory pathways. Repeated stimulation (up to 600 times) with normally imperceptible tactile stimuli caused unbearable pain in syphilitic patients whose dorsal columns had degenerated. [38] These experiments led Alfred Goldscheider to hypothesize that some form of central summation must occur in the nervous system so that pain scales with the intensity of multiple sensory inputs.[38] The Intensity Theory was

extended by the American psychologist John Nafe in 1929 as part of his "quantitative theory of feeling". In his view, somatosensory perception occurred in response to particular patterns of input – the pattern of peripheral nerve firing encoded the type of stimulus and drove the quality of the corresponding feeling.[42] An underlying assumption of this Pattern Theory was that all peripheral nerves are essentially the same – the specificity lies not in the nerve, but in the structure and timing of its activity. This challenge to specific sensory channels was supported by the discovery of the wide dynamic range neurons in the deep dorsal horn in 1966.[43]

It was in the context of the "bitter controversy" over these competing theories of pain that Melzack and Wall published their seminal paper 'Pain mechanisms: a new theory.'[44] They begin by reviewing the writings of the two camps – the Specificity Theory and the Pattern Theory (including its antecedent, Intensity Theory). Acknowledging that the experimental data could support either theory, they proposed a novel Gate Control mechanism that incorporated aspects of both. Briefly, they accepted the existence of specialized nociceptive and tactile afferents, but suggested the substantia gelatinosa acted as a gate that determined which peripheral inputs reach the brain. Small nociceptive fibres would open the gate, large fibres could close it, while the whole system was under descending control from the brain, providing an explanation for the clinical observation that pain often does not correlate with the extent of injury. Although influential, Gate Theory was hardly the final word on the matter. Clifford Woolf writes:

"My first exposure in the late 1970s to the Specificity versus Pattern Theory debate, repeated endlessly over too many pints of ale at the Jeremy Bentham pub near University College London, was from Pat Wall."[45]

Sadly the Jeremy Bentham pub is no more, turned into a cocktail bar midway through the writing of this thesis. The debates over Specificity and Pattern Theory, however, persist. The advent of *in vivo* imaging techniques to monitor the activity of many hundreds of cells simultaneously has reawakened controversy over the selectivity of sensory neuron responses.[46] No one can deny that investigations informed by Specificity Theory have been immensely fruitful, with the identification of multiple specific cell types, receptors and ion channels that appear to convey particular sensations.[47] However, the philosophical problems with Specificity Theory cannot be ignored. On the one hand, specific channels require an integrator to generate the overall perception, which skirts dangerously close to a 'Cartesian theatre' where the man-in-the-brain conveniently does

the perceiving.[48] On the other hand, there must be a limit to specificity otherwise one falls into the trap of requiring one neuron for every particular sensation *reductio ad absurdum* – the so-called Grandmother Neuron fallacy.[49]

In the clinic, theories of pain that acknowledge the central and emotional aspects of pain have been most influential, given they mesh best with the reality of the patient experience. Melzack proposed a neatly Trinitarian theory of pain, comprising equally important sensory-discriminative, affective-motivational, and cognitive-evaluative components processed in a simultaneously parallel and interacting fashion.[50] In this model, the protective and motivational behaviours associated with pain are not simple consequences of sensation but a fundamental and intrinsic part of the pain experience. This multidimensional view of pain has been given the stamp of official approval by the IASP definition of pain.[7] In recent years, the role of prior learning and experience has been recognized as important in pain. Howard Fields emphasizes the importance of expectancies and suggests that pain will be dampened by competing motivations.[51] A Bayesian view of the brain-in-pain is increasingly popular, where pain is seen as an inference based on nociceptive input and expectancies informed by prior experience.[52]

Even from this short survey, the great diversity of theories that seek to explain pain is apparent. It can be difficult to reconcile the battling theories and personalities, and to distinguish which explanation is most accurate or informative. Clearly, specialized receptors, nerves and ion channels exist. But it is also transparently true that the experience of pain is multidimensional and 'gated' by numerous external and internal factors. Basbaum reminds us that:

"The original discussion of specificity versus patterning was not a neurophysiological one. Rather, it was a perceptual one: How does the brain generate a pain percept?"[45]

We must be cautious not to confuse levels of explanation or analysis. A theory of pain is not a theory of nociception, and vice-versa. One theory may be best suited to explain central mechanisms of emotion and perception, while another most satisfactorily accounts for the peripheral mechanisms of detection and sensation. My thesis, which investigates ion channels and cell types specialized for specific painful and thermal sensations, doubtless contributes to the ever-accumulating evidence for a Specificity Theory of peripheral sensory neuron function. As to the respective roles of patterns, gates and Thomas Bayes in the sensory-emotional experience of pain, such questions are far beyond the scope of this work.

1.2 Sensory biology of nociception and pain

1.2.1 Physiology of peripheral nerves

Peripheral sensory neurons detect changes in the external environment and internal milieu to guide behavioural and homeostatic responses. My focus here is on the sensory neurons whose axons terminate in the skin, especially those involved in nociception and pain. With cell bodies located in the dorsal root and trigeminal ganglia, these cutaneous fibres provide the afferent sensory input that drives the conscious feeling of touch, temperature, itch and pain. Different forms of environmental energy – thermal, mechanical and chemical stimuli – are transduced at the peripheral nerve terminal into electrical impulses that propagate up sensory nerves to be interpreted and perceived by the central nervous system.

German anatomist Muller is usually credited with first suggesting that distinct sensory nerves carry information about different types of stimuli. He called this postulate his Law of Specific Nerve Energies, which formed a key argument for the Specificity Theory of pain.[37] Experimental support for such 'labelled lines' came from Von Frey and others, who showed that pinprick stimulation of tiny 'spots' of human skin gave rise to distinct experiences of pressure, heat, cold or pain. Histologists had previously described and eponymously named specialized end organs at nerve terminals – Pacinian corpuscles, Meissners corpuscles and the like – structures which Von Frey tried to correlate with specific sensations based on his 'spot' studies.[37] Physiologists toiling with home-made recording equipment gleaned many prescient insights into the function of peripheral nerves. In the 1920s, Lord Adrian's laboratory in Cambridge performed electrophysiological recordings directly from frog peripheral nerves – galvanometer traces from his group show irregular deflections in the recorded potential in response to various naturalistic stimuli, taken as evidence of selective responses by different fibres types.[53] Recordings of compound action potentials from the saphenous nerve of the cat by Gasser established a classification of different fibres based on conduction velocity, thickness and degree of myelination, still to be found in every textbook of neuroscience (**Table 1-1**).

As is common in the history of neuroscience, such detailed characterization of peripheral fibres was predicated on technological advances. Before the development of cathode ray oscilloscopes and improved vacuum tube amplifiers, Gasser wrote:

'The situation may be compared to the knowledge of geography before America was discovered. Our fiber world ended at gamma, with an uncertain and nebulous delta in sight beyond it. As soon as high gain amplifiers were built it was possible for us […] to see that there were two well-defined elevations that had not previously been recognized, those now labeled delta and C.'[54]

That a subset of these peripheral nerves were specialized to detect harmful or noxious stimuli was first hypothesized by Sherrington, who coined the term 'nociceptor.'[6] But the Specificity Theory was long taking root. Pain was expressly excluded from the five Aristotelian senses and, well into the 20th century, many psychologists and clinicians adhered to the Intensity or Pattern Theory, which saw pain as generated by excessive barrages of patterned activity in unspecialized nerves. Gasser, however, showed that driving or blocking activity in nerves contributing to particular components of the compound action potential implicated A-delta and C fibres in nocifensive reactions.[37] In consequence, A-delta and C fibres are conventionally associated with nociception and thermoception, while A-beta fibres provide tactile and proprioceptive signals (**Table 1-1**). However, it is now known that nociceptors encompass all classes of sensory nerves, including A-beta fibres.[55] In humans, application of a brief noxious stimulus evokes an early sharp and late dull sensation of pain, attributable to the faster A fibres and the slower C fibres, respectively.[56]

Fibre class	Diameter (μm)	Myelination	Conduction Velocity (ms)	Functional specialization
Aβ	6-22	Heavy	30-120	Tactile, proprioception, nociception
Aδ	1-4	Light	5-25	Tactile, mechano-nociception, cold
C	0.4-1.2	None	0.1-2	Nociception, heat, cold, tactile, pruriception

Table 1-1. Electrophysiological classification of peripheral nerves.

The traditional classification of sensory afferents based on conduction velocity, which is determined by diameter and the degree of myelination. Traditionally, C- and Aδ-fibres have been primarily associated with nociceptors. However, it is now appreciated that Aβ nociceptors also exist.[55]

A major difficulty facing physiologists investigating putative nociceptors, however, was that their thinness made unambiguously recording from single, identified C fibres technically daunting. When Zotterman recorded from the entire lingual nerve of the cat, he concluded the C fibre component signalled pain due to its high threshold of activation.[57] Three years later, however, he observed that C fibres apparently responded to innocuous tactile stimuli, speculating that these represented tickle-specific afferents.[58]

The demonstration of *bona fide* nociceptive fibres had to wait until the studies of Perl and colleagues who used the 'teased filament' technique to record from single afferent units. Perl recalled:

'Our routine of testing by gentle mechanical stimulation yielded no activity. After some minutes of fruitless trial, one of us, and we cannot remember whom, picked up a tissue forceps and pinched the skin in the middle of the nerve's receptive field. This evoked a burst of impulses. We looked at each other across the experimental table, both recognizing what we may have seen…'[34]

By recording many hundreds of individual units in a systematic and unbiased fashion, Perl and colleagues identified individual C and A-delta fibres that responded only to noxious stimuli. In agreement with Zotterman, however, not all C fibres were nociceptors. Of the nociceptive C fibres, most had 'polymodal' responses characteristics. A delta nociceptors were mainly activated by high-threshold mechanical stimuli, however other A delta fibres discharged to innocuous brushing.[41,40] Microneurographic recording of single afferent fibres in human volunteers demonstrated a correspondence between noxious stimulus, C fibre response and pain percept.[59] Using the recording electrode to stimulate nociceptors with a weak electrical current evoked pain in human subjects, corroborating that activity in peripheral nociceptors can drive the conscious experience of pain.[60] Wall and McMahon caution us against over-interpretation of these microneurographic studies, warning that the large size of the microelectrode tip in contact with the small fibres means we cannot be confident which fibre is being stimulated.[61] Nevertheless, on balance, nearly a century's worth of peripheral nerve recordings in humans and animals leave little doubt that specialized fibres that detect and encode noxious stimuli exist in mammals. Their contribution to different forms of physiological and pathological pain, however, remains an open question.

1.2.2 Molecular classification of sensory neurons

It was Ramon y Cajal who first recognized that neurons could be organized into a taxonomy of cell 'types'. Through careful study of Golgi stained nervous tissue, he identified discrete categories of neurons based on their diverse morphologies. This notion of cell 'type' lies at the foundation of modern neuroscience. Features such as morphology, developmental origin and gene expression are routinely used to profile and classify individual neurons. For sensory biologists, the great challenge has been to relate the physiological and anatomical specializations of afferent neurons to the cacophony of

molecules they express. By identifying molecular 'markers' that label subsets of afferents, it has been possible to characterize and experimentally manipulate defined sensory neuron subtypes in mice using molecular genetics (**Figure 1.3**).

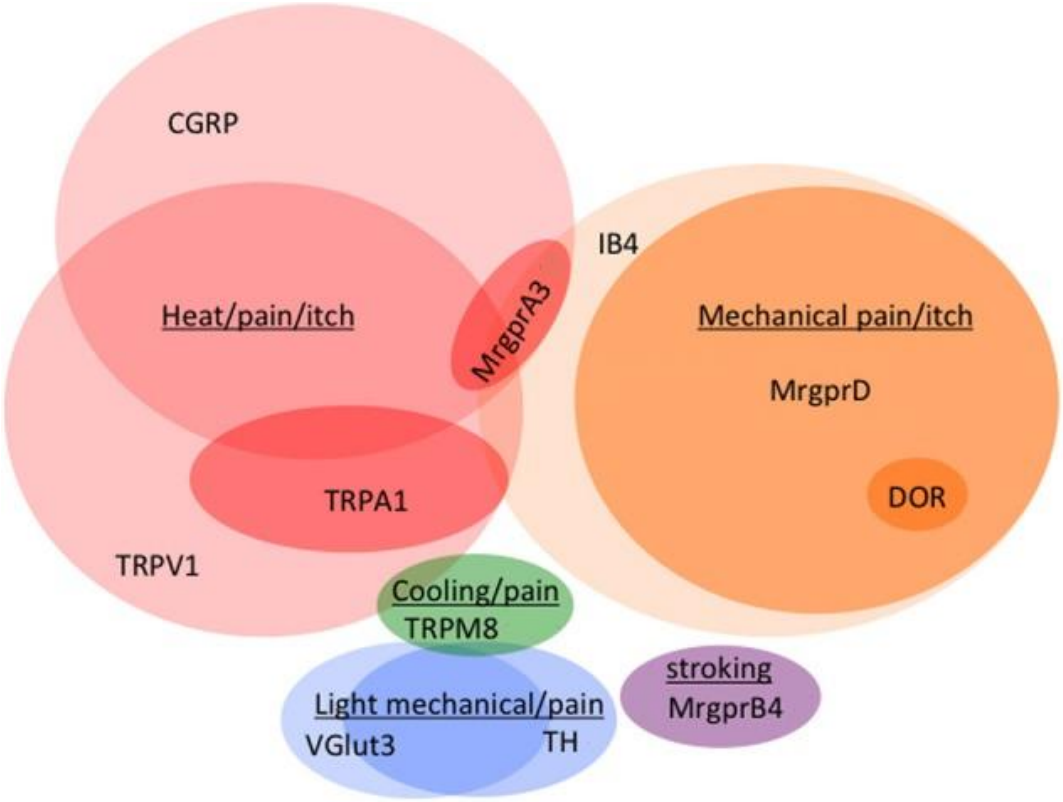

Figure 1.3 (*adapted from ref. 47*). Venn diagram illustrating the distribution of different molecular markers across different C fibre types determined by mouse genetic experiments.

This Venn diagram illustrates one interpretation of the different molecularly-defined subclasses of sensory neurons and their functional specializations. This classification is derived primarily from cell ablation experiments. Each colour represents a different modality and each circle represents a different molecular marker. Thus noxious heat requires cells expressing Trpv1, CGRPα and Trpa1, while cooling is encoded primarily by Trpm8-expressing neurons, but which are also positive for Trpv1.

We can, for example, relate neurochemical markers visible by immunostaining with the functional specializations of certain sensory neurons. Large 'light' sensory neurons stain for neurofilament 200 and correspond to the fast myelinated A fibres.[62] Small 'dark' sensory neurons – the nociceptive C fibres – are negative for neurofilament but can be identified by peripherin staining.[63] Putative nociceptors can then be divided into the peptidergic and non-peptidergic subclasses, although there is some overlap between them. Peptidergic neurons express neuropeptides such as CGRP and Substance P, while non-petidergic group are marked by their reactivity to the plant lectin IB4.[64] In a set of technically-impressive studies, Sally Lawson recorded intracellularly from the

sensory neurons of rats *ex vivo* and of guinea pig *in vivo*, first characterizing their electrophysiological properties, and then injecting a dye via the microelectrode for post-hoc identification of the recorded cells. These experiments revealed CGRP-positive neurons comprise both C and A-delta fibres, and account for fully half of all nociceptors.[65,66] Recently, targeted extracellular recording and calcium imaging of CGRP-expressing afferents revealed a unique population of A-delta mechanonociceptors that innervate the hairy skin with circumreferential endings, emphasizing the continuing relevance and utility of these traditional neurochemical markers.[67]

Equally informative has been understanding the developmental trajectory of peripheral sensory neurons to determine fate-specific labels. In particular, the diversity of low-threshold mechanosensors has been mapped using transcription factor and growth factor molecular markers. For example, the rapidly-adapting A-beta low threshold mechanosensors that innervate Meissner and Pacinian corpuscles have low TrkB levels and are defined by expression of the transcription factor cMaf.[68] The generation of TrkB-positive neurons, on the other hand, is driven by expression of the transcription factor Shox2.[64,69] The Ginty laboratory has exploited molecular genetics to survey and describe a large number of sensory neurons involved in touch.[70] In a particularly elegant example, the A-beta field LTMRs were targeted and characterized using an intersectional genetic strategy based on their co-expression of TrkC and Ret, illustrating how a few markers, exploited in a combinatorial fashion, guide the fine-grained dissection of a sensory neuron subset.[71]

Unsurprisingly, genes critical to specialized sensory neuron physiology – particularly ion channels – have proven useful as markers. For example, $Na_V1.8$, the TTX-resistant sodium channel expressed by small diameter C fibres, was used to target nociceptors.[72] Diphtheria toxin mediated ablation of Nav1.8-positive neurons in a Cre-dependent fashion kills the vast majority of nociceptors, abolishing the sensation of mechanical, cold and inflammatory pain.[73] Compare this to the phenotype of animals expressing diphtheria toxin receptor under the promoter for heat-sensitive ion channel Trpv1 – when these mice are given diphtheria toxin in adulthood, Trpv1-positive neurons are ablated and heat avoidance behaviour is all but absent.[74] In cultured sensory neurons, ion channel markers have been used for 'functional fingerprinting' – here the response of cells to multiple channel-specific agonists is measured by calcium imaging, allowing for the identification of subgroups by the unique 'constellation' of molecules they express, rather than based on the expression of one or two marker genes.[75]

The more features of a sensory neuron population are measured and used for classification, the more robust the taxonomy will be to new information. In recent years, single cell RNA sequencing has allowed for the unbiased classification of DRG neurons based on the expression of many thousands of transcripts. Patrick Ernfors' group analysed the transcriptomes of 622 single mouse dorsal root ganglia neurons. Through iterative principal component analysis, these neurons were assigned to eleven different subsets, which neatly corresponded to known sensory neuron types (**Figure 1.4A**).[76] Linarsson later profiled half a million cells from the entire mouse nervous system, identifying a hierarchy of twenty-two sensory neuron subsets (**Figure 1.4B**).[77] These studies were low-coverage, however, featuring partial transcriptomes. A higher-coverage analysis of sensory neurons identified ten subgroups – a classification corroborated by *in vivo* patch-clamp recordings combined with RNA extraction through the recording pipette and subsequent reverse transcriptase PCR (**Figure 1.4C**).[78,79] Note that single-cell transcriptomics is no panacea for sensory neuron taxonomy – sequencing depth, sampling methods and quality control greatly affect the eventual results. More fundamental objections include the relevance of analysing transcriptomes compared to, say, the translatome. Nevertheless, open-source single-cell transcriptome datasets are proving useful for exploratory analyses and hypothesis generation, highlighting both the utility of these classification studies and the importance of data-sharing in 21st century neuroscience.

Lurking beneath any census of cell subsets are philosophical issues surrounding the definition of biological 'type.' Reams have been written in the philosophy of biology warning would-be taxonomists against falling into the trap of essentialism.[80] The conceptual convenience of a cell 'type' must not obscure the fact that variation in gene expression within a class can be functionally important: for instance, thermal threshold of cold-sensing neurons defined by Trpm8 expression is actually set by reciprocal variation in Trpm8 and potassium channel levels.[81] Galanin, a putative marker of peptidergic nociceptors, changes greatly across time, spiking after nerve injury, suggestive of a pathological role.[82] Thus, while 'markers' provide an intuitive, binary way of defining cell identity, implicit in single-cell transcriptome-based clustering is that cell groupings depend on a set of multidimensional but statistically co-varying traits – in this case, expressed genes. Although I will regularly appeal to various taxonomies of DRG neurons in this thesis, these caveats must always be recognized.

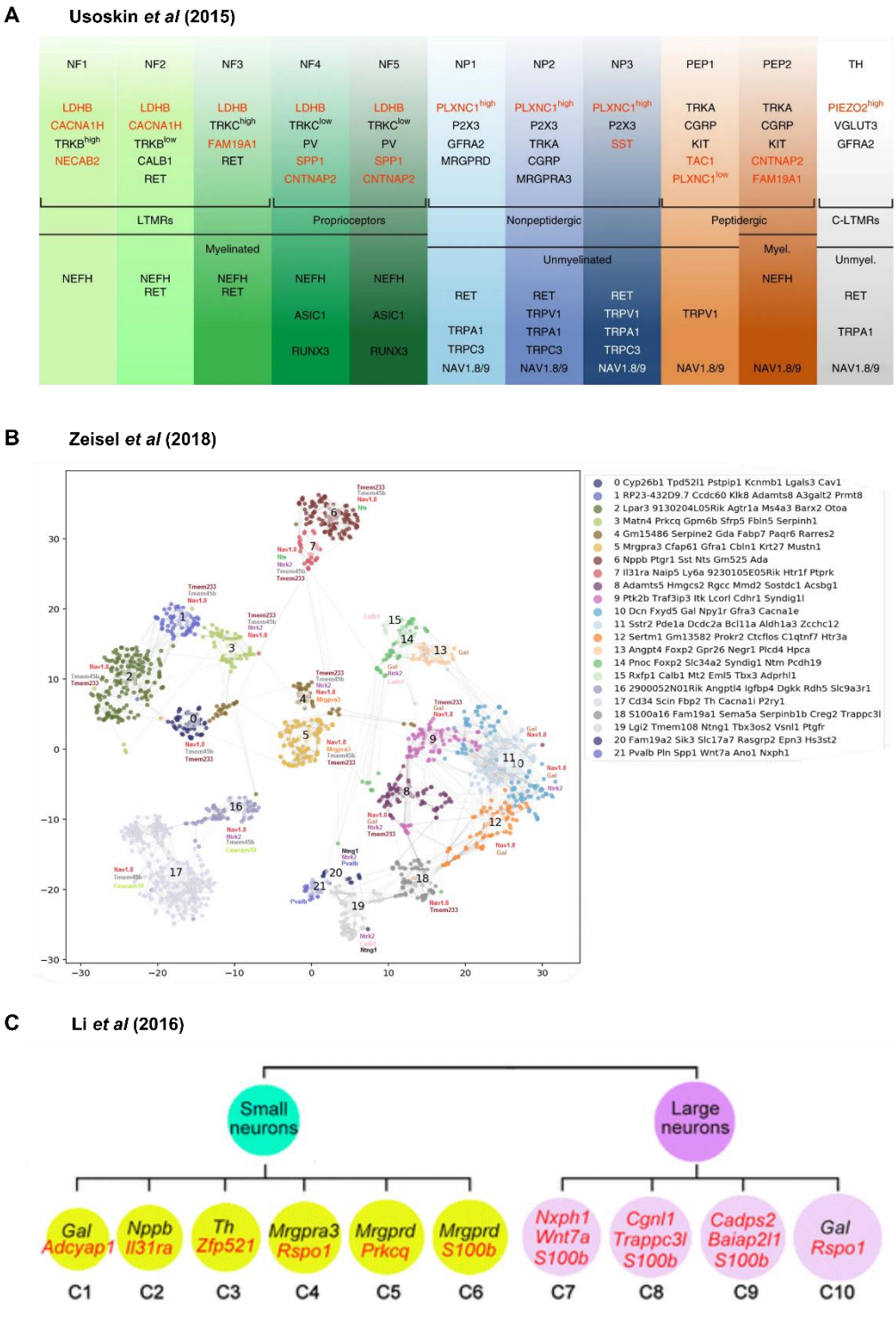

Figure 1.4. DRG neuron subtypes identified by unbiased classification using single cell RNA seq.

(A) The first classification of sensory neurons using single cell RNA sequencing by Ernfors and colleagues identified eleven different subtypes, here shown in tabular form. Marker genes are shown at the top, and below are functionally-important molecules such as ion channels expressed in each subtype.[76]

(B) The Linarsson lab subsequently identified 22 clusters, plotted here as a nearest neighbour graph projected on two dimensions. The most enriched genes for each cluster are listed on the top-right.[77]

(C) Li *et al* used high-coverage single cell RNA sequencing and hierachical clustering based on neuronal size revealed 10 different groups of neurons. Marker genes are shown within the circles[78,79]

1.2.3 Sensory transduction

Sensory neurons evolved to transform energy in the environment into behaviourally-relevant information in the nervous system. Thermal, mechanical or chemical energy gates a transducer molecule in the peripheral terminal, triggering a conformational change, leading to the opening or closing of an ion channel to alter the membrane potential. In the visual and olfactory systems, transducers are usually indirect: G-protein coupled receptors that modulate ion channels. For somatosensation, the transducer is typically the channel itself, whose opening at the nerve terminal triggers a generator potential – the first step in the pathway to detection of a sensory signal.

Identifying transducer molecules sheds light on the stimulus-specific responses of peripheral nerves. A great enigma of sensory biology was why certain plant products give rise to specific temperature percepts. To experience chillies as 'hot' and mint as 'cool' is apparently universal to all cultures, even if the enjoyment of spicy food is not.[83] The cloning of Trpv1 by Caterina and Julius in 1997 solved the mystery. In their seminal study, a cDNA library of DRG-specific mRNA was constructed, with different pools of clones transfected into HEK cells whose response to capsaicin was assayed by Fura-2 calcium imaging. In this way, a 3 kB cDNA insert was isolated that, by itself, conferred sensitivity to capsaicin and – importantly – also to high temperatures, explaining our perception of capsaicin as hot. Electrophysiological recording of recombinant Trpv1 revealed a non-specific cation channel that is gated by temperature above 43 °C, the psychophysical threshold for painful heat, thereby identifying a molecular transducer for noxious temperatures.[84]

Once a putative transducer has been cloned, to investigate the function of the molecule *in vivo*, researchers have turned to mouse genetics. Because of the paucity of good antibodies, to investigate Trpv1 expression in mice, PLAP and nLacZ markers were knocked in following the stop codon of Trpv1, thereby keeping upstream regulatory elements intact to ensure faithful marker expression. In adults, Trpv1 is enriched in peptidergic C fibres, polymodal nociceptors that respond to noxious heat.[85] To determine whether Trpv1 is required for heat nociception, two groups generated targeted Trpv1 gene knockout mice by homologous recombination in ES cells. Surprisingly, behavioural assessment of these lines showed little deficit in acute heat sensation, although the response to capsaicin is abolished and inflammatory heat hyperalgesia is impaired.[86,87] Biological function does not follow biophysical properties as night the day. An important caveat to gene knockout studies is that compensatory upregulation of other genes can

make up for loss-of-function during development. Indeed, it was recently shown that deletion of Trpv1, Trpm3 and Trpa1 is needed to completely abolish noxious heat sensation.[88] Such results emphasize redundancy in sensory pathways with channels compensating for each other, making traditional perturbations of single genes tricky to interpret.

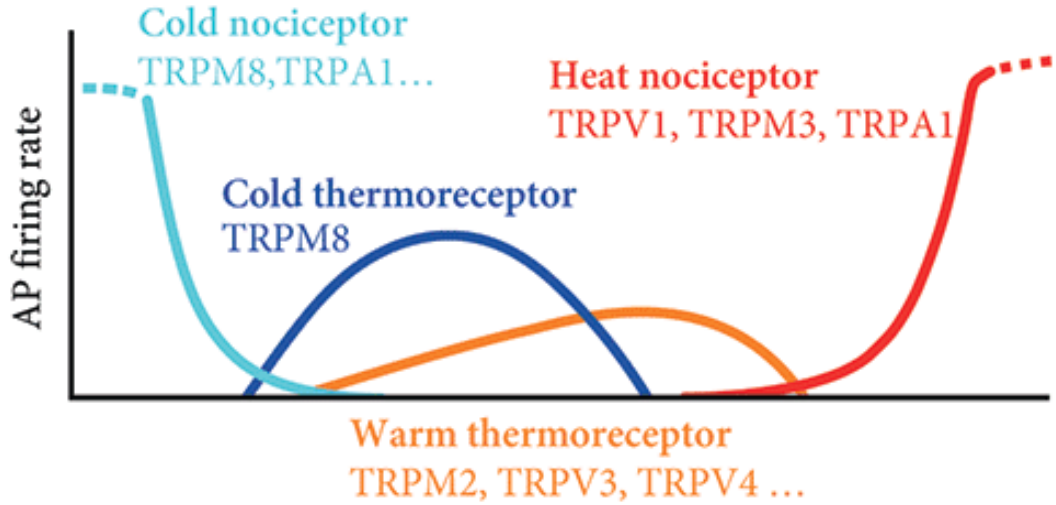

Figure 1.5 (*adapted from ref. 89*). Summary of action potential firing evoked by thermal stimuli in different classes of sensory afferent and the Trp channels proposed to mediate this activity.

This schematic illustrates the ion channels thought to transduce thermal stimuli into action potential firing (y-axis) in distinct sensory neurons (colours) within different relative temperature bands from cold to hot (x-axis). Absolute temperature values are omitted to avoid given a false impression of precision. Thus detection of noxious heat depends on a trio of Trp channels that drive a sharp increase in firing as temperature increases into the range associated with damage. As indicated by the ellipsis, there is still debate over which transducers mediate noxious cold and innocuous warmth sensation.

Although Trpv1 is by far the best studied, a multitude of putative transducers have been identified and characterized in sensory neurons, which we can only touch on briefly. These include other members of the Trp channel family, which are especially important for thermosensation (**Figure 1.5**). For example, the menthol receptor Trpm8 is necessary for innocuous cold sensation and will be considered in detail later (see Section 4.2.2).[90,91] In contrast, Trpm2 is reportedly essential for the detection of innocuous warmth.[92] Trpa1 responds to pungency, and apparently can contribute to heat, cold and mechanosensation.[88,93,94] A promiscuous channel, it appears to integrate multiple signals related to tissue damage.[95] Purinergic receptors likewise play a role in the response to injury, particularly P2X3 which is expressed on nociceptors and responds to ATP released into the extracellular space after cell breakdown.[96] ASICs, members of the ENaC ion channel family, are directly gated by extracellular protons, with nociceptor ASIC3

activated by tissue acidification during ischemia and inflammation.[97] A class of transducers particularly relevant to this thesis are background potassium channels, whose closure reduces the outward leak potassium current thereby depolarizing the membrane. TREK1 and TRAAK, for instance, are mechanically-gated and temperature-sensitive, controlling thresholds for warm and cold sensitivity.[98] Importantly, the expression and function of most transducers can change during injury and inflammation, triggering plasticity in nociceptor response properties.[16]

The last major class of transducers to be identified are the Piezo family of mechanically-gated ion channels. Using an RNAi screen, the Patapoutian group identified Piezo1 as mediating the mechanically-activated current recorded in N2A cells. Piezo1 and its cousin Piezo2 are large transmembrane proteins and can be considered as *bona fide* mechanosensors as they respond to pressure when expressed in heterologous systems.[99] Piezo2 mediates the rapidly adapting current in dorsal root ganglia neurons and when knocked out abolishes the response to light touch and proprioception in mice.[100,101] Human Piezo2 null mutants likewise show large deficits in discriminative touch and proprioception.[102] Interestingly, alternative splicing of Piezo2 produces channel variants with specialized biophysical properties that are expressed in different cell types.[103]

Discovering transducer molecules remains the holy grail of sensory biology. There are still many important questions waiting to be answered. The molecules underlying the slowly adapting mechanical current – likely responsible for noxious mechanosensation – are unknown, although the Tmem120a channel has recently proposed as the pore-forming subunit.[104] The role of non-neuronal skin cells is of increasing interest, such as purinergic transmission between keratinocytes and nerve terminals, or the role of cutaneous Schwann cells that are intrinsically mechanosensitive.[105,106] Detection of warmth, although ascribed to Trpm2, has recently come into question – warm perception in mice is impaired when cold, but not warm, transducers are ablated, results incompatible with labelled line theory and which point to a central comparator circuit.[107] Lastly, understanding what contribution particular transducers make to pathological pain states and under what conditions remains an area ripe for investigation.

1.2.4 Electrogenesis

Peripheral sensory neurons have some of the longest axons in the body. In sauropod dinosaurs, the recurrent laryngeal nerve would have reached up to 50 metres long.[108] Even in humans, the twists and turns of the sciatic nerve axons run into metre (**Figure 1.6**).

Because of the cable properties of the axon, the graded depolarizations produced by primary transducers would decay rapidly with distance if neurons carried sensory signals using the generator potential alone. Consequently, peripheral nerves must carry signals by all-or-none transmission of self-propagating action potentials. The number, frequency and temporal pattern of action potentials conveys information to the CNS about the sensory stimulus. Impulse generation and conduction are therefore important loci for molecular specialization and regulation in peripheral sensory neurons.

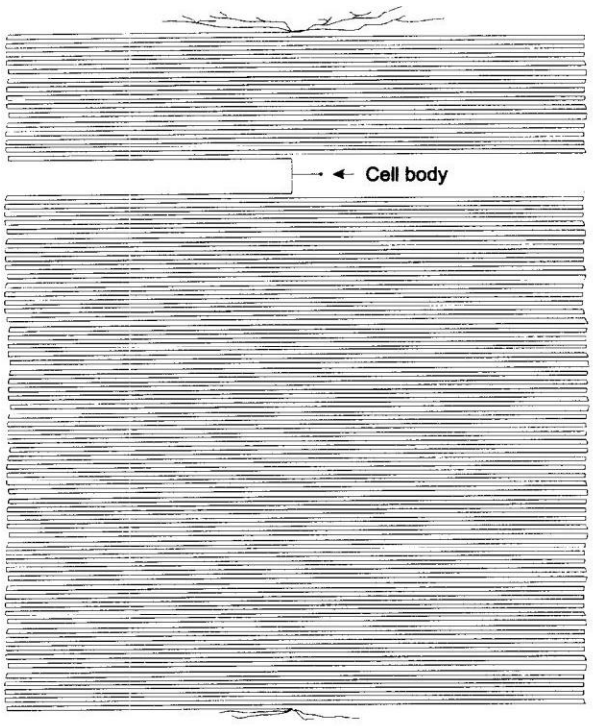

Figure 1.6 (*adapted from ref. 109*). Cartoon showing the anatomy of a dorsal root ganglia neuron.

In contrast to the textbook schematic, peripheral sensory neurons have immensely long peripheral and central axons. The cell is pseudo-unipolar, with a T-junction where the soma's stem axon joins the main axon. These features have important implications for action potential propagation, axonal trafficking and the interpretation of studies focussed on soma excitability.

The time course of the action potential was established by Bernstein, as long ago as 1865.[110] However, the ionic basis of these changes in membrane potential remained unknown. Nearly a 100 years later, Hodgkin and Huxley performed voltage-clamp recordings from the squid giant axon, choosing this preparation because the great thickness of the axon allowed for the insertion of an intracellular electrode.[111] By varying the holding potential and concentrations of ions in the extracellular solution, they successfully identified a fast, voltage-activated inward sodium conductance that triggered the rising phase of the action potential. A delayed, voltage-activated outward potassium

conductance drove the falling phase of the impulse.[112] Although computational modelling of these ionic components by hand-crank calculation successfully simulated the action potential, the physical nature of the conductances remained elusive. The later identification of compounds such as TTX, which selectively blocked the sodium but not potassium current flow, hinted at the existence of specialized pores or gates that passed particular ions in or out of the cell.[113] In 1976, Neher and Sakmann devised the patch-clamp which, in the cell-attached configuration, meant that the opening and closing of individual ion channels with unitary conductance could be observed, placing the physiological study of ion channels on a firm molecular footing.[114,115]

Voltage-gated sodium channels form a family of nine different alpha subunits, each expressed in different tissues and with its own biophysical properties.[116] By combining two-electrode voltage-clamp recording of oocytes with injection of message for exogenous expression of prospective clones, these subtypes were identified and characterized.[117,118] Sensory nerves express a unique complement of voltage-gated sodium channels that contribute to electrogenesis, including isoforms that are TTX-sensitive ($Na_V1.6$, $Na_V1.7$, $Na_V1.1$, and $Na_V1.3$) and TTX-resistant ($Na_V1.8$ and $Na_V1.9$).[119] The role of each of these channels in the different phases of the action potential are summarized in **Figure 1.7**. $Na_V1.7$, $Na_V1.8$ and $Na_V1.9$ are unique for being relatively selectively expressed in the periphery. Nociceptors are unusual in that they must generate action potentials even when the surrounding tissue is damaged, and the co-expression of mutually-redundant sodium channels may be an evolutionary solution to this. This is seen in $Na_V1.8$ knockout mice, whose loss-of-function is ameliorated by increased TTX-sensitive currents likely attributable to $Na_V1.7$.[120] $Na_V1.7$ is a promising analgesic drug target because it is essential for pain in humans and will be discussed at length later (see Section 3.2.3).

We focus here on the TTX-resistant sodium channels $Na_V1.8$ and $Na_V1.9$ as they are enriched in small-diameter peripheral neurons and play key roles in pain. $Na_V1.8$ knockout mice show deficits in mechanical, cold and inflammatory pain, while $Na_V1.9$-deficient animals exhibit impaired heat hyperalgesia and spontaneous pain.[120,121] Because nociceptors continue firing in response to stimuli that would normally damage neurons and prevent impulse generation, $Na_V1.8$ and $Na_V1.9$ display interesting biophysical adaptations that allow them to operate during extreme conditions. $Na_V1.8$ exhibits rapid repriming, slow inactivation and is thought to be the major driver of the rising phase of the action potential in nociceptors.[117,122] Consequently, gain-of-function $Na_V1.8$ mutations

in humans cause small fibre neuropathy with mechanical hypersensitivity and when the mutant channels are transfected into mouse DRGs, nociceptors become hyperexcitable.[123]

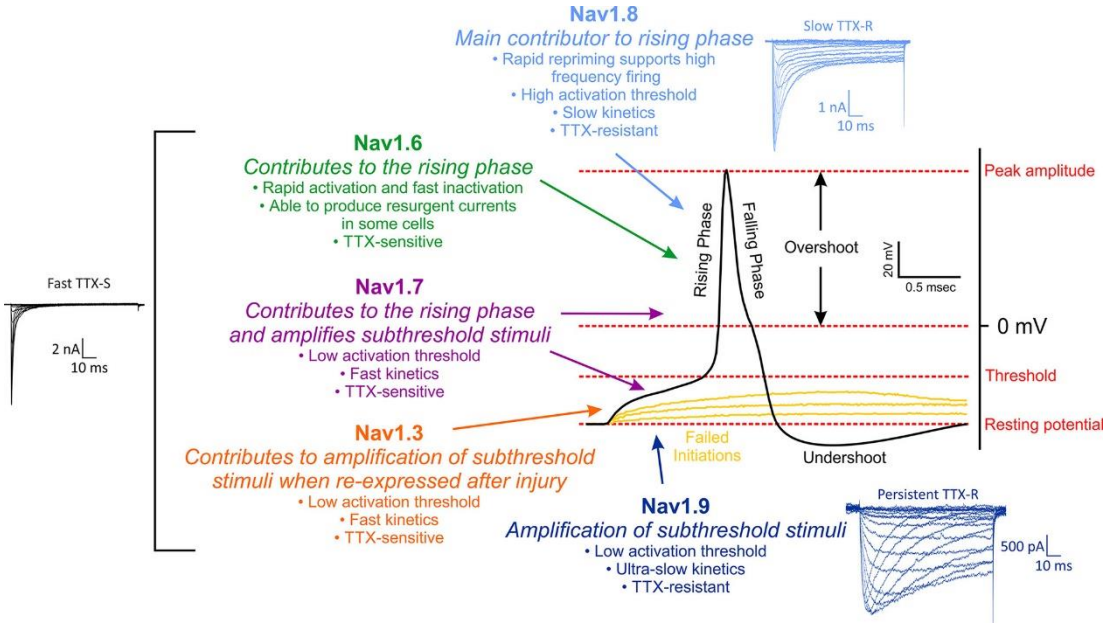

Figure 1.7 (*adapted from ref.* [119]). Peripheral voltage-gated sodium channels and their proposed role in electrogenesis.

This schematic illustrates the contribution of different voltage-gated sodium channel subtypes to action potential generation. A typical action potential waveform recorded from a presumptive nociceptor in culture is shown in the centre. Arrows denote which subtypes contribute to each stage of the action potential. Representative examples of fast TTX-sensitive currents from $Na_V1.3$, $Na_V1.6$, or $Na_V1.7$, slow TTX-resistant currents from $Na_V1.8$, and persistent TTX-resistant currents from $Na_V1.9$ are also shown.

Compared to $Na_V1.8$, the activation threshold of $Na_V1.9$ is hyperpolarized which, together with its slow inactivation, means it generates a persistent inward current at rest and is therefore hypothesized to function as an amplifier of subthreshold depolarizations.[124]An unfortunate consequence of $Na_V1.9$'s subthreshold activity, however, can be seen in two patients with congenital insensitivity to pain who carry gain-of-function mutations in the channel, causing excessive firing at rest and consequent sustained depolarization that prevents impulse generation.[125] Recently, Katharina Zimmerman's group discovered that $Na_V1.9$ actually undergoes a substantial gain-of-function with heating, and is therefore able to trigger action potentials at noxiously hot temperatures. The contribution of $Na_V1.9$ to heat pain *in vivo* proved difficult to test, however, and is only apparent when TTX-sensitive channels are blocked.[126]

$Na_V1.6$ is predominantly expressed by large-diameter neurons, displays fast inactivation kinetics and contributes 60% of the TTX-sensitive current in these cells.[127]

As the major isoform expressed at nodes of Ranvier, it is critical to action potential conduction in myelinated afferents.[128] Viral expression of Cre recombinase in sensory neurons to conditionally delete $Na_V1.6$ revealed a role for this channel in mechanical hypersensitivity after neuropathic pain.[127] A recent study using a $Na_V1.1$-selective spider toxin activator suggests this channel is also involved in acute mechanical pain, probably via A-delta mechanonociceptors, although there is as yet no loss-of-function data and the specificity of the agonist is in doubt.[129] $Na_V1.3$ does not appear to be required for excitability at basal conditions as it is not present in afferents during adulthood but is re-expressed following axotomy.[130] The channel's rapid recovery from inactivation suggests it could contribute to ectopic discharge and fast spiking in injured nerves.[131] However, $Na_V1.3$ knockout mice do not show deficits in chronic pain, presumably due to compensatory upregulation of other channels.[132]

Potassium channels show enormous variation in their functional and molecular properties, comprising around 78 genes in the human genome. 40 of those genes encode voltage-gated potassium channel subunits, which function to repolarize the membrane during the downstroke of the action potential, leading to de-inactivation of sodium channels.[133] We will focus on the Shaker-like K_V1 channels here as they are of particular relevance to the present work (see Section4.2.4).[134] The K_V1 subfamily are delayed rectifier channels activated by small membrane depolarizations and so act as excitability 'brakes' against stimulus-induced depolarizations. $K_V1.1$, $K_V1.2$ and $K_V1.6$ typically form heteromers located in the soma and juxtaparanodes of medium to large DRG neurons and are therefore poised to modulate excitability.[133] Knockdown of $K_V1.1$ with siRNA indeed leads to increased excitability in cultured sensory neurons identified as nociceptors based on their capsaicin sensitivity.[135] Consistent with this, $K_V1.1$ knockout mice exhibit reduced heat and mechanical pain thresholds and increased responses on the formalin test.[136] $K_V1.1$ and $K_V1.2$ also pass an intrinsically mechanically-sensitive hyperpolarizing current that acts to increased the activation threshold of fibres responding to pressure, with pharmacological inhibition of K_V1 using dendrotoxins sufficient to trigger mechanical pain, *in vivo*.[137] Compared to peripherally-enriched sodium channels, potassium channels are generally difficult to study *in vivo* as mouse knockouts or naturally-arising null mutants are often embryonic lethal or show pronounced seizure phenotypes that preclude behavioural testing.[138] Similarly, although many K_V1 channel mutations are described in humans, to the best of our knowledge, quantitative sensory testing is rarely performed, as ataxic or seizure symptoms typically dominate.[139,140]

Both sodium and potassium channels show exquisite spatial localization along the sensory neuron axon.[119,133] Yet studying them generally entails expressing the channels exogenously in HEK cells or recording from dissociated DRG neurons in culture. Such experiments therefore neglect the importance of the subcellular localization of different channel isoforms. For example, $Na_V1.8$ contributes to impulse conduction only in the distal portion of the nerve *in vivo*, whereas *in vitro* studies suggested it was the dominant sodium channel in nociceptors.[122,141] Likewise important is the unusual geometry of the bipolar axon – what Marshal Devor called the 'unexplained peculiarity' of the dorsal root ganglion.[109] The geometry of peripheral nerves impacts how they propagate action potentials – a recent experimental and computational study reported that intraganglionic GABA signalling depolarizes DRG somata, leading to depolarization block through sodium channel inactivation at the T junction, and subsequent filtering of action potentials incoming from the periphery.[142] Microfluidic methods for the culture of sensory neurons in a more 'native' state combined with imaging of the finer compartments is now opening up opportunities for characterizing the complex contribution of channels at the subcellular level.[143] That being said, as this thesis shows, insights into ion channel function and sensory neuron physiology that would be missed *in vitro* can be gleaned by studying the intact nerve in its native milieu, *in vivo*.

1.2.5 Synaptic transmission

Why do we rub where we've been slapped? The answer, according to Melzack and Wall, lies in their Gate Control Theory of Pain. In 1965, they proposed that myelinated afferents responding to innocuous touch can excite inhibitory interneurons in the spinal cord; these interneurons in turn suppress synaptic transmission from unmyelinated nociceptive afferents, thereby reducing pain.[44] Although the particularities of the original Gate Control Theory have been contested, the general point has stood the test of time. Like the retina, the dorsal horn circuitry is complex, filtering and modulating the incoming sensory signal from the periphery long before it reaches the brain.[144] The cells and molecules involved in synaptic transmission at the central terminals of nociceptive sensory neurons therefore govern peripheral drive in health and disease.

The classical features of fast synaptic transmission were determined by Katz at UCL in the 1950s. He performed intracellular microelectrode recordings from the frog neuromuscular junction, measuring the cholinergic end plate potential. Surprisingly, small and spontaneous depolarizations of the muscle were observed even when the motor nerve

was not stimulated – the so-called minis.[145] When the excitatory post-synaptic potential (EPP) was recorded under low calcium conditions, the fluctuations in EPP amplitude could be fit with a Poisson series, with each peak corresponding to an integer multiple of the mini amplitude.[146] The fundamental discovery that neurotransmitter release is quantal, probabilistic and Ca^{2+} dependent generalizes to other fast synapses, including peripheral afferents which mainly use glutamate as their fast transmitter. In the seventy years since Katz' experiments, the molecular mechanisms underlying vesicular release of neurotransmitters have been worked out in great detail. Briefly, when an action potential invades the presynaptic terminal, voltage-gated calcium channels are activated – the subsequent Ca^{2+} influx then couples to the Ca^{2+}-sensor synaptotagmin which triggers SNARE-mediated vesicular exocytosis of transmitter 'packets' that diffuse across the synaptic cleft to bind post-synaptic receptors.[147] At the central terminals of nociceptors, voltage-gated calcium channels have been studied in-depth due to their promise as analgesic targets. Gabapentin targets the $\alpha_2\delta$-1 subunit to provide relief from chronic pain, while the N-type channel $Ca_V2.2$ is critical for nociceptive transmission from peptidergic afferents and can be blocked by zicotonide.[148] Interestingly, a recent study suggested that disruption of $\alpha_2\delta$-1 strongly reduced the expression of Cav2.2 in the superficial dorsal horn *in vivo*, suggesting a common presynaptic mechanism of action for these drugs.[149]

Afferent terminations in the dorsal horn are segregated by fibre type into different laminae and somatotopically into spinal segments (**Figure 1.8**). Nociceptors synapse mainly in layers I and II of the dorsal horn, and use both glutamate and substance P as neurotransmitters. Genetic deletion of Vglut2 from $Na_V1.8$-expressing nociceptors prevents glutamate release and consequently abolished mechanical pain. Administration of a substance P antagonist blocked inflammatory pain in Vglut2-deficient animals but not controls, emphasizing that co-release of these transmitters is required for sensitized pain states.[150] Intriguingly, the morphology of nociceptor terminals in the dorsal horn varies by bodily origin: sparse genetic tracing of Mrgprd+ mechanonociceptors reveals a specialized structure for plantar-derived fibres compared to those from hairy skin, although their peripheral projections are similar, apparently explaining enhanced nociceptor sensitivity in the paw.[151] Functional studies of these afferent terminals are few and far between, however. One study used i*n vivo* imaging of GCaMP3-expressing MgrprB4-positive spinal projections, identifying them as C fibre low-threshold mechanoreceptors activated by massage-like stroking of the hairy skin, but insensitive to noxious stimulation.[152] Myelinated neurons also carry tactile information and generally

synapse in layer III to IV. The Ginty laboratory has produced an exhaustive description of the mechanosensory dorsal horn, finding enormous complexity, with multiple peripheral and central inputs onto up to eleven different classes of interneuron. Thus the importance of the spinal cord interneuron networks for regulating tactile input is likened to the retina for vision.[153]

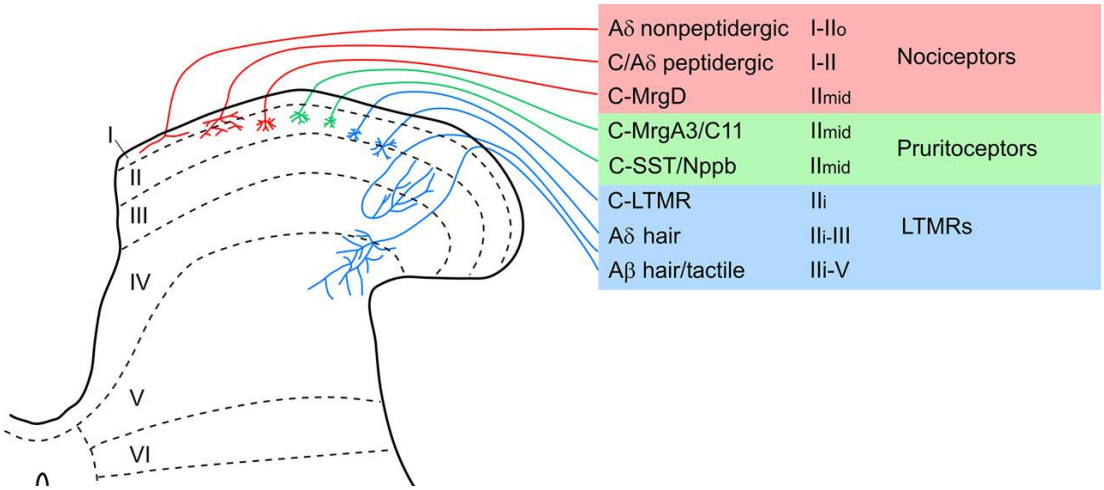

Figure 1.8 (*adapted from ref. 154*). Primary afferent projections to the dorsal horn.

Subsets of primary sensory neurons are shown in the table, together with their functional specializations. The lines represent their central axons, which terminate in different laminae of the dorsal horn, here shown in horizontal section. For example, nociceptors primarily terminate in the superficial laminae I and II, while low-threshold mechanoreceptors (LTRMs) have their endings mainly in the deeper laminae. Pruritoceptors are the sensory neurons responsible for itch-detection. Less is known about the central terminations of warm- and cold-sensing neurons, thus they are omitted here.

Nociceptive afferents synapse on both dorsal horn interneurons and projection neurons. The bulk of layer I-III neurons are interneurons whose axons terminate locally, including forming axo-axonic synapses with the afferent terminals, although nociceptive projections neurons can be found in layer I.[144] The lamina II interneurons have been most extensively studied. Perl and colleagues performed whole-cell recordings from rodent layer II interneurons followed by post-hoc morphological characterization, thereby classifying them into islet, central, vertical and radial cells.[155] Space constraints prevent us from discussing the menagerie of dorsal horn interneurons at length, however they have been studied and reviewed in detail by Andrew Todd.[156] In recent years, neurochemical markers such as galanin, dynorphin and neuropeptide-Y have been used to distinguish interneuron subtypes and gain genetic access to them. For instance, genetic ablation experiments showed that inhibitory interneurons defined by dynorphin expression act to prevent A-beta fibres from activating nociceptive excitatory neurons and thereby gate the

transmission of mechanical pain.[157] The importance of GABAergic and glycinergic inhibitory neurons for controlling pain is illustrated by a study where GABAergic progenitors from the medial ganglionic eminence were transplanted into the cord. Transplanted neurons integrated into the tissue and reversed the mechanical hypersensitivity associated with nerve injury.[158]

As well as being under local control through interneurons, the central terminals are a site of descending regulation by central nuclei. The dorsal horn receives serotonergic input from raphe nuclei and noradrenergic input from the locus coreleus, both neuromodulators that communicate by volume transmission. Although descending regulation generally inhibits nociceptive input, a facilitatory pathway has recently been described: Tac1-positive neurons in the parabrachial nucleus are activated by noxious stimulation and drive escape responses through the reticular formation by targeting the spinal cord to enhance pain.[159] While we have here focussed mainly on the spinal cord, pain can also be facilitated by direct monosynaptic contacts between orofacial nociceptors and the parabrachial nucleus, thought to explain the heightened affective component of orofacial pain.[160] Wherever they are found, then, the presynaptic terminals of nociceptors function as critical sites for both enhancing and dampening pain sensation.

1.3 Pathophysiology of chronic pain

Chronic pain is not a single disease involving a single disease mechanism. Like cancer, chronic pain is a constellation of disease states. A variety of pathophysiological and psychological triggers can drive the sensitization of the nervous system leading to persistent pain. Different pain conditions, although symptomatically and pathologically similar in some ways, may differ in important underlying mechanisms. We can for example divide chronic pain into inflammatory pain (due to prolonged inflammation) or neuropathic pain (due to injury or disease of the nervous system). However, many pain states display features of both (arthritis), do not fall into either category (cancer pain), or may be idiopathic.[161] In the following sections, I review the pathophysiology and treatment of chronic pain, and conclude by highlighting the promise of new optical approaches for shedding light on the mechanisms of chronic pain.

1.3.1 Preclinical models

To investigate the cell and molecular mechanisms driving human chronic pain conditions, we turn to rodent models of the disease, particularly mice. There are two key requirements for a good preclinical pain model. First, the model must display behavioural features that capture the relevant symptoms of the human pain condition. Second, the model must have good face validity – that is, be based on our best understanding of the human pathology and, ideally, mimic the time course of said pathological changes.[162] No animal model will satisfactorily capture all the features of a human disease, however much can and has been learnt from judicious study of mouse models of chronic pain.

The three cardinal symptoms of chronic pain are hyperalgesia, allodynia and spontaneous pain.[163] Correlates of the first two are readily apparent in rodents in the form of decreased reflex withdrawal thresholds, however spontaneous pain is trickier to study. In humans, hyperalgesia refers to increased pain in response to a usually noxious stimulus and is typically associated with inflammatory pain. Allodynia is when patients experience pain evoked by normally innocuous stimuli, and is a feature of many neuropathic pain states. Because rodents cannot verbalize their perception of pain, distinguishing these two symptoms is harder in mice. Most behavioural assays measure hypersensitivity to stimuli classed as noxious or innocuous based on the norms of the field and the experimenter's intuition. Heat hyperalgesia is studied using the Hargreaves Apparatus which measures the changes in the latency to paw withdrawal to radiant heat.[164] Mechanical hyperalgesia

is tested using the Randall-Selitto applied to the tail or paw.[165] Von Frey hairs can be used for punctate stimulation which allows for the assessment of both primary and secondary hyperalgesia.[166] It is debateable, however, whether Von Frey thresholds measure hyperalgesia or allodynia as Von Frey application can evoke withdrawal even under healthy conditions. Indeed, cotton swab application for testing dynamic allodynia – an innocuous stimulus if there ever was one – elicits withdrawal in naïve animals, casting doubt on the typical characterization of withdrawal as nocifensive.[100]

Importantly, withdrawal reflexes do not tell us if the animal is actually experiencing pain. Paw retraction persists even in decerebrate rats.[167] Whole-animal, spontaneous and affective components of behaviour are therefore increasingly studied to shed light on supraspinal pain pathways. Corder and colleagues usefully distinguish between reflexive and affective-motivational behaviours, defining the latter as:

"…temporally-delayed (relative to the noxious stimulus contact or removal of said stimulus), directed licking and biting of the paw (termed "attending"), extended lifting or guarding of the paw, and/or escape responses characterized by hyperlocomotion, rearing or jumping away from the noxious stimulus."[9]

Thermal place preference, for example, has been exploited to study mechanisms governing avoidance of particular temperatures.[168] To quantify ongoing pain, the mouse grimace scale could be used.[169] Although this assay requires a highly-trained scorer, deep neural networks are now being used to automate the process.[170] A recent paper used digging and burrowing behaviour as a measure of 'well-being' in arthritic mice to assess the effect of pain on day-to-day activities.[171] While spinal reflexes remain the most facile to test in mice, capturing quality-of-life indicators relevant to patients is likely to improve translation.

Care must be taken when performing any behavioural test. Experimenter confounds are especially strong with, for example, male experimenters causing stress-induced analgesia in mice.[172] Peculiarities of mouse biology can also impact results. It was recently reported that mice can transfer their pain state by olfactory cues to cage-mates, complicating assessment of hypersensitivity in co-housed mice.[173] Recently, efforts have been made to remove experimenter bias from pain behavioural assessments. Machine learning combined with high-speed videography can be used to objectively determine pain state in response to plantar stimulation.[174] Behaviour, which previously relied on laborious manual testing, is becoming Big Data. Deep Lab Cut, a machine learning algorithm for

automated behavioural tracking, presents enormous opportunities for dissecting out the fine grained components of pain behaviour.[175]

Of all chronic pain states, inflammatory pain is the simplest to model. Specific components of the inflammatory soup hypothesized to be involved in hyperalgesia can be injected such as PGE2. Alternatively, algogenic compounds that elicit a more generalized inflammatory response can be given to the animal like Complete Freud's Adjuvant (CFA) or carageenan.[161,162] A problem with these inflammatory models is their limited clinical relevance – short-term inflammatory pain is not a chronic pain state, but rather a form of physiological sensitization to promote tissue healing. The formalin model overcomes this caveat because it evokes a second phase response that is assumed to reflect a chronic state.[176] Hyperalgesic priming models that induce an injured state before injection of an algogenic compound have been developed to study the chronification of pain. For example, a recent study showed that primary afferent-derived BDNF is required for manifestation of priming elicited by carrageenan followed by PGE2 injection.[177]

Neuropathic pain is simulated using a variety of nerve injury preparations, originally developed in rats, but now widely used in mice.[178] There is inter-lab variability in the modality-specific behavioural changes, however. Chemotherapy-induced peripheral neuropathy can be modelled by treatment with various drugs like oxaliplatin and paclitaxel, however prolonged treatments are often required to induce pain.[179] Pain associated with both rheumatoid and osteoarthritis arthritis can be investigated in mice, for instance with the popular monoiodoacetate model.[180] Note that these models typically fail to capture many critical features of the disease including age effects and the time course of human pathology. A non-invasive joint loading model of osteoarthritis has now been described that displays the progressive development of pathology and pain that is observed in patients.[181]

An emerging alternative to mouse pain models is the use of human tissue samples. For instance, sensory neurons could be generated from patient-derived induced pluripotent stem cells and then investigated in the dish. Thus far such studies have focussed on patients with genetic mutations that drive chronic pain state such as inherited erythromelalgia.[182] However, such experiments obviously say little about pathophysiological changes at the level of the whole organism. Intriguingly, the Bennett group recently reported that injection of human autoantibodies against Caspr2 leads to tactile allodynia in mice. Caspr2 is a neurexin that forms a protein complex with $K_V1.1$ and $K_V1.2$ channels, genetic deletion of which also drove hypersensitivity associated with

reduced membrane K_V1.[183] As this work demonstrates, for mechanistic studies – even those involving patient samples – mice remain a reagent of choice. Because we can combine molecular genetic and systems neuroscience approaches with well-established chronic pain models, mice were the ideal model organism for the experiments described in this thesis.

1.3.2 Peripheral mechanisms

The conscious perception of pain occurs in the central nervous system. However, the sensory and emotional experience of pain results, usually, from peripheral nociceptive input. Importantly, removing this 'peripheral drive' with local anaesthetics that block sodium channels relieves both acute and chronic pain.[184] Similarly, patients with congenital insensitivity to pain due to mutations in peripheral sodium channels do not suffer from chronic pain, despite sustaining numerous injuries throughout their lives that would typically elicit persistent pain.[5] Such observations point to a critical role for peripheral sensory neurons in establishing and maintaining chronic pain states.

Many pain patients are hypersensitive to normally painful stimuli. These symptoms are mirrored by a pathologic hyperexcitability in peripheral nerves. During inflammation, nociceptors undergo 'sensitization', defined as a decrease in response threshold or an increase in response magnitude, a cellular correlate of hyperalgesia.[16] 'Peripheral sensitization' refers to a process where immunogenic and inflammatory mediators released after local tissue damage bind receptors on the nerve, increasing its excitability. A recent *in vivo* imaging study revealed the myriad alterations that occur in sensory neuron response properties after exposure to an 'inflammatory soup.'[185] Interestingly, fine-grained behavioural phenotyping combined with DRG transcriptomic profiling has revealed that immune responses also play an important role in neuropathic pain, with T cell or macrophage depletion abolishing mechanical allodynia.[186] Inflammatory mediators include histamine, bradykinin, protons, serotonin, prostaglandins and growth factors – they can be released from immune cells, damaged tissue or from the nerve itself and can directly or indirectly modify nociceptor excitability. For instance, protons released during tissue acidosis will directly sensitize Trpv1, reducing its heat activation threshold and triggering a burning pain sensation.[187] Components of the soup can also bind GPCRs or growth factor receptors to generate longer-lasting changes in afferent function. Injection of nerve growth factor (NGF) into human skin can induce localized pain and hyperalgesia within minutes,

while high levels of NGF mRNA and protein are observed in patients with chronic, mainly inflammatory, pain conditions.[188] NGF likely acts by TrkA expressed on nociceptors to cause hyperexcitability, transcriptional changes and sprouting.[189] Anti-NGF monoclonal antibodies have therefore been used to treat osteoarthritis, with fair success.[190] Recently, injection of non-functional NGF coupled to a phototoxic agent activated by near infrared light was shown to dramatically reduce nociception by retracting free nerve endings.[191]

Sensitization to noxious stimuli is not, however, what is most bothersome to patients. These stimuli can be avoided relatively easily. Mechanical allodynia, however, results in innocuous touch being experienced as pain – the mere brushing of clothes against skin can be agonizing for these patients. Both inflammatory and neuropathic pain states can elicit 'phenotypic switching' of peripheral nerves, such that mechano-nociceptors signalling damage acquire an inappropriate response to feather-light touch thereby driving mechanical allodynia. Interestingly, Piezo2 was recently shown to be absolutely required for tactile allodynia. Conditional knockout of Piezo2 in the caudal half of the mouse using Hoxb8 Cre blocked mechanical hypersensitivity after capsaicin and nerve injury.[192] These mouse data are supported by the compelling observation is that humans with loss-of-function Piezo2 mutations likewise fail to develop tactile allodynia after application of capsaicin cream, emphasizing the translational relevance of Piezo2 as a target for treating chronic pain. Imaging of Piezo2-deficient mouse trigeminal ganglia neurons *in vivo* revealed that Piezo2 is required for brush-evoked activity before and after injury, with no evidence of recruitment of nociceptors by touch stimulation.[193] Similarly, ablation of TrkB-positive cells in adulthood suggests these neurons – categorized as low-threshold D-hair and rapidly adapting Aβ light touch sensors – are absolutely required for dynamic, punctate and static tactile allodynia in neuropathic pain.[194] Collectively, these results suggest that peripheral input is required for mechanical allodynia, however there is no apparent sensitization or phenotypic switching of peripheral nociceptors.

After nerve injury, both damaged and non-injured nerves enter a hyper-excitable state, firing ectopic discharges that could underlie the spontaneous pain that is the primary complaint of the majority of patients. Changes in the expression and function of assorted voltage-gated channels may contribute to this change in afferent excitability. Increased expression of $Na_V1.8$ along the uninjured axons of the sciatic nerve is thought to drive aberrant activity in neuropathic pain, with antisense oligos against $Na_V1.8$ blocking nerve injury-induced pain.[195] Another study suggested, however, that $Na_V1.8$ is critical to the

development of spontaneous activity in the damaged axons of neuromas.[196] Controversy over the relative importance of injured versus uninjured nerves in driving ectopic activity rages on. A vast array of potassium channels have also been implicated in the etiology of chronic pain, and will be discussed in detail in the context of cold allodynia. Obviously, identifying ion channels that underlie pain pathogenesis is of great interest due to their utility as therapeutic targets. Conditional deletion of HCN2 in nociceptors blocks cAMP-dependent action potential firing and consequent inflammatory and neuropathic pain in mice.[197] Inhibitors of this channel are therefore under active exploration as potential analgesics.[198]

Multiple mechanisms operating at the molecular and cellular level may contribute to the pathogenesis and maintenance of chronic pain. Nociceptors may be sensitized or switch their phenotype to drive an enhanced nociceptive input. It must, however, be stressed that a peripheral component identified as necessary for chronic pain may not strictly be a pathogenic cause. The TrkB neurons required for tactile allodynia likely provide a mechanosensory input that is transformed into pain by malfunctioning central circuits. Care must be taken to distinguish between peripheral sensitization, which causes chronic pain, and peripheral drive, which merely maintains it. In the latter case, while targeting the periphery may ameliorate the pain by removing ascending input, the pathologic change occurs upstream in the central nervous system.

1.3.3 Central mechanisms

Pain was memorably defined by Sherrington as "the psychical adjunct of a protective reflex."[199] The psychological components of pain – that is, perceptual, affective and emotional responses – are implemented in the central nervous system. The relative importance of peripheral and central mechanisms in chronic pain is hotly debated. Pain is, in many cases, the sensory-emotional experience associated with nociceptor activity, however not all pain states fall under this bracket. Nociceptors do not sense pain, they detect damage. As suggested by Melzack and Wall, the resultant incoming sensory signal is then moulded and 'gated' at the level of cord and brain to trigger pain perception. We can thus usefully distinguish central mechanisms of pain in the following way. First, pain can depend on a peripheral input that is magnified by pathologic central processes. Second, we have pain originating from central circuits rendered aberrant by an initial peripheral insult. Last but not least, there is pain of purely central origin.

In 1983, Clifford Woolf, recording from motor efferents of nerve injured rats, observed an increase in the flexion reflex in response to noxious stimulation that was mediated by a central change in the spinal cord.[200] This central sensitization is a form of post-synaptic plasticity: in its barest essentials, synaptic efficacy is increased in an NMDA-receptor dependent manner through enhancement of post-synaptic receptors.[201,202] This, then, is an example of peripheral nociceptor input being magnified by a central facilitation. Central sensitization can be differentiated from wind-up because the former is a prolonged activity-dependent increase in synaptic strength, while the latter is a type of short-lasting temporal summation.[203] While the term central sensitization has been much abused, morphing into a woolly word for any central contribution to chronic pain, the specific pathophysiological changes described by Woolf remain of great medical relevance. It has been suggested that phantom limb pain can be prevented if peripheral nerve firing or NMDA receptor activity is silenced during surgery, thereby preventing barrages of activity from eliciting post-synaptic sensitization at the dorsal horn neurons that once received input from the amputated limb.[204] Note that phantom limb pain could thus be considered a form of chronic pain where peripheral insult evokes a change in central neurons that later drives pain in the absence of nociceptor activation.

We have already reviewed the role of dorsal horn interneurons and microcircuits in driving pain hypersensitivity in the context of Gate Theory. Suffice to say that multiple mechanisms operating in the cord can drive chronic pain, even in the presence of normal peripheral input. What has recently become apparent is the contribution of non-neural cells. Pharmacological block shows P2X4 receptors are necessary for pain after peripheral nerve injury.[205] However, these purinergic receptors are expressed only on microglial cells in the spinal cord, implicating microglia in the generation of chronic pain. Michael Salter showed that depleting microglia or inhibiting their signalling to dorsal horn neurons abolished mechanical hypersensitivity after nerve injury in mice. Intriguingly, microglia were only required for hypersensitivity in male animals. Females showed equivalent hypersensitivity, however this was dependent on the adaptive immune system, likely T lymphocytes.[206] What this sex difference emphasizes is that phenotypically identical pain states can have mechanistically-distinct underpinnings. In recent years, computational modelling studies have emphasized the many, interlocking and mutually-redundant mechanisms by which pain chronification can occur.[207] Such thinking was anticipated by Wall who cautioned against overtly reductionist approaches to investigating pain systems:

"[Reductionism] will never achieve an explanation of how such a system falls into stable pathological states, is immune to chemical and surgical lesions, oscillates spontaneously, shows a variable location of activity between individuals, and shows an ability to coordinate activity over long distances. That requires a distributed, widespread, interconnected population of cells with its own population abilities and deficiencies."[84]

The requirement for multiple interacting mechanisms perhaps explains why pain of solely central origin is rare. Occasionally, a lesion to the brain can induce a pathologic pain state. Examples include vascular injuries like stroke, Parkinson disease, multiple sclerosis, and brain tumours. Such lesions, however, are not necessarily always followed by pain.[208] Of more relevance to us are brain circuits that amplify or dampen pain via modulation of the pain pathway from the periphery. fMRI studies in human patients have identified a pain signature – often called a 'neuromatrix' – that is thought to mediate the subjective experience of pain.[209] Such correlative approaches have been questioned by a study which found similar networks activated in patients with congenital insensitivity to pain.[210] More convincingly, patients with basolateral amygdala lesions can detect noxious stimuli but there is no feeling of unpleasantness, confirming that brain networks are required for perceiving the negative quality of pain.[211] Recently, miniscope calcium imaging in mice identified an ensemble of neurons in the amygdala that encodes the affective dimension of pain, chemogenetic inhibition of which blocked affective pain behaviour in a nerve injury model.[212]

Both affective and perceptual components of chronic pain are strongly modulated by the internal state and environmental context of the organism. For example, in mice, withholding food can reduce inflammatory pain as the drive to reduce hunger overrides the pain. This suppression of chronic pain implemented by a projection from hypothalamic AgRP-positive feeding neurons to the parabrachial nucleus and is mediated by neuropeptide Y signalling.[213] Even at the level of acute reflexes, high-speed videography showed wakefulness modifies the withdrawal to optogenetic activation of nociceptors.[214] In human patients, arousal, acute stress and emotional state control the experience of pain. Accounts abounded after the Second World War of soldiers who fought on, feeling no pain, despite grievous injuries sustained during battle.[37] Such findings have led practitioners to subscribe to a Biopsychosocial Model, where pain is an outcome of both the underlying biology, as well the psychological and social factors affecting the patient. Gender, for example, strongly affects the manifestation of chronic pain. Pain conditions such as fibromyalgia are notably more prevalent in women than

men.[215] Interestingly, a recent study revealed that pain hypersensitivity conditioned by a prior noxious experience in the same environment could be observed in male mice and humans, but was absent in females of either species.[216]

One consequence of the relationship between pain and psychosocial factors is that the burden of pain is not spread equally in the population. Chronic pain is more common in patients of a lower socioeconomic status.[217] Diseases that drive pain – workplace injury, diabetes – invariably affect the poor and disadvantaged at greater rates.[218] Importantly, the actual manifestation of pain is increased by risk factors associated with poverty – chronic stress triggers brain changes that blunt the response to cortisol thereby facilitating chronic pain.[219] Basic biological research into nociception seeks to identify targets and mechanisms in the periphery that contribute to pain pathogenesis. Effective translation, however, will require an awareness that peripheral nociception in patients always occurs in the context of multifarious biopsychosocial factors that exert their effects via central circuits.

1.3.4 Analgesic treatment

Over two thousand years ago, Hippocrates was recommending infants chew willow-bark to treat pain.[220] Pain relief is the oldest pharmaceutical indication known to man, with witch-doctors and medicine-men the world over prescribing poppy, hemp and willow-bark to their patients for millennia. Even in the 21st century, two of the most widely used classes of analgesics – NSAIDs and opioids – are derived from these traditional remedies: willow-bark and poppy respectively. Although these popular analgesics successfully treat short-lasting pain, they show poor efficacy for chronic pain conditions. In a rapidly-ageing world, with a rising prevalence of persistent pain, our society faces a pressing need to identify new analgesic strategies, targets and compounds.

The active ingredient of willow-bark, salicylic acid, was first isolated by French and German chemists in the 19th century. As the new century dawned, acetylated forms of salicylic acid, christened aspirin, were generated on an industrial scale by Bayer and became enormously popular for treating pain, particularly rheumatoid arthritis.[221] It was not until 1971, however, that Ferreira, Moncada and Vane identified the mechanism of action of non-steroidal anti-inflammatory drugs (NSAIDs) like aspirin, for which Vane was awarded the Nobel Prize. Using dog spleen, they found that aspirin inhibited cyclooxygenases (COX1 and COX2), enzymes involved in the synthesis of eicosanoids such as prostraglandin and thromboxane from arachidonic acid, inflammatory mediators

known to cause pain.[222] Acetaminophen (i.e. paracetamol) is usually not considered an NSAID as it only has minor anti-inflammatory activity and does not appear to target COX2. Despite being the most widely-used painkiller in the USA and Europe, its mechanism of action remains mysterious. One study reported that acetaminophen metabolites activate Trpa1 and acetaminophen-induced analgesia is absent in Trpa1 knockout mice. Given Trpa1's known pro-nociceptive role, such findings appear counter-intuitive – the authors suggest activation of spinal Trpa1 by acetaminophen metabolites reduces sodium and calcium currents thereby alleviating pain.[223] However, a large body of work also indicates that acetaminophen metabolites stimulate CB1 receptors. Indeed, the analgesic effect of acetaminophen in mouse models of inflammatory pain was lost in CB1 knockout animals. Interestingly, injection of a CB1 blocker into the rostral ventromedial medullla blocked acetaminophen anti-nociception, supporting a pharmacological action at central CB1 receptors.[224] Such controversies indicate that widely used analgesics such as acetaminophen likely have multiple, interacting mechanisms of action that synergistically lead to analgesia.

Like willow-bark, opiates have been used for pain relief since antiquity. Homer tells us that opium was given by Helen, daughter of Zeus, to the friends of Odysseus "to lull all pain and anger and bring forgetfulness of every sorrow."[225] Opioids, including both plant-derived opiates like morphine and synthetic opioids like oxycodone, are generally very effective at alleviating short-term pain, such as after surgery. As agonists for the opioid receptors normally activated by endogenous opioids, they act by hijacking the nervous system's natural analgesic system. Endogenous opioids, also called endorphins, were first isolated from pig brain by Hughes and Kosterlitz in 1975 and shown to have similar agonist profiles to known opiate drugs.[226] There are four main families of endogenous opioids in the nervous system: β-endorphins, enkephalins, dynorphins, and nociceptin. These peptides are derived from larger precursor molecules that undergo enzymatic splicing and are packaged into dense core vesicles. For example, preproenkephalin can be cleaved into both met or leu-enkepahlin. Endogenous opioids are released as volume transmitters from axon terminals, diffusing to their – typically extrasynaptic – cognate receptors to dampen the activity of post-synaptic neurons, particularly in so-called pain pathways.[227] For instance, in a classic experiment, Jon Levine and Howard Fields showed that the opioid receptor antagonist naloxone blocked the placebo effect in patients with dental pain, implying placebo analgesia is dependent on endogenous opioid signalling.[228]

Opioid receptors were identified by Pert and Snyder via the binding of radiolabelled naloxone to discrete receptor sites in rat tissue.[229] Opioid receptors are G-protein coupled receptors forming four subtypes based on their relative sensitivity to different agonists: mu, delta, kappa, and nociceptin. Each subtype is encoded by a different gene, but share up to 60% similarity in amino acid composition.[227] All four subtypes signal via the $G_{\alpha i/o}$ pathway to inhibit adenylate cyclase, thereby reducing cyclic AMP production and consequently the activity of effectors such as protein kinase A. The $G_{\beta\gamma}$ subunit can also directly inhibit voltage-gated calcium channels, suppressing transmitter release, as well as opening GIRK potassium channels, thereby hyperpolarizing the membrane.[227] Lastly, arrestin-bound opioid receptors recruit different intracellular signalling pathways, such as the mitogen-activated protein kinase cascade. Biased agonists have therefore been developed that favour the $G_{\alpha i/o}$ over arrestin pathway, thought to maximize $G_{\alpha i/o}$-mediated analgesia while minimizing respiratory and gastrointestinal side-effects more dependent on arrestin signalling.[230]

Opioid receptors are expressed throughout the nervous system: in the periphery, spinal cord, and in brain areas such as the periaqueductal grey and the rostral ventromedial medulla, activation of which drives endogenous pain relief.[227] Each receptor isoform shows a unique spatial localization, and is functionally engaged in distinct components of pain – a recent study confirmed that mu and delta co-expression is rare in the CNS and, even in cells expressing both isoforms, the receptors function independently.[231] Because opioid receptors are distributed in multiple tissue sites unrelated to pain, this explains why opioid painkillers can cause numerous severe side effects, including respiratory depression, gastrointestinal problems, dependence and addiction, with the attendant risk of overdose. Tolerance, or even hyperalgesia, can develop if the drugs are taken for a long period of time. As noted earlier (see Section 1.1.2), inappropriate or over-prescription of opioids in the US has led to a widespread epidemic of opioid abuse, illustrating the importance of developing new analgesic drugs that do not target the opioid system.[232]

A perfect painkiller would reduce pain in a quantitative, controllable fashion without side effects, tolerance or addiction. There are purported panaceas aplenty in the pain field. Small molecule inhibitors of various pain-related ion channels have been developed. For example, multiple pharma companies have or had programs to find selective antagonists $Na_V1.7$, although these inhibitors did not prove particularly effective (see Section 3.2.3).[233] One recent area of promise is biologic therapies using antibodies. For example, monoclonal antibodies against CGRP have been very successful in treating

migraine and headache pain.[234] The pharma industry has also been interested in repurposing existing drugs for the treatment of pain. Cannabinoids have been used by self-medicating pain patients for years, and with the increasing social acceptance of these drugs, may become more widely used, although their effectiveness remains disputed. Interestingly, James Cox and co-workers recently reported on a patient with a microdeletion in a Fatty Acid Amide Hydrolase (FAAH) pseudogene that results in disrupted FAAH function and consequently enhanced endocannabinoid levels, leading to a pain- and anxiety-free phenotype.[235]

In the laboratory, circuit-based approaches to pain treatment are under active exploration by multiple groups. In humans, deep brain stimulation of anterior cingulate cortex has been used to treat chronic pain.[236] However, electrical stimulation activates neurons indiscriminately; technologies like chemo- and optogenetics are a means to more targeted manipulation of circuit function. In a proof-of-principle study, the Gereau lab used the inhibitory opsin archaeorhodopsin to silence bladder afferents to treat a mouse model chronic bladder pain.[237] A recent paper by the Bennett group described a novel ivermectin-gated chloride channel that could silence sensory neurons and reverse neuropathic pain.[238] An advantage of this tool is that it was expressed in sensory neurons by viral infection. This highlights an important issue: new circuit-based approaches require gene therapy. With the recent advances in Crispr technology for gene editing, it is no surprise that this kind of gene therapy is now much vaunted as a future pain therapeutic.

The sobering truth though is that the vast majority of therapies, whether small molecules, biologics or circuit based, fail in clinical trials. This is partly due to the strength of the placebo effect – peculiarly, the placebo effect has been increasing year-on-year in clinical trials, making distinguishing successful molecules more difficult.[239] However, many fundamental problems face anyone attempting to turn pre-clinical findings into treatments. Therapeutic approaches that work in mice often do not translate well to humans: mice may poorly model the human condition due to the young age and the homogeneity of inbred lab mice.[240] Deeper, structural issues also negatively impact preclinical research, especially with regard to improper use of statistics. Today, clinical trials are typically randomized, double-blind, and are pre-registered with outcome measures defined in advance. While most preclinical research is blinded, randomization procedures may not be used properly, while outcome measures are usually flexible. This leaves ample room for p-hacking and hypothesizing after the fact. Exploratory and

confirmatory research are usually not separated, while power calculations are rarely performed.[241] A review of the literature found numerous errors in statistical reporting in basic neuroscience papers published in high profile journals.[242] In general, poor use of statistics in basic neuroscience research likely contributes to the number of false positives that then fail in clinical trials.[243] Recently, a movement to tackle the crisis in reproducibility that began in psychology has entered basic preclinical science, with journals beginning to publish registered reports and requiring that data and analyses be openly available. Time will tell if these improvements are sufficient to widen the translational bottleneck for bringing analgesics from bench to bathroom cabinet.

1.3.5 *In vivo* imaging

Genetically-engineered calcium indicators have been widely adopted to monitor neural activity because they allow for the investigation of unprecedented numbers of neurons *in vivo*.[244] In the last few years, multiple groups have published studies using GCaMP indicators to visualize stimulus-evoked activity in peripheral sensory neuron somata.[67,185,245–248] These optical imaging methods allow us to combine cell-type molecular specificity with single cell-resolution, population-level imaging in intact, live animals. We thereby overcome the problems of traditional molecular studies of pain, where pathologic changes that occur in the intact peripheral nervous system may not be so apparent in the reduced preparations typically used for mechanistic investigations.

Consequently, imaging studies have reawakened interest in some previously under-studied aspects of peripheral sensory neuron biology. Using *in vivo* GCaMP3 imaging, our lab reported that previously silent nociceptors become activated by heat following intraplantar PGE2 injection.[245] Silent nociceptors were first observed in the articular nerve that innervates the knee joint of the cat.[16] They are defined as electrically excitable nerves that fail to respond to mechanical stimulation at baseline but become mechanically sensitive during inflammation. Silent nociceptors comprise ~15% of cutaneous afferents, but are hypothesized to be particularly important in visceral pain as they are commonest in the bladder and colon, as well as in the knee joint.[249] A recent study suggested CHRNA-expressing silent nociceptors are unmasked by NGF and depend on Piezo2 for their newfound mechanosensitivity.[250] In agreement with this, *in vivo* imaging experiments showed that pharmacological antagonism of Piezo2 using a tarantula toxin abolished the mechanical sensitivity of silent nociceptors awakened in a rat model of cancer induced bone cancer pain.[251]

Interestingly, mice treated with CFA also show increased numbers of GCaMP responses to noxious mechanical stimulation, however this was attributed to enhanced 'coupled' activation of neighbouring dorsal root ganglia neurons.[246] This provocative finding suggests that peripheral input is magnified through gap junction-mediated activation of adjacent sensory neuron somata. A critical issue with this study is that it did not control for the fact that 'conventional' sensitization leading to the activation of more neurons would increase the probability of neighbouring cells co-activating without necessarily being functionally coupled. On the other hand, pharmacological block of gap junctions and genetic deletion of connexin-43, which reduced the incidence of coupling, also decreased mechanical hypersensitivity, causally linking coupling to inflammatory pain sensitization. An important caveat is that increased activity in the central axon need not necessarily follow somatic depolarization due to the filtering function of the T junction.[142] Furthermore, coupling was not observed using the same imaging technique in a murine model of osteoarthritis.[252]

As with any new technique, there have been conflicting and contradictory findings using *in vivo* imaging. The robust debate concerning the preponderance of 'polymodal' neurons is a case in point.[46] Emery and colleagues reported that the vast majority of neurons had a modality-specific response: only 6.5% of the neurons sensitive to noxious pinch also responded to noxious heat, but polymodality increased after treatment with PGE2.[245] In the acute state, the lab of Xinzhong Dong also found limited overlap between noxious press and capsaicin-sensitive neurons – just 3.4% of neurons were polymodal, although noxious heat was not tested here.[246] The McMahon and De Koninck groups, however, report markedly higher rates of polymodality: 50-80% and ~50% respectively.[247,248] The Chesler lab also found nociceptors were mostly polymodal, consistent with classical physiology studies.[67] On the other hand, Sally Lawson recently revisited many years' worth of intracellular recording data, comprising >1000 recorded DRG neurons, concluding that most DRG neurons are unimodal, with 12% of mechanically-activated nociceptors also responding to heat.[55] These lower levels of polymodality are consistent with the modality-specific acute pain phenotypes of transgenic mouse lines in which specific sensory neuron subsets are ablated.[47] Owing to varying definitions of polymodality it can be difficult to compare results from different groups; the jury remains out on the question of polymodality.

Expressing GCaMP in a representative set of sensory neurons for *in vivo* imaging is not trivial. The vast majority of experiments in this thesis used Pirt-GCaMP3 knockin

mice where GCaMP3 is genomically-expressed and driven by the endogeneous Pirt promoter to label ~87% of DRG neurons.[253] Expressing GCaMP3 independently of Cre in Pirt-GCaMP3 mice is a great advantage to us as it allows for separate labelling of cell subsets of interest with Cre-driven tdTomato. Other groups have used AAVs injected intrathecally in adulthood or via the intraperitoneal route postnatally to express GCaMP6s, although this results in variable infection and consequent sampling of DRG neurons during imaging.[247,248] Each delivery route and GCaMP variant is suited to a different question. GCaMP3 is less sensitive and has worse signal to noise than GCaMP6s, but the probe is faster and brighter at rest.[254] Important for the present work, GCaMP3 can detect single action potentials in cultured DRG neurons, and *in vivo* imaging results from Pirt-GCaMP3 animals are comparable to those from Advillin-Cre GCaMP6s mice.[245] However, given GCaMP3 fluorescence change is highly dependent on baseline GCaMP3 levels, variable Pirt expression across different neurons could prove a problem. The cell type-specific physiology of different DRG neurons also clouds the interpretation of calcium imaging data independent of the indicator: action potentials may not always invade the soma, and may not always cause a calcium transient, due to differences in calcium buffering capacity. Reassuringly, a recent study combining DRG calcium imaging and electrophysiological recording of the same neuron which found a good correlation between somatic action potential firing and calcium signaling.[67]

The particulars of the preparation must be borne in mind. Stable anaesthesia before surgery was achieved in our experiments through ketamine-based anaesthetic cocktails – either with metodomidine (for chapter 3) or with xylazine and acepromazine (for chapter 4) – but other labs have used isofluorane or urethane.[246,247] I switched to ketamine, xylazine and acepromazine after observing the longer lasting preparation achieved by Wang and colleagues using this cocktail at Université Laval.[248] There is a risk that such a pharmacopeia of anaesthetics will differentially impact DRG neuron activity. Indeed, *in vivo* imaging of DRG in awake, but restrained animals, demonstrated that anesthesics suppressed activity in a large numbers of sensory neurons.[255] Many of these are likely to be proprioceptors, which respond when the animal moves and are thus silenced during anesthesia.

The imaging modality will also impact the quality of imaging. To image the ganglia in our animals, I used confocal microscopy of a single image plane from the L4 DRG. The great boon of optical sectioning is that there is little ambiguity in distinguishing separate cells. One group abrogated this advantage by opening the pinhole to its full

extent, performing confocal microscopy without the confocality.[247] Another used confocal imaging to collect z-stacks through the DRG, maximizing the number of cells imaged, but at the cost of a very slow frame rate.[246] Widefield epifluorescence imaging has been successfully used by Ghitani *et al* to obtain video-rate recordings from the trigeminal ganglia, however this relies on sparse expression of GCaMP6f to ensure satisfactory spatial resolution.[67] Impressively, the de Koninck group combined the optical sectioning of two-photon imaging with video-rate recording, producing images of notable quality.[248]

Although conscious of its limitations, I believe *in vivo* GCaMP imaging is currently the best approach for monitoring population-wide activity of peripheral sensory neurons and is therefore ideally suited to studying novel mechanisms of chronic pain. *In vivo* imaging lets us watch pain plasticity in action. We can investigate changes in the response properties of hundreds of sensory neurons simultaneously in live animals exposed to naturalistic stimuli and gain insights impossible to obtain using traditional, single-fibre electrophysiological approaches. With this method, we can combine cutting-edge systems neuroscience with molecular genetics to identify novel mechanism and targets involved in triggering persistent pathological pain. The present work thus aims to elucidate cell and molecular mechanisms of nociception and pain using novel imaging methods, combined with more traditional electrophysiological, behavioural and molecular approaches.

1.4 Aims and structure of the work

The over-arching aim of this thesis was to use optical, electrophysiological and molecular genetic techniques to investigate the role of peripheral sensory neurons in different pain states. In particular, I wanted to leverage new *in vivo* imaging techniques for monitoring activity in peripheral sensory neurons to shed light on the cell and molecular mechanisms driving (1) congenital insensitivity to pain and (2) cold allodynia associated with neuropathic pain.[245] Both these pain states represent maladaptive responses by the nociceptive system to sensory stimuli. In congenital insensitivity to pain, noxious stimuli fail to elicit the aversive response needed to avoid tissue damage.[5] In cold allodynia, normally innocuous cooling triggers pain that serves no physiological purpose.[256]

1.4.1 The mechanism of analgesia in $Na_V1.7$ null mutants

Mice and humans lacking sodium channel $Na_V1.7$ are insensitive to pain, but peripherally-targeted pharmacological blockers of $Na_V1.7$ fail to relieve pain in the clinic.[5,257,258] To resolve this paradox, I aimed to identify the locus and mechanism of analgesia in $Na_V1.7$ null mutants.

The prevailing hypothesis in the field is that analgesia in $Na_V1.7$ nulls results from impaired excitability of nociceptor peripheral terminals leading to nociceptor silencing.[259] To test this, I first used *in vivo* calcium imaging to monitor sensory neuron responses to acute and inflammatory noxious stimuli at the level of the dorsal root ganglia in sensory neuron-specific $Na_V1.7$ knockout mice. To my surprise, I found that peripheral excitability was essentially normal in mice lacking $Na_V1.7$.

Next, I hypothesized that noxious sensory input to the central nervous system was instead lost at the central terminal due to a deficit in synaptic transmission. To test this, I developed a glutamate imaging technique using iGluSnFR to monitor volume glutamate transmission from sensory neuron central terminals in spinal cord slices from mice lacking $Na_V1.7$.[260] Using this novel method, I observed impairments in neurotransmitter release from nociceptor terminals.

It has been suggested that analgesia in $Na_V1.7$ null mutants requires opioid receptors.[261] I therefore investigated the effect of blocking opioid receptors on glutamate and substance P release in spinal cord of $Na_V1.7$ KO mice and saw that opioid blockade rescued the synaptic deficits. To test if this opioid-mediated suppression of transmitter release drove analgesia in $Na_V1.7$ nulls, I investigated the effect of different opioid

antagonists on nociceptive thresholds in mice lacking $Na_V1.7$. I found that central, but not peripheral, opioid receptors were required for analgesia in $Na_V1.7$ null mutants.

1.4.2 Silent cold-sensing neurons drive cold allodynia in neuropathic pain

Neuropathic pain patients often suffer from cold allodynia where innocuous cooling is experienced as excruciating pain.[256] My aim was to use *in vivo* imaging to investigate how neuropathic pain states affect sensory neuron responses to cold and to identify the cells and molecules mediating these changes.

I hypothesized that neuropathic pain states might alter the peripheral representation of cold. To test this hypothesis, I imaged activity in response to cooling in three different mouse models of neuropathic pain that display cold hypersensitivity. In all three models, I found neuropathy caused a set of normally cold-insensitive large-diameter neurons to gain an inappropriate response to cooling. I named these cells silent cold-sensing neurons.

I hypothesized silent cold-sensing neurons were nociceptors that became cold-sensitive thereby driving pain. To test this, I used an *in vivo* screen to identify the molecular markers they expressed and found they were positive for peptidergic nociceptor markers *Calca* and *Scn10a*. Consequently, I showed genetic ablation of *Scn10a*-expressing nociceptors decreased cold hypersensitivity in neuropathic pain.[73]

To identify molecules involved in driving *de novo* cold sensitivity, I used fluorescence activated cell sorting followed by microarray analysis to characterize the transcriptome of presumptive silent cold-sensing neurons, finding they were enriched with K_V1 potassium channel message. I hypothesized that K_V1 channel activity normally suppresses cold-induced action potentials in silent cold-sensing neurons and that removal of this 'brake' triggers *de novo* cold sensitivity.[262] To test this, I pharmacologically blocked K_V1 channels, and found this was sufficient to elicit cold sensitivity in silent cold-sensing neurons.

2 Materials and Methods

2.1 Mouse Genetics

2.1.1 Transgenic mice

All animal procedures carried out at University College London were approved by University College London ethical review committees and conformed to UK Home Office regulations. All animal procedures carried out by collaborators at the University of Saarland were approved by the Institutional Animal Care and Use Committee of the University of Saarland School of Medicine and were in accordance with the laws for animal experiments issued by the German Government.

For experiments using wild-type mice, adult C57/BL6 mice from Charles River were used. Transgenic mouse lines used in this thesis are summarized in **Table 2-1**, with identifiers. Breeding strategies for most of these lines have been previously described in detail.[73,245,257,263,264] Peripheral $Na_V1.7$ knockout mice expressing GCaMP3 were generated by crossing conditional knockout animals with mice homozygous for floxed $Na_V1.7$ and homozygous for Pirt-GCaMP3.[253] Cre-dependent tdTomato mice expressing GCaMP3 were generated by crossing subset-specific Cre mice with animals homozygous for Rosa-flox-stop tdTomato and homozygous for Pirt-GCaMP3. $Na_V1.8$-Cre-dependent tdTomato and diphtheria toxin mice expressing GCaMP3 were generated by crossing $Na_V1.8$ Cre mice with animals heterozygous for Rosa-flox-stop tdTomato, heterozygous for Rosa-flox-stop DTA and homozygous for Pirt-GCaMP3.

Mice were housed on a 12:12 hour light-dark cycle with food and water available *ad libitum*. Both male and female animals were used for all experiments, in equal numbers where possible, bearing in mind the limitations of generating complex transgenic crosses. These studies were not however designed to test for sex differences, and sexes were pooled for analysis. Adult (>6 weeks) mice were used for all studies, with the exception of glutamate imaging and Substance P ELISA experiments, where younger animals were used to improve viability of the spinal cord preparation. The number of animals used to generate each dataset is described in individual figure legends.

MOUSE LINE	IDENTIFIER	CITATION	STOCK
Pirt-GCaMP3	Pirt^{tm2Xzd}	Kim *et al*, 2014[253]	N/A
$Na_V1.7$ flox	Scn9a$^{tm1.1Jnw}$	Nassar *et al*, 2004[265]	N/A
Advillin Cre	B6.129P2-*Avil*$^{tm2(cre)Fawa}$/J	Zhou *et al*, 2010[266]	032536
Wnt1 Cre	*H2az2*$^{Tg(Wnt1-cre)11Rth}$ Tg(Wnt1-GAL4)11Rth/J	Danielian *et al*, 1998[267]	003829
OMP Cre	B6;129P2-*Omp*$^{tm4(cre)Mom}$/MomJ	Weiss *et al*, 2011[263]	006668
Rosa-flox-stop tdTomato (Ai9)	B6;129S6-*Gt(ROSA)26Sor*$^{tm9(CAG-tdTomato)Hze}$/J	Madisen *et al*, 2010[268]	007905
Calb1-Cre	B6;129S-*Calb1*$^{tm2.1(cre)Hze}$/J	Nigro et al[269]	028532
TrkB-CreERT2	B6.129S6(Cg)-*Ntrk2*$^{tm3.1(cre/ERT2)Ddg}$/J	Rutlin et al (2014)[270]	027214
Trpv1-Cre	B6.129-*Trpv1*$^{tm1(cre)Bbm}$/J	Cavanaugh et al (2011)[85]	017769
$Na_V1.8$-Cre	Scn10a$^{tm2(cre)Jnw}$	Nassar *et al* (2004)[265]	N/A
Tmem45b-Cre	Tmem45b$^{tm1.1Hsue}$	N/A	N/A
CGRPα-CreERT2	Calca$^{tm1.1(cre/ERT2)Ptch}$	Song *et al* (2012)[271]	N/A
$Na_V1.8$ KO	Scn10a^{tm1Jnw}	Akopian *et al* (1999)[120]	N/A
Rosa-flox-stop DTA	*Gt(ROSA)26Sor*$^{tm1(DTA)Jpmb}$/J	Ivanova et al (2005)[272]	006331

Table 2-1. Summary of transgenic mouse lines used in this thesis.

2.1.2 Cre recombinase/loxP system

Cre (cyclization recombination) recombinase is a 38 kDa protein from bacteriophage P1 protein that catalyzes recombination of the DNA sequence between two 34-bp loxP recognition sites, depending on their orientation.[273] When the two sites are placed in the same direction, the flanked sequence is excised, but when placed in opposite directions, the flanked sequence is inverted (**Figure 2.1**). To generate a conditional KO mouse, two transgenic mouse lines are required: one expresses Cre driven by a promoter of interest (e.g. Advillin-Cre), the other has loxP sites facing the same direction and flanking part of the gene of interest (e.g. exon 14 and 15 of *Scn9a*); crossing these two lines results in Cre-mediated excision of the flanked DNA sequence, causing deletion of that gene only in

tissues expressing the promoter that drives Cre expression. To generate a conditional reporter mouse, the animal expressing Cre (e.g. $Na_V1.8$-Cre) is crossed to mice where a loxP-flanked transcriptional stop sequence prevents transcription of the fluorescent reporter (e.g. rosa-floxstop-tdTomato). Cre-mediated excision of the stop sequence leads to expression of the reporter protein only in cells expressing the promoter that drives Cre-expression.

Temporal control of Cre recombination can be achieved using the CreERT2 system.[274] A tamoxifen-binding estrogen receptor domain is fused to Cre recombinase; in the absence of tamoxifen, the mutant recombinase is sequestered in the cytoplasm, where it remains inactive. When tamoxifen is introduced, the mutant recombinase is shuttled to the nucleus where site-specific recombination at the loxP sites can now occur, allowing for inducible gene deletion or expression (e.g. CGRPα-CreERT2). In this study, animals were given three 200 µl doses of a 1% tamoxifen solution on consecutive days at 6-10 weeks of age. Tamoxifen was made-up in a 15% ethanol/85% sunflower oil.

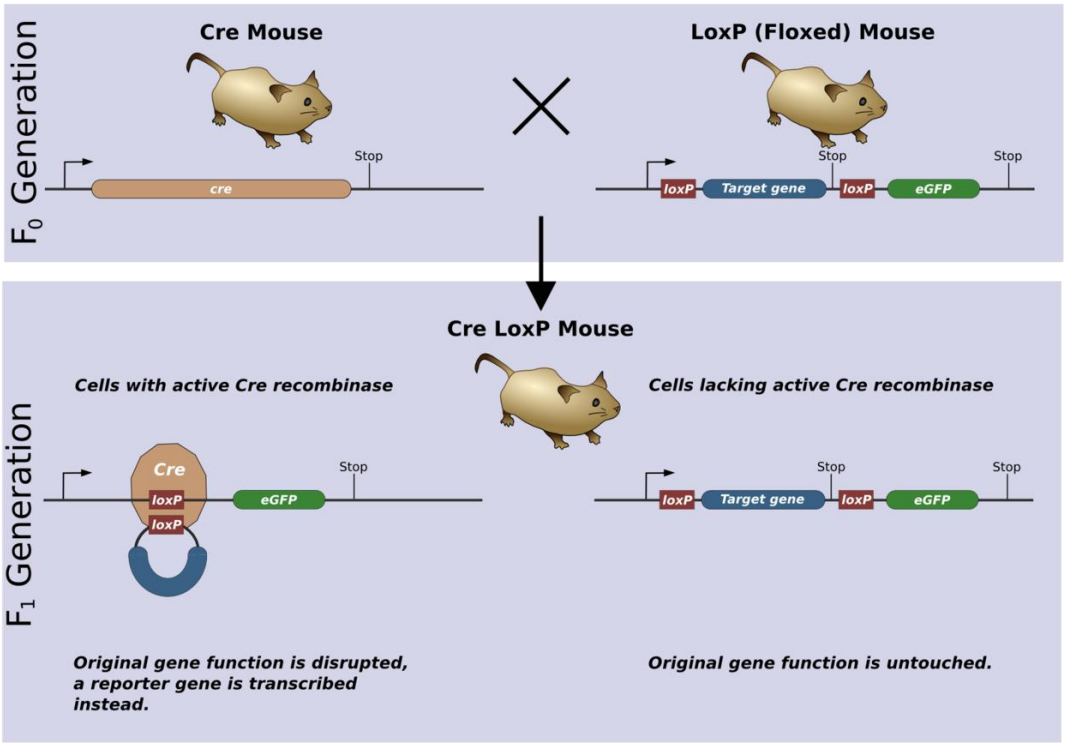

Figure 2.1 (*adapted from Wikimedia Commons*). Cartoon of Cre recombinase/loxP system.

Crossing the Cre-expressing mouse with the mouse carrying the floxed allele generates offspring where Cre-mediated recombination and excision of the floxed allele results in tissue-specific deletion of the target gene only in cells expressing Cre recombinase. In this example, the removal of the stop codon also leads to transcription of a reporter gene eGFP, as a control for successful recombination.

2.1.3 Diphtheria toxin system

The diphtheria toxin system is used to conditionally ablate specific subsets of cells.[272] Diphtheria toxin has two fragments. Fragment B binds the cell surface receptor, allowing it to insert into the phospholipid bilayer and facilitate transfer of the enzymatically-active fragment A. This A fragment suppresses protein synthesis by catalysing the transfer of the ADP-ribose moiety of nicotinamide adenine dinucleotide to elongation factor-2. Cell-type specific diphtheria toxin activity can be achieved in two ways. First, diphtheria toxin receptor is expressed at very low levels in the mouse; over-expression of the receptor in specific cell types using Cre/loxP, BAC transgenesis or knockin strategies therefore means that when mice are treated with diphtheria toxin, only in the cell type of interest can the toxin act to shut down protein synthesis.[74] Second, fragment A can be expressed in a Cre-dependent manner in the cell type of interest; as fragment A is already intracellular, only this fragment is needed to inhibit protein synthesis and thus kill the cell (e.g. rosa-floxstop-DTA).[73]

2.1.4 Genotyping

Ear tissue samples were taken from mice and digested in 30μl lysis buffer with Proteinase K for 180 minutes at 55°C and then for 5 minutes at 95°C to inactivate Proteinase K. Samples were vortexed, spun down and stored at 20°C. A typical polymerase chain reaction (PCR) consisted of: 10 μl Dreamtaq PCR Mastermix (Thermo Scientific), 7 μl H2O, 1 μl each primer (10 μM), 1 ng template DNA. Note that Dreamtaq contains all components necessary for PCR (dNTPs, Taq, buffer). Samples underwent PCR in conditions appropriate for Dreamtaq and specific for each primer set. Samples were run on a 1% agarose gel by gel electrophoresis to separate bands by size. Gels were prepared by dissolving 0.5g agarose (Sigma) per 50ml 1X TAE buffer (40 mM Tris-acetate, 1 mM EDTA). Ethidium bromide (EtBr) was added (0.5 μg/ml) and the gel was set. 5 μl of an appropriate molecular weight marker was run alongside samples in each gel. Samples were run for 30 minutes at 100 volts to separate bands which were visualised using a Biodoc System. Primers used are summarized in **Table 2-2**.

PCR PRODUCT	FORWARD PRIMER	REVERSE PRIMER
Pirt-GCaMP3		
Pirt WT (300 b.p.)	TCCCCTCTACTGAGAGCCAG	GGCCCTATCATCCTGAGCAC
GCaMP3 (400 b.p.)	TCCCCTCTACTGAGAGCCAG	ATAGCTCTGACTGCGTGACC
Na_V1.7 flox		
Na_V1.7 WT (382 b.p.)	CAGAGATTTCTGCATTAGAATTTG TTC	GCAAATCATAATTAATTCATGACAC AG
Na_V1.7 flox (527 b.p.)	CAGAGATTTCTGCATTAGAATTTG TTC	GCAAATCATAATTAATTCATGACAC AG or AGTCTTTGTGGCACACGTTACCTC
Na_V1.7 KO (395 b.p.)	CAGAGATTTCTGCATTAGAATTTG TTC	GTTCCTCTCTTTGAATGCTGGGCA
Advillin-Cre		
Advillin WT (480 b.p.)	CCCTGTTCACTGTGAGTAGG	AGTATCTGGTAGGTGCTTCCAG
Cre (180 b.p.)	CCCTGTTCACTGTGAGTAGG	GCGATCCCTGAACATGTCCATC
Wnt1-Cre		
Wnt1-Cre (628 b.p.)	CTCATTGTCTGTGGCCCTGA	AAATGTTGCTGGATAGTTTTTACT GCC
OMP-Cre		
OMP WT	TGGCAACAGCTGTAGCACTT	ACAGAGGCCTTTAGGTTGGC
Cre	CATTTGGGCCAGCTAAACAT	CCCGGCAAAACAGGTAGTTA
Rosa-flox-stop tdTomato (Ai9)		
WT (297 b.p.)	AAGGGAGCTGCAGTGGAGTA	CCGAAAATCTGTGGGAAGTC
tdTomato (196 b.p.)	CTGTTCCTGTACGGCATGG	GGCATTAAAGCAGCGTATCC
Calb1-Cre		
Calb1 WT (311 b.p.)	AGAACATAATGGCCTTGTG	TACTGACTGGCCTAAGCATGG
Cre (144 b.p.)	AGAACATAATGGCCTTGTG	ACACCGGCCTTATTCCAAG

PCR PRODUCT	FORWARD PRIMER	REVERSE PRIMER
TrkB-CreERT2		
Ntrk2 WT (302 b.p.)	GACACGCACTCCGACTGACT	ACACCTGCCTGATTCCTGAG
CreERT2 (500 b.p.)	GCATGAAGTGCAAGAACGTG	ACACCTGCCTGATTCCTGAG
Trpv1-Cre		
Trpv1 WT (490 b.p.)	TTCAGGGAGAAACTGGAAGAA	TAGTCCCAGCCATCCAAAAG
Cre (102 b.p.)	GCGGTCTGGCAGTAAAAACTATC	GTGAAACAGCATTGCTGTCACTT
$Na_V1.8$-Cre		
$Na_V1.8$ WT (258 b.p.)	CAGTGGTCAGGCTGTCACCA	ACAGGCCTTCAAGTCCAACTG
Cre (346 b.p.)	CAGTGGTCAGGCTGTCACCA	AAATGTTGCTGGATAGTTTTTACTGCC
Tmem45b-Cre		
Tmem45b-Cr (368 b.p.	AGGCCAATGAGAAGTCCTGTGT	GGTATGCTCAGAAAACGCCTGG
CGRPα-CreERT2		
CreERT2 (900 b.p.)	TGCGGCGGATCCGAAAAGAA	TGCCAGGTTGGTCAGTAAGC
$Na_V1.8$ KO		
$Na_V1.8$ WT (258 b.p.)	GAGTGATGCATATGATGTCAT	GCCTTCACTGTTGTTTACACCT
$Na_V1.8$ KO (346 b.p.)	GAGTGATGCATATGATGTCAT	GCAGCGCATCGCCTTCTATC
Rosa-flox-stop-DTA		
WT (600 b.p.)	AAAGTCGCTCTGAGTTGTTAT	GGAGCGGGAGAAATGGATATG
DTA (250 b.p.)	AAAGTCGCTCTGAGTTGTTAT	GCGAAGAGTTTGTCCTCAACC

Table 2-2. Primers used for mouse line genotyping.

2.2 Viral injections

Neonatal pups (P1-P3) were injected with 5 μl of AAV particles (titre ≥ 1×10^{13} vg/mL) via the intraperitoneal route using a Hamilton syringe connected to a 30G needle cannula. Care was taken to minimize exposure to foreign scents to ensure re-acceptance of pups by parents upon return to breeding cage. Viruses used in this study are summarized in **Table 2-3**.

VIRUS	TITRE	CITATION	IDENTIFIER
pAAV.CAG.GCaMP6f.WPRE.SV40	≥1×10^{13} vg/mL	Chen *et al*, 2013[254]	Addgene AAV1; 100836-AAV1
pAAV.hSyn.iGluSnFr.WPRE.SV40	≥1×10^{13} vg/mL	Marvin *et al*, 2013[260]	Addgene AAV9; 98929-AAV9

Table 2-3. Summary of viruses used in this study.

2.3 Pharmacology

The key drugs and compounds used in this study are summarized in **Table 2-4**. Drugs were made up to stock solutions on arrival and diluted on the day of the experiment to the working concentration, as detailed in the methods for each experiment.

REAGENT	SOURCE	IDENTIFIER
PF 05089771	Tocris	5931; CAS: 1430806-04-4
Prostaglandin E2	Merck (Sigma)	P0409; CAS: 363-24-6
Naloxone hydrochloride dihydrate	Merck (Sigma)	N7758; CAS: 51481-60-8
Naloxone Methiodide	Merck (Sigma)	N129; CAS: 93302-47-7
Capsaicin	Merck (Sigma)	M2028; CAS; 404-86-4
Captopril	Merck (Sigma)	C4042; CAS: 62571-86-2
Phosphoramidon disodium salt	Merck (Sigma)	R7385; CAS: 119942-99-3
Dithiothreitol	Merck (Sigma)	D9779; CAS: 3483-12-3
Thiorphan	Merck (Sigma)	T6031; CAS: 76721-89-6
Bacitracin	Merck (Sigma)	B0125; CAS: 1405-87-4
Oxaliplatin	Merck (Sigma)	O9512; CAS: 61825-94-3
Ciguatoxin-2	Richard Lewis, University of Queensland	N/A
Tamoxifen	Merck (Sigma)	T5648; CAS: 10540-29-1
TTX	Merck (Sigma)	T8024; CAS: 4368-28-9
4,9-anhydrousTTX	Tocris	6159; CAS: 13072-89-4
Veratridine	Merck (Sigma)	V5754; CAS: 71-62-5
4-aminopyridine	Merck (Sigma)	275875; CAS: 504-24-5
α-dendrotoxin	Alomone labs	D-350; CAS: 74504-53-3
k-dendrotoxin	Alomone labs	D-400; CAS: 119128-61-9
RIIIJ	Alomone labs	STC-660; CAS: N/A

Table 2-4. Summary of key drugs and compounds used in this study.

2.4 *In Vivo* Calcium Imaging

2.4.1 Acquisition

The rig used for *in vivo* calcium imaging experiments is shown in **Figure 2.2**. Adult mice expressing GCaMP3 or GCaMP6f (8 to 14 weeks, male and female) were anesthetized using ketamine (120 mg/kg) and medetomidine (1.2 mg/kg) in Chapter Three, or ketamine (100 mg/kg), xylazine (15 mg/kg) and acepromazine (2.5 mg/kg) in Chapter Four. Anesthetics were delivered by intramuscular injections into the hindlimb contralateral to the DRG used for imaging. The animal was re-dosed every 20-30 minutes. Depth of anaesthesia was assessed by monitoring the pedal reflex in all four paws. Absent whisker movement and steady breathing rate were used as additional indicators of deep anesthesia. The surgery was begun only once the pedal reflex was entirely absent in all four limbs, whisker movement was absent and breathing was steady.

Animals were maintained at a constant body temperature of 37°C using a heated mat (VetTech). Although this was a terminal procedure, all surgical instruments were heat sterilized using a bead sterilizer. Lateral laminectomy was performed at spinal level L3-5. In brief, the skin was incised longitudinally, and the paravertebral muscles were cut to expose the vertebral column. Transverse and superior articular processes of the vertebra were removed using microdissection scissors and OmniDrill 35 (WPI). To obtain a clear image of the sensory neuron cell bodies in the ipsilateral dorsal root ganglion (DRG), the dura mater and the arachnoid membranes were carefully opened using microdissection forceps (**Figure 2.3**). The animal was mounted onto a custom-made clamp attached to the vertebral column (L1), rostral to the laminectomy (**Figure 2.4**). Bleeding was controlled using sterilized orthodontic sponges. The trunk of the animal was slightly elevated to minimize interference caused by respiration. Artificial cerebrospinal fluid [containing 120 mM NaCl, 3 mM KCl, 1.1 mM $CaCl_2$, 10 mM glucose, 0.6 mM NaH_2PO_4, 0.8 mM $MgSO_4$, 1.8 mM $NaHCO_3$ (pH 7.4) with NaOH] was perfused over the exposed DRG during the procedure to maintain tissue integrity, or the DRG was isolated by coating with silicone elastomer.

Images were acquired using a Leica SP8 confocal microscope. A 10x dry, 0.4-N.A. objective with 2.2 mm working distanced was used, with image magnification of 0.75-3x optical zoom. GCaMP3 or GCaMP6f was excited using a 488 nm laser line (1-15% of maximum laser power). tdTomato was excited using a 552 nm laser line (1-15% of

maximum laser power). The absolute maximum laser power output in Watts was not measured and is not known. Filtering and collection of the emission light was optimized to maximize yield and minimize cross-talk (Leica Dye 164 Finer, LasX software, Leica). GCaMP was detected using a hybrid detector (100% gain) and tdTomato using a photomultiplier tube (500-600V gain). 512 x 512 pixel images were captured at a frame rate of 1.55 Hz, bidirectional scan speed of 800 Hz, and pixel dwell time of 2.44 μs.

Noxious and innocuous stimuli were applied to the left hindpaw, ipsilateral to the exposed DRG. For thermal stimuli, the paw was immersed with ice-water (0°C), acetone (100%) or water heated to 37°C or 55°C using a Pasteur pipette. For delivery of precise temperature stimuli, I used a Peltier-controlled thermode (Medoc). For mechanical stimuli, I used noxious pinch with serrated forceps, and innocuous brushing with a small paint-brush (ProArte-2) or cotton-swab. An interval of at least 30 s separated each stimulus application.

PGE2 (500 μM in 20 μl saline for 10 minutes) was applied to the paw by intraplantar injection. Naloxone (2 mg/kg in saline for 20 minutes) was delivered by subcutaneous injection into the scruff of the neck. TTX (20 μM in 20 μl saline for 20 minutes), 4,9-anhydro-TTX (20 μM in 20 μl saline for 20 minutes), 4-aminopyridine (10 mM in 20 μl saline for 20 minutes), α-dendrotoxin (100 μM in 20 μl saline for 20 minutes), k-dendrotoxin (100 μM in 20 μl saline for 20 minutes), conotoxin kappaM-RIIIJ (100 μM in 20 μl saline for 20 minutes) and veratridine (100 μM in 20 μl saline for 20 minutes) were all applied to the paw by intraplantar injection.

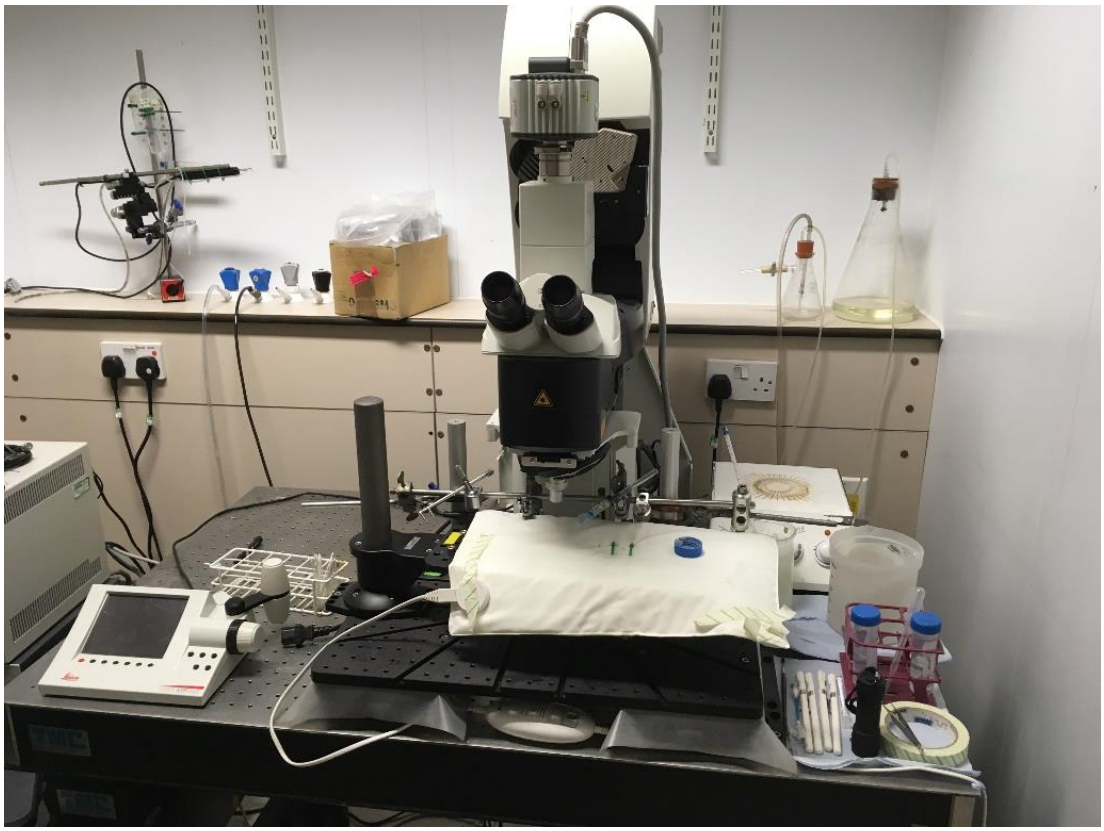

Figure 2.2. Photograph of in vivo imaging rig.

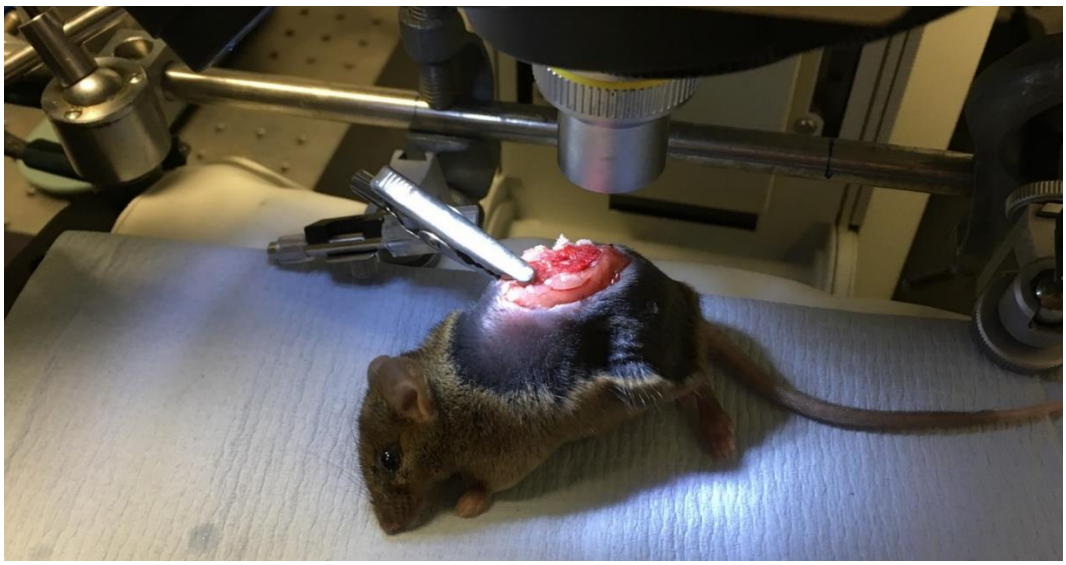

Figure 2.3. Photograph of a mouse with exposed dorsal root ganglion prepared for in vivo imaging

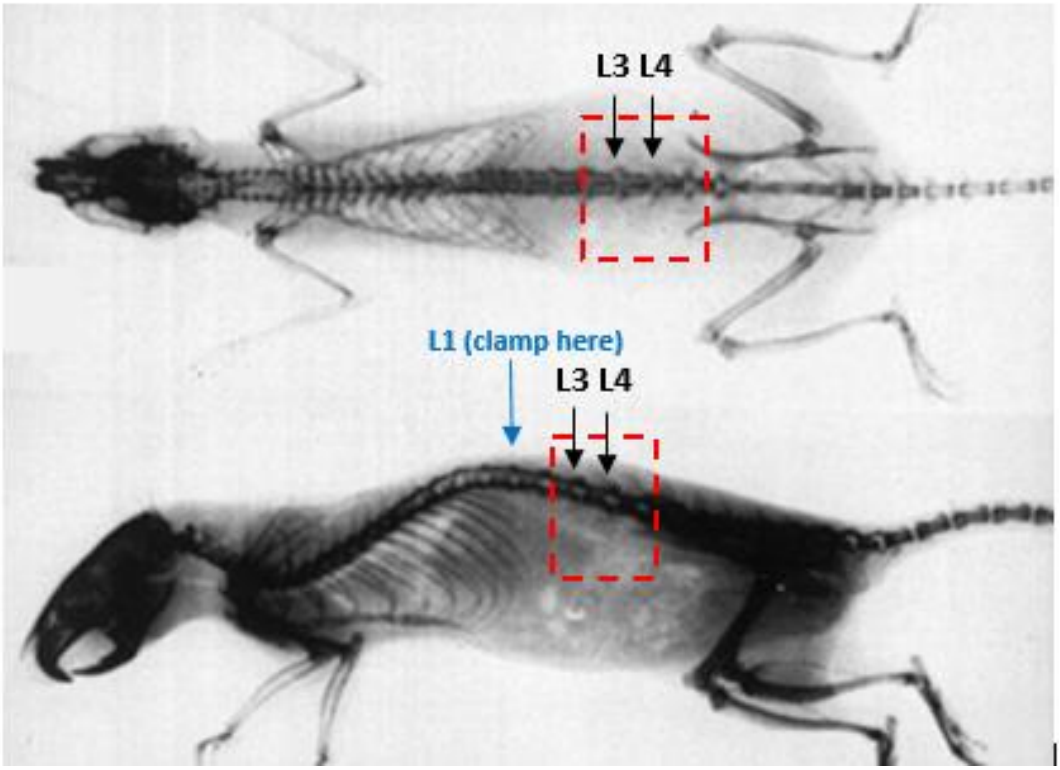

Figure 2.4. X-ray image of mouse showing location of DRGs

2.4.2 Analysis

Image stacks were registered to a reference image – typically, the first frame in the series – using the FIJI plugin TurboReg (accurate rigid body transformation) to correct for XY drift. Stacks that showed excessive Z movement were excluded from analysis. Stacks from DRGs that showed excessive blood flow or damage due to surgery were also excluded

Regions of interest (ROI) were manually drawn around apparently responding cells using the free hand tool in FIJI (**Figure 2.5**). ROIs encompassed the entire cell, not cytosol alone. DRG neuron somata vary greatly in size and morphology, however there is little neuropil contamination, which makes manual identification of cells relatively easy and reliable. Manually identifying responding cells depended on a number of factors: a characteristic cell morphology, a visible darker nucleus with less GCaMP signal, an increase in fluorescence following sensory stimulation, the absence of fluctuating fluorescence changes not locked to the stimulus indicative of non-sensory activity and the absence of a prolonged high GCaMP signal indicative of cell death or damage. The absence of GCaMP3 signal in the satellite glia cells that surround and separate neighbouring DRG somata was advantageous for differentiating adjacent cells, as well as preventing overlap in the fluorescence signal.

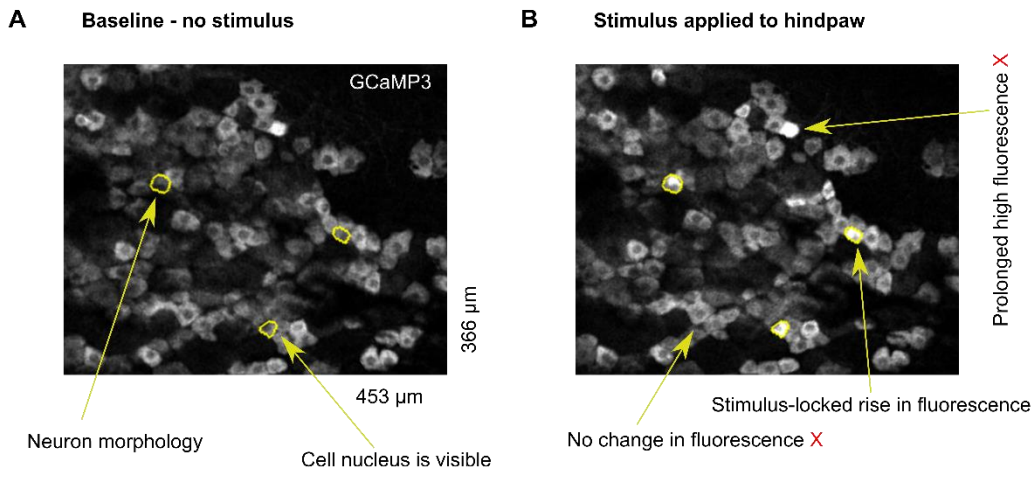

Figure 2.5. Manual identification of regions of interest

(A) Confocal image of a region of the L4 dorsal root ganglion from a Pirt-GCaMP3 mouse. Sensory neuron somata are readily identifiable by neuronal morphology and darker cell nuclei using the GCaMP3 signal alone. Note the absence of neuropil. Pirt is not expressed by satellite glia cells therefore satellite glia, which normally envelope the neuronal somata, are not visible, allowing for easy segregation of neighbouring neurons.

(B) Regions of interest (ROI, yellow shapes) are drawn around the cells that show a rise in fluorescence locked to the stimulus. Cells that show no fluorescence increase or that show a prolonged high fluorescence are excluded.

Mean pixel intensity over time for each ROI was extracted in Fiji and analysed. The time series of mean pixel intensity for each ROI was smoothened by a four time point moving average to remove high-frequency noise. Next, I calculated the derivative of the mean pixel intensity. I calculated a mean baseline derivative for the 10 s preceding stimulus application. Neurons were classed as responders if, within 30 s of stimulus application, the maximum derivative was greater than the baseline derivative plus five standard deviations – that is, a Z-score of at least 5. I then calculated the $\Delta F/F_0$ value for each response to obtain a normalized measure of change in fluorescence. Neurons which showed a $\Delta F/F_0$ less than 0.25 were then discarded. Each trace was then manually screened as a further precaution against false positives. The remaining neurons that made up the responding population were then used for statistical analysis.

Cross-sectional area for each ROI in μm^2 was also extracted in Fiji and analysed. Because nuclei are visible in the cells analysed here, we can justify comparing the areas of the cells present in the image as measures of their relative size.

The red channel of the reference image was used determine whether a cell was positive for tdTomato. Five regions of interest were drawn in background areas of the image clearly negative for tdTomato and average red fluorescence measured to calculate the mean and standard deviation of the background red fluorescence. Red fluorescence in responding cells was Z-scored versus the background value, and cells were counted as tdTomato positive if the Z-score was greater than 5.

2.5 Behavioural Testing

All animal experiments were performed in accordance with Home Office Regulations. I was blinded to treatment and/or genotype. Animals were acclimatized to handling and every effort was made to minimize stress during the testing. Both male and female animals were used.

2.5.1 Randall-Selitto

The threshold for mechanonociception was assessed using the Randall-Selitto test.[165] Animals were restrained in a clear plastic tube. A 3 mm^2 blunt probe was applied to the tail of the animal with increasing pressure until the mouse exhibited a nocifensive response, such as tail withdrawal. The pressure required to elicit nocifensive behavior was averaged across three trials. The cut-off was 500 g.

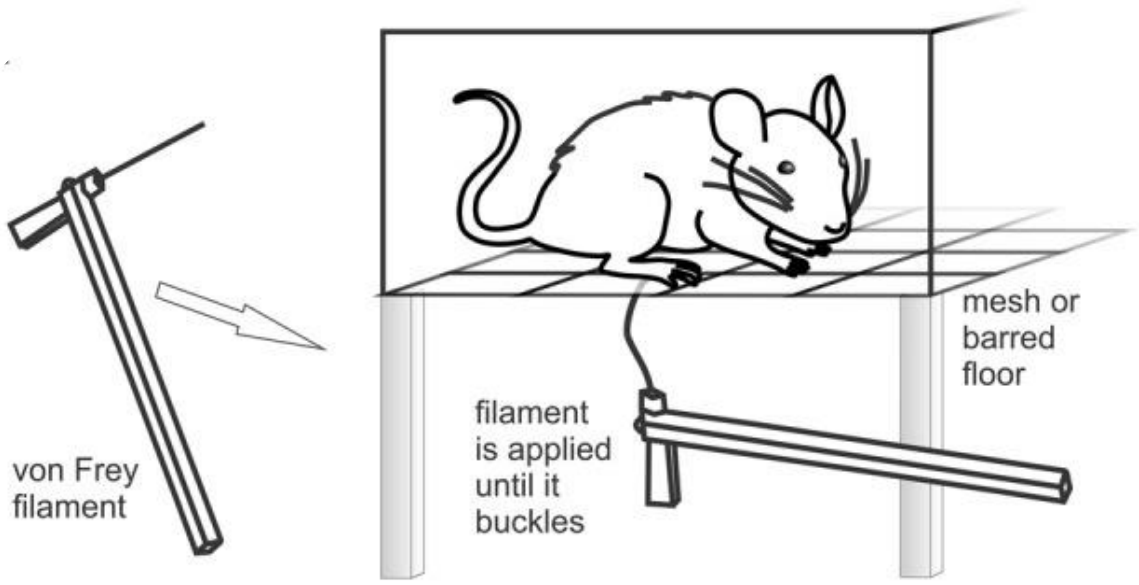

Figure 2.6. Cartoon of Von Frey test

2.5.2 Von Frey

Punctate mechanical sensitivity was measured using the up-down method of Chaplan to obtain a 50% withdrawal threshold (**Figure 2.6**).[275] Mice were habituated for one hour in darkened enclosures with a wire mesh floor. A 0.4 g von Frey filament was applied to the plantar surface of the paw for 3 s. A positive response resulted in application of a filament

of lesser strength on the following trial, and no response in application of a stronger filament. To calculate the 50% withdrawal threshold, five responses surrounding the 50% threshold were obtained after the first change in response. The pattern of responses was used to calculate the 50% threshold = $(10[\chi+\varkappa\delta])/10{,}000)$, where χ is the log of the final von Frey filament used, $\varkappa$ = tabular value for the pattern of responses and δ the mean difference between filaments used in log units. The log of the 50% threshold was used to calculate summary and test statistics, in accordance with Weber's Law.

2.5.3 Hargreaves' Test

Spinal reflex responses to noxious heat stimulation were assessed using the Hargreaves' test (**Figure 2.7**).[164] Mice were habituated for an hour in plexiglass enclosures with a glass base. Before testing, the enclosures were cleaned of faeces and urine. Radiant heat was then locally applied to the plantar surface of the hindpaw until the animal exhibited a nocifensive withdrawal response. Average latencies were obtained from three trials per animal, with inter-trial interval of 15 mins. Cut-off time was 30 s. The effect of intraplanar PGE2 (500 μM in 20 μl) on heat sensitivity was assessed using the Hargreaves' test. A baseline withdrawal latency was obtained and then measured again 10 minutes following PGE2 treatment. The effect of subcutaneous opioid blockers naloxone and naloxone methiodide (2 mg/kg for 20 minutes) or intrathecal naloxone (3 mM in 5 μl) was also assessed using this assay, 20 minutes following drug treatment. For intrathecal injections, mice were anesthetized using 2-3% isofluorane and drugs delivered via a 30G needle cannula attached to a Hamilton syringe.

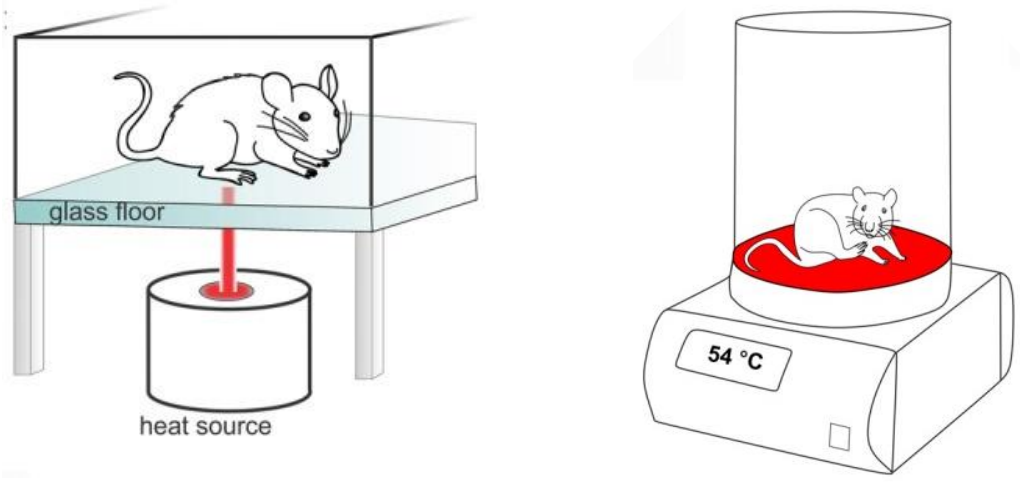

Figure 2.7. Cartoon of heat pain behavioural tests

2.5.4 Hot plate

The Hot Plate test measures suprasinal nociceptive behaviours in response to extreme heat (**Figure 2.7**).[276] Mice were placed on the Hot Plate apparatus held at 50°C or 55°C. The tested ended when the animal showed a withdrawal behavior or licked its hindpaw. Cut-off time was 60 s for 50°C and 30 for 55°C.

2.5.5 Cold Plantar

Spinal reflex responses to cooling were assessed using the Cold Plantar test (**Figure 2.8**).[277] Mice were placed in Plexiglass enclosures with glass flooring and acclimatized for one hour. Before testing, faeces and urine were removed and the animal was left to settle. Dry ice was compacted into a blunt 2 ml syringe and applied to the glass surface just below the hindpaw. The time to withdrawal was measured. Cut off was 30 s. Testing was repeated 3 times, and averaged, with a waiting period of 15min between stimulations.

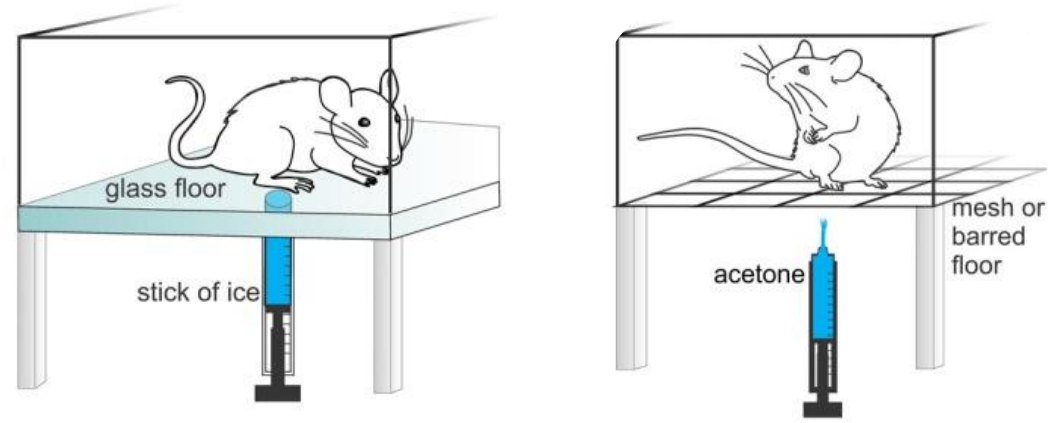

Figure 2.8. Cartoon of cold pain behavioural tests

2.5.6 Cold Plate

Mice were placed on the Cold Plate apparatus.[278] The Cold Plate was maintained at 5°C for 5 minutes while the animal was free to move around on the plate and the number of pain-like behaviours (shaking, lifting, licking, guarding, biting) displayed by each paw were counted by the observer.[279] In the unilateral Cold Plate test, animals were restrained, the ipsilateral paw was placed directly onto the plate maintained at 10°C and the time until paw withdrawal was then measured. This was repeated three times and a trial averaged response obtained.

2.5.7 Acetone Test

The acetone evaporation test measures the nociceptive behaviours triggered by evaporative cooling of the hindpaw (**Figure 2.8**).[280] Mice were habituated for 1 hour in enclosures with a wire mesh floor. Using a home-made syringe, a 50 μl drop of acetone was applied to the ventral side of the ipsilateral hindpaw. The cumulative time where the ipsilateral hindpaw was engaged in nociceptive behaviours (lifting, shaking, licking, guarding, biting) over the ensuing 60 s was then counted. An average of three trials was obtained, with at least 10 minutes between trials.

2.6 Neuropathic pain models

2.6.1 Oxaliplatin

Chemotherapy-induced neuropathy was studied in mice using the intraplantar oxaliplatin model first described by Jennifer Deuis and Irina Vetter because this treatment recapitulates the rapid onset of cold allodynia in human patients infused with this drug.[279] Oxaliplatin (Sigma) was made up in 5% glucose solution to an equivalent dose of 80 μg in 40 μl. Mice were treated by intraplantar injection. Vehicle was 5% glucose solution. Behavioural testing or imaging was assessed at least 3 hours after injection. Note that oxaliplatin is unstable in chloride-containing saline solution.

2.6.2 Partial Sciatic Nerve Injury

Peripheral nerve injury was studied in mice using a modified version of the Setlzer model.[281] Surgical procedures were performed under isoflurane anaesthesia (2–3%) in adult mice. After the left thigh area was shaved and the skin sterilized with 70% ethanol, a longitudinal skin incision was made at the level of the femur. With the help of forceps, the muscle fibres were separated to allow for visualization of the sciatic nerve. The partial nerve injury was induced by tying a tight ligature with 6-0 silk suture around approximately 1/3 of the diameter of the sciatic nerve. The skin was then closed with 6-0 Vicril suture and animals kept in a warm enclosure until complete recovery.

2.6.3 Ciguatoxin-2

Ciguatera poisoning was studied in mice using the intraplantar ciguatoxin model as this treatment isolates the sensory effects of the disease from the central and gastrointestinal symptoms.[282] Ciguatoxin-2 (P-CTX-2) was a gift from Richard Lewis (University of Queensland). P-CTX-2 is highly-lipophilic and sticks to plastic surfaces. P-CTX-2 was therefore made up to 10 μM in 50% methanol solution, stored in a glass vial at -20°C and aliquoted using a metal/glass Hamilton syringe. The stock solution was diluted in saline containing 1% BSA to produce a final concentration of 100 nM. Mice undergoing imaging or behavioural testing were injected intraplantar with 20 μl of 100 nM P-CTX-2, and the effect of the drug measured 20-30 minutes after. Vehicle treatment was a 50% methanol solution diluted 100-fold in 1% BSA.

2.7 Electrophysiology

2.7.1 *In vitro* electrophysiology:

Adult mice were killed by inhalation of a rising CO_2 concentration followed by cervical dislocation to confirm death. Dorsal root ganglia (DRG) were dissected from the entire length of the spinal column and then digested in a pre-equilibrated enzyme mix for 45 minutes (37 °C, 5% CO_2). The enzyme mix consisted of Hanks' balanced salt solution containing collagenase (type XI; 5 mg/ml), dispase (10 mg/ml), HEPES (5 mM) and glucose (10 mM). DRGs were then gently centrifuged for 5 minutes at 300 revolutions per minute, the supernatant was discarded and replaced with warmed Dulbecco's modified Eagle's medium (DMEM), supplemented with L-glutamine (1%), glucose (4.5 g/litre), sodium pyruvate (110 mg/litre) and 10% fetal bovine serum (FBS). Next, DRGs were mechanically triturated with three fire-polished glass Pasteur pipettes of gradually decreasing inner diameter. Dissociated cells were then centrifuged again at 300 revolutions per minute, the supernatant was discarded and cells were re-suspended in the required volume of DMEM supplemented with FBS and nerve growth factor (50 ng/ml). Finally, cells were plated onto 12 mm glass coverslips coated with poly-L-lysine (1 mg/ml) and laminin (1 mg/ml). Cells were incubated at 37 °C in 5% CO_2 and recordings were performed at room temperature 24 – 72 hours after dissociation.

Functional deletion of $Na_V1.7$ was assessed by pharmacological isolation of putative $Na_V1.7$-mediated currents. Patch pipettes (tip resistance of 3-5 MΩ) were filled with intracellular solution containing: 140 mM CsF, 1 mM EGTA, 5 mM NaCl and 10 mM HEPES. To isolate macroscopic sodium currents, neurons were continuously perfused with room temperature extracellular solution containing: 35 mM NaCl, 75 mM Choline-Cl, 30 mM TEA-Cl, 4 mM KCl, 1.8 mM $CaCl_2$, 1 mM $MgCl_2$, 10 mM HEPES, 5 mM Glucose and 0.1 mM $CdCl_2$. Whole-cell recordings were obtained using an Axopatch 200B amplifier, filtered at 10 kHz and digitized at 50 kHz via a Digidata 1322A (Axon Instruments). Medium diameter neurons from WT and $Na_V1.7$ KO mice were voltage-clamped at -70 mV. Series resistance compensation was at least 60%. To measure the voltage-dependence of sodium channel activation, the holding command was dropped to -120 mV to de-inactivate all sodium channels and then a step-protocol from -80 to 20 mV was applied, in increments of 5 mV, to activate sodium channels. To determine the contribution of $Na_V1.7$ to the total sodium current, the $Na_V1.7$ blocker PF 05089771 was applied for 5 minutes at 100 μM. As PF 05089771 is a state-dependent blocker that binds

only to the inactivated state of the channel, the holding command was increased to -40 mV to inactivate sodium channels for the duration of drug application.

Functional deletion of $Na_V1.8$ was assessed by pharmacological isolation of TTX-resistant currents. Patch pipettes (tip resistance of 3-5 MΩ) were filled with intracellular solution containing: 140 mM CsF, 1 mM EGTA, 5 mM NaCl, 10 mM HEPES. Neurons were perfused with extracellular solution containing in: 70 mM NaCl, 70 mM Choline-Cl, 3 mM KCl, 1 mM $MgCl_2$, 20 mM TEA-Cl, 0.1 mM $CdCl_2$, and 10 mM Glucose. 5nM TTX was included in the extracellular solution to isolate TTX-resistant currents. Whole-cell recordings were obtained using an Axopatch 200B amplifier, filtered at 10 kHz and digitized at 50 kHz via a Digidata 1322A (Axon Instruments). Medium to large-diameter tdTomato-expressing neurons from heterozygous and homozygous $Na_V1.8$-Cre mice were voltage-clamped at -70 mV. Series resistance compensation was at least 60%. To measure the voltage-dependence of sodium channel activation, the holding command was dropped to -120 mV to de-inactivate all sodium channels and then a step-protocol from -80 to 20 mV was applied, in increments of 5 mV, to activate sodium channels.

2.7.2 *Ex vivo* slice electrophysiology:

These experiments were performed by Dr Sascha Alles, Dr Filipe Nascimento and Prof Marco Beato. Spinal cord preparations were obtained from male or female mice, between 30 and 60 days old, from either wild-type C75Bl/6 (WT) or conditional $Na_V1.7$ knockout ($Na_V1.7$ KO). Animals were anesthetized via intraperitoneal injection of a ketamine/xylaxine mix (80 mg/kg and 10 mg/kg respectively) and decapitated. The spinal cord was dissected in ice cold aCSF containing: 113 mM NaCl, 3 mM KCl, 25 mM NaHCO3, 1 mM NaH2PO4, 2 mM CaCl2, 2 mM MgCl2, and 11 mM D-glucose. Once dissected free from the vertebral column, the spinal cord was carefully cleaned from connective tissues and dorsal roots were cut at approximately 2 mm length. The spinal cord was then glued to an agar block and glued to the slicing chamber of a HM 650V vibratome (Microm, ThermoFisher Scientific, UK). The slicing solution contained: 130 mM K-gluconate, 15 mM KCl, 0.05 mM EGTA, 20 mM HEPES, 25 mM D-glucose, 3 mM kynurenic acid, 2 mM Na-Pyruvate, 3 mM Myo-Inositol, 1 mM Na-L-Ascorbate, and pH 7.4 with $NaOH_4$. Slices were incubated for 40 minutes at 35°C and then allowed to equilibrate at room temperature for further 30 minutes before starting the recordings.

Voltage clamp recordings were performed using either a Molecular Devices Multiclamp 700B (Scientifica, UK) or an ELC-03X amplifier (NPI electronics, Germany).

Signals were filtered at 5KHz, acquired at 50 KHz using a Molecular Devices 1440A A/D converter (Scientifica, UK) and recorded using Clampex 10 software (Molecular Devices, Scientifica, UK). Electrodes were pulled with a Flaming-Brown puller (P1000, Sutter Instruments, USA) from borosilicate thick glass (GC150F, Harvard Apparatus, UK). The resistance of the electrodes, following fire polishing of the tip, ranged between 3 and 5 MΩ. Bridge balance was applied to all recordings. Intracellular solution contained 125 mM K-gluconate, 6 mM KCl, 10 mM HEPES, 0.1 mM EGTA, 2 mM Mg-ATP, pH 7.3 with KOH, and osmolarity of 290–310 mOsm. Cells were targeted for patching in the inner and outer Lamina II and visualized through an Eclipse E600FN Nikon microscope (Nikon, Japan) equipped with infrared differential interference contrast (IR-DIC) connected to a digital camera (Nikon, DS-Qi1Mc).

Dorsal root was stimulated via a suction electrode connected to an isolated current stimulator (DS3, Digitimer, UK). The stimulation intensity was fixed at 5×threshold for evoking the low threshold response in the recorded cell (typically 50-100 μA), at either 1Hz or 0.1 Hz. Cells were voltage-clamped at -70 mV and the stimulus-evoked EPSC was recorded. Latencies were calculated from 1Hz trials and the mono or polysynaptic nature of the response was classified based on the 0.1 Hz response. Spontaneous EPSCs were automatically detected using ClampFit in a 5 s window for each cell. Cells were voltage-clamped at -70 mV and spontaneous excitatory post synaptic currents (sEPSCs) recorded. sEPSCs were automatically detected using ClampFit in a 5 s window for each cell.

2.7.3 *Ex vivo* olfactory bulb electrophysiology

These experiments were performed by Dr Jan Weiss in the lab of Prof Frank Zufall. Acute olfactory bulb slices were prepared from 4 - 11 week old mice (male and female) anesthetized with CO_2 before decapitation. OBs were rapidly dissected in ice-cold oxygenated (95% O_2, 5% CO_2) solution containing the following (in mM): 83 NaCl, 26.2 NaHCO3, 1 NaH2PO4, 2.5 KCl, 3.3 $MgCl_2$, 0.5 $CaCl_2$, 70 sucrose, pH 7.3 (osmolarity, 300 mOsm/l). The tissue was mounted on a vibratome (VT1000S; Leica Microsystems, Nussloch, Germany) and horizontal olfactory bulb slices (275 μm thick) were cut in the same solution. Slices were stored at 30 - 35° C for 15 - 20 min in standard extracellular solution and afterwards at room temperature until use. The extracellular solution contained the following (in mM): 125 NaCl, 25 $NaHCO_3$, 2.5 KCl, 1.25 NaH_2PO_4, 1 $MgCl_2$, 2 $CaCl_2$ and 10 glucose (continuously bubbled with 95% O_2, 5% CO_2). Tissue slices were placed in the recording chamber and superfused at a rate of ~2 ml/min (gravity

flow) with extracellular solution bubbled with carbogen (95% O_2, 5% CO_2). Cells were visualized in intact tissue slices with a 40x water immersion objective lens (Olympus) using infrared-optimized differential interference contrast optics and fluorescent illumination and a GFP filter set attached to the microscope to elucidate the morphology of lucifer yellow-filled mitral and tufted cells (BX50WI, Olympus).

Slice recordings were carried out at room temperature using an EPC-9 automated patch-clamp amplifier (HEKA Elektronik, Lambrecht, Germany) and Pulse 8.11 software as described previously.[263] Patch pipettes were pulled from borosilicate glass tubing (World Precision Instruments, Germany). The signals were filtered using an eight-pole Bessel filter built into the EPC-9 amplifier (VR-10B, Instrutech Corp.). The sampling rate during all recordings was 10 kHz. Recording pipettes had resistances of 3 - 6 MΩ. Cells were voltage-clamped in the whole-cell patch-clamp mode. M/T cells had an ellipsoid-shaped cell body with a diameter of >10 μm, were located in the mitral cell layer or in the external plexiform layer. Mitral cells and tufted cells were not discriminated within the group of M/T cells. M/T cells were filled with lucifer yellow during the recording and were afterwards visually inspected using fluorescent illumination.

The intracellular solution contained (in mM): 140 CsCl, 1 EGTA, 10 HEPES, 2 ATP Na-salt, 1 GTP Mg-salt, 5 QX-314 (a lidocaine derivative; Sigma-Aldrich, Taufkirchen, Germany), 0.1 lucifer yellow, 0.4 neurobiotin (Vector Laboratories, Burlingame, CA, USA); pH 7.1; osmolarity 290 mosm). The theoretical liquid junction potential between intracellular and extracellular compartments was calculated to be 4.1 mV and was not corrected.

After establishing a whole-cell recording, cells were voltage clamped to −60 mV. Data acquisition began after 2 minutes to allow for equilibration of intracellular solution into the dendrites. Electrical stimulation of the olfactory nerve layer was applied via a glass electrode filled with extracellular solution and connected to an Isolated Pulse Stimulator Model 2100 (A-M Systems Instruments, USA). Electrodes were visually positioned in close proximity to the corresponding glomerulus of the recording site and stimulus duration and intensity was 1 ms and 100 V, respectively. Extracellular solution containing the opioid receptor antagonist naloxone (300 μM, Sigma Aldrich, Germany) was perfused to the olfactory bulb slice for at least 10 minutes.

All electrophysiological data were analyzed using Igor Pro software (WaveMetrics) and Excel (Microsoft). For pharmacological experiments, amplitudes of evoked EPSCs were assessed.

2.7.4 *In vivo* electrophysiology:

These experiments were performed by Dr Shafaq Sikandar and Dr Ana Luiz. Electrophysiological recordings were performed by a blinded experimenter. Mice were anaesthetized with isofluorane (4%; 0.5 l/min N_2O and 1.5 l/min O_2) before being secured in a stereotaxic frame. Depth of anaesthesia was reduced and maintained at 1.5% isoflurane during the experiment. Lateral laminectomy was performed to expose the L4 DRG, as described above for *in vivo* imaging. Multi-unit extracellular recordings were made from DRG neurons using parylene-coated tungsten electrodes (A-M Systems). Mechanical and thermal stimuli were applied to the peripheral receptive field of hindpaw glabrous skin ipsilateral to the exposed DRG. Natural stimuli (dynamic brush, von Frey hairs 0.16–26 g, noxious prod 100 and 150 g/cm^2 mechanical stimulation, thermal water jet 35–55°C and iced water) were applied in ascending order of intensity to receptive fields for 10 s and the total number of evoked spikes recorded. Ethyl chloride was applied for 1s as a noxious cold stimulus and the total number of evoked spikes in 10 s was quantified. Evoked activity of neurons was visualized on an oscilloscope and discriminated on spike amplitude and waveform basis using a CED 1401 interface coupled to Spike2 software (Cambridge Electronic Design) to record waveform templates and carry out principal component analysis. For naloxone experiments, 2 mg/kg naloxone in saline was injected subcutaneously into the scruff of the neck, and the stimulation protocol repeated again 20 minutes after naloxone injection.

2.8 Glutamate Imaging

2.8.1 In vitro characterization

Dorsal root ganglia neurons were dissociated and cultured onto glass coverslips as described above. Neurons were treated with iGluSnFR AAV9 particles diluted in culture media at dilutions varying from 1/100 to 1/4000. After 2-5 days treatments, neurons expressed the virus at all tested dilutions. Coverslips were transferred to an imaging chamber and perfused with extracellular solution containing: 140 mM NaCl, 4 mM KCl, 1.8 mM CaCl2, 1 mM MgCl2, 10 mM HEPES and 5 mM glucose, with pH 7.4. Images were acquired using a Leica SP8 confocal microscope with 20x immersion objective and iGluSnFR was excited using a 488 nm laser (1-5% laser power). Glutamate was applied at various concentrations in the bathing solution resulting in fluorescence increases localized to the plasma membrane. For analysis, ring-shaped regions of interest were drawn around the membrane and mean pixel intensity extracted and converted to $\Delta F/F_0$. Three-parameter dose-response curves were fit using GraphPad prism with a standard Hill Slope of 1.

2.8.2 Two-photon imaging

Lumbar spinal cord slices were prepared for glutamate imaging from P9-P21 mice virally expressing iGluSnFr in sensory afferents.[260] Mice were culled by intraperitoneal injection of a ketamine (60mg/kg) and xylazine (12mg/kg) cocktail followed by decapitation and exsanguination. Spinal cords were dissected in an ice-cold oxygenated (5% CO_2 / 95% oxygen) dissection solution containing: 215 mM sucrose, 3 mM K-gluconate, 1.25 mM NaH_2PO_4, 26 mM $NaHCO_3$, 4 mM $MgSO_4$-$7H_2O$, 10 mM d-glucose, 1 mM kynurenic acid and 1 mM $CaCl_2$. Spinal cords were embedded in low-melting point agarose (2-3%) in ASCF and then sectioned using a vibrating microtome into 500 um thick transverse slices in oxygenated ACSF. Slices were incubated for at least an hour in oxygenated ACSF at 37°C. The ACSF contained: 111 mM NaCl, 3.085 mM KCl, 10.99 mM d-glucose, 25 mM $NaHCO_3$, 1.26 mM $MgSO_4$-$7H_2O$, 2.52 mM $CaCl_2$, and 1.1. mM KH_2PO_4.

Slices with dorsal roots attached were transferred to the recording chamber and pinned using a harp. Using a 10x air objective on a Brüker 2P microscope, the dorsal roots were visualized and approached with the suction electrode. Roots were gently suctioned into the suction electrode, allowing a tight seal to form. An Isoflex (Molecular Devices) stimulus isolator was used to deliver negative current pulses of varying amplitudes. The

stimulus isolator was triggered directly from the imaging software (Prairie View) and stimulation was timelocked to image acquisition. The temporal profile of the output waveform was controlled from the imaging software, with pulse duration of 400 μs, and, in paired pulse experiments, with an inter pulse interval of 25-250 ms. To ensure accurate time-locking, the output from the stimulus isolator was also recorded by the imaging software.

Images were acquired using a 2-photon microscope (Bruker) with a 20x high NA water immersion objective. iGluSnFr was excited using a 920 nm laser line (Insight DS, Spectra-Physics) and 525/70 nm emission acquired by a GaAsP PMT (Hamamatsu) with gain set to maximum. The location of layer II of the dorsal horn was estimated using physical and fluorescent landmarks and a 250 x 125 pixel field of view drawn, equivalent to 195 x 98 μm. Images of glutamate release in response to different single pulse stimulus intensities were acquired at 10 Hz. For linescan experiments, straight lines (1024 pixels; 200 μm) were scanned through manually identified regions of interest and acquired at a speed of ~500 Hz. Glutamate transmission was evoked using a peri-maximal stimulus intensity previously determined as sufficient to elicit peak release. Throughout the experiments slices were perfused with oxygenated room temperature ACSF and, in some experiments, the bathing solution contained naloxone (100 uM), which was applied for at least 20 minutes.

2.8.3 Analysis

Image stacks were analyzed in Fiji. Trials were concatenated and then registered to the first image in the stack (accurate rigid body transformation). Regions of interest were manually identified by a blinded experimenter and the mean pixel intensity over time per ROI extracted. Manual identification was based on identifying regions which showed an increase in fluorescence and corresponded to a single afferent process. Signals were converted to $\Delta F/F_0$. Glutamate release events time-locked to the stimulus were z-scored and considered significant if $z>4$. This dataset was then used for subsequent statistical analysis. For linescan experiments, the line profile over time was extracted per ROI and events were again considered significant where $z>4$. For events that passed this threshold, a trial averaged response was obtained by calculating the median at every timepoint. For paired pulse experiments, the signal attributed to release evoked by the second pulse was estimated by subtracting the signal due to a single pulse from the signal elicited by paired stimulation.

2.9 Cell Sorting and Microarray

These experiments were performed by Dr Edward Emery. Dorsal root ganglia neurons were extracted, acutely dissociated, and resuspended in extracellular solution containing (in mM): 140 Na, 4 KCl, 1.8 $CaCl_2$, 1 $MgCl_2$, 10 HEPES, 5 Glucose. DNAse 1 was also added to the cell suspension at 10 mg/mL. Cells were immediately sorted using Fluorescent Activated Cell Sorting (FACS; FACSAria III; BD Biosciences) at 4°C (**Figure 2.9B**). Neuronal populations were gated based on their fluorescence. A non-fluorescent sample was used before each sorting experiment to ensure the exclusion of auto-fluorescent neurons (**Figure 2.9A**). A 37°C sample was run to ensure accurate gating of the cold-activated GCaMP population (**Figure 2.9C**). Sorted populations were immediately placed into lysis buffer and were used for RNA extraction. Cell lysis and RNA extraction was performed using the PureLink RNA Micro kit (Invitrogen, UK). Extracted RNA was then used for microarray analysis (AffyMetrix Microarray Analysis; ThermoFisher, UK).

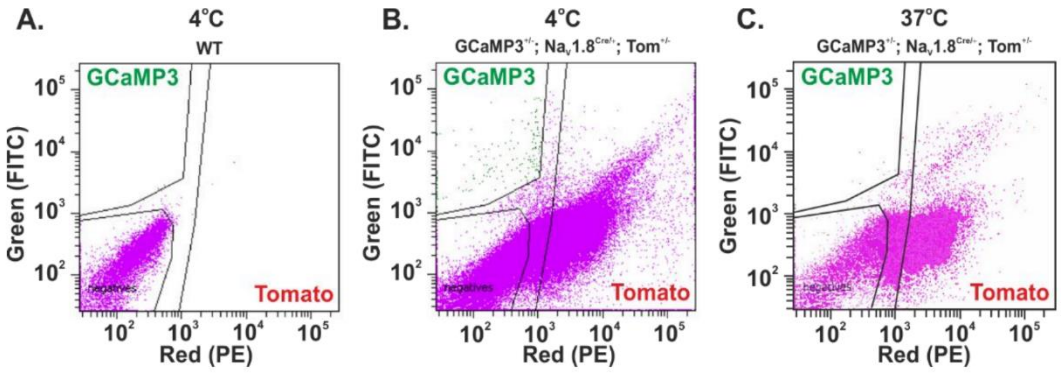

Figure 2.9. Fluorescence-activated cell sorting of DRG neurons at 4°C and 37°C.

FACS plots of individual DRG neurons from WT (A.) and GCaMP3+/− ; $Na_V1.8$-Cre+/- ; tdTomato+/− (B. and C.) mice, at 4°C (A. and B.) and 37°C (C.). Gating was performed to isolate GCaMP3 and tomato fluorescence, as well as to remove non-fluorescent cells.

2.10 Substance P ELISA

Thoraco-lumbar transverse spinal cord slices were prepared from P14-40 WT and KO^{Adv} mice. Mice were culled by intraperitoneal injection of a ketamine (60mg/kg) and xylazine (12mg/kg) cocktail followed by decapitation and exsanguination. Spinal cords were removed from the spinal column by hydraulic extrusion and embedded in low-melting point agarose (2-3%) before sectioning using a vibratome (Leica) into 300 μm thick coronal slices in ice-cold oxygenated ACSF. Slices were then incubated for at least an hour in oxygenated ACSF at 37°C. The ACSF solution used throughout was the same recipe as used for glutamate imaging.

Following incubation, slices were treated with either 1 mM naloxone or vehicle for 20 minutes in 37°C oxygenated ACSF. Slices were then transferred to a 48 well plate, with 10 slices per well. To evoke substance P release, slices were treated with 2 uM capsaicin with and without naloxone for 20 minutes while being shaken at 300 rpm. The treatment solution also contained 0.1% BSA and a cocktail of peptidase inhibitors to maximize recovery of substance P. The cocktail contained (in μM): 200 captopril, 2 phosphoramidon disodium salt, 12 dithiothreitol, 20 thiorpan and 40 bacitracin. Following treatment, the superfusate was immediately collected and substance P concentration measured using a commercially-available Substance P competitive binding assay (R&D systems). All samples were run in duplicate (50 μl per sample) following the manufacturer's instructions and optical density measured using a microplate reader. Sample substance P concentrations were interpolated from a standard curve run in parallel (**Figure 2.10**).

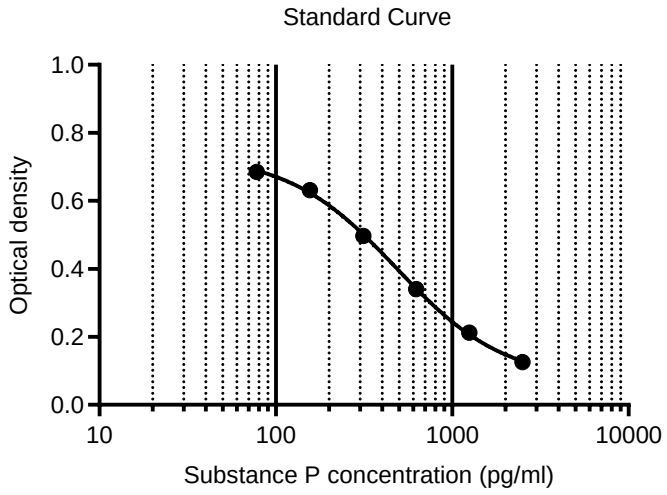

Figure 2.10. Example standard curve from substance P ELISA showing relationship between substance P concentration and optical density

2.11 Immunohistochemistry

This experiment was performed by Dr Martina Pyrski, in the lab of Prof Frank Zufall. One day prior to the experiment, mice were distributed onto individual homecages. Naloxone was dissolved in phosphate buffered saline (PBS) pH 7.4 and systemically applied by intraperitoneal injection of 2 mg/kg bodyweight, while negative controls received vehicle (PBS) alone. Tested mice (n=3 each genotype) were Nav1.7^{control} [(flox/–)(OMP/–)(Cre/–)] and Nav1.7 KO^{OMP} [(fx/fx) (OMP/–)(Cre/–)] mice. For each mouse, three consecutive intraperitoneal injections with 30 min time intervals were performed. After each injection, mice were returned to their odour-rich home cages. At 24 hours after the last injection, mice were anesthetized, subjected to transcardial perfusion, followed by tissue preparation for tyrosine hydroxylase immunohistochemistry. Mouse tissue preparation followed previously described methods.[263,283] Adult mice (7-9 weeks-of-age) were anaesthetized using a mixture of 165 mg/kg body weight ketamine and 11 mg/kg body weight xylazine, and were transcardially perfused with phosphate-buffered saline (PBS) pH 7.4, followed by 4% paraformaldehyde in PBS. Olfactory bulbs (OBs) were dissected, incubated for 2 h in fixative and for overnight in 30% sucrose in PBS at 4°C, embedded in O.C.T. (Tissue-Tek), and snap-frozen in a dry ice/2-methylbutane bath. Frozen tissue sections (18 μm) were collected on a cryostat (Microm HM525, Walldorf, Germany) and stored at -80°C until subjected to immunohistochemistry. For tyrosine hydroxylase (TH) immunostaining, tissue sections were rinsed in PBS, treated for 1 h with blocking buffer containing 0.3% Triton X-100 and 4% normal horse serum (NHS, Vector Laboratories) prepared in PBS, followed by incubation in TH primary antibody (mouse monoclonal, cat# 22941, RRID:AB_572268, ImmunoStar, Hudson, WI, USA) diluted 1:2000 in blocking solution. Tissue sections were washed three times 10 min in PBS and incubated in Alexa-Fluor 488 conjugated goat-anti-mouse secondary antibody (1:1000, Thermo Fisher Scientific cat# A-11029, RRID:AB_2534088) for 1 h in the dark. Tissue sections were rinsed in PBS, the nuclei counterstained with Hoechst 33342 (1:10,000 in PBS, Invitrogen) for 10 min, rinsed again in PBS, and cover slipped using fluorescence mounting medium (DAKO). All procedures were conducted at room temperature with the exception of tissue incubation in primary antibody solution at 4°C. Confocal fluorescence images were acquired on a Zeiss LSM 880 confocal microscope containing a 32-channel GaAsP-PMT and 2-channel PMT QUASAR detector. Each image shown in Figure 6C refers to a single 2.5 μm thick optical section. Images were assembled and minimally adjusted in brightness using Adobe PhotoShop Elements 10.

2.12 Human Sensory Testing

2.12.1 Human Subjects

These experiments were performed by Dr Flavia Mancini and Prof Giandomenico Iannetti. Two male $Na_V1.7$ null participants and one age and gender matched healthy control were tested. All participants gave written informed consent. The study was approved by the UCL Research Ethics Committee. Both males are compound heterozygous nulls and have been previously described.[284,285] Mutations are summarized in **Table 6-1** in Chapter Six.

2.12.2 Testing

Perception of tonic radiant heat was assessed at baseline and during intravenous administration of saline or naloxone (12 mg), in a randomized order. The perception of long-lasting, tonic nociceptive stimuli is generally considered to be less confounded by attention than transient noxious stimuli, involving rapid, attentional shifts that can confound perceptual measures.[286] Psychophysical assessment was carried out by an experimenter blind to the pharmacological condition. Tonic radiant heat was generated by a CO_2 laser, whose power is regulated using a feedback control based on an online measurement of skin temperature at the site of stimulation (Laser Stimulation Device, SIFEC, Belgium). The CO_2 laser selectively stimulates both A-delta and C fibers. On each trial, tonic radiant heat was delivered to the forearm for 25 s and kept constant at either 45 or 48 °C.[287] Participants were asked to rate the intensity of the thermal sensation on a visual analogue scale throughout the trial (0=no sensation, 100=worst pain imaginable). Three trials per stimulus temperature were given on each session (baseline, saline and naloxone) in a randomized order.

2.13 Quantification and Statistical Analysis

2.13.1 Statistical Power

For *in vivo* imaging experiments, n refers to the number of cells responding to any stimulus. For electrophysiology experiments, n refers to the number of recorded cells. For glutamate imaging experiments, n refers to the number of regions of interest. For all imaging and physiology data, the number of animals used is indicated in the legend. For behavioural and substance P experiments, n refers to the number of animals.

For the majority of behavioural experiments, I used six animals per group. For imaging experiments and all other experiments using animal tissue, I typically obtained individual replicates from at least three animals. In the small number of cases where fewer mice were used, this was due to limited availability of transgenic animals generated from complex crosses.

No power calculations were performed for these studies. A limitation of the statistical analysis in this thesis is that no distinction was made between data gathered for exploratory research and for hypothesis testing.

2.13.2 Summary statistics

Datasets are presented using appropriate summary statistics as indicated in the legend, typically accompanied by raw data points or a representation of the underlying distribution. Normality was assessed by visual inspection of the raw data, as only gross departures from normality affect the robustness of the statistical tests used here. Error bars denote mean ± 95% confidence interval or mean ± SEM, as indicated in the legend.

Normality was not assumed for datasets where failure to detect the quantity being measured was scored as zero. For example, all GCaMP response magnitudes in Chapter Four where treated as non-normal, because non-responders were defined as $\Delta f/f_0=0$, thus mean values would be artificially deflated. Normality was also not assumed when comparing cell cross-sectional areas in Chapter Four as many of these distributions were clearly multimodal. For non-normal data, medians with quartiles, or cumulative probability plots, were used to summarize the data.

For *in vivo* imaging experiments, cells from all animals were pooled for analysis, as is typical in the field.[67,248] Because there was substantial variation in the number of cells recorded per animal, this avoided skewing of the dataset by summary values calculated

from animals where very few cells were recorded. Imaging data presented here were often categorical: for instance, whether a cell was polymodal. To give a measure of the uncertainty around percentages calculated from these pooled datasets, 95% confidence intervals around proportions were estimated using the Wilson-Brown method.

2.13.3 Test statistics

Tests of statistical comparison for each dataset are described in detail in figure legends. When comparing two groups, unpaired *t* test or Mann-Whitney test was used, depending on whether normality was assumed. When comparing the distribution of cell cross-sectional areas for two groups, the Kolmogorov-Smirnov test was used. For more than two groups, One-Way ANOVA or Kruskall-Wallis test was used with post-hoc tests corrected for multiple comparisons. When comparing the effect of two factors on multiple groups, a repeated-measures Two-Way ANOVA was used, with post-hoc tests corrected for multiple comparisons. For categorical data, proportions were compared using χ^2 test, with Yates' correction where appropriate. Curve fitting was performed using linear regression or non-linear regression functions.

Statistical tests were all performed using GraphPad Prism 7. An α-value of $p=0.05$ for significance testing was used. All p-values resulting from planned hypothesis testing are reported.

Please note, where data were collected and analyzed by other investigators, their original analytical choices were retained, even where this was inconsistent with the assumptions and analyses used on my own data. This was to avoid *p*-hacking by repeatedly analyzing the same data in multiple ways.

3 The mechanism of analgesia in $Na_V1.7$ null mutants

3.1 Summary

Genetic deletion of the voltage-gated sodium channel $Na_V1.7$ in mice and humans leads to profound pain insensitivity. Paradoxically, peripherally-targeted pharmacological antagonists of $Na_V1.7$ fail to relieve pain in the clinic. This could be linked to endogenous opioid signalling that is enhanced in $Na_V1.7$ null mutants but is not activated by $Na_V1.7$ blockers. Importantly, $Na_V1.7$ is expressed at both the peripheral and central terminals of nociceptors.

To determine the locus and mechanism of analgesia in $Na_V1.7$ null mutants, I used optical, electrophysiological and behavioural methods to investigate the impact of peripheral $Na_V1.7$ deletion on nociceptor function. Surprisingly, both calcium imaging and extracellular recording of $Na_V1.7$-deficient sensory neurons *in vivo* revealed limited deficits in the response to noxious stimuli. Synaptic transmission from sensory neuron central terminals in the spinal cord was however compromised following $Na_V1.7$ deletion. Importantly, deficits in both glutamate and substance P release were reversed by blocking opioid receptors. Consistent with this, I found central – but not peripheral – opioid receptors were required for behavioural analgesia in $Na_V1.7$ knockout mice. Extending these observations to humans, nociception was enhanced in a male $Na_V1.7$ null individual after infusion with an opioid receptor antagonist.

Collectively, these data demonstrate that action potentials evoked by noxious stimuli propagate at least as far as the soma in nociceptors lacking $Na_V1.7$. Noxious sensory input is instead lost at the central terminal, likely through opioid receptor-mediated inhibition of synaptic transmission. My findings thus account for the failure of peripherally-targeted $Na_V1.7$ blockers and point to a central mechanism of analgesia in $Na_V1.7$ null mutants that requires opioid receptors.

3.2 Introduction

Chronic pain afflicts a fifth of the population, but effective analgesics are few.[18] We urgently need new molecular targets to develop improved painkillers. A successful strategy is to identify genes involved in rare human monogenic pain disorders. Loss-of-function mutations in the gene SCN9A encoding the peripheral voltage-gated sodium channel $Na_V1.7$ lead to congenital insensitivity to pain (CIP), but innocuous sensation remains intact.[5] Gain-of-function mutations in *SCN9A* are conversely associated with ongoing pain.[288–290] Dubbed the "volume knob" for pain by the popular press, this channel represents one of the most promising, human-validated drug target for pain relief.[291]

Pharmacological blockers of $Na_V1.7$ are of enormous interest to the pharmaceutical industry, with a number of compounds tested in clinical trials for chronic pain. Unfortunately the peripherally-targeted antagonists of $Na_V1.7$ studied so far have not proven successful as painkillers.[258] Paradoxically, pharmacological block of the channel does not recapitulate the analgesia associated with functional deletion of the SCN9A gene. Our understanding of the mechanisms underlying pain insensitivity in $Na_V1.7$ null mutants *in vivo* is incomplete. Studies of mice engineered to lack $Na_V1.7$ have revealed the complex contribution of $Na_V1.7$ to pain pathways.[292] To develop rational therapies targeted at $Na_V1.7$, we need to resolve how exactly $Na_V1.7$ loss-of-function leads to the absence of pain. Here I review genetic, structural and pharmacological studies of $Na_V1.7$, and end by highlighting the hypotheses thus far proposed to explain the complete analgesia of $Na_V1.7$ null mutants.

3.2.1 Human genetics of $Na_V1.7$

In 2006, James Cox and Geoff Woods reported on three consanguineous Pakistani families whose members showed an unusual clinical phenotype characterized by a complete inability to feel pain.[5] All had injuries to their lips and tongue due to self-mutilation in childhood. All experienced cuts and bruises without pain, and most suffered painless fractures. Importantly, innocuous sensation was preserved, with patients able to feel touch, warming, cooling and tickling. These individuals carried homozygous recessive nonsense mutations in the gene *SCN9A* encoding the alpha subunit of the TTX-sensitive voltage-gated sodium channel $Na_V1.7$. Expression of mutant channels in HEK cells confirmed complete channel loss-of-function. These genetic data indicate $Na_V1.7$ is essential for transmission of nociceptive signals to the CNS in humans.

Since then numerous $Na_V1.7$ mutations have been identified in congenital insensitivity to pain (CIP) patients **(Figure 3.1**). Most mutations described thus far cause channel truncations, mis-splicing or defective trafficking, totally eliminating $Na_V1.7$-mediated sodium currents.[292] Emery and colleagues characterized three mutations in two compound heterozygous CIP patients where some residual channel function was retained, however. These three mutations reduced the peak voltage-dependent sodium current as well as causing a depolarizing shift in activation or hyperpolarizing shift in steady-state fast inactivation.[293] $Na_V1.7$ null mutants are typically distinguished from the Hereditary Sensory Autonomic Neuropathy (HSAN) category of pain-free disorders based on normal autonomic function, however one Japanese group described three patients with $Na_V1.7$ loss-of-function accompanied by autonomic dysfunction, hypohydrosis and delayed onset of pain insensitivity.[294] This arguably represents a different genetic condition and reflects expression of $Na_V1.7$ in sympathetic neurons.[292] Nevertheless, even these patients eventually show the expected loss of pain.

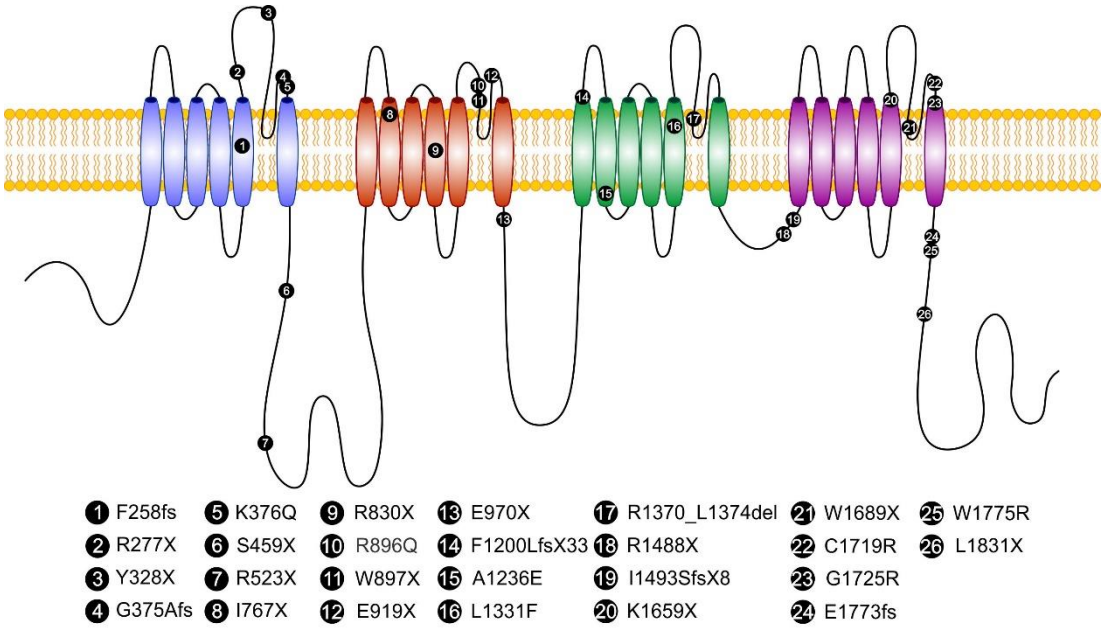

Figure 3.1 (adapted from Ref. *119*). Secondary structure of Nav1.7, showing amino acids affected by different CIP mutations.

Gain-of-function mutations in *SCN9A* contrastingly cause extreme and ongoing pain. Inherited erythromelalgia (IEM) is a rare autosomal dominant disorder characterized by attacks of burning pain in the extremities triggered by warming, exercise and stress. No effective treatments exist; patients resort to immersing hands and feet in ice to relieve the pain. In 2004, Yang *et al* used linkage analysis and candidate gene sequencing to identify gain-of-function mutations in SCN9A causing IEM in a Chinese pedigree.[288]

Electrophysiological analysis by Steve Waxman's group subsequently found mutated channels showed hyperpolarized voltage-dependence of activation, slower inactivation kinetics and enhanced ramp currents.[295] Mutations characterized since are found mainly in domains I to IV and result in enhanced channel activation, presumably leading to nociceptor hyperexcitability.[296] Importantly, IEM is aggravated by warming, while electrophysiological studies are typically performed at room temperature. When studied at 35 °C, IEM mutations show a depolarizing shift in steady-state fast inactivation, as well as the typical hyperpolarized activation threshold.[297] Conclusively linking biophysical alterations in mutant channels to changes in excitability in sensory neurons is difficult, however. To overcome this, investigators now study excitability in human nociceptors differentiated from ISPCs derived from IEM patients.[182]

Paroxysmal extreme pain disorder (PEPD) is a $Na_V1.7$ channelopathy distinct from IEM. It is characterized by intolerable pain localized to the rectum, ocular or submandibular region that is triggered by defecating or eating. It is caused by gain-of-function mutations in domains II and III that mainly affect fast inactivation or enhance persistent, ramp and resurgent currents.[289,292] While IEM results in heat pain, PEPD is characterized by mechanical pain; these phenotypic differences have been ascribed to the fact PEPD and IEM mutations primarily impair inactivation and activation, respectively.[233] Small fibre neuropathy, characterized by burning pain in the feet and associated degeneration of small-calibre fibres, is also linked to $Na_V1.7$ mutations, with ~30% of idiopathic SFN patients carrying gain-of-function $Na_V1.7$ mutations.[290] Recently, genetic analysis of a deeply phenotyped cohort of diabetic neuropathy patients found 12 rare $Na_V1.7$ variants in 10 of the 111 patients reporting pain, but no variants in the 78 patients without pain. Five of these variants had previously been characterized for small fibre neuropathy.[298] Taken together, these genetic studies support a critical role for $Na_V1.7$ in nociception in humans, with multifarious mutations either enhancing or eliminating pain.

3.2.2 Mouse models of congenital insensitivity to pain

$Na_V1.7$ was first cloned and identified as a peripheral sodium channel, enriched in trigeminal, dorsal root and sympathetic ganglia, with little expression in brain.[299] $Na_V1.7$ is highly expressed in peripheral sensory neurons of all sizes, in rodents, humans and other primates.[292] In guinea pig, intracellular recording followed by subsequent dye injection and immunolabelling of sensory neurons confirms $Na_V1.7$ is expressed in all C fibre

nociceptors and most A delta nociceptors.[300] Importantly, $Na_V1.7$ is found all along the length of the nociceptor, at high levels in the soma, peripheral terminal and central terminal.[301] A recent immuno-EM study also found small numbers of $Na_V1.7$ particles in post-synaptic dorsal horn neurons.[302] $Na_V1.7$ is additionally expressed by olfactory sensory neurons, but not in the post-synaptic mitral cells.[303,263] In rodents, $Na_V1.7$ is detected in pituitary gland, subfornical organ, and hypothalamic nuclei.[304] Interestingly, $Na_V1.7$ ensures near-perfect synaptic integration in hypothalamic neurons controlling energy regulation; its deletion in different cell types bidirectionally modulates feeding and weight gain in mice.[305] In primates, however, $Na_V1.7$ is very weakly expressed in hypothalamic nuclei and other brain sites.[306] This is consistent with no reports of CNS deficits in human null mutants, including appetite. Because $Na_V1.7$ shows relatively selective expression in the periphery, it is the loss of $Na_V1.7$ in nociceptors that likely leads to pain insensitivity.

This hypothesis is supported by the finding that conditional knockout of *Scn9a* in the peripheral sensory neurons of mice largely recapitulates the pain insensitivity of human $Na_V1.7$ null mutants. The acute pain phenotypes of the various conditional $Na_V1.7$ knockout mouse lines are summarized in **Table 3-1**, accompanied by the global KO line for comparison. The first of these lines was published in 2004, before the mapping of human null mutations.[265] LoxP sites were inserted into introns flanking exon 14 and 15 of SCN9A which encode most of domain II of $Na_V1.7$. These animals were crossed to mice where Cre was knocked in to the *Scn10a* locus, leading to Cre-dependent deletion of $Na_V1.7$ in the subset of nociceptors expressing $Na_V1.8$ ($Na_V1.7$ $KO^{1.8}$)[72] These mice exhibited impaired mechanical and inflammatory pain, but heat nociception on the Hargreaves' apparatus was spared. When $Na_V1.7$ was deleted in all sensory neurons using Advillin-Cre ($Na_V1.7$ KO^{Adv}), the mice were hyposensitive on the Hargreaves' apparatus, indicating $Na_V1.7$ is required in distinct subsets of sensory neurons for different pain modalities.[257] Notably, no hot plate phenotype was apparent in either sensory neuron KO line. In contrast, in Wnt1-Cre $Na_V1.7$ knockouts ($Na_V1.7$ KO^{Wnt}), mice did not respond at all on the hot plate test, typically going to cut-off. Wnt1-Cre is expressed in all neural crest-derived neurons, including sympathetic ganglia that are normally enriched with $Na_V1.7$. Sympathectomy of Advillin-Cre $Na_V1.7$ KO mice made the animals insensitive on the hot plate test, suggesting deletion of $Na_V1.7$ in sympathetic neurons is required for impaired hot plate behaviour. Different chronic pain models showed a unique dependence on $Na_V1.7$ in distinct cell types, and some forms of chronic pain were spared

in all KO lines.[307] This is consistent with the human literature with one report of neuropathic pain developing in a $Na_V1.7$ null mutant in adulthood.[308]

Modality		**Test**	**$Na_V1.8$-Cre** 257,265,309	**Advillin-Cre** 257,261,309,310	**Wnt1-Cre** 257,309–311	**Global** 312
Acute:	**Heat:**	**Hargreaves' Apparatus:**	—	↓	↓	
		Hot Plate (50 °C & 55 °C):	—	—	↓	↓
	Mechanical:	**Randall-Selitto (tail):**	↓	↓	↓	↓ (tail clip)
		Randall-Selitto (paw):	—	—	—	
		Von Frey Hairs (paw):	—	—	—	
		Von Frey Hairs (abdomen):	—	↓	↓	
	Cold:	**Acetone:**	—	↓	↓	
		Thermal Place Preference (Cold):	—	—	—	
		Thermal Place Preference (Cool):		↓		
Sensitized	**Heat Hyperalgesia:**	**Complete Freund's Adjuvant:**	↓			↓
		Carageenan:	↓			
		Nerve Growth Factor:	↓			
	Mechanical Allodynia:	**Complete Freund's Adjuvant:**	↓	↓	↓	
		Formalin:	↓	↓	↓	↓

Table 3-1. Behaviorual phenotypes of conditional $Na_V1.7$ knockout mice.

The symbol ↓ denotes hyposensitivity and the symbol — denotes no change. The cell is left blank where the behavioural assay was not tested.

Initial efforts to establish a global $Na_V1.7$ knockout mouse foundered due to the death of pups shortly after birth, which was unexpected given that human *SCN9A* null mutations are non-lethal. It turned out this was due to anosmia in these animals leading to failure to feed.[265] Subsequent studies showed human $Na_V1.7$ null mutants are also anosmic and that conditional deletion of $Na_V1.7$ in olfactory sensory neurons caused anosmia in mice.[263] Hand-rearing of global $Na_V1.7$ knockout mice circumvented the deficits in olfactory-guided feeding. In adulthood, these mice were profoundly hyposensitive to noxious mechanical, thermal, chemical and inflammatory stimuli, but with no touch or motor deficits.[312] Genenetch later generated a mouse where $Na_V1.7$ was deleted in adulhthood using a tamoxifen-inducible global CreERT2. These animals showed similar phenotypes to global knockouts, confirming analgesia does not arise from developmental effects.[313] Recently, a $Na_V1.7$ knockout rat has been described that shows deficient thermal, chemical and neuropathic pain.[314] For the most part, these three global knockout lines recapitulate the phenotype of the KO^{Wnt} mouse, indicating that while loss of $Na_V1.7$ in sensory neurons is the main driver of analgesia, deletion of $Na_V1.7$ in the sympathetic system is also required.' Collectively, behavioural analysis of transgenic animals lacking $Na_V1.7$ points to $Na_V1.7$ in the periphery as being critical for nociception and the attendant pain experience.

3.2.3 Structure and pharmacology of $Na_V1.7$

Hundreds of millions of dollars have been invested in developing inhibitors of $Na_V1.7$ to treat chronic pain. Development of sodium channel antagonists is hampered, however, by the need for subtype specificity, to avoid unwanted cardiac or CNS side effects. This is made difficult by the high sequence similarity of different sodium channel isoforms, with 53-88% of amino acid residues shared between any two alpha subunit sequences.[292] The sodium channel alpha subunit was first cloned in the 1980s and consists of a single polypeptide chain folded into four homologous domains linked by intracellular loops.[315] Each domain has six transmembrane segments with S1-S4 forming the voltage-sensing domain and S5-S6 the pore domain. Voltage-gating depends on the presence of conserved positively charged amino acids at every third position in the S4 helices, with membrane potential changes moving these gating charges to cause conformational changes and opening of the channel.[316] In recent years, the solving of crystal structures for both bacterial and eukaryotic sodium channels has greatly enhanced our understanding of

sodium channel structure and function.[317–319] In 2019, two CryoEM of structures of $Na_V1.7$ were published, which will likely aid the rational design of channel inhibitors.[320,321]

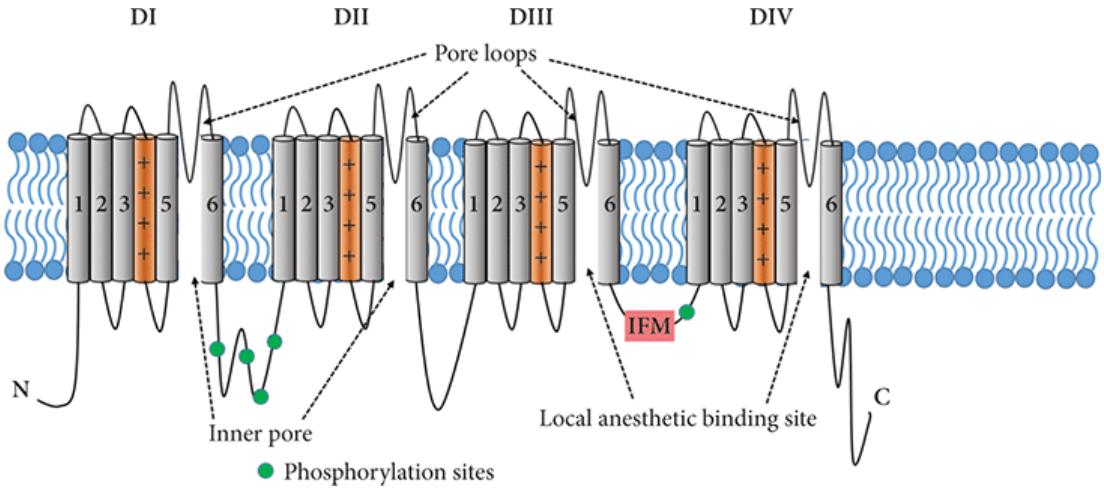

Figure 3.2 (*adapted from ref. 322*). Secondary structure of mammalin voltage-gated sodium channel.

$Na_V1.7$ inhibitors can broadly be classed as either pore blockers or gating modulators. Classical non-specific sodium channel inhibitors bind to the pore region of the channel, either extracellularly in the case of TTX, or in intracellularly in the case of local anesthetics like lidocaine. Lidocaine was developed in the 1940s by Swedish scientists and revolutionized surgery, but has also proved useful as a painkiller in both acute and neuropathic pain, highlighting the potential of sodium channels as analgesic targets.[322,323] Because the pore domain is highly conserved between alpha subunit isoforms, it is difficult to achieve subtype specificity with pore blockers. The channel domains controlling voltage-gating show greater sequence divergence, and are thus the target of most $Na_V1.7$ inhibitors currently under active investigation. One pore blocker, vixotrigine, originally thought to be $Na_V1.7$ specific, is now widely considered non-selective and has failed in clinical trials for several forms of chronic pain[258,324] It is important to note that both pre-clinical and human data support the idea that $Na_V1.7$-independent forms of chronic pain exist – the choice of chronic pain condition to test compounds on is thus of crucial importance.[307,308]

The earliest reported truly selective blockers of $Na_V1.7$ were animal toxins. For example, ProTxII is a tarantula venom peptide identified by Merck. Despite showing potent and 85-fold selective inhibition of $Na_V1.7$ in electrophysiological assays, as well as block of action potential propagation in nociceptors, neither intrathecal nor intravenous

dosing of this peptide was analgesic for inflammatory pain.[325] Lack of efficacy was blamed on the slow on-rate and poor perineurium penetration of this drug, illustrating the importance of pharmaco-kinetic and –dynamic profile. Peptide selectivity depended on a residue close to the extracellular loop of S3 in domain II – the so-called paddle motif.[119] However, substantial inhibition of $Na_V1.7$ in the absence of effects at other isoforms could not be achieved, and higher doses of the drug were lethal. A new generation of venom peptides have improved on this narrow therapeutic index. Like ProTxII, these toxins trap the voltage sensing domain of $Na_V1.7$ in a closed configuration thus inhibiting activation of the channel. The tarantula peptide Pn3a showed 40-1000fold selectivity and reduced TTX-sensitive currents in small diameter DRG neurons. Although analgesic in a mouse model of pain induced by activation of $Na_V1.7$, there was no effect in inflammatory pain models after systemic administration, except when delivered with subtherapeutic doses of opioids.[326] Somewhat perplexingly, the same group later found that the compound alone was sufficient to relieve pain in a mouse model of acute postsurgical pain.[327]

Among small molecule inhibitors of $Na_V1.7$, the aryl sulphonamides have been extensively studied. These drugs bind preferentially to the slow inactivated state, shown by structural studies to prevent recovery from inactivation, and demonstrate good target engagement *in vitro*.[328,329] In a particularly elegant study, Waxman generated iPSCs from four IEM patients with different $Na_V1.7$ mutations. Hyper-excitability was evident in nociceptors differentiated from these iPSCs and aggravated by warming. The aryl sulfonamide $Na_V1.7$ blocker PF-05089771 ameliorated hyperexcitability in the dish and caused a modest reduction in heat-evoked pain in most of the patients.[330] However, this same drug failed to meet its pre-determined efficacy criteria in a trial for diabetic neuropathy, and also did not modify pain thresholds in healthy volunteers.[331,332] Because of the preference for the slow inactivated state, these drugs may not be able to bind and inhibit sufficient numbers of channels *in vivo*. Bafflingly, there is no published data of PF-05089771 eliciting analgesia in animal models; notwithstanding this, it was brought forward to human testing on the basis of the genetic data.[292] A similar compound PF-04856264 failed to elicit analgesia in inflammatory pain in mice, despite inhibiting pain evoked by selective activators of $Na_V1.7$.[326,333] Recently, a humanized mouse expressing human $Na_V1.7$ with the IEM mutation I848T was developed and sodium activator-induced pain was used as a target engagement assay to test a new generation of $Na_V1.7$-selective acyl sulphonamides: GX-201 and GX-585. These compounds show longer

residence time at the receptor than the aryl sulphonamides, but bind to the same voltage sensor domain 4. As well as blocking pain driven by sodium channel activation, these compounds ameliorated inflammatory and neuropathic pain in mice.[334] Although this analgesic efficacy was reproduced in a separate study, time will tell if these GX-201 or GX-585 prove efficacious in humans.[313]

Drug candidate	Sponsor	Modality	Development status
PF-05089771	Pfizer	Small-molecule inhibitor	Discontinued in 2015 after failed phase II trial in painful diabetic peripheral neuropathy
TV-45070	Teva/Xenon	Small-molecule inhibitor	Discontinued in 2017 after failed phase II trial in post-herpetic neuralgia
RG-6029/GDC-0310	Roche/Genentech/Xenon	Small-molecule inhibitor	Discontinued in 2018 prior to phase II initiation
Vixotrigine	Biogen	Small-molecule inhibitor	Discontinued in painful lumbosacral radiculopathy after phase II failure in 2018; phase III trial planned in trigeminal neuralgia; phase II trial ongoing in small fibre neuropathy
BIIB-095	Biogen	Small-molecule inhibitor	Phase I trial for neuropathic pain ongoing
ST-2427	SiteOne	Small-molecule inhibitor	IND for post-operative pain
AM-6120, AM-8145 and AM-0422	Amgen	Peptide derived from tarantula venom	Discovery
Nav1.7-targeted mAb	Shionogi	mAb	Discovery
VY-NAV-01	Voyager Therapeutics	Gene therapy Nav1.7 knockdown	Discovery

Table 3-2 (*adapted from ref. 258*). Selected $Na_V1.7$ inhibitors currently and formerly in development.

As we have seen, numerous purportedly $Na_V1.7$-selective drugs have been tested in both pre-clinical models and human clinical trials. **Table 3-2** summarizes the litany of failures. Despite the enormous investment in this target, why the lack of success? In other words, why does inhibition of $Na_V1.7$ fail to recapitulate the consequences of functional deletion of the channel? A number of explanations have been highlighted here. Doubtless $Na_V1.7$ is not particularly druggable, with selectivity and bioavailability remaining key

challenges. Many compounds also show a preference for particular states of the channel, which may not translate into the required channel occupancy *in vivo*. Importantly, there is no consensus about the mechanism by which loss of $Na_V1.7$ gives rise to pain insensitivity. Without a good mechanistic understanding of analgesia in $Na_V1.7$ null mutants rooted in preclinical research, I would argue that drug development is but shooting in the dark.

3.2.4 Mechanisms of analgesia in $Na_V1.7$ null mutants

Because pharmacological inhibition of $Na_V1.7$ fails to recapitulate the effects of gene deletion, understanding how exactly loss of $Na_V1.7$ leads to pain insensitivity is thus of critical importance to developing better therapies targeting the channel. Four major mechanisms have been proposed to account for absent pain in $Na_V1.7$ null mutants: reduced excitability or silencing of peripheral terminals, absent intra-epidermal nerve fibres, impaired synaptic transfer at central terminals, and enhanced endogenous opioid signalling. Evidence can be found to support any of these mechanisms – they are not necessarily mutually-exclusive and may act in concert to drive analgesia.

Given the biophysical properties of the channel, $Na_V1.7$ is proposed to control action potential initiation in peripheral nociceptors. Because $Na_V1.7$ exhibits slow closed-state inactivation, the channel is less likely to inactivate during sub-threshold depolarizations and mediates a ramp current thought to function as an amplifier of generator potentials at nociceptor peripheral terminals.[335] In patch-clamp studies of cultured mouse sensory neurons and human iPSC-derived nociceptors, $Na_V1.7$ deletion impairs action potential firing upon depolarization of the soma.[284,313,336] FGF13 is required for heat nociception because it ensures $Na_V1.7$ is available in the membrane for sustained heat-evoked action potential firing.[337] Hence the prevailing hypothesis – and rationale for developing peripherally-targeted inhibitors – is that analgesia after $Na_V1.7$ loss-of-function arises from reduced excitability of the nociceptor peripheral terminal. This was borne out by microneurographic recording of superficial peroneal nerve from three human null mutants, which found no evidence of C fibre nociceptors, based on activity-dependent slowing profiles (but not on the response to noxious stimuli). [284] Similar results were obtained in KO^{Adv} mice through recording of compound action potentials.[338] However, equating nociceptors with C fibres is problematic; nociceptors are defined by their ability to respond to and encode noxious stimuli.[7]

A provocative explanation for the apparent lack of C fibres is that $Na_V1.7$ null mutations lead to retraction of peripheral axons so that terminals at not physically present

for the transduction of noxious stimuli into action potentials. Skin biopsy of three null mutant patients showed markedly reduced or absent intra epidermal fibre density (IEFD) in the distal leg and thigh, indicative of a small fibre pathology.[284] Two other studies have reported reduced IEFD.[339,340] This contrasts with the original description of $Na_V1.7$ null mutants, which were distinguished from the HSAN disorders based on the absence of neuropathy.[5] Interestingly, both global $Na_V1.7$ KO mice and rats show normal IEDF, suggesting a species difference.[312,314] But is decreased IEFD actually causal for analgesia? This would seem incompatible with $Na_V1.7$ inhibitors causing analgesia acutely in animals. An alternative explanation might be that reduced nociceptor activity throughout life causes the reduction of peripheral terminals. Evidence for this comes from a three year old boy with $Na_V1.7$ loss of function who had normal sensory nerve conductions and IEFD.[341]

$Na_V1.7$ is expressed along the entire length of the nociceptor, including at the central terminals in the spinal cord. [301] Although nociceptors are peripheral neurons, these central terminals actually extend beyond the blood brain barrier into the CNS. Importantly, spinal cord wide dynamic range neurons show less stimulus-evoked activity in mice lacking $Na_V1.7$ in sensory neurons, implying a reduction of nociceptive input to the CNS.[257] Although this could be due to the aforementioned peripheral silencing, an alternative hypothesis is that the signal is lost due a deficit in synaptic transfer from the central terminal to second order spinal cord neurons. Substance P release is completely abolished in $Na_V1.7$ KOs, while application of $Na_V1.7$ inhibitors to spinal cord slices reduces synaptic transmission from afferents.[257,326,329] This is analogous to the role of $Na_V1.7$ in olfactory sensory neurons (OSNs) – OSN-specific deletion of $Na_V1.7$ completely abolishes synaptic transfer from OSN presynaptic terminals to postsynaptic mitral cells, although somatic excitability to odorant stimuli is normal.[263]

Analgesia in mice and humans lacking $Na_V1.7$ can be reversed by opioid antagonists or opioid receptor deletion, indicating the endogenous opioid system is essential to the maintenance of pain insensitivity.[261,311] This results from both enhanced PENK production and opioid receptor function.[261,342] Case reports of unmapped CIP patients support a contribution of the opioid system to analgesia, while non-specific sodium channel blockers show synergistic analgesia when paired with opioid drugs.[343,344] A snag in this hypothesis lies in the fact that deletion of the transcription factor NFAT5 leads to elevated *Penk* message, but without corresponding analgesia.[311] Enhanced opioid receptor signalling, and not elevated opioid tone, may thus be the predominant

mechanism triggering analgesia in $Na_V1.7$ KO mice.[342] This is consistent with recent observations that peptide antagonists of $Na_V1.7$ elicit analgesia in mice that is reversed by naloxone, and which synergizes with low dose opioids.[326,327]

Which mechanism of analgesia proves correct will raise important questions about how to optimally design analgesics targeted against $Na_V1.7$. Existing strategies implicitly assume that $Na_V1.7$ is required for electrogenesis in peripheral terminals, and that acute, peripherally-targeted block should be sufficient to reduce pain. But for how long does $Na_V1.7$ need to be inhibited? If reduced IEFD is required for analgesia, short-lasting channel blockade is unlikely to be sufficient. Where along the nociceptor does the blocker need to act? If the locus of analgesia is the central terminal, then blood brain barrier penetrant antagonists are needed to block the $Na_V1.7$ channels that control synaptic transfer And what proportion of channels need to be blocked to relieve pain? If the opioid hypothesis turns out to be accurate, close to 100% channel block may be required, and alternate approaches such as gene therapy might need to be pursued.[345]

3.2.5 Aims

The goal of this work is to determine the pathophysiological mechanism driving analgesia in individuals with $Na_V1.7$ loss-of-function mutations. The conditional $Na_V1.7$ KO 'mouse model' of CIP is ideally suited to mechanistic investigations of $Na_V1.7$ loss-of-function that link genotype to phenotype. To determine the mechanism of analgesia in $Na_V1.7$ null mutants, I used complementary optical, electrophysiological and pharmacological methods to study nociceptor function *in vivo* in mice and humans lacking $Na_V1.7$.

3.3 Results

3.3.1 Peripheral knockout of $Na_V1.7$ decreases pain sensitivity

I used a genetic strategy to conditionally delete *Scn9a* in peripheral sensory neurons of mice, encompassing nociceptors, the presumed locus of analgesia in $Na_V1.7$ null mutants. As previously reported, Advillin-Cre or Wnt1-Cre was used to excise the floxed *Scn9a* allele, resulting in knockout of $Na_V1.7$ restricted, respectively, to sensory neurons or to neural crest-derived neurons. I performed whole-cell voltage-clamp recordings of voltage-gated sodium currents in cultured sensory neurons from control animals homozygous for the floxed $Na_V1.7$ allele, here called wild-type (WT). Application of the $Na_V1.7$-specific antagonist PF-05089771 (PF-771, 100 nM for 5 minutes) showed that ~50% of the peak sodium current in medium diameter nociceptor-like neurons can be attributed to $Na_V1.7$ (**Figure 3.3A&B**).[329] In contrast, PF-771 did not markedly affect voltage-gated sodium currents recorded in sensory neurons from either Advillin-Cre $Na_V1.7$ knockout (KO^{Adv}) or Wnt1-Cre $Na_V1.7$ knockout (KO^{Wnt}) mice, confirming functional loss of the channel (**Figure 3.3C&D)**.

Next, I performed blinded behavioural testing on these animals across a battery of nociceptive assays for different modalities. KO animals showed increased withdrawal thresholds to noxious mechanical stimuli assessed using the Randall-Selitto apparatus on the tail, with the mean WT value of 176 ± 14.3 g doubling to 393.3 ± 26.8 g in KO^{Wnt} and 352.1 ± 30.4 g in KO^{Adv} animals (**Figure 3.4A**). The response to punctate mechanical stimuli on the Von Frey Test was unaltered (**Figure 3.4B**). Using the Hargreaves' assay for heat nociception, the WT mean withdrawal latency was 13.06 ± 1.29 s, which was increased to 21.21 ± 1.31 s in the KO^{Adv} and 23.34 ± 2.37 s in the KO^{Wnt} line (**Figure 3.4C**). Lastly, using the Cold Plantar (i.e. 'dry ice') test, I found no significant effect of deleting $Na_V1.7$ on withdrawal latency to cooling **(Figure 3.4D**). Thus, as previously reported and in common with human $Na_V1.7$ null mutants, I found both lines of conditional $Na_V1.7$ KOs exhibit a profound analgesic phenotype for heat and mechanical pain, with no change in tactile or cold sensitivity.

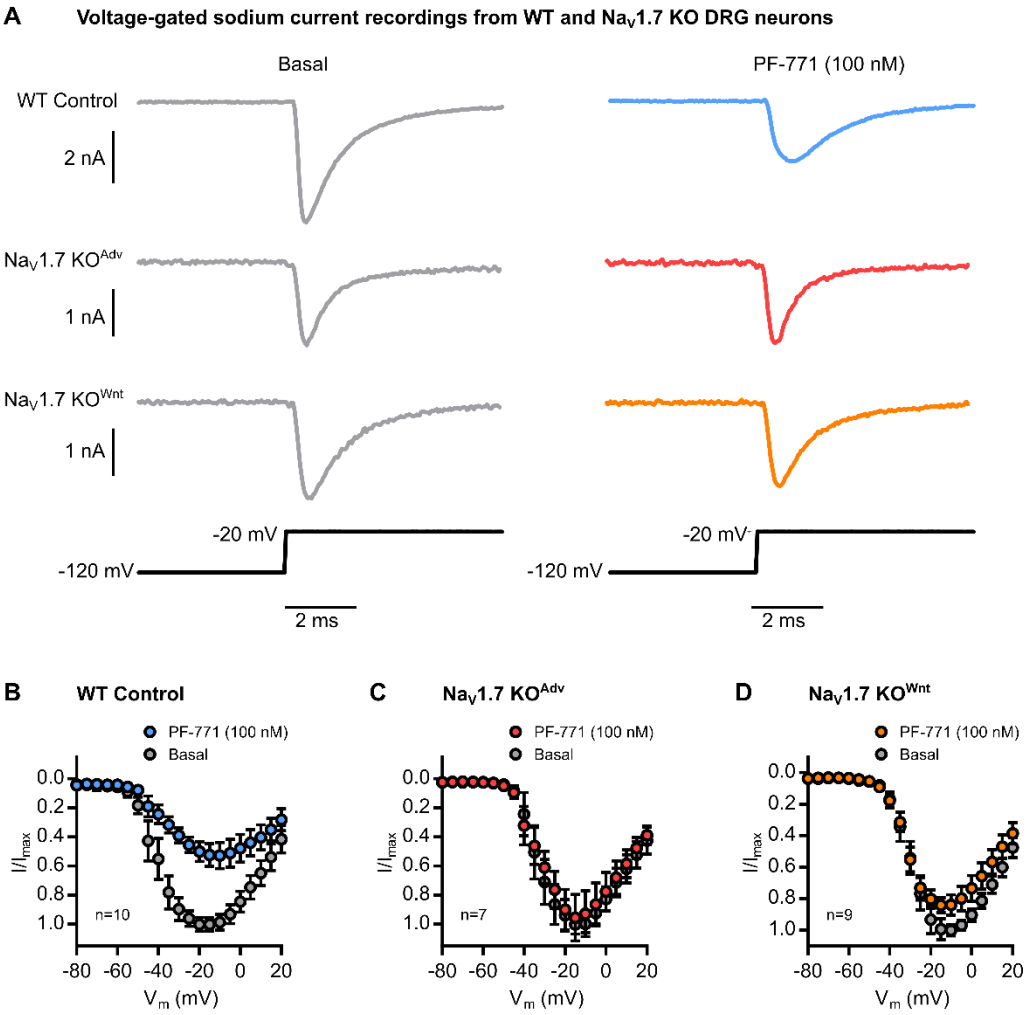

Figure 3.3. Conditional deletion of *SCN9A* in sensory neurons abolishes voltage-gated sodium currents attributed to Nav1.7.

(A) Example current traces showing voltage-gated sodium currents activated by a 100 mV voltage-step from -120 mV to 20 mV recorded from WT and Nav1.7 KO DRG neurons (grey). Application of the Nav1.7-specific antagonist PF-05089771 (PF-771, 100 nM for 5 minutes) caused a marked reduction in sodium currents in WT neurons (blue) but not in cells from KO^{Adv} (red) or KO^{Wnt} (orange) mice.

(C) Current-voltage (I-V) curve showing that application of the Nav1.7-specific antagonist PF-771 reduces voltage-gated sodium currents in WT sensory neurons. n=10 cells.

(C) I-V curve showing PF-771 did not markedly affect voltage-gated sodium currents in sensory neurons from Nav1.7 KO^{Adv} mice. n=7 cells.

(D) I-V curve showing PF-771 did not markedly affect voltage-gated sodium currents in sensory neurons from Nav1.7 KO^{Wnt} mice. n=9 cells.

Error bars denote standard error of the mean.

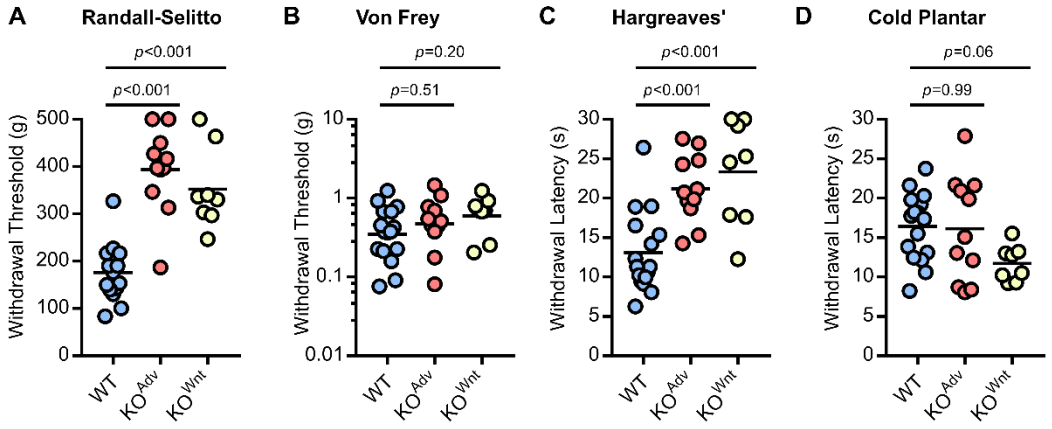

Figure 3.4. Peripheral $Na_V1.7$ knockout mice show reduced pain sensitivity

(A) Both $Na_V1.7$ KO lines show increased withdrawal thresholds to noxious mechanical stimuli on the Randall-Selitto test.

(B) $Na_V1.7$ deletion has no effect on withdrawal thresholds to punctate tactile stimuli on the Von Frey test

(C) Both $Na_V1.7$ KO lines show increased withdrawal latencies to radiant heat stimuli on the Hargreaves' test.

(D) $Na_V1.7$ KO^{Adv} show unchanged withdrawal latencies to dry ice stimuli on the Cold Plantar test compared to control, however $Na_V1.7$ KO^{Wnt} display a small, but insignificant, hypersensitivity.

For (A) to (D), means for each KO line were compared to WT control using One-Way ANOVA followed by post-hoc Dunnett's test. n=16 mice for WT, n=11 mice for KO^{Adv} and N=8 mice for KO^{Wnt}.

3.3.2 Deletion of $Na_V1.7$ in sensory neurons does not silence nociceptors

Given the purported role of $Na_V1.7$ in action potential generation, the pain insensitivity of $Na_V1.7$ KO mice may reflect reduced excitability or silencing of peripheral nociceptors. To test the hypothesis that $Na_V1.7$ deletion renders nociceptors hypo- or inexcitable, I monitored the responses of peripheral sensory neurons to noxious stimulation using *in vivo* calcium imaging.[245] First, I generated conditional $Na_V1.7$ KO and WT mice on a Pirt-GCaMP3 background, where GCaMP3 is knocked in at the Pirt locus resulting in calcium indicator expression in all peripheral sensory neurons.[253] Using laser-scanning confocal microscopy, I imaged calcium signals in sensory neuron somata within the dorsal root ganglia of live animals (**Figure 3.5A**). Interestingly, $Na_V1.7$-deficient sensory neurons readily responded to all noxious stimuli applied to the hindpaw (**Figure 3.5B** & **Figure 3.6).** I classified responding neurons into functionally-defined cells types. Every cell type was present in both WT and KO animals, but differences were apparent in the distribution of responses (**Figure 3.5C**). Fewer cells responded to noxious pinch in KO^{Adv} (44/197, 22%) and KO^{Wnt} (70/262, 27%) compared to WT (206/516, 40%). I observed additional cold-sensing neurons in KO^{Adv} (73/197, 37%) and KO^{Wnt} (117/262, 45%) versus WT (132/516, 26%). Importantly, the relative number of cells responding to noxious heat was not consistently altered between WT (234/516, 45%), KO^{Adv} (95/197, 48%) and KO^{Wnt} (88/262, 34%) lines, despite behavioural insensitivity to heat. I wondered whether classical polymodal nociceptors were silenced by loss of $Na_V1.7$, here defined as pinch-sensitive cells that also respond to thermal stimuli. Polymodality did not differ between genotypes and was similar to previous reports, with 21% of WT, 25% of KO^{Adv} and 16% of KO^{Wnt} neurons categorized as polymodal (**Figure 3.5D**).[46,55,245,248] Finally, I measured the peak calcium signal ($\Delta F/F_0$) as a surrogate measure of single neuron excitability. Interestingly, when I quantified this for each stimulus type, there was no effect of $Na_V1.7$ deletion on the maximum calcium response (**Figure 3.5E**). Overall, although the distribution of cold and mechanical responses was altered, I found little evidence using calcium imaging of decreased nociceptor excitability in animals lacking $Na_V1.7$, with no change in peak response magnitude to any stimulus, prevalence of polymodality or number of noxious heat responses.

As a further corroboration, I imaged sensory neuron responses in WT and KO^{Adv} mice virally expressing GCaMP6f. AAV1-CAG-GCaMP6f virus was delivered by intraperitoneal injection at P2, as this route of administration results in preferential expression in peripheral afferents.[160] In adulthood, GCaMP6f expression was detectable

in sensory neurons of all sizes (**Figure 3.7A**). Neurons were again classified into functionally-defined cell types, all of which were present in the KO^{Adv} animals (**Figure 3.7B**). Note that cold-responsive cells were few in number in both genotypes, presumably because viral GCaMP6f targets different sets of sensory neurons to the Pirt-GCaMP3 mouse line. There were however no significant differences in the distribution of cell types between genotypes. The degree of polymodality was not noticeably affected by $Na_V1.7$ deletion, with 18% of WT and 24% of KO^{Adv} neurons classed as polymodal (**Figure 3.7C**). Lastly, quantification of the peak response magnitude ($\Delta F/F_0$) for each stimulus modality revealed no change due to loss of $Na_V1.7$ (**Figure 3.7D**). Thus, using a different GCaMP delivered to sensory neurons through a different expression strategy, I again find no major effect of $Na_V1.7$ deletion on peripheral nociceptor excitability.

While calcium imaging is ideally suited to monitoring population activity, it cannot directly measure action potential firing. This method may not be sensitive to subtler effects of $Na_V1.7$ deletion on excitability. My colleague Dr Shafaq Sikandar with Dr Ana Luiz therefore performed multi-unit extracellular recordings from dorsal root ganglia of live $Na_V1.7$ KO and WT animals. To analyse these experiments, we pooled data obtained from both KO^{Adv} and KO^{Wnt} lines, quantifying the number of action potentials fired in 10 seconds by presumptive polymodal nociceptors to peripheral stimuli of various modalities (**Figure 6.1A**). Firing evoked by noxious mechanical prodding was unchanged after deletion of $Na_V1.7$ (**Figure 6.1B**). Intriguingly, although firing in response to most von Frey stimuli was normal, that evoked by the 8, 15 and 26 g gram hairs showed a small reduction (**Figure 6.1C**). This is in spite of the normal hind-paw von Frey thresholds of $Na_V1.7$ KO mice (see **Figure 3.4B**). As expected, innocuous brush stimuli evoked action potentials equally well in WT and KO animals (**Figure 6.1D**). There was no appreciable change in the number of spikes triggered by ice water (**Figure 6.1E**) or noxious heat stimuli (**Figure 6.1F**). Taken together, these electrophysiology data corroborate that diminished sensitivity of $Na_V1.7$ KO mice to noxious heat or mechanical stimuli cannot be explained by decreased peripheral nociceptor excitability.

The foregoing experiments focussed on sensory neuron responses to acute noxious stimuli. Of particular clinical interest, however, is the fact $Na_V1.7$ null mutant humans and mice show deficient pain sensitization. Prostaglandin E2 (PGE2) is an important inflammatory mediator and potent pro-algesic.[245] To investigate the mechanism by which $Na_V1.7$ deletion impedes pain sensitization, I compared the effect of intraplantar injection of PGE2 (500 μM for 10 minutes) on whole-animal behavioural versus sensory

neuron calcium responses to noxious heat stimuli, *in vivo* (**Figure 3.8A**). First, I assessed the impact of PGE2 on heat withdrawal latencies using the Hargreaves apparatus (**Figure 3.8B**). In WT mice, PGE2 reduced withdrawal latency from 11.4 ± 0.7 s to 4.6 ± 0.7 s, but saline had no effect. In contrast, both lines of conditional $Na_V1.7$ KO mice failed to develop heat hyperalgesia after PGE2. In KO^{Adv} animals, withdrawal latency was 20.1 ± 1.6 s at baseline and 16.7 ± 2.2 s after PGE2, but this difference was not significant. In KO^{Wnt} animals, withdrawal latency was 21.0 ± 2.6 s at baseline and 20.4 ± 4.0 s following PGE2 treatment. In parallel imaging experiments, intraplantar injection of PGE2 unmasked silent nociceptors and increased heat responses in both WT and KO^{Adv} animals virally expressing GCaMP6f, indicating this form of peripheral sensitization is intact in mice lacking $Na_V1.7$ (**Figure 3.8C**). I also observed robust sensitizing effects of PGE2 in KO^{Wnt} animals expressing GCaMP3, although the number of silent nociceptors awoken was slightly less than WT (**Figure 3.8D**). $Na_V1.7$ deletion therefore impairs heat hyperalgesia but paradoxically does not abolish its physiological correlate: peripheral sensitization of nociceptors.

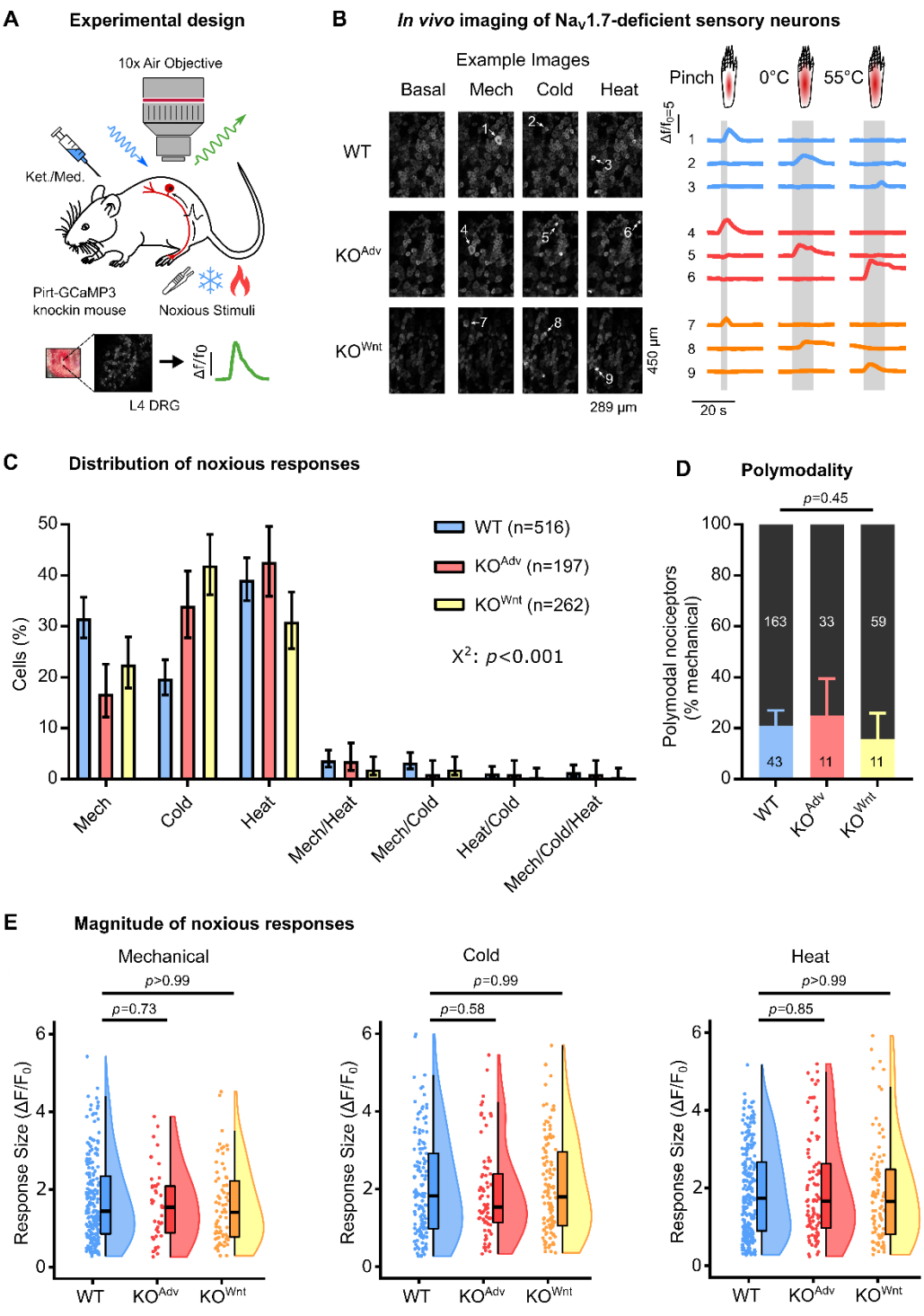
A
Experimental design
10x Air Objective
Ket./Med.
Pirt-GCaMP3
knockin mouse
Noxious Stimuli
L4 DRG
Δf/fo
B
In vivo imaging of NaV1.7-deficient sensory neurons
Example Images
Basal
Mech
Cold
Heat
WT
KOAdv
KOWnt
450 µm
289 µm
Pinch
0°C
55°C
Δf/f0=5
20 s
C
Distribution of noxious responses
Cells (%)
WT (n=516)
KOAdv (n=197)
KOWnt (n=262)
X2: p<0.001
Mech
Cold
Heat
Mech/Heat
Mech/Cold
Heat/Cold
Mech/Cold/Heat
D
Polymodality
p=0.45
Polymodal nociceptors (% mechanical)
163
33
59
43
11
11
WT
KOAdv
KOWnt
E
Magnitude of noxious responses
Mechanical
p>0.99
p=0.73
Cold
p=0.99
p=0.58
Heat
p>0.99
p=0.85
Response Size (ΔF/F0)
WT
KOAdv
KOWnt

Figure 3.5. $Na_V1.7$-deficient sensory neurons respond to noxious stimuli at the level of the soma, *in vivo*

(A) Schematic of *in vivo* dorsal root ganglion imaging setup.

(B) Example images and traces showing sensory neurons respond to noxious mechanical and thermal stimuli in WT and both $Na_V1.7$ KO mouse lines. Each numbered trace corresponds to one cell. The data in this figure were obtained from 19 WT, 8 KO^{Adv} and 11 KO^{Wnt} animals.

(C) Bar plot summarizing the distribution of all sensory neurons that responded to different noxious stimuli in WT and $Na_V1.7$ KO animals. The error bars represent 95% confidence intervals and proportions were compared using Chi-Square test. n=516 cells from WT (blue), n=187 cells from KO^{Adv} (red) and n=262 cells from KO^{Wnt} (yellow).

(D) Bar plot showing similar prevalence of polymodal nociceptors in WT and $Na_V1.7$ KO mice. Polymodal nociceptors are defined as pinch-sensitive neurons that respond to any noxious thermal stimulus (colour) and are expressed as a fraction of mechanically-sensitive cells (black). The error bars represent 95% confidence intervals and proportions were compared using the Chi-Square test. n=206 cells from WT, n=44 cells from KO^{Adv} and n=70 cells from KO^{Wnt}.

(E) Raincloud plots showing similar peak calcium responses ($\Delta F/F_0$) evoked by different noxious stimuli for WT and $Na_V1.7$ KO lines. Mean response magnitude of KO lines was compared to WT control using One-Way ANOVA followed by post-hoc Dunnett's test. Mechanical: n=206 cells from WT, n=44 cells from KO^{Adv} and n=70 cells from KO^{Wnt}. Cold: n=132 cells from WT, n=73 cells from KO^{Adv} and n=117 cells from KO^{Wnt}. Heat: n=234 cells from WT, n=95 cells from KO^{Adv} and n=88 cells from KO^{Wnt}.

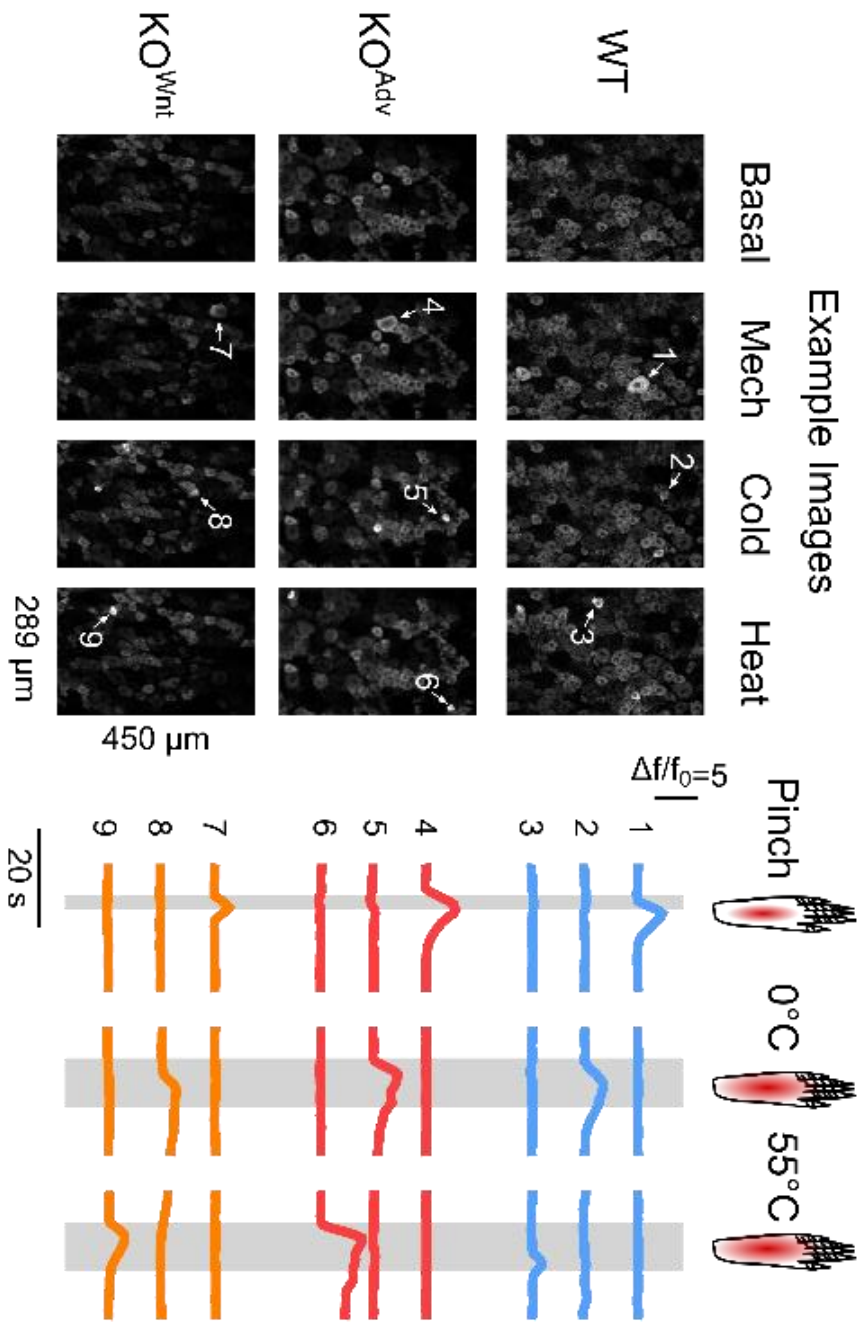

Figure 3.6. *In vivo* imaging of $Na_V1.7$-deficient sensory neurons (enlarged).

Example images and traces showing fluorescence signal in GCaMP3-expressing sensory neurons in response to noxious mechanical and thermal stimuli in WT and two $Na_V1.7$ KO mouse lines. Each numbered trace corresponds to one cell. Responses to all tested modalities are evidence in each genotype. Note using this preparation, most responses to noxious stimuli are modality-specific. The data in this figure were obtained from 19 WT, 8 KO^{Adv} and 11 KO^{Wnt} animals.

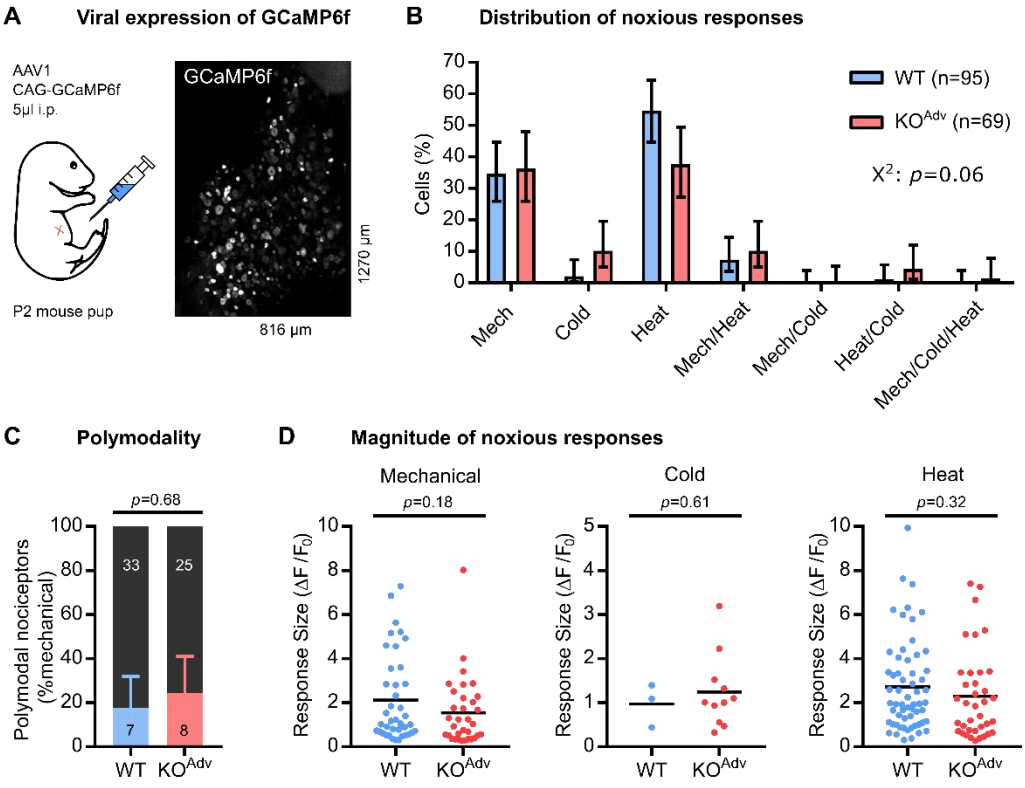

Figure 3.7. ***In vivo*** **calcium imaging of $Na_V1.7$-deficient sensory neurons virally expressing GCaMP6f**

(A) Confocal z-stack of L4 DRG *in vivo* from a $Na_V1.7$ KO^{Adv} mouse virally expressing GCaMP6f. AAV1-CAG-GCaMP6f was delivered by intraperitoneal injection into P2 mouse pups.

(B) Bar plot summarizing the distribution of all sensory neurons that responded to different noxious stimuli in WT and KO^{Adv} animals. The error bars represent 95% confidence intervals and proportions were compared using Chi-Square test. n=95 cells from 4 WT mice (blue) and n=69 cells from 4 KO^{Adv} mice (red). Markedly fewer cells responded to cold in these animals compared to in Pirt-GCaMP3 mice, likely due to biased expression of the virally-delivered GCaMP6f.

(C) Bar plot showing similar prevalence of polymodal nociceptors in WT and KO^{Adv} mice. Polymodal nociceptors are defined as pinch-sensitive neurons that respond to any noxious thermal stimulus (colour) and are expressed as a fraction of mechanically-sensitive cells (black). The error bars represent 95% confidence intervals and proportions were compared using the Chi-Square test with Yates Correction. n=40 cells from WT and n=33 cells from KO^{Adv}.

(D) Scatter plots showing similar peak calcium responses ($\Delta F/F_0$) evoked by different noxious stimuli for WT and KO^{Adv}. Mean response magnitude of KO^{Adv} was compared to WT control using an unpaired t test. Mechanical: n=40 cells from WT and n=33 cells from KO^{Adv}. Cold: n=3 cells from WT and n=11 cells from KO^{Adv}. Heat: n=60 cells from WT and n=37 cells from KO^{Adv}.

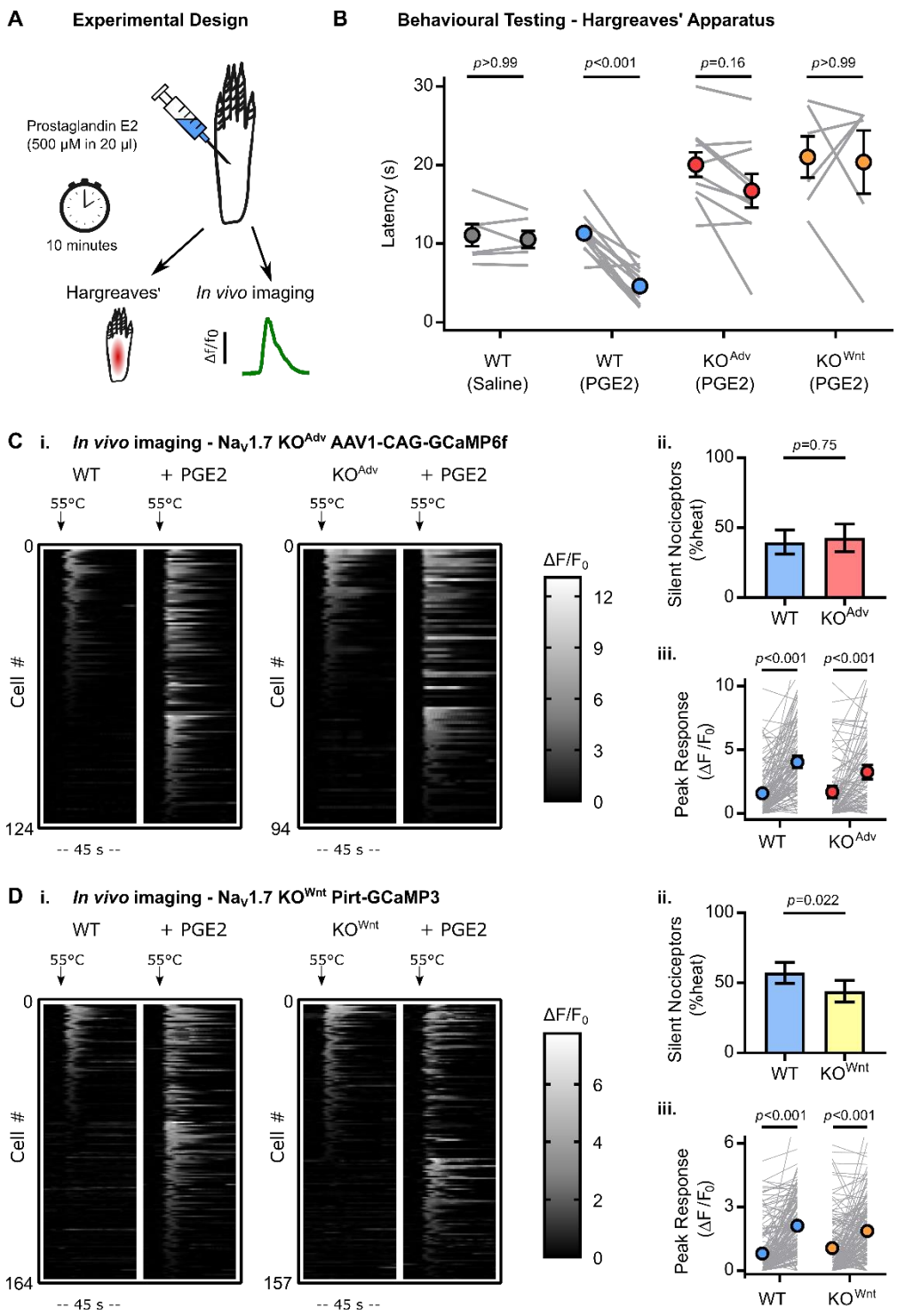
A
Experimental Design
Prostaglandin E2
(500 µM in 20 µl)
10 minutes
Hargreaves'
In vivo imaging
Δf/f0
B
Behavioural Testing - Hargreaves' Apparatus
p>0.99
p<0.001
p=0.16
p>0.99
Latency (s)
30
20
10
0
WT
(Saline)
WT
(PGE2)
KOAdv
(PGE2)
KOWnt
(PGE2)
C i. In vivo imaging - NaV1.7 KOAdv AAV1-CAG-GCaMP6f
WT
+ PGE2
KOAdv
+ PGE2
55°C
55°C
55°C
55°C
Cell #
0
124
94
-- 45 s --
ΔF/F0
12
9
6
3
0
ii.
p=0.75
Silent Nociceptors
(%heat)
100
50
0
WT
KOAdv
iii.
p<0.001
p<0.001
Peak Response
(ΔF /F0)
10
5
0
WT
KOAdv
D i. In vivo imaging - NaV1.7 KOWnt Pirt-GCaMP3
WT
+ PGE2
KOWnt
+ PGE2
55°C
55°C
55°C
55°C
Cell #
0
164
157
-- 45 s --
ΔF/F0
6
4
2
0
ii.
p=0.022
Silent Nociceptors
(%heat)
100
50
0
WT
KOWnt
iii.
p<0.001
p<0.001
Peak Response
(ΔF /F0)
6
3
0
WT
KOWnt

Figure 3.8. $Na_V1.7$ deletion abolishes inflammatory pain without affecting peripheral sensitization

(A) Schematic illustrating induction of acute inflammatory pain using PGE2.

(B) Behavioural assessment of the effect of PGE2 on Hargreaves' withdrawal latencies in WT and $Na_V1.7$ KO animals, showing KO mice do not develop heat hyperalgesia. The error bars represent standard error of the mean. Mean latencies before and after PGE2 were compared using repeated measures Two-Way ANOVA followed by post-hoc Sidak's test. n=6 animals for WT vehicle, n=12 for WT PGE2, n=10 for KO^{Adv} PGE2, and n=6 for KO^{Wnt} PGE2.

(C) Heat maps (i.) and quantification (ii. & iii.) showing unmasking of silent heat nociceptors by PGE2 in both WT and $Na_V1.7$ KO^{Adv} animals virally transduced with GCaMP6f. n=124 cells from 4 WT animals and n=94 cells from 4 KO^{Adv}. The time scale per trial is 45 seconds.

(D) Heat maps (i.) and quantification (ii. & iii.) showing unmasking of silent heat nociceptors by PGE2 in both WT and $Na_V1.7$ KO^{Wnt} animals expressing GCaMP3. n=164 cells from 8 WT animals and n=157 cells from 11 KO^{Wnt} animals.

For both (C) and (D), the effect of genotype on PGE2-induced unmasking of silent nociceptors was compared using the Chi-Square test with Yates' Correction for proportions (i.) and repeated measures Two-Way ANOVA followed by post-hoc Sidak's test for mean response size (ii.). Error bars represent 95% confidence intervals.

3.3.3 Loss of $Na_V1.7$ impairs synaptic transmission from nociceptor central terminals in the spinal cord

That nociceptor activity is little altered by $Na_V1.7$ deletion is incompatible with a mechanism of $Na_V1.7$ analgesia arising from reduced peripheral excitability. Is the loss of function occurring further upstream at the level of the nociceptor central terminal? As part of another study, my colleagues Dr Sascha Alles, Dr Filipe Nascimento and Prof. Marco Beato performed patch-clamp recordings from lamina II neurons in spinal cord slices, which receive input from afferents expressing $Na_V1.7$.[302] Cells were held at -70 mV in voltage-clamp thus excluding the contribution of post-synaptic $Na_V1.7$ and minimizing outward currents.[302] Dorsal root stimulation was used to bypass the peripheral compartment of the nociceptor and directly activate the central axons. Mono and poly-synaptic responses were evident (**Figure 6.2Ai**). When I analysed their data, I observed a substantial reduction in the prevalence of the slower polysynaptic inputs in $Na_V1.7$ KO^{Adv} animals (**Figure 6.2Aii**). When I examined spontaneous EPSCs, a measure of the summed input to the dorsal horn neuron, there was a reduction in frequency but not amplitude, consistent with impaired presynaptic release (**Figure 6.2B**). These data indicate deficient synaptic transfer at the level of the dorsal horn associated with a decrease in putative slow fibre-mediated EPSCs.

Due to the complex interneuron circuitry of the dorsal horn, it proved difficult using this dataset to isolate post-synaptic responses reflecting afferent input alone, without polysynaptic contamination. I therefore used the fluorescent glutamate sensor iGluSnFR to directly measure glutamate release from sensory afferent central terminals in spinal cord slices. Note the approach I used here measures volume glutamate transmission, not exclusively intra-synaptic transmission. First, I virally transfected cultured dorsal root ganglia neurons with iGluSnFR. iGluSnFR signal was evident on the cell membrane and along neurites (**Figure 3.9A**). Bath application of a range of glutamate concentrations confirmed the sensitivity of the probe to extracellular glutamate concentrations within the physiological range (**Figure 3.9B**). I then virally transduced sensory neurons *in vivo* with iGluSnFR by intraperitoneal injection of AAV9-synapsin-iGluSnFR virus at P2 (**Figure 3.9C**). Spinal cord slices were prepared for 2-photon imaging experiments at P9-21. In the dorsal horn, I observed iGluSnFR fluorescence in the central processes of incoming afferents, but no spinal cord cell bodies were labelled (**Figure 3.9D**). In contrast, confocal imaging showed iGluSnFR was widely expressed in

the cell bodies of sensory neurons in the dorsal root ganglion, *in vivo*, confirming the successful targeting of iGluSnFR to afferents (**Figure 3.9E**).

To image glutamate transmission in the spinal cord, dorsal root stimulation was used to evoke release from central afferent terminals expressing iGluSnFR in WT and KO^{Adv} mice (**Figure 3.10A**). I restricted my imaging of glutamate signals to layer II of the spinal cord, where nociceptor afferents terminate. Two-photon imaging at 10 Hz showed glutamate release was readily evoked across a range of single pulse stimulus intensities in dorsal horn of spinal cord slices, with iGluSnFR signals showing spatial localization to regions of interest (**Figure 3.10B** and enlarged in **Figure 3.11**). Interestingly, the mean minimum stimulus current required to elicit release in slices from KO^{Adv} animals was 891 μA, threefold greater than the control value of 279 μA (**Figure 3.10Ci**). The EC_{50} current was also reduced in the KO^{Adv} animals (**Figure 3.10Cii**). Even when perimaximal stimuli were used, the peak fluorescence change ($\Delta F/F_0$) was reduced in the KO^{Adv} slices (**Figure 3.10Ciii**). These data are consistent with a reduction in glutamate release at the central terminal of sensory neurons in $Na_V1.7$ KO^{Adv} animals due to dampened excitability of the central afferent.

Such imaging experiments allowed me to look at bulk glutamate release from afferents, however we could not resolve fast synaptic events. I thus performed linescans through identified regions of interest (~500 Hz), using a perimaximal stimulus intensity, to more closely investigate fast synaptic transmission. I used paired pulse protocols to estimate the release probability. For shorter inter pulses intervals, the slow decay kinetics of iGluSnFR (decay $t_{50\%}$=92 ms) meant individual glutamate transients overlapped.[260] I thus subtracted the signal evoked by a single pulse from the signal evoked by two pulses, giving us an estimate of the signal attributed to the second pulse. To calculate the paired pulse ratio (PPR), I divided this estimated second pulse signal by the signal elicited by one pulse (**Figure 3.12A**). In both genotypes, PPR was, as expected, lower at longer inter pulse intervals. Interestingly, I found that PPR was increased overall in the KO^{Adv} animals, with release showing facilitation at 25 ms IPI, while WT release was depressive (**Figure 3.12B**). These data are thus consistent with a reduction in the release probability of afferent glutamate transmission in KO^{Adv} mice. Interestingly, the peak glutamate transient in response to a perimaximal single pulse stimulus was also significantly reduced in KO^{Adv} animals (**Figure 3.12C**). Such alterations in basic synaptic physiology may account for the heightened nocifensive thresholds of mice lacking $Na_V1.7$ and associated diminished nociceptive input to the CNS.

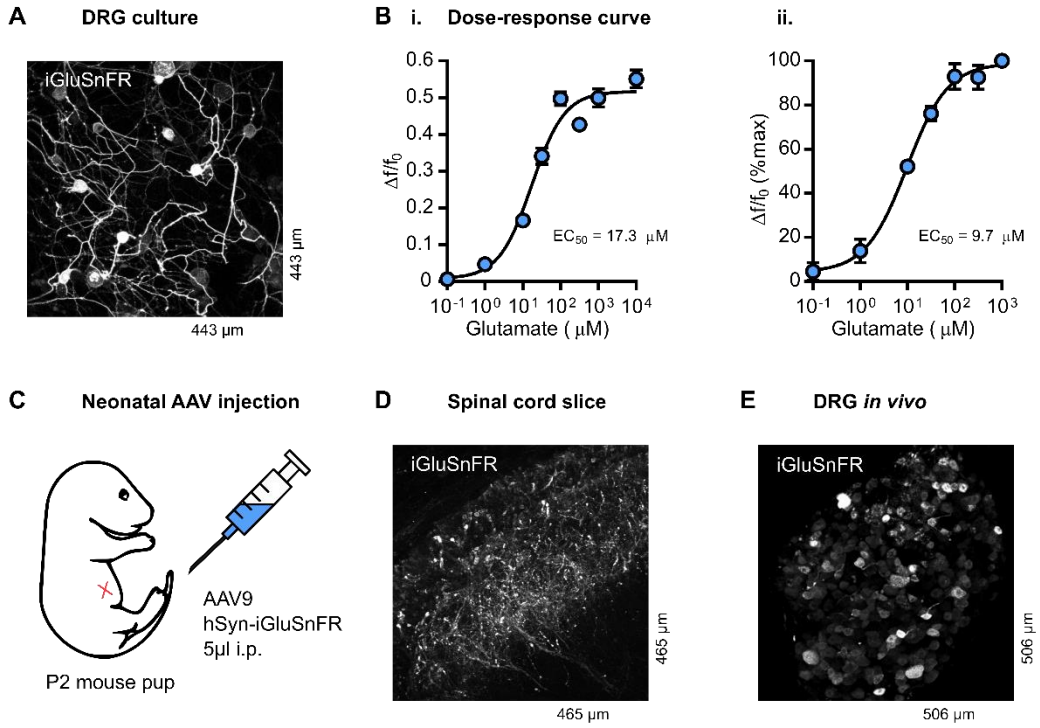

Figure 3.9. Expression and function of iGluSnFR in sensory afferents

(A) Confocal z-stack of iGluSnFR-expressing cultured dorsal root ganglia neurons, *in vitro*.

(B) (i.) Dose-response curve of raw iGluSnFR fluorescence ($\Delta F/F_0$) in cultured DRG neurons against extracellular glutamate concentration. n=36-154 neurons depending on tested concentration. EC_{50}=17.3 µM. r^2=0.426. (ii.) Dose-response curve of normalized iGluSnFR fluorescence (% maximum) in cultured DRG neurons against extracellular glutamate concentration. In this experiment, each cell was exposed to all glutamate concentrations tested. n=45 neurons. EC_{50}=9.7 µM. r^2=0.625.

(C) Schematic of neonatal virus injection.

(D) Two-photon z-stack of iGluSnFR-expressing sensory afferent terminals in spinal cord dorsal horn, *ex vivo*.

(E) Confocal z-stack of iGluSnFR-expressing sensory afferent cell bodies in L4 dorsal root ganglion, *in vivo*.

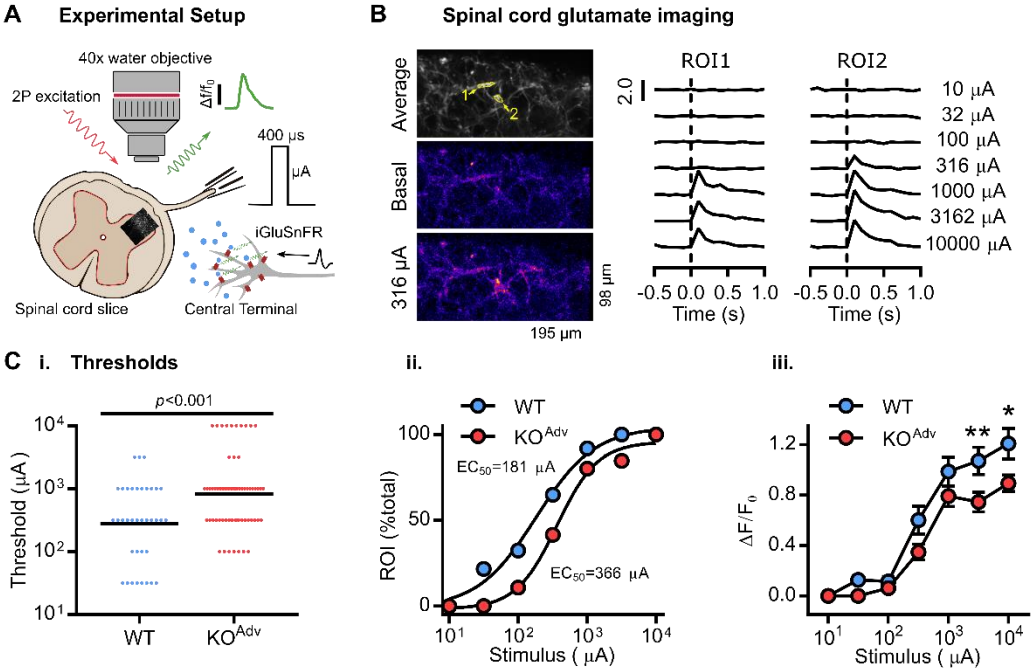

Figure 3.10. Decreased neurotransmitter release from the central terminals of $Na_V1.7$-deficient sensory neurons

(A) Schematic illustrating two-photon imaging of iGluSnFR-expressing afferent terminals in the dorsal horn of spinal cord slices. Data were obtained from 4 WT and 6 KO^{Adv} animals.

(B) Example images and traces of volume glutamate release from afferent terminals in response to single-pulse dorsal root stimulation in spinal cord slices obtained from a $Na_V1.7$ KO^{Adv} mouse. ROI=region of interest.

(C) Plots showing the threshold current required to evoke glutamate release is decreased in slices from KO^{Adv} mice. For (i.), the mean absolute threshold was compared between genotypes using an unpaired t test. For (ii.), WT: EC_{50}=181 µA, r^2=0.99 and KO^{Adv}: EC_{50}=366 µA, r^2=0.99. For (iii.), mean evoked glutamate release ($\Delta F/F_0$) was compared between genotypes using repeated measures Two-Way ANOVA followed by post-hoc Sidak's test. **p=0.007, *p=0.010. n=37 ROIs for WT. n=65 ROIs for KO^{Adv}.

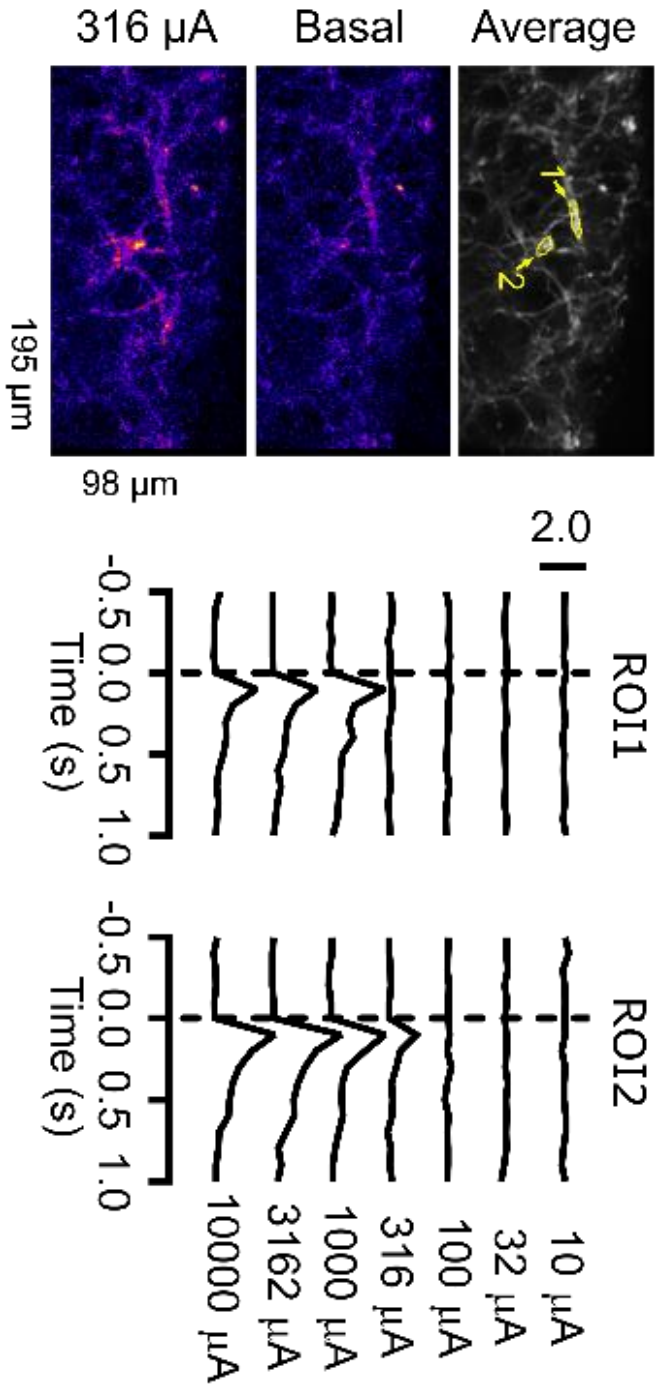

Figure 3.11. Spinal cord glutamate imaging (enlarged).

Example images and traces of volume glutamate release from afferent terminals in response to single-pulse dorsal root stimulation in spinal cord slices obtained from a $Na_V1.7$ KO^{Adv} mouse. The average image (top) shows the structure and morphology of afferent processes in the dorsal horn of the spinal cord. The pseudo-coloured images show baseline fluorescence (middle) and fluorescence after a current stimulation of the dorsal root (bottom). The highlighted regions of interest (ROI) show different thresholds for activation of glutamate release, as evident in the example traces.

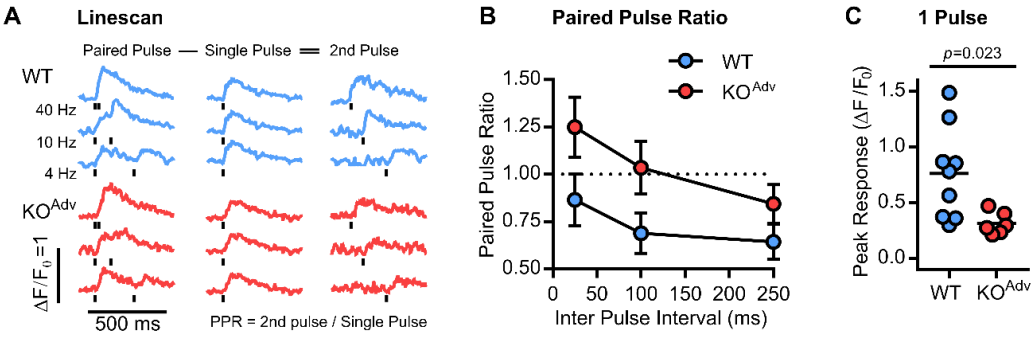

Figure 3.12. $Na_V1.7$ deletion increases paired pulse ratio for glutamate release

(A) Example traces obtained by performing linescans through ROIs in response to paired and single pulse dorsal root stimulation using a perimaximal stimulus intensity.

(B) Plot showing the paired pulse ratio (PPR) is increased in KO^{Adv} mice. Mean PPR across inter pulse intervals was compared between genotypes using repeated measures Two-Way ANOVA followed by post-hoc Sidak's test. There was a significant main effect of genotype: p=0.05.

(C) Plot showing diminished release ($\Delta F/F_0$) in KO^{Adv} mice using a single pulse stimulus. Mean peak responses were compared between genotypes using an unpaired t test. For both (B) and (C), n=6 ROIs for WT and n=9 ROIs for KO^{Adv}.

3.3.4 Opioid receptors are required for synaptic deficits in nociceptors but not olfactory sensory neurons lacking $Na_V1.7$

It has previously been shown that analgesia in $Na_V1.7$ null mutants requires opioid receptors. This is due to both upregulation of pre-pro-enkephalin and enhanced opioid receptor signalling caused by $Na_V1.7$ deletion.[261,311,342] Does increased opioid signalling account for the synaptic deficits we observe in $Na_V1.7$ KOs? I first investigated the effect of systemic naloxone injection *in vivo* (2 mg/kg subcutaneously for 20 minutes) on peripheral excitability of nociceptors. To my surprise, *in vivo* imaging experiments revealed that naloxone increased the number of responding cells in both WT and KO^{Adv}, suggesting tonic endogenous opioid activity is present in my preparation. Importantly, however, the effect of naloxone on the number and size of responses was comparable across genotypes (**Figure 3.13A**). My colleague Dr Shafaq Sikandar performed additional *in vivo* extracellular recordings of sensory neurons from WT and KO^{Adv} and we found no effect of naloxone on action potential firing in response to noxious heat, mechanical or cold stimuli (**Figure 3.13B**).

As naloxone did not markedly affect peripheral excitability, I examined the relationship between opioid receptors and synaptic dysfunction in $Na_V1.7$ KOs. Spinal cord slices from $Na_V1.7$ KO^{Adv} animals were treated with either vehicle or naloxone for at least 20 minutes before measuring dorsal root stimulation-evoked glutamate release using iGluSnFR. Vehicle-treated KO^{Adv} slices showed a mean minimum stimulus current for eliciting release of 690 μA. This was reduced to 302 μA in naloxone-treated KO^{Adv} slices, comparable to the 279 μA threshold I previously observed in WT slices (**Figure 3.13C**). The EC_{50} current was 457 μA in the vehicle-treated group, and decreased to 173 μA after naloxone, similar to the WT value of 181 μA (**Figure 3.14A**). Next, I performed linescan experiments, estimating release probability as before by calculating the paired pulse ratio. As expected, vehicle-treated KO^{Adv} slices showed facilitation at IPI=25 ms, but this was unchanged by naloxone treatment (**Figure 3.14B**).

Next, I asked if the deficits in substance P release previously observed in KO^{Adv} mice are also dependent on opioid receptors.[257] Electrical stimulation of hemisected spinal cord with dorsal roots attached was originally used to show a deficit in substance P release in KO^{Adv} mice. Here I used the potent pain-producing TRPV1 ligand capsaicin to selectively depolarise nociceptor terminals in spinal cord slices from WT and KO^{Adv} mice. Using a competitive binding immunoassay, I measured the amount of substance P release elicited by 2 μM capsaicin stimulation in both genotypes with and without 1 mM naloxone

(**Figure 3.13D**). In KO^{Adv} slices, a mean of 35 ± 35 pg / ml of substance P was detected. Treatment with naloxone increased release to 418 ± 135 pg / ml. In WT slices, there was no significant difference between vehicle (282 ± 92 pg / ml) and naloxone conditions (414 ± 169 pg / ml). The diminution in substance P release from nociceptor central terminals lacking $Na_V1.7$ is thus rescued by block of opioid receptors.

Mice lacking $Na_V1.7$ in olfactory sensory neurons (Nav1.7 KO^{OMP}) are totally anosmic due to a loss of transmitter release from olfactory nerve terminals.[263] Our collaborators in the Frank Zufall lab performed a series of experiments to investigate if these synaptic deficits are also dependent on opioid receptors. Jan Weiss recorded M/T cells in horizontal olfactory bulb slices of KO^{OMP} mice. As expected, electrical stimulation (1 ms, 100 V) of the olfactory nerve layer harbouring the olfactory sensory neuron axon terminals did not elicit a postsynaptic current in M/T cells of Nav1.7 KO^{OMP} (**Figure 6.3A**). To test if the opioid receptor antagonist naloxone can restore transmitter release at this synapse, we bath-applied 300 μM naloxone for at least 10 minutes and recorded olfactory nerve-evoked responses in 17 M/T cells (5 animals). Naloxone did not lead to an increase in EPSC amplitude (**Figure 6.3B**) (control -14 ± 0.4 pA vs Nav1.7KO^{OMP} -13.9 ± 0.03 pA). To exclude the possibility that naloxone affects transmitter release in general at this synapse, he additionally recorded M/T cells of control mice (WT, 7 cells in 4 animals). Olfactory nerve stimulation caused activation of characteristic inward currents in M/T cells of control mice with amplitudes of -165 ± 20 pA. Application of naloxone to the slice had only minor effects on evoked EPSCs (-148 ± 37 pA) (**Figure 6.3A&B**). As a further corroboration, Martina Pyrski injected animals intraperitoneally 3 times (30 minute interval) with naloxone (1 mg/kg) or PBS and kept in the odour-rich environment of their homecage for the next 24 hours to allow expression of tyrosine hydroxylase (TH). Afterwards animals were sacrificed, perfused and olfactory bulb coronal sections stained against TH protein. There was no obvious difference between PBS and naloxone treated animals in their amount of TH expression, with low to no expression of TH in KO^{OMP} mice, and high expression in control mice (**Figure 6.3C**). These results are consistent with the finding that, in WT mice, treatment with a cocktail of opioid receptor agonists did not affect EPSCs evoked by olfactory nerve stimulation (**Figure 6.3D**). TTX, on the other hand, completely abolished synaptic transmission from OSNs to M/T cells (**Figure 6.3E**)

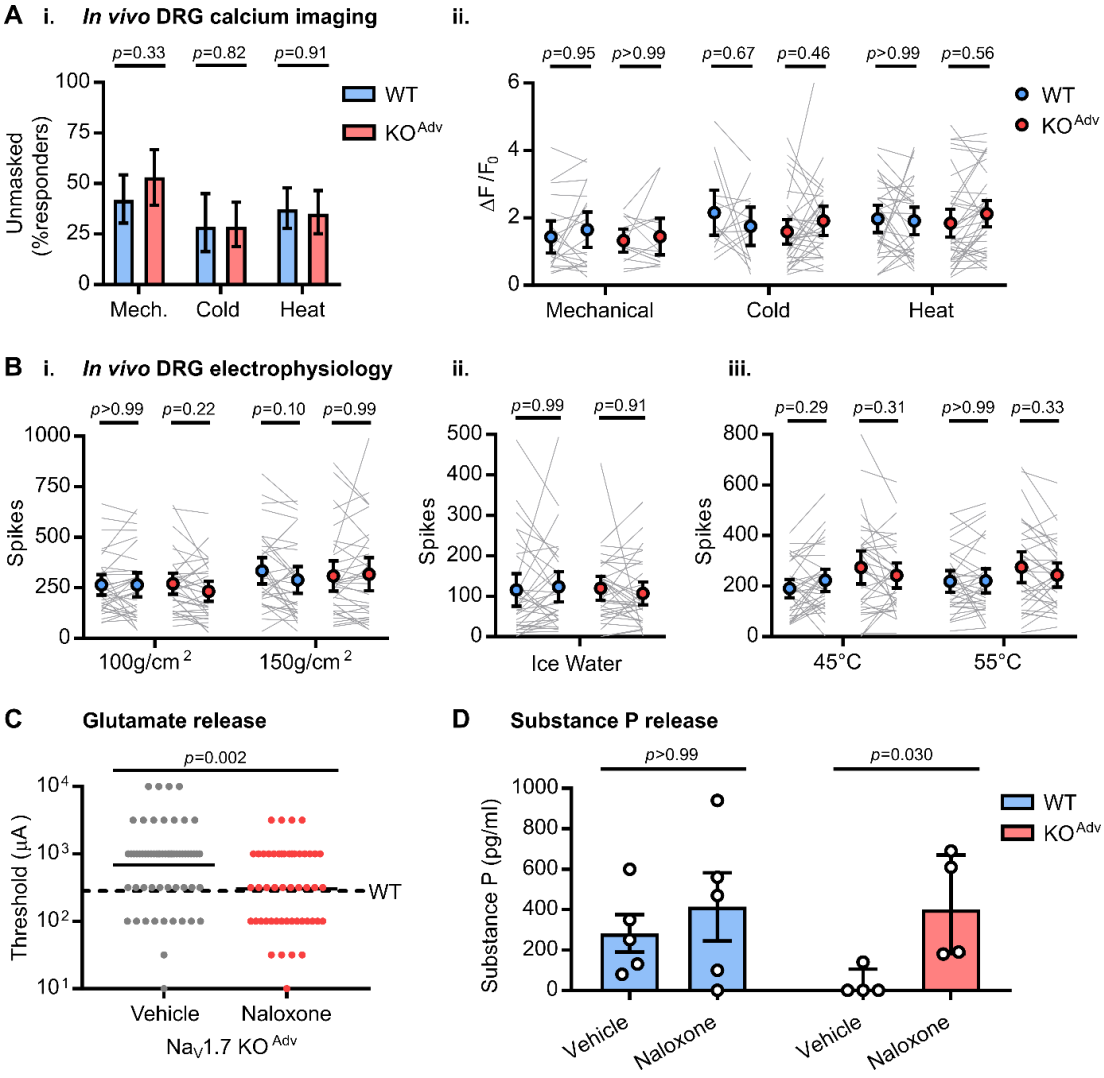
A i. In vivo DRG calcium imaging
p=0.33 p=0.82 p=0.91
Unmasked (%responders)
100
75
50
25
0
Mech. Cold Heat
WT
KOAdv
ii.
p=0.95 p>0.99 p=0.67 p=0.46 p>0.99 p=0.56
ΔF/F0
6
4
2
0
Mechanical Cold Heat
WT
KOAdv
B i. In vivo DRG electrophysiology
p>0.99 p=0.22 p=0.10 p=0.99
Spikes
1000
750
500
250
0
100g/cm2 150g/cm2
ii.
p=0.99 p=0.91
Spikes
500
400
300
200
100
0
Ice Water
iii.
p=0.29 p=0.31 p>0.99 p=0.33
Spikes
800
600
400
200
0
45°C 55°C
C Glutamate release
p=0.002
Threshold (μA)
10^4
10^3
10^2
10^1
WT
Vehicle Naloxone
NaV1.7 KOAdv
D Substance P release
p>0.99 p=0.030
Substance P (pg/ml)
1000
800
600
400
200
0
Vehicle Naloxone Vehicle Naloxone
WT
KOAdv

Figure 3.13. Opioid receptor blockade rescues impaired neurotransmission after $Na_V1.7$ deletion but does not affect peripheral excitability

(A) *In vivo* imaging of sensory neuron activity before and after treatment with systemic naloxone (2 mg/kg subcutaneously for 20 minutes) in WT (blue) and $Na_V1.7$ KO^{Adv} (red) mice. (i.) Naloxone unmasked previously silent neurons in both WT and KO^{Adv} mice. Proportions were compared using Chi square test with Yates' correction. (ii.) Naloxone had no effect on the peak calcium responses evoked by noxious stimuli in either genotype. Mean peak calcium responses before and after naloxone were compared using repeated measures Two-Way ANOVA followed by post-hoc Sidak's test. Data were obtained from 4 WT and 6 KO^{Adv} animals. Mechanical: n=62 cells from WT, n=47 cells from KO^{Adv}. Cold: n=35 cells from WT, n=63 cells from KO^{Adv}. Heat: n=86 cells from WT, n=74 cells from KO^{Adv}.

(B) *In vivo* extracellular recording of sensory neuron action potential firing before and after treatment with systemic naloxone (2 mg/kg subcutaneously for 20 minutes) in WT (blue) and $Na_V1.7$ KO^{Adv} (red) mice. Naloxone had no effect on spiking evoked by noxious mechanical (i.), ice water (ii.) or heat (iii.) stimuli. Mean spikes fired before and after naloxone were compared using repeated measures Two-Way ANOVA followed by post-hoc Sidak's test. n=33 from 6 WT animals, and n=33 from 7 KO^{Adv} animals.

(The extracellular recording data were collected and analysed by Dr Shafaq Sikandar, with Dr Ana Luiz. They are provided here in the main results for comparison with my imaging data on the effect of naloxone.)

(C) *Ex vivo* iGluSnFR imaging of glutamate release from sensory neuron central terminals in dorsal horn of spinal cord slices from 6 KO^{Adv} animals treated with vehicle (grey) or 100 μM naloxone (red). Naloxone reduced mean threshold current required to elicit release to WT levels (dashed line). n=62 regions of interest for vehicle and n=50 for naloxone.

(D) Measurement of substance P release from spinal cord slices obtained from 5 WT and 4 KO^{Adv} animals. Treatment with 1 mM naloxone rescued diminished substance P release in KO^{Adv} slices, but had no effect in WT. Data were compared using Kruskall Wallis test.

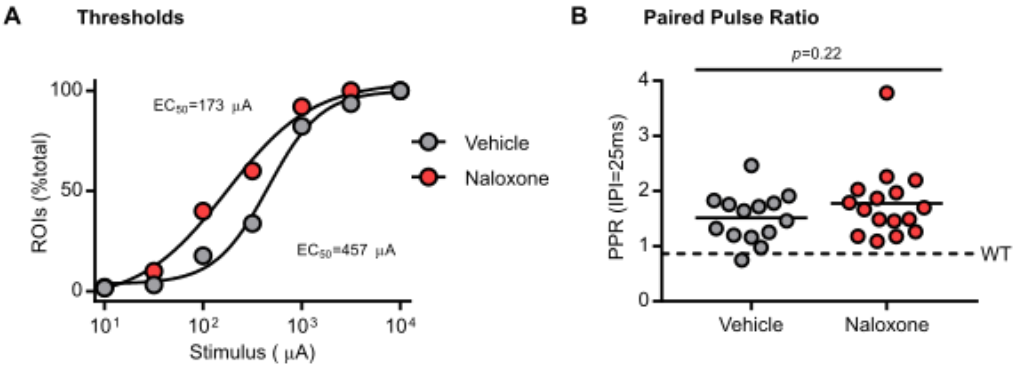

Figure 3.14. Effect of naloxone on synaptic deficits in $Na_V1.7$ KOs

(A) Naloxone normalized the EC_{50} current stimulation required for evoking glutamate release in KO^{Adv} slices to WT levels. n=62 ROIs for vehicle and n=50 for naloxone.

(B) In KO^{Adv} slices, Naloxone did not affect the paired pulse ratio of glutamate release determined for individual ROIs using perimaximal current stimuli. Means were compared using t test. n=14 ROIs for vehicle and n=16 for naloxone.

3.3.5 Pain insensitivity of mice and humans lacking $Na_V1.7$ depends on endogenous opioid signalling at central opioid receptors

Is the suppression of synaptic transmission by the opioid system required for analgesia of $Na_V1.7$ null mutants *in vivo*? Peripherally-restricted opioid receptor antagonists fortuitously gave me a means of causally testing this in awake behaving animals, by selectively blocking opioid receptors in either the peripheral, central or both compartments of the nociceptor (**Figure 3.15A**). For these experiments, I used withdrawal latencies to radiant heat stimuli as a read-out, because KO^{Adv} mice take twice as long to respond on the Hargreaves' apparatus as WT animals. Systemic administration of naloxone methiodide (2 mg/kg) – a naloxone analogue that does not cross the blood-brain barrier – had no impact on withdrawal latencies in either WT or KO^{Adv} mice, comparable to the effect of vehicle injection. In contrast, systemic injection of naloxone (2 mg/kg) caused a ~71% reversal of analgesia in the KO^{Adv} group (**Figure 3.15B**), reproducing our previously published observations.[261,311] To test if central opioid receptors are required, naloxone (3 mM in 5 μl) was delivered by intrathecal injection directly into the spinal column. Centrally-administered naloxone was sufficient to reverse thermal hyposensitivity in $Na_V1.7$ by ~76%. There was no effect of intrathecal vehicle injection (**Figure 3.15C**). Thus, central – but not peripheral – opioid receptors are essential for the maintenance of analgesia in mice lacking $Na_V1.7$ (**Figure 3.15D**).

It has previously been shown that naloxone infusion restores nociception in a single rare female $Na_V1.7$ null human.[261] Here we extended these findings to two male humans with compound heterozygous $Na_V1.7$ loss-of-function mutations (**Table 6-1**).[284,285] Our collaborator Flavia Mancini, with Gian D. Iannetti, applied tonic radiant heat stimuli (25 s) to the forearm, while participants rated online the perceived intensity using a visual analogue scale (**Figure 6.4**). In Male 1, naloxone strongly enhanced pain sensation, mimicking the effect on the previously reported female participant.[261] In Male 2, there was no apparent effect of naloxone. In an age and gender-matched control, pain ratings were consistently higher than the $Na_V1.7$ null individuals and not enhanced by naloxone. Thus, in 2 of the 3 human with $Na_V1.7$ null mutations tested so far, block of opioid receptors enhances pain sensitivity, supporting a role for opioid signalling in driving analgesia associated with $Na_V1.7$ loss-of-function.

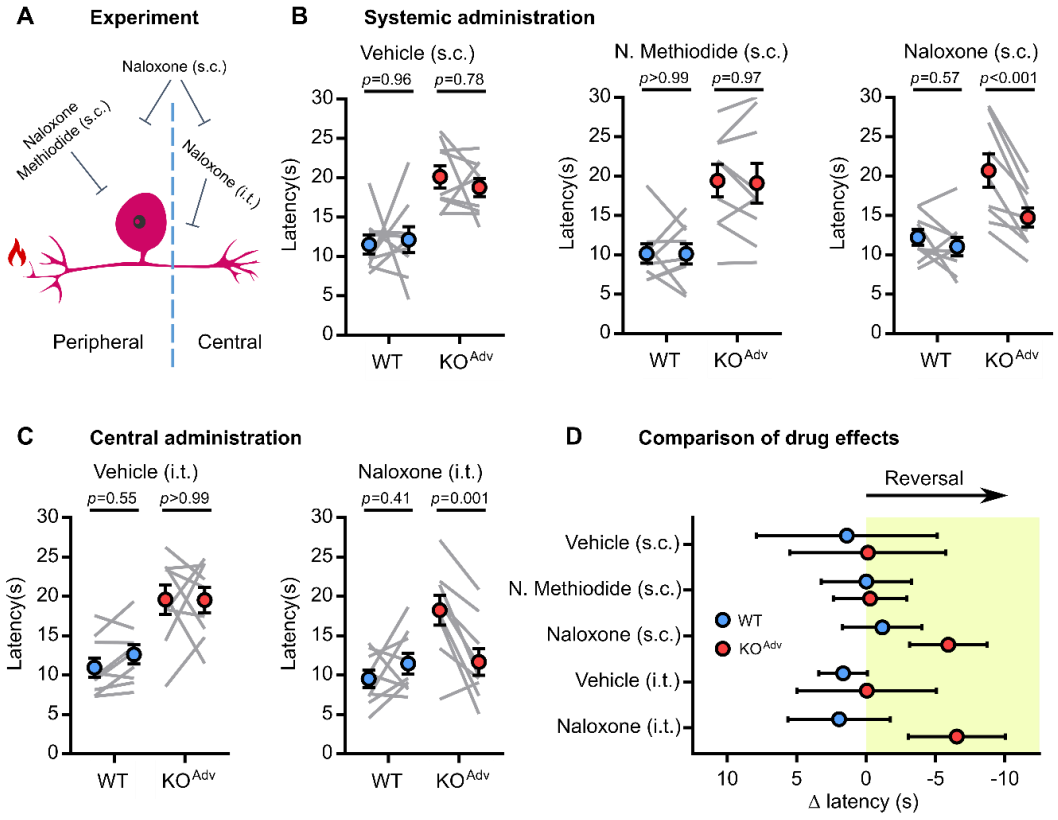

Figure 3.15. Local block of central, but not peripheral, opioid receptors reverses analgesia in $Na_V1.7$ knockout mice

(A) Schematic of behavioural pharmacology experiment.

(B) Behavioural assessment of the effect of saline vehicle and the opioid receptor blockers naloxone (2 mg/kg for 20 minutes) and naloxone methiodide (N. methiodide, 2 mg/kg for 20 minutes) administered systemically by subcutaneous injection. N. methiodide is peripherally-restricted and does not cross the blood brain barrier.

(C) Behavioural assessment of the effect of saline vehicle and naloxone (3 mM in 5 µl for 20 minutes) administered centrally by intrathecal injection.

For both (B) and (C), the error bars represent standard error of the mean. Mean latencies before and after drug treatment were compared using repeated measures Two-Way ANOVA followed by post-hoc Sidak's test. n=9 animals for WT and n=9 animals for KO^{Adv}.

(D) Summary plot comparing the effects of all drug treatments across genotypes. The error bars represent confidence intervals around the mean change in latency after drug.

3.4 Discussion

Deletion of *SCN9A* encoding the peripheral sodium channel $Na_V1.7$ in humans causes insensitivity to pain and anosmia.[5,263] Peripheral neuron $Na_V1.7$ KO mice are pain-free in assays of mechanical, heat and inflammatory pain and show decreased spinal cord wide-dynamic range neuron firing to noxious stimuli.[257,265] The main driver of analgesia must thus be the loss of $Na_V1.7$ in sensory neurons. In this study, I sought to determine the locus and mechanism of analgesia in $Na_V1.7$ null mutants and so inform the development of better therapies targeting this channel. Using imaging and extracellular recording of sensory neuron activity, I found that peripheral excitability was essentially unchanged by $Na_V1.7$ deletion. In contrast, synaptic transmission from afferent terminals in the spinal cord was compromised in an opioid-dependent manner. Importantly, pain insensitivity was reversed by blocking central opioid receptors, causally linking analgesia with these synaptic deficits.

3.4.1 Peripheral silencing

$Na_V1.7$ is highly-expressed in sensory neurons and passes a ramp current hypothesized to function as an amplifier of generator potentials at nociceptor peripheral terminals.[335] It has been assumed that pain insensitivity in $Na_V1.7$ null mutants results from reduced excitability of the nociceptor peripheral terminal and that pharmacological block of the channel at this locus should produce analgesia.[292] Using *in vivo* imaging and electrophysiology, this study directly tested whether loss of $Na_V1.7$ causes peripheral silencing of nociceptors in live mice.[245] Surprisingly, nociceptor excitability at the level of the DRG was largely unchanged, with normal levels of heat, polymodal and silent nociceptors, and normal calcium and spike response profiles. Nonetheless, in GCaMP3 – but not GCaMP6f – experiments, I did observe a modest reduction in the number of cells responding to noxious mechanical stimuli. This is consistent with *in vitro* recordings that found ~30% of $Na_V1.7$-deficient putative nociceptors are electrically silenced in culture.[336] Other groups have also found some deficits in excitability associated with $Na_V1.7$ loss-of-function using cultured mouse DRG neurons, iPSC-derived nociceptors, mouse compound action potential recording and human microneurographic recordings.[284,313,338] In my hands, however, nociceptors were present, functional and excitable *in vivo* in both lines of mice lacking $Na_V1.7$.

How confident can we be that peripheral excitability is largely unchanged in $Na_V1.7$ knockout mice? A key limitation of the imaging experiments is that only responding cells can be identified and analysed, therefore proportions for each cell type are presented as a function of the responding population, as is common in the field.[193] If there was broad silencing of all cell types, this could be missed in this analysis. However, this is unlikely given the modality-specific behavioural analgesia of conditional $Na_V1.7$ KO animals.[257] The mild reduction in noxious mechanical responders was seen only in Pirt-GCaMP3 mice and not in the animals virally expressing GCaMP6f. Importantly, the distribution of response types was different between the genomically-expressed GCaMP3 and virally-expressed GCaMP6f, so these data are not directly comparable. Cold neurons were rarely seen in the GCaMP6f mice, presumably reflecting preferential expression of the virus in other subsets of cells, and highlighting how dependent the cell population imaged is on the expression strategy.[245,247,248]

To circumvent the issue of analysing only responding cells, I used the PGE2 model of inflammatory pain because the relative effect of PGE2 can more easily be compared between genotypes. Emery *et al* previously showed that PGE2 had dramatic effects on the representation of heat in the periphery.[245] The PGE2 experiments showed that silent heat nociceptors were unmasked and heat response magnitude was increased in $Na_V1.7$ KO mice in a manner similar to WT. In contrast, $Na_V1.7$ deletion abolished PGE2-induced heat hyperalgesia on the Hargreaves' apparatus. This is consistent with previous reports that all standard inflammatory pain treatments fail to sensitize pain behaviour in mice lacking $Na_V1.7$ in nociceptors.[265] In my opinion, this experiment is the most compelling demonstration of intact nociceptors in $Na_V1.7$ KOs using an inflammatory pain stimulus that unequivocally does not elicit pain in these animals.

It is conceivable that analgesia might not require total silencing; a graded reduction in excitability of responding afferents could be enough to reduce nociceptive input to CNS. I therefore quantified peak calcium signals in response to different noxious stimuli in Pirt-GCaMP3 mice and observed no effect of $Na_V1.7$ deletion. GCaMP3 has lower signal-to-noise (SNR) and slower kinetics than later generations of GCaMP so may not be sufficiently sensitive to capture finer-grained changes in excitability.[254,346] However, I reproduced these same observations using GCaMP6f, which has higher SNR and faster kinetics. To establish whether action potential firing in the responding population was altered by loss of $Na_V1.7$, we performed extracellular recording and observed only minor changes in the number of spikes fired to noxious stimulation. The analyses were rather

superficial, expressed as number of spikes recorded in the 10 s following stimulation, and risk missing changes in the pattern of firing. In the main, however, these imaging and extracellular recording data indicate action potentials are initiated and propagate as far as the soma in $Na_V1.7$-deleted sensory neurons *in vivo*. $Na_V1.7$ is therefore not required for action potential generation at the nerve terminal or conduction along the peripheral nerve. The locus of analgesia is thus unlikely to be the peripheral terminal. Taken together, my findings are incompatible with the 'peripheral silencing' hypothesis of $Na_V1.7$ null analgesia and therefore account for the failure of peripherally-targeted inhibitors of $Na_V1.7$.

Importantly, my observation of functional nociceptors in $Na_V1.7$ KO mice also precludes die-back of peripheral nerves driving analgesia in mice lacking $Na_V1.7$. As noted earlier, several studies of human null mutants found reduced intra-epidermal fibre density.[284,339,340] In the most high profile study, this reduction was associated with absent C fibre nociceptor-associated activity-dependent slowing profiles using microneurgraphy (although Aδ fibres were present). Contrastingly, a case report of one null mutant child found normal epidermal innervation with loss of pain, however it is unclear if this study distinguished epidermal and dermal fibre counts.[341] Although the evidence supports decreased IEFD in null mutants, I believe die-back is unlikely to be causal to analgesia for the following reasons. First, not all nociceptors that respond to peripheral stimulation innervate the epidermis; many nerve endings have receptive fields located deeper.[55] Second, global $Na_V1.7$ KO mice and rats show profound analgesia, yet IEFD is completely normal, consistent with my observation of functional nociceptors.[312,314] Third, the preservation of neurogenic inflammation and axonal flare in $Na_V1.7$ null humans in response to algogens and pruritogens indicates functional nociceptors that can propagate action potentials are present.[119,284] Fourth, $Na_V1.7$ is also lost from innocuous touch sensing neurons that do not seem to die back or dysfunction.[77] What causes the die-back? One explanation for neuropathy may be retraction due to lack of nociceptor activity throughout life, but this is inconsistent with my observation of normal excitability. The effect could be developmental, but there was no intrinsic change in neurite outgrowth in CIP iPSC-derived nociceptors.[284] Alternately, die-back may occur as a consequence of the injuries these patients sustain throughout life. What causes the reduced epidermal innveration therefore remains mysterious but, on balance of probability, appears unlikely to be the principle mechanism of analgesia.

3.4.2 Synaptic transmission

Sodium channels are required for action potential invasion into presynaptic terminals and thus poised to regulate synaptic transmission.[292] $Na_V1.7$ is expressed along the length of sensory neurons, including at the central terminal, where it associates with many proteins including synaptotagmin-2.[301,347] Given normal peripheral excitability, but reduced spinal cord wide dynamic range neuron firing in $Na_V1.7$ KOs, an alternative explanation for analgesia is that nociceptive input is lost through a failure of synaptic transmission from nociceptors to CNS neurons.[257] Indeed, application of $Na_V1.7$ inhibitors to spinal cord slices reduces synaptic transmission from afferents.[326,329] Using glutamate imaging, electrophysiology and a substance P immunoassay, I observed deficits in pain-related neurotransmitter release in the spinal cord of mice lacking $Na_V1.7$. As I directly activated dorsal roots of spinal cord slices, these experiments preclude any contribution of impaired peripheral excitability to the observed synaptic deficits. Echoing this, direct stimulation of dorsal roots in one CIP patient failed to elicit pain.[348] These findings agree with the function of $Na_V1.7$ in the olfactory system. Anosmia in $Na_V1.7$ null mutants is wholly explained by impaired synaptic transmission from first-order olfactory sensory neurons, although somatic excitability to odorant stimuli is normal.[263] However, in the olfactory system, evoked EPSCs are completely absent after $Na_V1.7$ deletion; the changes I observed in spinal cord were nowhere near as large, despite substantial behavioural analgesia.

Does this reflect a less significant role for $Na_V1.7$ in spinal cord transmission, or a limitation of the assays used? The layer II dorsal horn electrophysiology experiments were performed for a different purpose, and re-analysed opportunistically.[302] Although dorsal roots were routinely stimulated as part of the protocol, critically, the roots were relatively short and different stimulus amplitudes were not tested. Thus I could not distinguish EPSCs resulting from C and A fibre stimulation. I was limited to measuring latency to the first event; a crude analysis which nonetheless showed the absence of slower polysynaptic events in the KO^{Adv} slices. In the future, it is crucial that a proper electrophysiological characterization of dorsal horn synaptic transmission in $Na_V1.7$ KOs is performed, using the standard protocols.[349] The reduction in frequency but not amplitude of spontaneous EPSCs is consistent with presynaptic dysfunction, however this measure reflects all input to the recorded cell and not sensory afferents alone. The decreased frequency of sEPSCs could result from the known dampened excitability of dorsal horn neurons after peripheral $Na_V1.7$ deletion.[302] To overcome this, it would be

useful to look at capsaicin-induced spontaneous or miniature EPSCs as a direct measure of the fraction of synaptic release coming from nociceptive afferent terminals.[350,351]

To directly monitor transmitter release from afferent terminals I developed an iGluSnFR imaging technique where glutamate release is monitored optically. The threshold current required to evoke glutamate release was increased in KOs. What does this mean? The central terminal may be less excitable. As with the electrophysiology experiments, a critical problem with the electrical stimuli used here is we cannot distinguish A and C fibre stimulation. On reflection, I ought to have used stimulus protocols that preferentially activate C and A fibres.[352] I did try to use capsaicin stimulation, however bleaching of the fluorophore made these chemical stimulation experiments uninterpretable. Optogenetic activation with the opsin genetically restricted to nociceptors is an alternative strategy, however care would need to be taken that the activation did not overlap with that required to excite iGluSnFR.[9] The final flaw in these experiments was that the lack of a structural marker meant I could not localize the imaging to defined release sites, with pre and postsynaptic termini apposed. Thus, the signal recorded here results from volume glutamate transmission, rather than solely intra-synaptic transmission. Nonetheless, even with these caveats, I have successfully measured bulk glutamate release optically in dorsal horn for the first time and developed an assay that, with some refinement, could be exploited by others to study excitatory transmission in the spinal cord.

Using line scans to acquire the signal more rapidly, I also saw a reduction in release probability, measured by increased paired pulse ratio (PPR). I used perimaximal stimuli determined on the fly. One problem was the slow kinetics of iGluSnFR meant the signal attributable to the second pulse overlapped with the first, thus I had to use subtraction to estimate its amplitude.[260] Faster variants of iGluSnFr could be used, as has been done in hippocampal slice cultures.[353] For determining PPR, more traditional electrophysiological characterization may be more appropriate. Interpreting the findings presents its own difficulties. Population changes in synaptic parameters may reflect the fact that some synapses or afferents are silenced by $Na_V1.7$ deletion. Non-nociceptive afferents might therefore be over-represented in the population, causing a change in the population average, and so the PPR change would have little relevance to analgesia. The key next step would be to use iGluSnFR to measure glutamate release *in vivo* in the cord, as this would allow for naturalistic stimulation, and enable a direct comparison with the peripheral imaging data. In my hands, iGluSnFR could be imaged in DRG *in vivo* but not in the cord

using confocal microscopy. A two photon microscope would thus be required to overcome the problem of light scattering in the white matter, as has been achieved by one group when imaging GCaMP.[152]

Finally, I used capsaicin to selectively activate nociceptor terminals in spinal cord slices and measured the resultant release of Substance P. I reproduced the previous observations of decreased substance P release driven by C fibre stimulation.[257] Collectively, then, the data presented here, together with previous findings, are consistent with impaired synaptic release in $Na_V1.7$ KO mice. This may account for decreased nociceptive input to the CNS and associated loss of pain.

3.4.3 Endogenous opioids and opioid receptors

How does loss of $Na_V1.7$ impair neurotransmitter release? Immunostaining for $Na_V1.7$ or epitope-tagged $Na_V1.7$ clearly demonstrates presynaptic expression of the channel in afferent central axons in the superficial laminae of the dorsal horn.[301,302] Is $Na_V1.7$ essential for the propagation of the action potential along the central axon and subsequent invasion into the presynaptic terminal?[292] Alexandrou *et al* found PF-05198007 applied to the dorsal root decreases and slows C fibre-mediated EPSCs onto dorsal horn heurons. The data in this paper consists of single "representative" experiments, thus it is difficult to gauge the size and significance of this effect.[329] Deuis *et al* found the spider toxin Pn3a reduced C fibre EPSCs magnitude by ~40% and Aδ EPSCs by ~20%.[326] Intrathecal delivery of $Na_V1.7$ inhibitors is reported to be analgesic in rodents, consistent with the direct effects of channel loss on excitability causing diminished transmitter release.[354,355] However, intrathecal injection of Pn3a had no effect on the development of inflammatory pain, despite impairing synaptic transmission in the slice experiments.[326]

Analgesia in mice and humans lacking $Na_V1.7$ can be substantially reversed by opioid antagonists or opioid receptor deletion.[261,311] This results from both enhanced PENK production and opioid receptor signalling.[261,342] As opioids are known to potently suppress substance P and glutamate release from spinal cord afferent terminals, I wondered if the synaptic impairments I saw in $Na_V1.7$ KOs are dependent on opioid receptors.[356,357] Deficits in both glutamate and substance P release were reversed by naloxone. Note that the altered P_r apparent in paired-pulse experiments was not rescued by naloxone. Both μ and δ opioid receptors are expressed at the central terminals in non-overlapping sets of nociceptors, where they are poised to control synaptic transmission. This explains why both subtypes are required for analgesia in $Na_V1.7$ nulls.[9,311,358] Opioid

receptor signalling both promotes opening of potassium channels and inhibits voltage-gated calcium channels. Inhibition of the voltage-gated calcium channels that control transmitter release is reported to be the principal mechanism operating in dorsal horn nociceptor terminals.[357] However, how exactly opioid receptors suppress release in $Na_V1.7$ nulls remains to be answered. One powerful assay would be to study transmitter release using mechanistic pharmacology in co-culture using human $Na_V1.7$ null iPSC-derived nociceptors and dorsal horn neurons.[284]

Opioid receptor block did not differentially affect activity in sensory neuron cell bodies of WT and KO mice, as judged by calcium imaging or electrophysiology, despite functional expression of opioid receptors in dorsal root ganglia somata and peripheral axons.[227] Given deletion of $Na_V1.7$ had little impact on peripheral excitability, it is not surprising I saw no KO-specific opioid effect. Interestingly, however, naloxone actually increased the number of responsive cells in both genotypes, indicating there is endogenous opioid tone or constitutive receptor activity present in the dorsal root ganglion that normally suppresses somatic calcium signals. This was not apparent when looking at peak transients which may be linked to the non-linearity of the calcium indicator. The origin of the opioid activity in WT mice observed using our imaging preparation is worthy of further investigation.

In contrast to spinal cord synaptic transmission, our collaborators in the Zufall lab found synaptic transfer from olfactory sensory neurons was not rescued by naloxone treatment. This is unsurprising given a single cell RNA sequencing study demonstrates olfactory sensory neurons do not express opioid receptors.[359] $Na_V1.7$ is the only sodium channel available in olfactory sensory neuron nerve terminals; thus its loss completely blocks electrical activity presynaptically, consistent with the abolition of transmitter release by TTX reported here.[263,303] In contrast, nociceptors express numerous other sodium channels that can support electrogenesis in the absence of $Na_V1.7$ when the inhibitory effect of opioids is removed.[76,77] Observations using a DRG neuron and dorsal horn neuron microfluidic co-culture systems suggest inhibition of $Na_V1.7$ alone is not sufficient to block synaptic transfer.[360] TTX does not fully block C-fibre mediated EPSCs because $Na_V1.8$ and $Na_V1.9$ alone are sufficient to support synaptic transmission.[361] Interestingly, mice lacking both $Na_V1.8$ and $Na_V1.7$ show pronounced heat insensitivity that is normal in the nociceptor-specific $Na_V1.7$ KO animal.[362]

Opioid action at the central terminal is causally involved in pain insensitivity because central administration of naloxone was sufficient to reverse analgesia, but

systemic administration of a peripherally-restricted opioid antagonist was not. Intrathecal naloxone would result in a high concentration locally in the CSF, thus preferentially antagonizing spinal cord opioid receptors. Diffusion to the DRG cannot be ruled out though as the CSF also bathes part of the DRG.[363] However, the failure of naloxone methiodide to reverse analgesia precludes peripheral opioid receptors contributing to pain insensitivity.[364]

In humans, naloxone infusion enhanced sensitivity to nociceptive stimuli in 2 of the 3 $Na_V1.7$ null mutants thus far tested. Why did naloxone have no effect on heat sensitivity in Male 2? This participant is hyposensitive to warmth, and during adolescence developed the ability to detect noxious stimuli by a 'tingling' sensation that was not perceived as unpleasant.[285] These unusual phenotypic characteristics could impact his perception of the tonic heat stimuli used here, which he rated zero throughout. In general, subjective pain scales designed for healthy subjects and chronic pain patients may not work well with CIP patients, who, by definition, have never experienced pain. In the future, we envisage testing these patients using noxious capsaicin cream as a prolonged, unambiguously painful stimulus that they do not experience, that lacks the confound of touch and that is unequivocally dependent on nociceptors.[284] I would predict that capsaicin flare would develop normally due to intact action potential propagation and neurogenic inflammation.[119]

Numerous other case reports in the clinical literature attest to the dependence of CIP-like phenotypes on the opioid system, and sodium channel inhibitors produce synergistic analgesia in combination with opioid drugs.[259,343,344] In one particularly elegant experiment, intrathecal injection of CSF from a CIP patient reduced heat nociception in rats. As this effect was blocked by naloxone, CSF opioids acting centrally are sufficient to recapitulate CIP-associated analgesia in animals.[365] Further studies support the role of CSF opioids within the HPA axis that can modulate spinal nociceptive processing.[366,367] I wanted to reproduce this transfer experiment using Hargreaves' in mice as read-out with CSF from $Na_V1.7$ patients and controls delivered intrathecally. However, no CSF was available and the need for lumbar puncture would make it difficult to recruit human participants.

Importantly, the centrally-acting, opioid-dependent mechanism of analgesia I have identified here solves a long-standing mystery about the functional consequences of $Na_V1.7$ deletion. According to single-cell RNA sequencing studies, $Na_V1.7$ is widely expressed in all sensory neuron subtypes, apart from proprioceptors.[76,77] Yet null mutants

are insensitive only to noxious stimuli. If $Na_V1.7$ deletion results in electrical silencing of sensory neurons, why is touch sensation not lost? Opioid receptors are not expressed by neurons expressing markers for low-threshold mechanoreceptors. Only in cells expressing opioid receptors can $Na_V1.7$ deletion drive impaired synaptic transmission in an opioid-dependent manner, thereby blocking nociception but not touch.

3.4.4 Enhanced opioid signalling

How does loss of $Na_V1.7$ lead to increased opioid drive? This is a controversial area: experimental studies are few and there are numerous unanswered questions. Two broad explanations have been put forward that are not necessarily mutually exclusive. First, increased production and release of endogenous opioid peptides.[261] Second, enhanced efficacy of opioid receptors and their associated intracellular signalling pathways.[342] Both these events are hypothesized to result from a decrease in intracellular sodium due to absent $Na_V1.7$ channels.

In support of the first explanation, we know that *Penk*, which encodes the endogenous opioid precursor preproenkephalin, is transcriptionally upregulated in $Na_V1.7$-deficient mice. Changes in intracellular sodium concentration have also been causally linked to elevated transcription of *Penk*. Treating DRG neurons with the sodium ionophore monensin, but not the calcium ionophore ionomycin, decreased the level of *Penk* transcript.[261] In contrast, 6 hour incubation with TTX dose-dependently increased the amount of *Penk* message.[261] The sodium-regulated transcription factor NFAT5, which has binding motifs upstream of *Penk*, is present in sensory neurons, and may link intracellular sodium and *Penk* transcription.[76,77] Indeed, genetic deletion of NFAT5 leads to enhanced *Penk* expression.[311] The slow onset of analgesia in adult-onset inducible knockouts of $Na_V1.7$ supports the idea that transcriptional changes are required, however this could just be due to slow protein turnover.[307,313]

Does transcriptional upregulation of *Penk* actually result in increased endogenous opioid peptides? Minett *et al* found increased Met-enkephalin protein in the dorsal horn of $Na_V1.7$ KO^{Adv} mice based on immunohistochemistry.[261] This is consistent with my finding of tonic opioid inhibition of neurotransmitter release. The paradox remains: if synaptic transmission from nociceptor terminals is reduced, but the opioid peptides are sensory neuron-derived, how are they themselves released? My hypothesis is that *Penk* is predominantly over-expressed in non-nociceptive afferents that do not express opioid receptors. These afferents release opioid peptides to suppress transmitter release from

nociceptors. Consistent with this, the genes downregulated in the $Na_V1.7$ KO transcriptome are mainly expressed in non-nociceptors.[76,261] RNAscope imaging of *Penk* message with co-staining for different DRG neuron subsets would be the obvious test of this hypothesis.

A major problem for the endogenous opioid explanation is that the NFAT5 KO mouse does not show higher pain thresholds, despite elevated *Penk*.[311] This implies increased Penk is not sufficient to cause analgesia. Importantly, *Penk* mRNA was undetectable in the $Na_V1.7$ KO human iPSC-derived nociceptors, casting doubt on the relevance of these findings to humans.[284] The level of met-enkephalin was also not altered in a historical case of naloxone-reversible CIP.[368] In contrast, in a case of naloxone-resistant CIP, total opioid peptides in the CSF were increased.[348] Both these cases were unmapped. Should CSF samples from $Na_V1.7$ nulls ever become available, it is critical they be tested for increased opioid peptide content.

Enhanced opioid receptor signalling, and not elevated endogenous opioid tone, may thus be the crucial component for analgesia in $Na_V1.7$ KO mice.[342] The evidence for this alternative explanation is indirect. Isensee *et al* showed opioid receptor-mediated reduction of protein kinase A (PKA) was markedly increased in $Na_V1.7$-deficient sensory neurons using an immunocytochemical single cell assay of PKA phosphorylation. PKA phosphorylates five serine residues in the first intracellular loop of $Na_V1.8$, increasing the TTX-resistant current, which can be inhibited by opioid-mediated block of PKA.[369] The opioid fentanyl therefore more effectively inhibits TTX-resistant sodium currents in $Na_V1.7$ KO mice.[342]

How does $Na_V1.7$ deletion upregulate opioid receptor signalling? This could occur by numerous means such as altered receptor expression, stability, internalization, or by 'biasing' intracellular signalling pathways. However, by varying intracellular sodium in WT sensory neurons via the patch pipette, it has been shown that fentanyl-evoked inhibition of TTX-resistant sodium current is increased at lower sodium concentrations. Importantly, at 0 mM, the effect of fentanyl is no different between WT and $Na_V1.7$ KO sensory neurons.[370] Thus it has been proposed that loss of $Na_V1.7$ decreases intracellular sodium which in turn increases the efficacy of opioid receptor signalling. Indeed, opioid receptors have a sodium binding site, and ligand binding is affected by sodium concentration.[371,372]

The recent observations that peptide antagonists of $Na_V1.7$ that acutely elicit analgesia in mice can be inhibited by naloxone is consistent with enhanced opioid receptor signalling as the primary driver of analgesia.[327,373] It is conceivable that intracellular sodium concentration in the narrow structures of the axon and presynaptic terminal is sensitive to the pharmacological block of persistent and voltage-dependent $Na_V1.7$ currents. This needs to be tested using sodium-sensitive dyes. The profound analgesic synergy between $Na_V1.7$ blockers and low-dose opioids is thus explicable.[233,326,327] I would propose that $Na_V1.7$ block enhances opioid receptor signalling in nociceptors alone, reducing the effective concentration of opioids required to inhibit synaptic transmission from terminals.

Interestingly, interactions between other pain-related ion channels and opioid receptors have also been reported. Trpv1 activation blocks opioid-dependent phosphorylation and internalization of the μ opioid receptor, thereby preventing receptor desensitization.[374,375] This was shown to be important for opioid-mediated analgesia that promotes the recovery from inflammatory pain.[375] Insensitivity to noxious mechanical stimuli in Trpa1 KO mice is reversed by kappa opioid receptor antagonists.[376] This is entirely analogous to analgesia in $Na_V1.7$ null mutants, as it is not loss of the channel itself that confers analgesia, but the subsequent engagement of the opioid system.

A significant objection to both explanations of analgesia proposed here is the following: if opioid-mediated analgesia is related to altered intracellular sodium, why does loss of other peripherally-expressed sodium channels not also lead to increased opioid drive? Why is the reduction in intracellular sodium and subsequent activation of the opioid system specific to $Na_V1.7$ deletion? One hypothesis is that $Na_V1.7$ is physically associated with the μ opioid receptor. This is based on the finding that $Na_V1.7$ interacts with Gprin1, an opioid receptor-binding protein.[347,370] It is tempting to speculate that sodium ingress through $Na_V1.7$ associated with opioid receptors normally inhibits opioid receptor function and that removal of this brake when the channel is deleted leads to opioid-dependent analgesia. What makes this hypothesis appealing is that it only requires a local alteration of sodium concentration near the receptor.

3.4.5 Therapeutic prospects

What are the implications of a central, opioid-dependent mechanism of $Na_V1.7$ null analgesia for therapeutic strategies targeting the channel? I have shown here that peripheral excitability is effectively normal in $Na_V1.7$ nulls. Acute blockade of $Na_V1.7$ at

the peripheral terminal and axon of nociceptors is therefore unlikely to drive analgesia. Others contest this: a state-independent peptide blocker of $Na_V1.7$ that produced modest thermal analgesia in non-human primates was present at very low concentrations in CSF, and thus claimed to act peripherally.[377] Do inhibitors actually need to penetrate the blood brain barrier to suppress transmitter release to drive analgesia? My finding that impaired synaptic transmission is opioid-dependent suggests that transient block of $Na_V1.7$ to make central axons less excitable is also not likely to produce pain relief.

If analgesia is primarily driven by enhanced receptor signalling at the central terminal, then inhibitors would still need to penetrate the blood-brain barrier to block $Na_V1.7$. This helps explain why $Na_V1.7$ blockers that are not on their own analgesic show analgesic synergy with low-dose opioids or enkephalinase inhibitors.[233,326,327] Comparatively low amounts of $Na_V1.7$ block at the CNS could result in analgesia if accompanied by the additional opioid drive provided by normally subtherapeutic opioid doses or suppression of enkephalinases that degrade endogenous opioid peptides. Clinical trials of low dose opioids with $Na_V1.7$ blockers have yet to be performed, however. In the context of the current Opioid Epidemic, this seems a promising strategy to reduce the risk of addiction when prescribing opioids. Interestingly, the $Na_V1.7$ blocker Pn3a also synergizes with the $GABA_B$ antagonist baclofen, but not with gabapentin.[326,327] The mechanism of this synergy is unknown.

If analgesia is driven by enhanced *Penk* transcription, then it is not clear in which cellular compartment the channel must be silenced to drive transcriptional changes. Close to 100% channel block may be required to drive the changes in opioid function responsible for analgesia, as only very high concentrations of TTX could mimic the effects of channel deletion on *Penk* message production.[261] This level of block is unlikely to be achievable by most currently available pharmacological inhibitors, without resulting in side effects at sodium channel isoforms.

How else can we inhibit $Na_V1.7$? One promising new approach has been to disrupt trafficking of $Na_V1.7$ by manipulating post-translational modification of its binding partner CRPMP2 protein.[347,378] SUMOylation of CRPM2 is required to maintain cell surface expression of $Na_V1.7$.[379] Over-expression of a SUMO-impaired mutant of CRMP2 triggers $Na_V1.7$ internalization, resulting in diminished channel activity and attenuated mechanical allodynia in a rat model of neuropathic pain.[380,381] Intrathecal injection of a peptide designed to block Ubc9-mediated SUMOylation of CRPM2 also resulted in analgesia.[382] The Khanna lab has subsequently developed a small molecule inhibitor of

CRMP2 SUMOylation that selectively reduces $Na_V1.7$ membrane expression and channel activity. Crucially, this molecule upregulated *Penk* message and produced a marked analgesia that was reversible by naloxone.[383] The challenge of achieving antagonist selectivity was thus overcome by the novel approach of targeting a post-translational modification on a $Na_V1.7$ interacting protein that is required for the cell surface trafficking of the channel.

Alternatively, gene therapy strategies that mimic genetic loss-of-function could also be successful. CRISPR gene editing to induce CIP mutations in *SCN9A* in patient nociceptor neurons is perhaps not the best strategy: these changes would be permanent and cause analgesia with all the attendant problems of CIP. Moreno *et al* employed CRISPR interference to dial down expression of *Scn9a* in mouse sensory neurons *in vivo*.[345] They used a catalytically inactivated 'dead' Cas9 that is unable to cleave DNA but can still bind to the genome via a guide-RNA for *Scn9a*. By fusing Cas9 to a KRAB repressor domain, this approach results in selective but not permanent suppression of *Scn9a* expression. Viral expression of this construct by AAV injection resulted in analgesia in mouse models of inflammatory and neuropathic pain. Curiously, these mice were not hyposensitive to acute noxious heat, despite sensory neuron-specific KOs showing this phenotype. Gene therapy faces numerous regulatory hurdles to progress to human trials. However, given CRISPR interference does not permanently alter the genome, this treatment may well be tested in end-of-life patients experiencing intolerable pain in the not too distant future. Thus, with the advent of gene therapy and the development of improved pharmacological approaches, together with an improved mechanistic understanding of $Na_V1.7$ null analgesia, I am positive that hope remains for $Na_V1.7$ as a drug target for chronic pain.

3.5 Conclusions

Taken together, these data support a mechanism where pain insensitivity of mice and humans lacking $Na_V1.7$ principally involves opioid receptors (**Figure 3.16**). Diminished peripheral excitability and die-back may also contribute to analgesia, but opioid-mediated suppression of neurotransmitter release plays a major role. Endogenous opioids inhibit synaptic communication between the central terminals of peripheral nociceptors and post-synaptic neurons in the spinal cord, resulting in diminished nociceptive input to the central nervous system. Importantly, nociceptor activity at the level of the dorsal root ganglion is largely unaffected by $Na_V1.7$ deletion, despite behavioural analgesia. The critical locus of analgesia in $Na_V1.7$ nulls is therefore the central terminal and not, as once thought, the periphery. My findings consequently provide a biological explanation for the failure of peripherally-targeted $Na_V1.7$ inhibitors to cause analgesia, and point to central terminal $Na_V1.7$ and associated opioid signalling pathways as alternative therapeutic targets for pain relief.

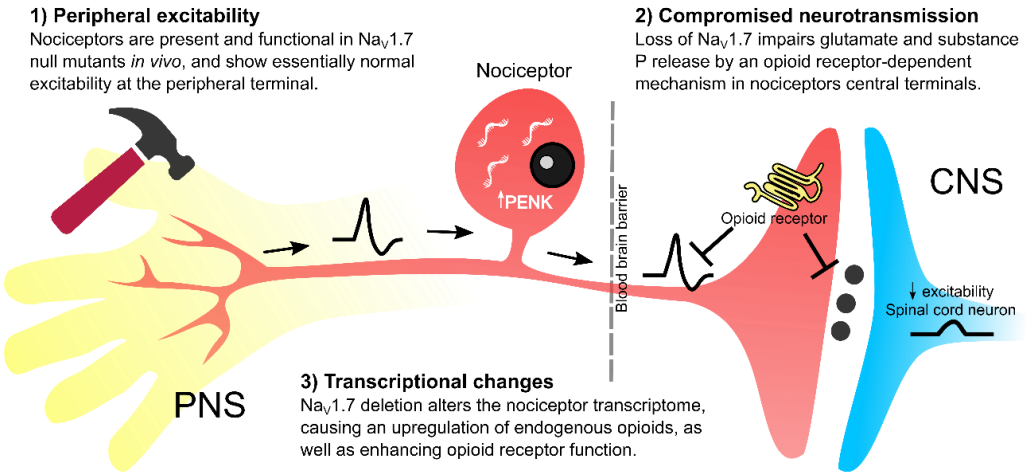

Figure 3.16. The mechanism of analgesia in Na$_V$1.7 null mutants

Cartoon showing the effects of Na$_V$1.7 deletion on nociceptor function.

1) *Peripheral excitability:* Some, but not all, humans with Na$_V$1.7 null mutations show reduced intra-epidermal fibre density, while Na$_V$1.7-deficient sensory neurons are less excitable *in vitro*. But, *in vivo*, terminal excitability is essentially normal, and neurogenic inflammation is preserved. Thus the peripheral terminal is not the locus of analgesia.

2) *Compromised neurotransmission:* Synaptic transfer from nociceptor terminals to spinal cord dorsal horn neurons is impaired after loss of Na$_V$1.7. These synaptic deficits depend on opioid receptors, which can suppress both synaptic release and terminal excitability. Dorsal horn neurons are also less excitable due to absent post-synaptic Na$_V$1.7.

3) *Transcriptional changes:* Loss of Na$_V$1.7 leads to an upregulation of PENK, encoding pre-preproenkephalin, resulting in increased endogenous opioid signalling. Concomitantly, reduced sodium ingress following deletion of Na$_V$1.7 leads to enhanced opioid receptor function inhibiting neurotransmitter release. Analgesia in mice and humans lacking Na$_V$1.7 is thus dependent on opioids.

4 Silent cold-sensing neurons drive cold allodynia in neuropathic pain

4.1 Summary

Chronic pain patients suffering from cold allodynia experience normally innocuous cooling as excruciating pain. While cold sensation in the healthy state is well understood, the cells and molecules that drive cold allodynia remain elusive. I therefore used *in vivo* calcium imaging of dorsal root ganglia to investigate how the activity of peripheral cold-sensing neurons was altered in three mouse models of neuropathic pain: oxaliplatin-induced neuropathy, peripheral nerve injury and ciguatera poisoning.

In control mice, cold-sensitive neurons were rare and had small diameters. In neuropathic animals exhibiting cold allodynia, a set of normally cold-insensitive, large-diameter neurons acquired a *de novo* responsiveness to cooling. These 'silent' cold-sensing neurons were identified as peptidergic nociceptors based on their response to noxious mechanical stimulation and expression of nociceptor markers $Na_V1.8$ and CGRPα. Consistent with this, diphtheria toxin-mediated ablation of silent cold-sensing neurons decreased neuropathic cold hypersensitivity.

Voltage-gated potassium channels $K_V1.1$ and $K_V1.2$ – hypothesized to mediate a hyperpolarizing 'brake' current against cooling-induced depolarization – were highly expressed in silent cold-sensing neurons under naïve conditions. Pharmacological inhibition of $K_V1.1$ consequently induced cold responsiveness in cold-insensitive neurons within minutes *in vivo*, pointing to functional downregulation of $K_V1.1$ channel activity as triggering pathological cold activation.

Here I identify the silent-cold sensing neurons that contribute to cold allodynia in diverse neuropathic pain conditions and identify a molecular mechanism driving de novo cold sensitivity, *in vivo*. Cold allodynia associated with neuropathic pain is thus a profound form of peripheral sensitization that depends on altered nociceptor excitability.

4.2 Introduction

The sensation of cooling is essential for survival, with animals evolving multiple strategies to mitigate, avoid and escape low temperatures. Cold sensation depends on peripheral input from specialized sensory neurons that detect drops in temperature through cutaneous nerve endings. In recent years, the scientific study of cold sensation has been revolutionized by the discovery and characterization of cold transducer molecules – ion channels expressed in sensory neurons that are gated by decreasing temperature.[384] Activation of these ion channels by cooling leads to membrane depolarization, action potential firing, and ultimately the perception of cold by the nervous system.[385]

Extreme cold is experienced as pain because cold is a noxious stimulus that causes profound, irreversible tissue damage at temperatures above and below freezing.[89] In healthy individuals, the temperature at which skin cooling begins to evoke pain and subsequent protective behaviour is about 20 °C, minimizing exposure to dangerously cold stimuli. Among the most unpleasant symptoms of people suffering from chronic pain, however, is cold allodynia, when cooling to normally innocuous temperatures is experienced as excruciating pain (**Figure 4.1**). Chronic pain afflicts a fifth of people worldwide, with many patients refractory to treatment.[18] Of these patients, cold allodynia is a common complaint of people suffering from neuropathic pain triggered by chemotherapy, ciguatera poisoning, peripheral nerve injury and post-herpetic neuralgia (**Figure 4.2**).[163]

Cold allodynia is a maladaptive and inappropriate response of the nociceptive sensory system to mild cooling. Despite advances in identifying cold-gated ion channels, the molecular mechanisms driving pathological cold-evoked pain are unclear.[386] To develop better treatments for chronic pain, it is imperative we understand cold sensation at the molecular level in both health and disease. Here we highlight the ion channels that detect cooling and extreme cold, discuss their contribution to pathological cold pain and end by reviewing the potential cellular and molecular mechanisms driving cold allodynia in neuropathic pain.[387]

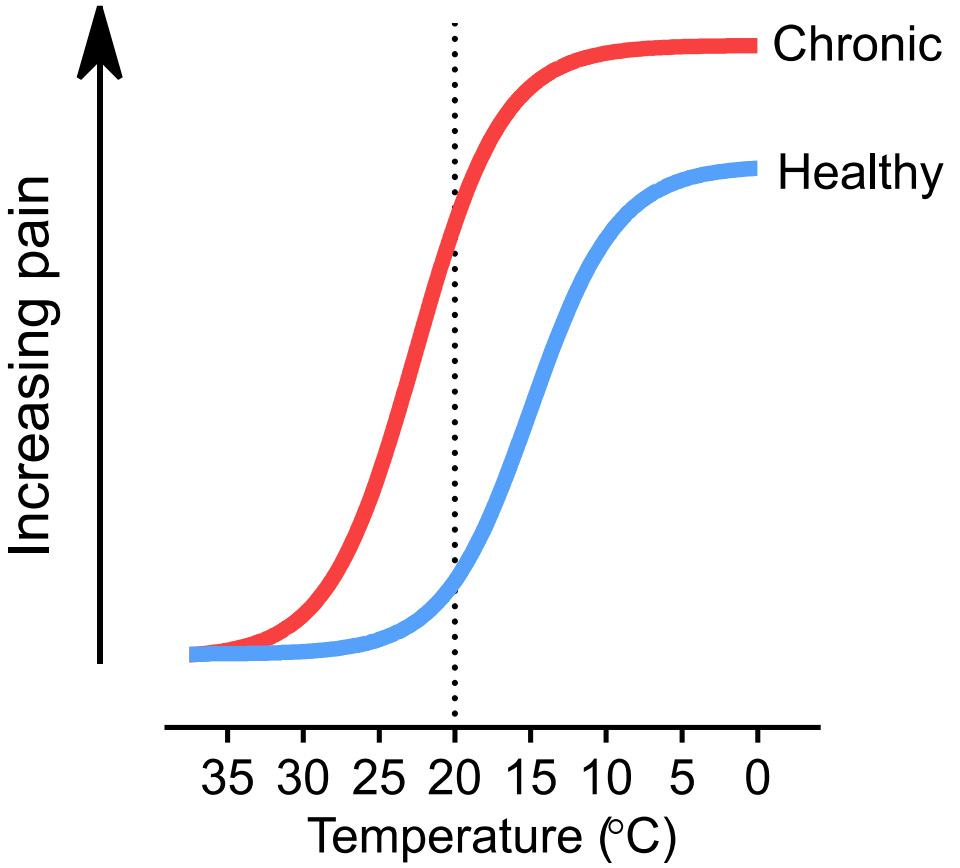

Figure 4.1. Schematic of human cold pain sensitivity in health and disease.

In chronic pain conditions, the sensitivity to decreasing temperature is increased, which typically manifests as an increase in cold-induced pain. The dashed line represents the approximate threshold at which cooling begins to evoke noticeable pain in healthy individuals.

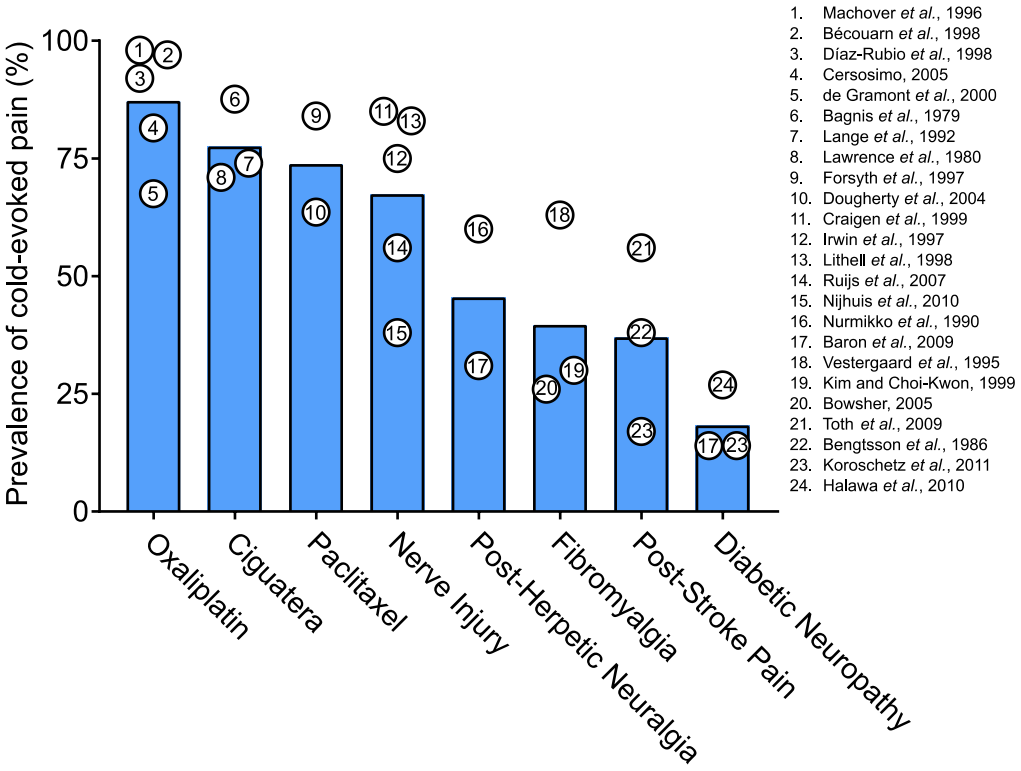

Figure 4.2. Average estimated prevalence of cold-evoked pain in different human pain states.

Data points represent the prevalence of pain evoked by cooling or cold stimuli reported among chronic pain patients in individual clinical studies, and bars represent the mean.[388–411]

4.2.1 Sensory biology of cooling and cold pain

Peripheral sensory neurons have cell bodies in the dorsal root and trigeminal ganglia and conduct action potentials via pseudo-unipolar axons from peripheral tissues to the central nervous system in response to noxious and innocuous stimuli. Although thermosensation is not as extensively studied as touch or nociception in humans, afferents in glabrous skin that respond to cooling have been identified by microneurography.[412] Cold-responsive nerves were first recorded in classical electrophysiological experiments carried out in cats and monkeys.[57,413] The dorsal root ganglia neurons that detect cooling project mainly to the superficial laminae of the dorsal horn: layers I, II and III. Here incoming sensory signals drive reflex arcs and are molded by spinal cord interneuron networks before being transmitted to the brain to drive appropriate behavioural responses.

Cold-sensing afferents encompass a menagerie of different poly- and unimodal, small and large fibre types.[256] Low-threshold thermoreceptors respond to mild cooling, while high-threshold cold nociceptors are activated by extreme cold. C and A-delta low-threshold thermoceptors are spontaneously active at neutral skin temperatures, but their firing frequency increases in response to small temperature drops, and rapidly adapts once steady-state temperature is reached. In contrast, the high-threshold cold nociceptors are normally quiescent, but show prolonged, lower frequency and delayed firing after extended cooling into the noxious temperature range. While low-threshold cold thermoreceptors are usually unimodal, the cold nociceptors also fire in response to noxious heat and mechanical stimuli. Lastly, temperatures below 0°C cause all normally cold-insensitive nociceptors to fire, presumably via freezing-induced tissue damage.[414]

The psychophysical threshold for cooling perception in healthy humans is a drop of just 1-2°C, with cold pain perceived below about 20°C, and a distinct stinging cold sensation felt at subzero temperatures.[163] Despite inter-individual variability, these values generally do map onto sensory afferent cold thresholds. Interestingly, mice have a similar detection threshold for cooling of ~2°C.[415] Compared to other stimulus modalities, cold sensation is trickier to study in mice. The Cold Plate test, for example, measures the time to hindpaw lifting of animals placed on a cooled surface. Latencies reported in the literature range from 5 to 200 s for a plate held at 0°C, as mice adopt a pose that minimizes exposure to the cold.[416] An understanding of both the ethological validity and translational relevance of these tests is crucial to interpreting mouse behavioural phenotypes arising from genetic perturbations of cells and molecules controlling cold sensation. For

convenience, I summarize in **Table 4-1** the impact of genetically manipulating a range of ion channels on selected assays of acute cold sensitivity.

Hitherto these single ion channel genes have proved fruitful as genetic markers to define the cellular code for cold sensation through ablating specific subsets of neurons. However, the advent of single-cell RNA sequencing has allowed for unbiased classification of DRG neurons based on the expression of many thousands of unique transcripts, revealing unexpected complexity in the peripheral coding of cold.[76] The latest study distinguishes three types of Trpm8-positive cold-sensing neuron: two putative C fibre and one putative Aδ fibre population.[77] These chime conveniently with the three functional archetypes of cold-sensing neuron recently uncovered by *in vivo* calcium imaging of cooling-evoked activity in the trigeminal ganglion.[417,418]

In vivo imaging studies are pivotal to investigating the global representation of cooling in the periphery. There does appear to be a specific unimodal 'labelled line' encompassing neurons that detect both mild and noxious cooling, as well as a group of polymodal cells activated by the cold.[245,247,248,264,417,418] Cold-sensing neurons typically exhibit graded responses to enhanced cooling, consistent with a population code where decreasing temperature is correlated with increasing number and strength of neuronal responses.[247,264,417] Wang *et al* propose a contrasting combinatorial strategy where cold-sensing neurons are tuned to respond only within a certain band of temperatures, and it is the pattern of co-activated neurons that reflects the degree of cooling.[248] Given the clear molecular heterogeneity among cold-sensing neurons, it may be that distinct coding strategies are operating simultaneously in different cells. Indeed, Leijon *et al* observed individual neurons that followed either coding scheme.[418] How exactly a unique complement of ion channels endows each cold-sensing neuron with its coding characteristics remains elusive.

Mouse Line			Behavioural Assay			
	Channel (s)	Manipulation	Dry Ice	Acetone	Thermal Preference	Cold Plate
Trp	*Trpm8*	KO	↓[74,419]	↓[90,91,420]	↓[74,90,91,420,421]	↓[91,420,422,423], —[90]
		DTR	↓[74]	↓[420]	↓[74,420]	↓[420]
	Trpa1	KO	—[419]	↓[424]		↓[93,423,425], —[424]
		DTR			—[417]	
	Trpa1/Trpm8	Double KO			↓[421,426]	
	Trpc5	KO			—[427]	—[427]
K2P	*TRAAK*	KO			—[98]	—[98]
	TREK1	KO		—[428]		
	TRAAK / TREK1	Double KO			↑[98]	↑[98]
	TREK2	KO			↑[429]	—[429]
	TRAAK / TREK1 / TREK2	Triple KO			↑[429]	↑[429]
	TASK-3	KO	↑[419]	↑[419]		
	TRESK	KO	↑[430]		↑[430]	↑[430]
Na_V	*$Na_V1.7$*	Avil-Cre KO		↓[257]	—[257], ↓[309]	
		Wnt1-Cre KO		↓[257]	—[257]	
	$Na_V1.8$	KO	—[264]	—[257,264]	↓[257]	↓[264,431]
		DTA	↑[264]	↑[264]	—[309]	↓[431], ↑[264]
	$Na_V1.9$	KO			↓[432]	↓[432], —[433]

Table 4-1. Acute cold sensitivity of ion channel KO and cell ablated mice.

The symbol '↓' denotes reduced cold sensitivity, '↑' denotes cold hypersensitivity and '—' denotes unchanged cold sensitivity on different cold behavioural assays following genetic manipulation of ion channels and sensory neuron subsets.

4.2.2 Molecular transduction of cooling by Trp channels

Menthol, the active ingredient in mint, is used by toothpaste and chewing gum manufacturers to simulate freshness and cooling. This is because menthol activates and sensitizes low-threshold cold thermoreceptors, pointing to a commonality in the detection of cold and the detection of menthol-containing substances. The cloning of a gene encoding the non-selective cation channel Trpm8 – gated both by menthol and decreasing temperatures – revolutionized the field by identifying a molecular substrate for cold-sensing.[434,435] Trpm8 is expressed mainly in small diameter sensory neurons, akin to the C fibre cold thermoreceptors. Fluorescent tracing using Trpm8-eGFP knockin mice show Trpm8-positive afferents terminate centrally in layer I of the spinal cord dorsal horn and peripherally in the epidermis, where they are optimally positioned to sense changes in ambient temperature.[436]

Global deletion of Trpm8 impairs cold sensation in mice, with reduced avoidance behaviour for temperatures between 30°C and 15°C on the thermal place preference test and a loss of firing in sensory afferents to low-threshold cooling stimuli.[90,91,422] Trpm8 knockout (KO) animals are also unable to learn a perceptual task where mice are trained to respond to cooling of the forepaw from 32°C to 22°C.[415] Trpm8 KO animals exhibit decreased core body temperature when housed in the cold, pointing to Trpm8 playing a crucial role in cold-induced thermoregulation.[437] Avoidance of noxious cold is, however, preserved in Trpm8 KO mice, suggesting another transducer is required for detection of high-threshold cold stimuli. When Trpm8-positive neurons are killed in adulthood by diphtheria toxin injection into Trpm8-DTR mice, cold discrimination and cooling-induced analgesia is abolished, but residual cold-sensing is present at lower temperatures.[74,420]

In vivo imaging of the spinal cord reveals that mild, but not noxious, cooling-evoked activity in dorsal horn neurons is diminished in Trpm8-DTR mice, confirming that Trpm8-expression defines a subset of peripheral neurons responsible for innocuous cold input.[438] Imaging of trigeminal ganglia where GCaMP5 was restricted to Trpm8-positive neurons using Trpm8-Cre confirms these cells are overwhelmingly selective for oral cooling, with 90% responding to cold alone.[417] A later *in vivo* imaging study found 87% of menthol-responsive trigeminal neurons responded to cooling. Contrastingly, only 32% of all cold-sensing neurons were activated by menthol.[418] This is consistent with a study of cutaneous cold-sensitive afferents in Trpm8-EGFP mice using the *ex vivo* somatosensory preparation which preserves intact the hairy skin, saphenous nerve, dorsal

root ganglia and spinal cord. Intracellular recordings of dorsal root ganglia somata revealed numerous Trpm8-negative cold afferents among all fibre classes.[439]

What mediates Trpm8-independent cold transduction? Trpa1 is directly activated by cooling below 10°C in recombinant systems and so could control the sensation of painful cold.[440] However, the channel is promiscuous and integrates numerous noxious stimuli, including force, heat, inflammatory mediators and pungent compound.[95] Whether Trpa1 is a *bona-fide* cold sensor *in vivo* remains contentious. Two studies of Trpa1 KO mice indicate the channel is essential for nocifensive behaviours evoked by the 0°C Cold Plate, while another found no differences across multiple, more robust cold pain behavior tests.[93,424,425] No cold responses, even to 1°C stimulation, were detected by imaging of murine trigeminal ganglia expressing GCaMP in Trpa1-positive neurons.[417] A two-plate avoidance test also showed normal avoidance of 5°C by Trpa1-DTR mice, although complete ablation of all Trpa1-expressing neurons was not confirmed in this study.[417]

Cold-sensitive dorsal root ganglia neurons have been observed in culture that lack responses to both menthol and AITC, and therefore probably do not express Trpm8 or Trpa1.[441] This finding is recapitulated *in vivo* – only 36% of trigeminal cold neurons responded to canonical Trp agonists in the oral cavity.[418] Both Trpa1 and Trpm8 have also been shown to be dispensable for the noxious cold sensitivity of the dental pulp.[442] Interestingly, ablation of Trpv1 lineage neurons – a heterogeneous set of nociceptors and thermoreceptors – causes a reduction in noxious cold sensation significantly greater than that seen in mice lacking Trpm8 cells alone, but which cannot be ascribed to Trpa1.[74] This is corroborated by the loss of spinal cord responses to strong cold in Trpv1 DTR mice.[438] Clearly, there is a 'missing sensitivity' to noxious cold in mammalian sensory neurons that cannot be accounted for by Trpm8 or Trpa1.

4.2.3 Structure and function of a cold transducer

As the only cold transducer for which the evidence is unequivocal, Trpm8 has been studied in great detail at the molecular and structural level. Trpm8 channels form homotetramers, with cytosolic N and C terminal domains and six transmembrane domains. Early structure-function studies focused on defining the molecular basis of agonist-sensitivity. Using a high-throughput random mutagenesis screen of ~14,000 mutant Trpm8 channels, residue Y745, mapped to transmembrane segment 2, and residue L1009, in the TRP domain of the C terminal, were pinpointed as crucial for menthol, but not cold sensitivity.[443] A CryoEM structure for Trpm8 from collared flycatcher has

recently been reported at ~4.1 Å – interestingly, residue Y745 was actually identified on transmembrane segment 1 facing the centre of the voltage-sensitive like domain cavity.[444] CryoEM structures of Trpm8 in complex with icilin and menthol analog WS-12 have now conclusively demonstrated that the binding site for cold mimetics is within this voltage-sensitive like domain cavity.[445]

Reconstitution of Trpm8 in a planar lipid bilayer results in a channel that is activated by cooling, in a manner dependent on PIP2, indicative of a direct gating by the cold.[446] Trpm8, like most Trp channels, is weakly voltage-sensitive and bears a topographic similarity to voltage-gated potassium channels. Mutagenesis screens have identified Trpm8 mutants affecting voltage-dependence that also result in altered thermal activation and menthol-sensitivity.[447] For example, substitution of R842 in the S4 and S4-5 linker domain with alanine to neutralize the positive gating charge shifted the voltage-dependence of activation to more depolarized potentials, resulting in reduced agonist and thermal sensitivity.[447] Cooling and cold mimetics may therefore act via the voltage-sensor to shift the voltage-dependence of activation to more hyperpolarized potentials, through an integrative mechanism of channel gating.

A promising approach for identifying residues involved in cold sensitivity is to study orthologues of the channel. For example, hibernating rodents must withstand prolonged exposure to the winter cold. Ground squirrels and Syrian hamsters, both hibernating species, show enhanced cold tolerance on the thermal place preference test compared to non-hibernating mice. Interestingly, cold-sensing neurons from ground squirrels showed normal activation by Trpm8 agonists but reduced sensitivity to the cold. Substitution of the squirrel Trpm8 transmembrane core domain with a rat orthologue rescues cold sensitivity. By systematically replacing individual amino acids, six residues were identified in the transmembrane core that were sufficient to confer normal cold sensitivity to squirrel Trpm8 and that therefore likely control the response to temperature of rodent Trpm8.[448]

Such comparative studies provide unique insights into how evolution operates at the molecular level on the Trpm8 gene to control thermoregulation across different climatic conditions. Recently, the sequencing of the woolly mammoth genome allowed for the resurrection of the mammoth Trpm8 channel which displayed intact agonist-sensitivity but effectively absent cold sensitivity, consistent with the adaptation of this extinct species to Ice Age conditions.[449] In humans, a single nucleotide polymorphism (SNP) variant rs10166942 ~1 kB upstream of Trpm8 shows enormous variation across

the population. Allele frequencies range from 5% in Nigeria to 88% in Finland and strongly correlate with latitude and temperature in a manner indicative of strong positive selection. Interestingly, genome-wide association studies show the same variant is strongly associated with migraine, and Trpm8 modulators have been proposed to treat migraine.[450,451] Although no functional data is available, the SNP is predicted to play a regulatory role and may contribute to the control of Trpm8 expression, tuning thermosensation in different populations to the local climate.[452] That distinct molecular alterations in the Trpm8 coding gene and associated regulatory elements can be linked to gross evolutionary adaptations to the cold in humans and animals further evidences that Trpm8 is the major detector of ambient cooling and primary 'molecular thermostat' for cold-induced thermoregulation in mammals.

4.2.4 Control of excitability at low temperatures by voltage-gated ion channels

Cold-sensing neurons must, by definition, reliably fire action potentials at low temperatures unfavourable to spike initiation due to cooling-induced inactivation of sodium channels. Evolution provides an elegant solution to this paradox. The sensory neuron-enriched TTX-resistant sodium channels $Na_V1.8$ and $Na_V1.9$ display unusual biophysical adaptations to operate during extreme cooling. $Na_V1.8$ does not show cold-induced slow inactivation and so can propagate action potentials at 10 °C when all other sodium channels are inactive. Behavioural tests suggest the channel is essential for pain at low temperatures.[431] Consistent with the purported role of $Na_V1.8$ in cold pain, Cre-dependent diphtheria toxin-mediated ablation of $Na_V1.8$-positive neurons abolishes escape behavior in response to ongoing extreme cold.[73] Corroborating these findings, we recently found that $Na_V1.8$ deletion reduces the activity of neurons responding to prolonged cooling *in vivo*, mirrored by absent jumping when the mice are exposed to a -5 °C cold plate.[264]

Compared to $Na_V1.8$, the activation threshold of $Na_V1.9$ is hyperpolarized which, together with its slow inactivation, means it generates a persistent inward current at rest.[124] Functional upregulation of $Na_V1.9$ in cold-responsive nociceptors thus amplifies subthreshold potentials evoked by cooling enabling prolonged spiking in the cold. $Na_V1.9$ KO mice are consequently less responsive to noxious cold.[432] A heterozygous gain-of-function missense mutation in SCN11A encoding $Na_V1.9$ (p.V1184A) has been identified in a human family by whole-exome sequencing. Family members carrying the mutation experience attacks of pain in the extremities that are triggered and aggravated by cooling.

Mutant channels show hyperpolarized voltage-dependence of activation and cause cold-resistant hyperexcitability when transfected into mouse nociceptors, supporting a contribution of $Na_V1.9$ to nociception at low temperatures.[453]

Despite compelling evidence for a role of $Na_V1.8$ and $Na_V1.9$ in acute cold pain, single cell RNA sequencing of DRG neurons shows these channels have limited overlap in expression with the known cold transducer Trpm8.[76] Indeed, Trpm8-expressing neurons fire TTX-sensitive action potentials, with a substantial contribution from $Na_V1.1$.[454] This begs the question which sodium channel triggers the action potential in the innocuous cold detectors, if the cold-resistant isoforms are unavailable? A possible solution comes from a recent study of corneal afferents, notable for their high incidence of cold sensitivity, which showed that the action potential initiation zone is physically removed from the peripheral terminal, located further along the intraepithelial fibres.[455] In Trpm8-positive cold sensors, sodium channels and the spike initiation zone may be sufficiently distant from the peripheral terminal to be unaffected by local cooling of the receptive field.

Trpm8-expressing cold afferents exhibit enormous variability in their thermal thresholds. Using *in vivo* imaging, we have shown that cold-sensing neurons are small in size and have thresholds that tile the whole range of non-zero temperatures below skin thermoneutrality.[264] How is it that thresholds *in vivo* so widely differ? One answer emerges from differential expression of voltage-gated potassium channels that determine the probability of action potential firing. By recording from identified cold-sensing cells in culture, Madrid *et al* demonstrated that the thermal threshold of a given neuron is reciprocally determined by the functional levels of Trpm8 and a 4-AP-sensitive voltage-gated potassium current.[81] This excitability brake current, I_{KD}, is a voltage-gated hyperpolarizing current that acts to suppress depolarization induced by the cold. The molecular substrate of this current is yet to be conclusively determined, however, its block by dendrotoxins points to heteromers of the Shaker-like $K_V1.1$ and $K_V1.2$ channels as probable candidates.[81] These findings have been replicated by an unbiased constellation pharmacology screen, which demonstrated enhanced dendrotoxin-sensitivity of high-threshold versus low-threshold cold-sensing neurons.[75] Consistent with its purported role as an excitability brake, $K_V1.2$-containing channels have also been shown to blunt cold responses purportedly mediated by Trpa1.[456] Ion channels differentially expressed between low and high-threshold cold-sensing neurons are summarized in **Figure 4.3**.

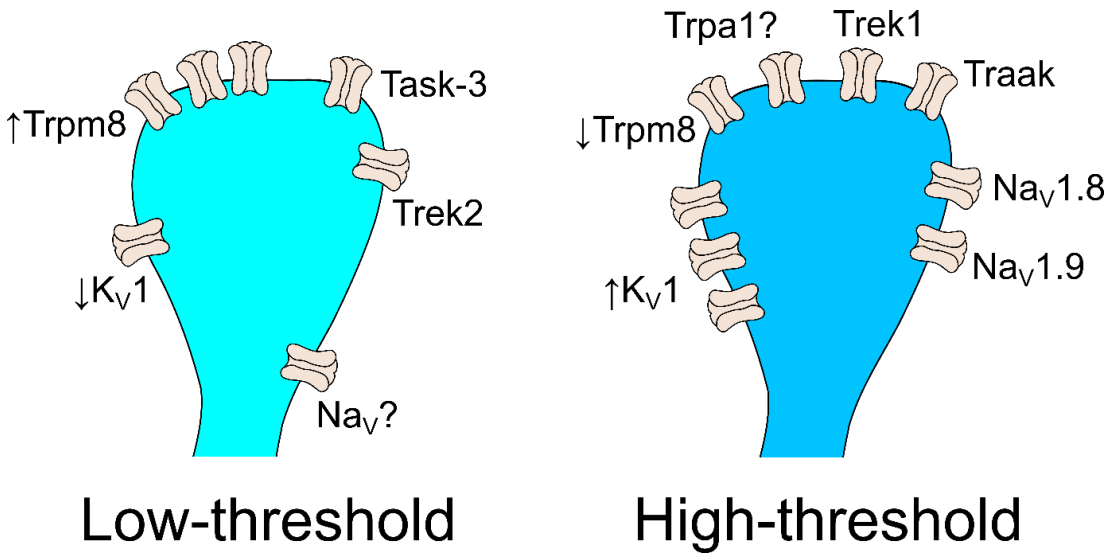

Figure 4.3. Ion channels defining low- and high-threshold cold-sensing neurons.

Schematic illustrating the ion channels expressed in cold-sensing neurons that transduce cooling and control terminal excitability at low temperatures.

4.2.5 Pathophysiology of cold allodynia

While there is a wealth of data on the ion channels and sensory neurons controlling cold-sensing in the healthy state, the role of these cells and molecules in cold allodynia remains unclear. Mouse models of neuropathic pain exhibiting hypersensitivity to cooling are useful tools for mechanistic investigation of cold allodynia *in vivo*, with most studies focused on peripheral nerve injury- and chemotherapy-induced neuropathy.[178] Although these studies are hampered by the challenges involved in assessing cold-evoked pain in mice, a number of molecules have been implicated in cold allodynia through behavioural experiments on KO and cell ablated animals (**Table 4-2**).[166]

Different chronic pain conditions present with similar cold-evoked pain symptoms, but the underlying disease mechanism driving cold allodynia is often distinct. This is evident even in the mouse KO literature, where studies exist that either support or conflict with a role for a given channel or cell type in cold allodynia. Both Trpm8 KO and Trpm8-DTR mice show deficits in cold allodynia monitored by acetone responses after chronic constriction injury.[74,422] Likewise, cold allodynia evoked by artemin, NGF, or morphine-induced hyperalgesia is dependent on the Trpm8 channel.[457,458] On the other hand, Trpm8 deletion has no effect on cold allodynia in a mouse model of ciguatera poisoning. Ciguatoxin-evoked cold hypersensitivity depends instead on Trpa1, corroborated by the emergence in culture of Trpa1-dependent cold responses in a set of normally cold-insensitive neurons.[282] Interestingly, Trpa1 and Trpm8 were both dispensable for acute cold allodynia evoked by a single intraplantar injection of oxaliplatin, reaffirming that alternative transducers mediating pathological cold pain must exist.[279] This is in contrast to systemic models of oxaliplatin where both KOs do apparently show deficits.[459,460]

Which sodium channel isoforms are required for afferent excitability in cold allodynia is equally controversial. $Na_V1.9$ is absolutely required for cold allodynia induced by a single intraperitoneal injection of the chemotherapeutic oxaliplatin.[432] On the other hand, $Na_V1.9$ deletion did not affect cold allodynia in the intraplantar oxaliplatin model of cold allodynia; rather, $Na_V1.6$ was shown to be essential through pharmacological block.[279] This fits with findings that oxaliplatin increases persistent and resurgent $Na_V1.6$ currents in large diameter DRG neurons in culture. [461] Given these divergent findings about the role of sodium channels in oxaliplatin neuropathy, it is clear that even within a chronic pain model with a well-defined etiology, the method of administration, time course and behavioural tests used can all impact the manifestation of gene KO

phenotypes, pointing to mechanistic redundancy at the molecular level. Constitutive gene KO can also cloud interpretation of the phenotype due to compensatory changes in ion channel expression.[120]

Given the limitations of gene deletion experiments, investigation of transgenic mice where subsets of neurons are genetically ablated has been instructive in defining the cellular basis of cold allodynia. In the periphery, cold allodynia and tactile allodynia appear to require distinct 'labelled lines.' Ablation of all Trpv1 lineage neurons prevents cold, but not mechanical, allodynia in the spared nerve injury model.[186] In contrast, ablation of TrkB-positive cells in adulthood suggests these neurons are absolutely required for dynamic, punctate and static tactile allodynia, but dispensable for cold allodynia in the same model.[194] The Trpv1 lineage encompasses diverse types of sensory neuron, however, including cells corresponding to nociceptors and thermosensors, both C and A fibres.[462]

Mouse Line			Disease Model			
Type	Channels (s)	Manipulation	CFA	CCI	Oxaliplatin	Ciguatera
Trp	*Trpm8*	KO	↓[420,422]	↓[420,422]	↓[460], —[279]	—[282]
		DTR	↓[420]			
	Trpa1	KO			↓[459], —[279]	↓[282]
K2P	*TRAAK*	KO		—[98]		
	TREK1	KO		↓[428]		
	TRAAK / TREK1	Double KO		↑[98]	↓[460]	
	TREK2	KO			↓[429]	
	TRAAK / TREK1 / TREK2	Triple KO			↓[429]	
	TRESK	KO			↓[430]	
Na_V	*$Na_V1.7$*	Avil-Cre KO		↓[257,307]	—[307]	
		Wnt1-Cre KO		↓[307]	—[307]	
	$Na_V1.8$	KO		↓[307,463]	—[279,307]	↓[282]
		DTA			—[307]	↓[282]
	$Na_V1.9$	KO		↓[307,463]	↓[432], —[279,307]	—[282]

Table 4-2. Cold allodynia phenotype of ion channel KO and cell ablated mice.

The symbol '↓' denotes reduced or absent cold allodynia, '↑' denotes enhanced cold allodynia and '—' denotes unchanged cold allodynia in different mouse models of neuropathic pain following genetic manipulation of ion channels and sensory neuron subsets. CFA=Complete Freud's Adjuvant. CCI=Chronic Constriction Injury.

4.2.6 Mechanisms of cold allodynia

How might different ion channels and sensory neurons drive cold allodynia? We can distinguish three major hypotheses or mechanisms by which normally innocuous cooling could elicit pain. In the first mechanism, cold-activated nociceptors that normally respond to extreme cold can become responsive to milder temperature drops and consequently drive cooling-evoked pain. Calcium imaging of dissociated sensory neurons found altered activation thresholds of cold-sensitive cells may be responsible for cold allodynia.[262,430] An *in vivo* imaging study which examined cold activity after ultraviolet burn injury did find greater activity with smaller temperature drops, suggesting that threshold shifts may contribute to this form of cold allodynia.[247] This change in threshold has been attributed to functional downregulation of voltage-gated potassium channels, which normally act to limit neuron depolarization in the cold.[464]

In the second mechanism, cold-insensitive nociceptors that normally provide noxious sensory input acquire a *de novo* sensitivity to cooling. A recent *in vivo* imaging study of trigeminal ganglia showed that, following burn injury of the oral cavity, previously 'silent' neurons became newly sensitive to cooling.[417] These neurons were identified as peptidergic nociceptors on the basis of post-hoc immunohistochemical labelling for CGRPα. Tellingly, spared nerve injury-evoked cold allodynia can be temporarily reversed by optogenetic silencing of CGRPα-positive afferents expressing the inhibitory opsin archaerhodopsin-3, hinting at a contribution of these cells to cold allodynia.[465] That nociceptors are recruited to become cold-sensitive during chronic pain is supported by a microneurography study of a human patient with idiopathic small fibre neuropathy whose C-fibre nociceptors show aberrant cold-sensitivity associated with cold allodynia.[466]

In the third mechanism, nociceptive input is unchanged and sensitization to innocuous cold input occurs centrally.[200] According to this hypothesis, afferent activity in response to cooling is normal and drives pain through aberrant spinal cord and brain circuits. A role for non-nociceptive cold neurons is supported by mouse experiments where quaternary lidocaine derivative QX-314 is targeted to silence only Trpm8-expressing neurons.[467] In humans, preferential blockade of large fibres abolishes cold allodynia in both non-freezing cold injury and oxaliplatin neuropathy, demonstrating a requirement for A fibres typically categorized as non-nociceptive.[468,469] The three mechanisms outlined here are not mutually exclusive and may act in concert to drive cold allodynia.

4.2.7 Aims

The goal of this work is to determine the cellular and molecular changes that drive cold allodynia in neuropathic pain. To investigate the mechanism of cold allodynia, I used *in vivo* calcium imaging to ask how the activity of cold-sensitive sensory neurons is altered in different mouse models of neuropathic pain. By combining imaging with molecular genetic, pharmacological and behavioural experiments, this work aims to define the pathophysiological basis of cold-evoked neuropathic pain.

4.3 Results

4.3.1 Functional characterization of cold-sensing neurons using *in vivo* imaging

To investigate the cellular basis of cold-evoked pain, I used Pirt-GCaMP3 mice to image peripheral sensory neuron responses to cooling during health and disease. These mice constitutively express the genetically-encoded calcium indicator GCaMP3 in all somatosensory neurons in a manner that is independent of Cre recombinase. As GCaMP3 is knocked in to the endogenous *Pirt* locus, the heterozygous Pirt-GCaMP3 mice used here lack one copy of the *Pirt* gene. Pirt protein is a positive regulator of Trpm8 function in sensory neurons and homozygous *Pirt* null mice show impaired cold sensation.[470] I therefore conducted a battery of behavioural tests on heterozygous Pirt-GCaMP3 animals to ensure mice hemizygous for *Pirt* showed no deficit in pain behaviour. There was no difference in sensory thresholds between WT and heterozygous Pirt-GCaMP3 animals for all tested pain modalities, validating the use of this mouse line for studies of neuropathic pain (**Figure 4.4A-F**).

As a proof-of-principle, I used *in vivo* imaging to characterize the response of sensory neurons in the L4 dorsal root ganglion to mild and extreme cooling in the naïve state. Different cooling stimuli were applied to the glabrous surface of the ipsilateral hindpaw using a Peltier-controlled thermode. Using both a staircased (**Figure 4.5Ai**) and a drop (**Figure 4.5Aii**) temperature stimulus, I recorded 134 cold-sensing neurons that displayed thresholds that tiled a wide range of cold temperatures (25°C to 0°C). For the staircased stimulus, thresholds were distributed across this range, albeit with fewer found at the very lowest tested temperature (**Figure 4.5B**). For the drop temperature stimulus, the number of responding neurons showed an almost perfect linear rise with increasing temperature drops (**Figure 4.5C**). All cold-sensing neurons observed here were small in size, and cross-sectional areas were fit by a Gaussian distribution centred on mean of 253.6 μm^2 (**Figure 4.5D**). When I compared the activation thresholds estimated by the two stimulus protocols, the mean drop threshold was linearly related to the threshold estimated by the staircase stimulation (**Figure 4.5E**). These results suggests that cold is encoded in the periphery by a graded population code, where the number of responding neurons increases proportionately with the degree of cooling, and thermal activation thresholds are distributed across the whole range of temperatures below skin thermoneutrality.

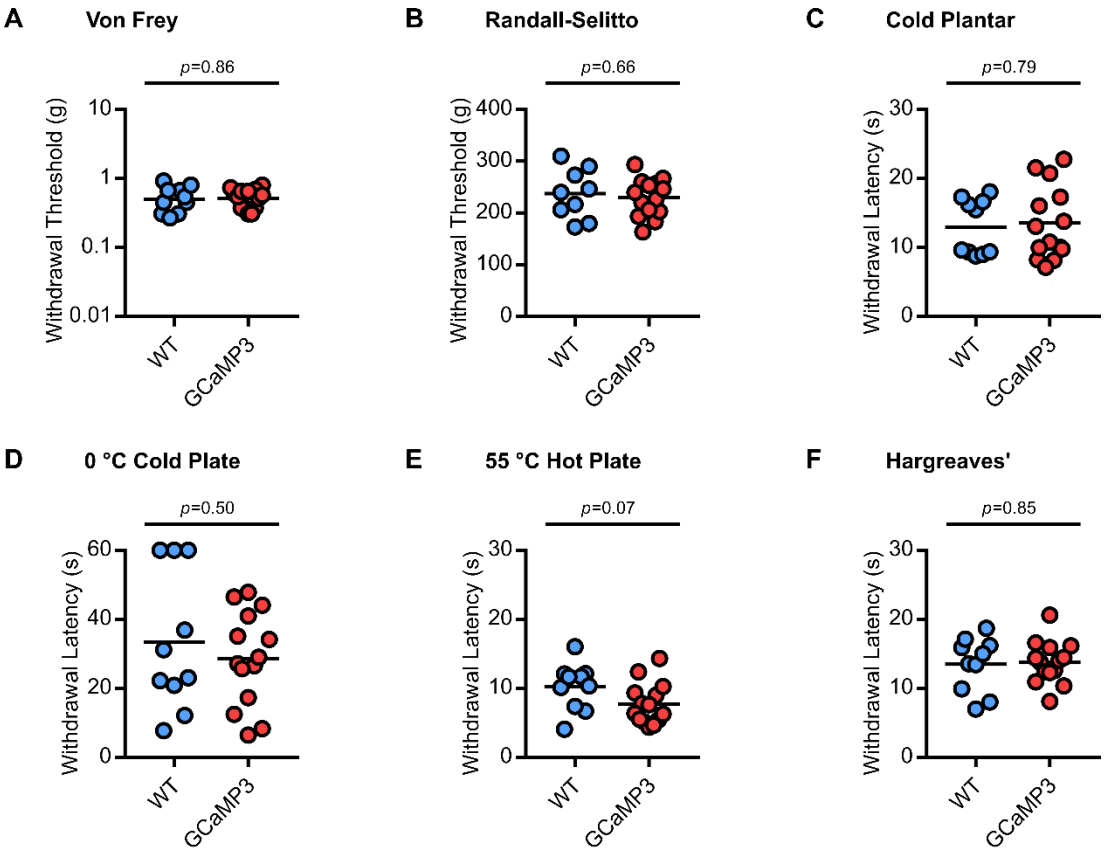

Figure 4.4. Pirt-GCaMP3 mice show normal pain behaviour.

(A) Sensitivity to punctate mechanical stimuli measured using Von Frey hairs is not altered between WT (blue, n=10) and heterozygous Pirt-GCaMP3 mice (red, n=14).

(B) No change in the response to noxious mechanical stimulation measured using Randall-Selitto apparatus.

(C) No change in the sensitivity to mild cooling stimuli applied in the Cold Plantar (Dry Ice) test.

(D) No change in sensitivity to extreme cold measured on 0°C cold plate.

(E) No change in sensitivity to extreme heat measured 55°C hot plate.

(F) No change in sensitivity to radiant heat measured using the Hargreaves' apparatus.

The means are indicated by lines and compared between genotypes using unpaired t tests.

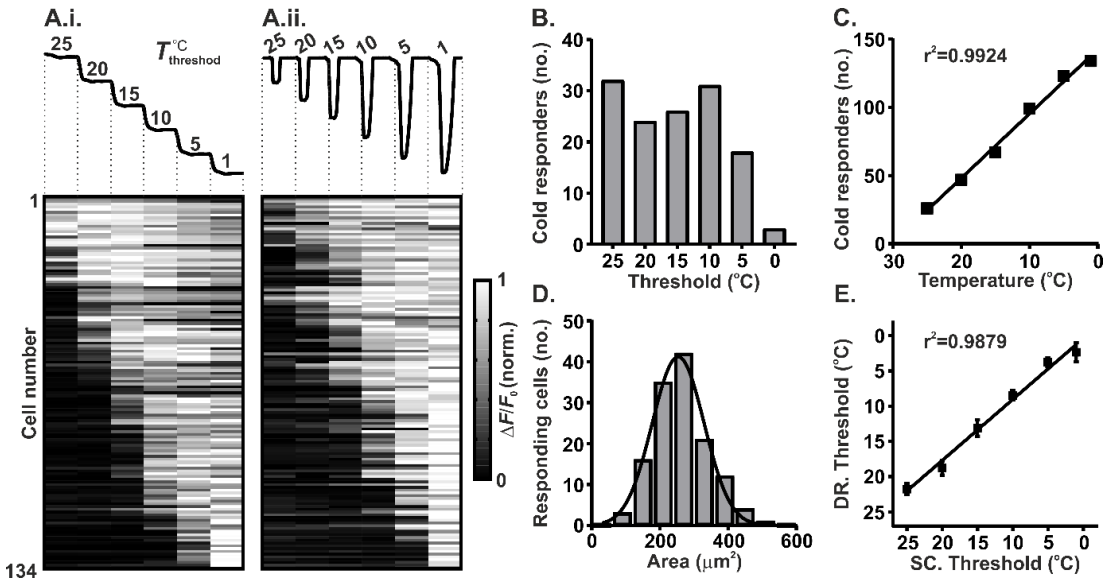

Figure 4.5. *In vivo* calcium imaging of peripheral sensory neurons reveals variable thermal activation thresholds of cold-sensing neurons.

*(*A) Normalised fluorescence response from 134 cold-sensitive neurons from 21 animals expressing GCaMP3 following a staircased (A.i.) or drop temperature stimulus (A.ii.). The cooling protocols are shown at the top of the figure. Each row represents the response from the same neuron to each stimulus protocol.

(B) Summary of the threshold of cold-sensing neuron activation observed following a staircased cooling protocol as in (A.i.).

(C) Number of neurons activated by different cooling temperature drops as in (A.ii.) (linear regression: $y = -4.715 * x + 142.4$).

(D) Histogram of cell area for cold-sensing neurons (Least squares Gaussian; Bin width is 60 μm2 ; Mean=253.6 μm^2 , Std. Dev. 76.06 μm^2).

(E) Relationship between mean thresholds of activation in response to a drop (DR) cooling stimulus versus a staircased (SC) cooling stimulus (linear regression: $y = 0.8652 * x + 0.3839$). Error bars denote S.E.M.

4.3.2 *In vivo* imaging of cold-sensing neurons during chemotherapy-induced neuropathy

To investigate the mechanisms of cold allodynia, I used *in vivo* calcium imaging to explore how sensory neuron responses to cooling are altered in different mouse models of neuropathic pain. I focused initially on chemotherapy-induced neuropathy because ~90% of cancer patients treated with the chemotherapeutic drug oxaliplatin develop cold allodynia (**Figure 4.2**). Pirt-GCaMP3 mice expressing GCaMP3 in all sensory neurons were treated with the chemotherapeutic drug oxaliplatin (80 μg/40 μl by hindpaw intraplantar injection). Three hours after injection mice displayed extreme cold hypersensitivity as measured by the number of pain-like behaviours (lifting, licking, guarding or shaking of the ipsilateral hindpaw) when the animal was placed on a 5 °C Cold Plate (**Figure 4.6A**). The short-latency cold hypersensitivity observed after a single clinical dose of oxaliplatin (~3mg/kg) in this model mimics the rapid onset of cold allodynia in patients.[279] Importantly, oxaliplatin-injected mice also developed punctate tactile allodynia assessed by Von Frey testing, but no heat hyperalgesia was evident on the Hot Plate, consistent with a neuropathic phenotype (**Figure 4.6A**).

Using laser-scanning confocal microscopy, I imaged cold-evoked calcium signals in sensory neuron somata within the L4 dorsal root ganglion of animals treated with vehicle (n=82 cold-sensing neurons) and oxaliplatin (n=179). There was a dramatic change in the peripheral representation of cold following oxaliplatin treatment (**Figure 4.6B** and enlarged in **Figure 4.7**). In vehicle-treated mice, cold-sensing neurons were sparse and small in size, in agreement with previous observations.[248,264] When I measured the size of neurons responding to either ice-water or acetone, cross-sectional areas were normally distributed and had a mean value of 214.9 μm^2 (**Figure 4.6C**). In oxaliplatin-treated animals, small cells also responded to cold, however a novel, normally cold-insensitive population of medium-to-large diameter neurons also became activated by cooling. These cells had cross-sectional areas that lay more than three standard deviations from the mean value for vehicle (>446.77 μm^2) (**Figure 4.6C**). These larger neurons essentially never respond to cooling under physiological conditions but acquire a *de novo* sensitivity to cold following oxaliplatin. I therefore decided to name them 'silent cold-sensing neurons' as they are reminiscent of the silent nociceptors that are unmasked during inflammation.[245]

The increase in the size of neurons responding to cold after oxaliplatin was apparent for both ice-water and acetone stimuli when considered individually (**Figure**

4.8A). There was no marked change in cross-sectional area for mechanically-sensitive neurons (**Figure 4.8A**). The heat-activated population showed a small, but statistically significant, shift towards larger cells (**Figure 4.8A**). Interestingly, in oxaliplatin-treated animals, the response of many larger cold cells to acetone was temporally-delayed and continued for tens of seconds beyond the initial delivery of the stimulus (**Figure 4.6B**). Consistent with this, when oxaliplatin-treated animals were tested with acetone, the animals showed profound pain-like behavior localized to the ipsilateral paw for nearly the entire minute following acetone stimulation; the contralateral paw showed a minimal response (**Figure 4.8B**). The unmasking of normally silent, large-diameter cells to become cold-activated by oxaplatin was reflected in an increase in the relative number of cold-sensitive cells from 21% (82/383) to 33% (179/542) (**Figure 4.6D**). There was no increase in the number of cells responding to other modalities (**Figure 4.8C**). Thus oxaliplatin treatment results in a modality-specific expansion in the peripheral representation of cold.

I wondered whether oxaliplatin also increased the sensitivity of cold-sensing neurons so that more cells had thermal activation thresholds at higher temperatures. To my surprise, there was no significant change in the distribution of cold thresholds when the hindpaw was stimulated with drop temperature stimuli delivered by a Peltier-controlled thermode (**Figure 4.6E**). Next, I quantified the peak fluorescence signal activated by cold as a surrogate for excitability before and after oxaliplatin. For this analysis, cold-sensing neurons in the oxaliplatin-treated group were divided into a basal population (within three standard deviations of the mean cross-sectional area for the vehicle group), and a silent population (greater than three standard deviations away from the mean, >446.77 μm^2). Both the basal and silent population showed no change in cold-evoked activity after oxaliplatin when compared to the vehicle group (**Figure 4.6F**). In addition, the magnitude of responses to mechanical stimuli was not altered, although the response to heat was reduced (**Figure 4.8D**). Collectively, these data indicate oxaliplatin does not markedly affect the activation thresholds or excitability of the basally-active cold-sensing neurons.

What is the functional identity of silent cold-sensing neurons? It has been shown before that nociceptor polymodality is increased by treatment with inflammatory mediators that cause pain.[245] Interestingly, there were visibly more polymodal neurons in the oxaliplatin-treated group (**Figure 4.6B**). Oxaliplatin increased the proportion of mechano-heat neurons from 19% (26/136) to 32% (61/193) (**Figure 4.8E**). In vehicle-

injected animals, very few cold-sensing neurons responded to heat, and this was unaffected by oxaliplatin (**Figure 4.6Gi**). By contrast, oxaliplatin markedly increased the prevalence of cold-sensing neurons also responding to mechanical stimuli (**Figure 4.6Gii**). For ice-water, this rose from 16% (8/51) to 33% (27/81) and for acetone from 12% (7/58) to 37% (53/145). Note this number is likely an under-estimate because the application area of pinch stimuli is less than that of ice-water or acetone and thus targets a smaller receptive field. These mechano-cold neurons were mainly large-diameter cells (**Figure 4.6Giii**). Many silent cold-sensing neurons therefore also respond to noxious mechanical stimuli, consistent with a functional identity as nociceptors.

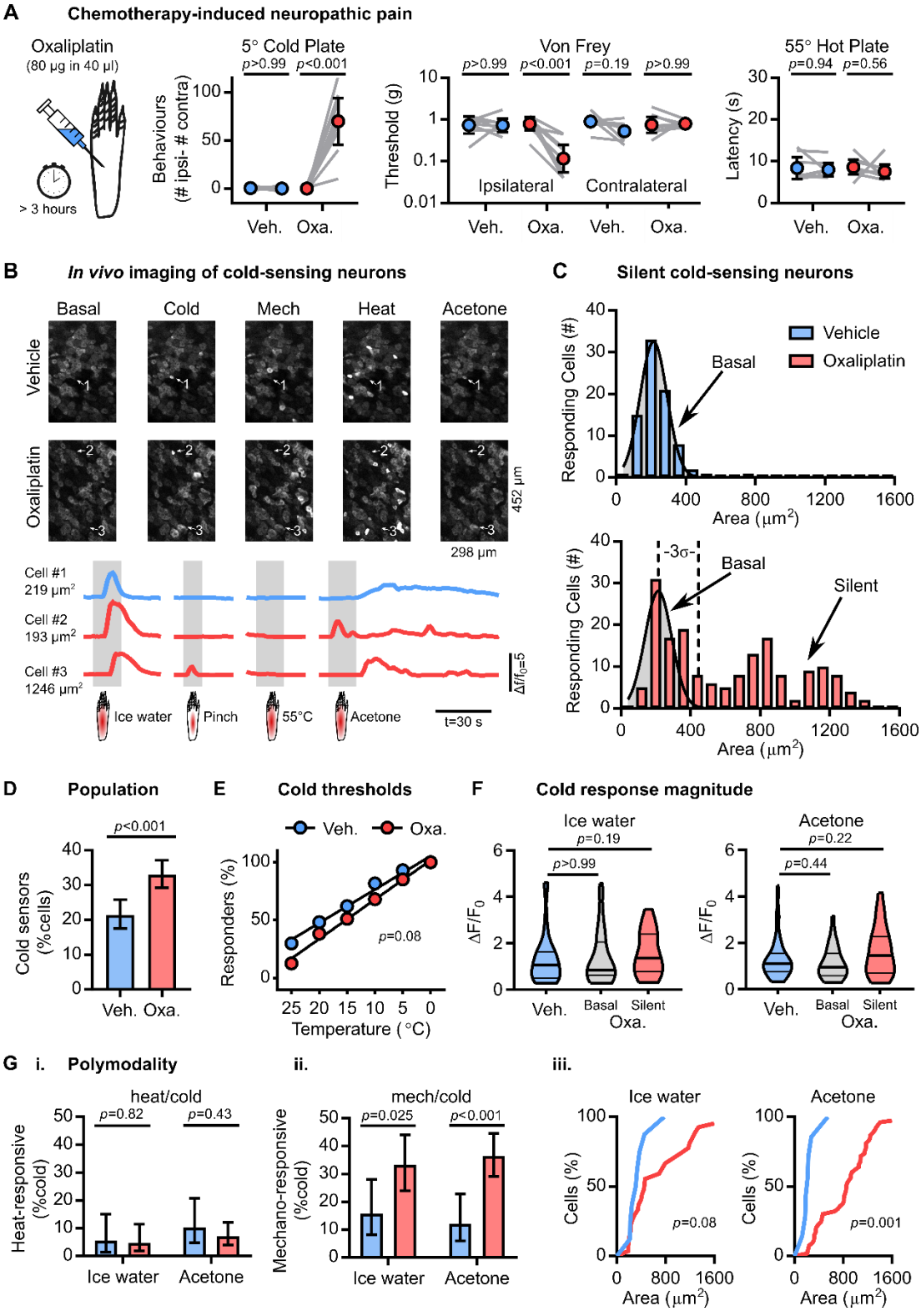
A
Chemotherapy-induced neuropathic pain
Oxaliplatin
(80 µg in 40 µl)
> 3 hours
5° Cold Plate
p>0.99 p<0.001
Behaviours (# ipsi- # contra)
Veh. Oxa.
Von Frey
p>0.99 p<0.001 p=0.19 p>0.99
Threshold (g)
Ipsilateral
Contralateral
Veh. Oxa. Veh. Oxa.
55° Hot Plate
p=0.94 p=0.56
Latency (s)
Veh. Oxa.
B
In vivo imaging of cold-sensing neurons
Basal Cold Mech Heat Acetone
Vehicle
Oxaliplatin
452 µm
298 µm
Cell #1
219 µm²
Cell #2
193 µm²
Cell #3
1246 µm²
Ice water
Pinch
55°C
Acetone
t=30 s
C
Silent cold-sensing neurons
Responding Cells (#)
Vehicle
Oxaliplatin
Basal
Area (µm²)
-3σ-
Silent
D
Population
p<0.001
Cold sensors (%cells)
Veh. Oxa.
E
Cold thresholds
Veh. Oxa.
Responders (%)
p=0.08
Temperature (°C)
F
Cold response magnitude
Ice water
p=0.19
p>0.99
Acetone
p=0.22
p=0.44
ΔF/F0
Veh. Basal Silent
Oxa.
G
i. Polymodality
heat/cold
p=0.82 p=0.43
Heat-responsive (%cold)
Ice water Acetone
ii.
mech/cold
p=0.025 p<0.001
Mechano-responsive (%cold)
Ice water Acetone
iii.
Ice water
Acetone
Cells (%)
p=0.08
p=0.001
Area (µm²)

Figure 4.6. Silent cold-sensing neurons are activated by oxaliplatin-induced neuropathy.

(A) Behavioural testing of the effect of oxaliplatin on different sensory modalities. n=8 for vehicle and n=9 for oxaliplatin. Mean values before and after treatment were compared using repeated measures 2-way ANOVA followed by post-hoc Sidak's test. Error bars denote 95% confidence interval.

(B) Example images and traces of cold-responding neurons in vehicle- and oxaliplatin-treated animals expressing GCaMP3. Cell #1 is a small-diameter cold-sensing neuron in the vehicle condition, Cell #2 is a small-diameter basal cold-sensing neuron after oxaliplatin and Cell #3 is a large-diameter silent cold-sensing neuron unmasked by oxaliplatin that also responds to noxious mechanical stimuli

(C) Histograms of cross-sectional area of all neurons responding to any cold stimulus in vehicle (top, blue, n=82) and oxaliplatin (bottom, red, n=179) groups. The distribution of areas for vehicle was fit by non-linear regression (least squares Gaussian; Bin width is 80 μm^2 ; Mean=214.9 μm^2 , Std. Dev. 77.29 μm^2). This model is plotted over the oxaliplatin data to aid comparison with the dashed line denoting three standard deviations from the mean. The different in the distribution of areas between groups was assessed by Kolmogorov-Smirnov test (p<0.001).

(D) Bar plot of the percentage of responding neurons sensitive to any cold stimulus in vehicle and oxaliplatin groups. Proportions were compared using a χ^2 test, and error bars denote 95% confidence intervals.

(E) Relationship between the number of responding cells and the drop in temperature can be fit by linear regression for both groups. For vehicle, $y = -3.442 * x + 105.2$, r^2=0.9809, n=87. For oxaliplatin, $y = -3.392 * x + 101.6$, r^2=0.9921, n=47. The slopes are not significantly different.

(F) Violin plots showing the peak responses evoked by cold stimuli in the vehicle group and separately in the basal and silent cold-sensing neurons from the oxaliplatin group. Ice water: n=51 for vehicle, n=40 for basal, and n=41 for silent. Acetone: n=58 for vehicle, n=57 for basal, and n=88 for silent. Medians were compared by Kruskall-Wallis test followed by Dunn's multiple comparison's test.

(G) Quantification of the proportion of cold-sensing neurons responding to either heat (i.) or mechanical (ii.) stimuli in vehicle and oxaliplatin groups. The proportion of polymodal neurons was compared using χ^2 test, and error bars denote confidence intervals. Ice water: n_{veh}=51, n_{oxa}=81 for oxaliplatin. Acetone: n_{veh}=58, n_{oxa}=145. (iii.) Cumulative probability plots showing mechano-cold neurons have larger cross-sectional areas in the oxaliplatin group, as determined by the Kolmogorov-Smirnov test. Ice water: n_{veh}=8, n_{oxa}=62. Acetone: n_{veh}=7, n_{oxa}=53.

For this experiment, 383 neurons responding to any stimulus were recorded in 8 vehicle-treated mice and 542 cells were recorded from 9 oxaliplatin-treated animals.

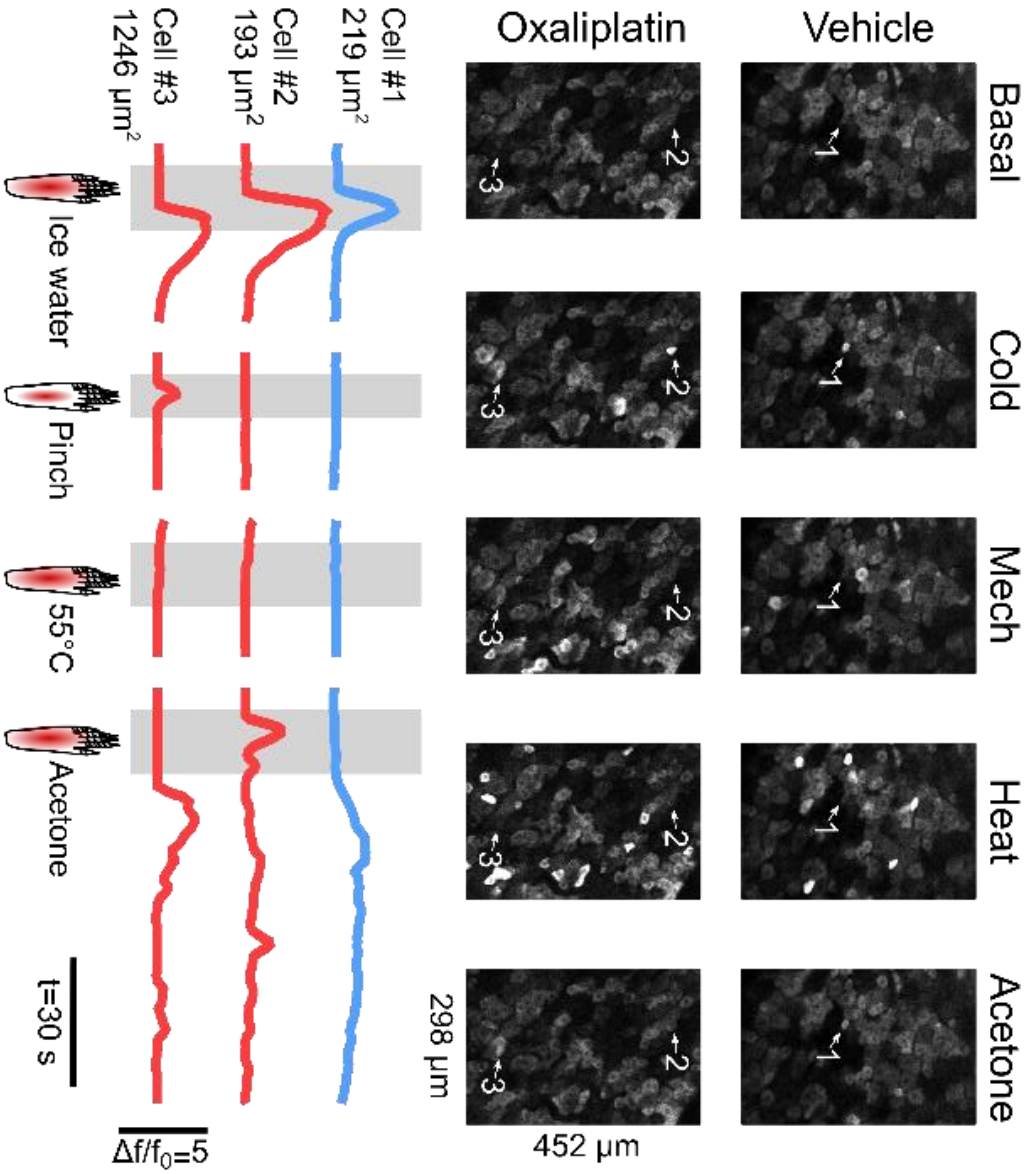

Figure 4.7. ***In vivo*** **imaging of cold-sensing neurons during oxaliplatin neuropathy (enlarged)**

Example images and traces of cold-responding neurons in vehicle- and oxaliplatin-treated animals expressing GCaMP3. Cell #1 is a small-diameter cold-sensing neuron in the vehicle condition, Cell #2 is a small-diameter basal cold-sensing neuron after oxaliplatin and Cell #3 is a large-diameter silent cold-sensing neuron unmasked by oxaliplatin that also responds to noxious mechanical stimuli

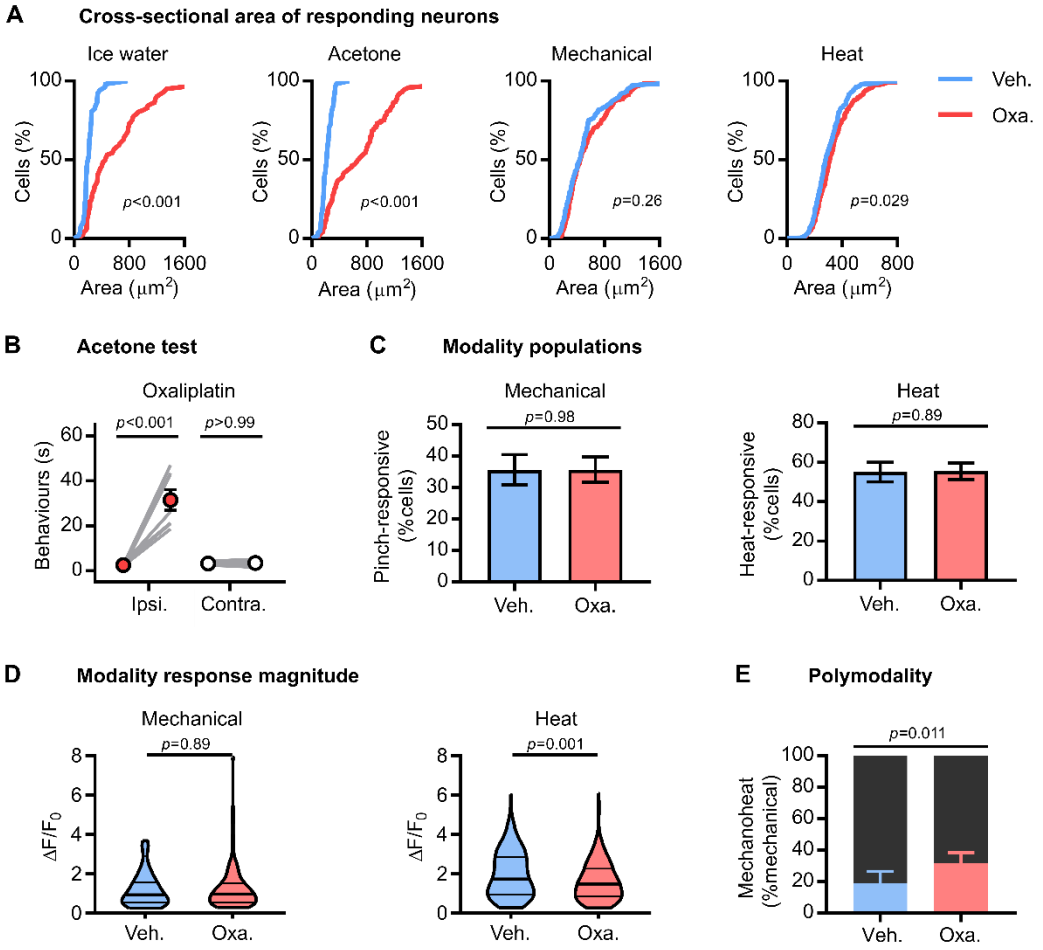

Figure 4.8. Modality-specific effects of oxaliplatin on sensory neuron physiology.

(A) Cumulative probability plots of cross-sectional areas for cells responding to each stimulus modality, compared using Kolmogorov-Smirnov test.

(B) Effect of oxaliplatin on acetone-evoked pain behaviour. Means before and after treatment were compared using repeated measures 2-way ANOVA with post-hoc Sidak's test. n=7 for both.

(C) Bar plots showing the proportion of all responding neurons responding to heat or mechanical stimuli, compared using χ^2 test. Error bars denote 95% confidence interval.

(D) Violin plots showing peak response evoked by each stimulus modality, compared using Mann-Whitney test.

(E) Proportion of mechanically-sensitive neurons also responding to noxious heat, compared using χ^2 test. Error bars denote 95% confidence interval.

Ice-water: n_{veh}=51, n_{oxa}=81. Acetone: n_{veh}=58, n_{oxa}=145. Mechanical: n_{veh}=136, n_{oxa}=193. Heat: n_{veh}=211, n_{oxa}=301.

4.3.3 *In vivo* imaging of cold-sensing neurons during peripheral nerve injury

Are silent cold-sensing neurons recruited in other neuropathic pain states? To mimic chronic neuropathic pain associated with nerve injury, I performed partial sciatic nerve ligation (PNL) on Pirt-GCaMP3 mice (**Figure 4.9A**). Two weeks after surgery, nerve injured animals developed mechanical, but not cold, hypersensitivity. At four weeks, I saw both mechanical and a modest cold hypersensitivity, but no difference in heat withdrawal latencies. I therefore performed *in vivo* imaging of both nerve-injured and sham-operated mice between 4 and 5 weeks post-surgery, when cold allodynia was present (**Figure 4.9B** and enlarged in **Figure 4.10**). As expected, in sham-operated mice, cold-sensing neurons were small in size with a mean of 222.7 μm^2 (n=113) (**Figure 4.9C**). But after nerve injury, a set of normally cold-insensitive, large-diameter neurons began to respond to cooling (n=109) (**Figure 4.9C**). Neurons with cross-sectional areas greater than three standard deviations away from the mean sham value (>405.4 μm^2) were again classified as silent cold-sensing neurons. The recruitment of large cells by cold after nerve injury was apparent for both ice-water and acetone stimuli (**Figure 4.11A**). Consistent with the less profound behavioural cold hypersensitivity, silent cold-sensing neurons were fewer in number in nerve injured animals compared to the effect of oxaliplatin treatment. This was reflected in the relatively modest expansion of the cold-responsive population from 30% (113/373) to 37% (109/291). (**Figure 4.9D**).

As with oxaliplatin, there was no detectable shift in the thermal activation thresholds of cold-responsive neurons after nerve injury (**Figure 4.9E**). The effect of nerve injury on the excitability of cold-sensing neurons was complex. Acetone-evoked activity was enhanced in the basal population, while ice-water response magnitude was less in the silent cells (**Figure 4.9F**). There was no change in the prevalence of heat/cold polymodal neurons (**Figure 4.9Gi**), however the proportion of mechano-cold cells was significantly increased (**Figure 4.9Gii**). For ice-water, this rose from 5% (3/64) to 20% (14/71) and for acetone from 0% (0/95) to 10% (7/73). Mechano-cold cells comprised both the basal and silent cold-sensing neurons, based on cell size (**Figure 4.9Giii**). Thus, the effects of nerve injury on the peripheral representation of cold is qualitatively similar to the effect of oxaliplatin, characterized by an unmasking of silent cold-sensing neurons that also often respond to noxious mechanical stimuli.

Nerve injury had varying consequences on other modalities. There was no change in the cell area distribution for mechanical stimuli, but the heat-activated population was larger in size (**Figure 4.11A**). By contrast, more neurons responded to pinch (38% vs.

28%), and there was a trend towards fewer responses to heat (40% vs. 47%) (**Figure 4.11B**). I saw no difference in the response to noxious heat, but pinch-evoked activity was decreased (**Figure 4.11C**). Unlike oxaliplatin, there was no enhancement of mechano-heat polymodality (**Figure 4.11D**). Taken together, although some of the effects of nerve injury on other modalities are dissimilar to oxaliplatin, the consequences for peripheral cold sensation are comparable.

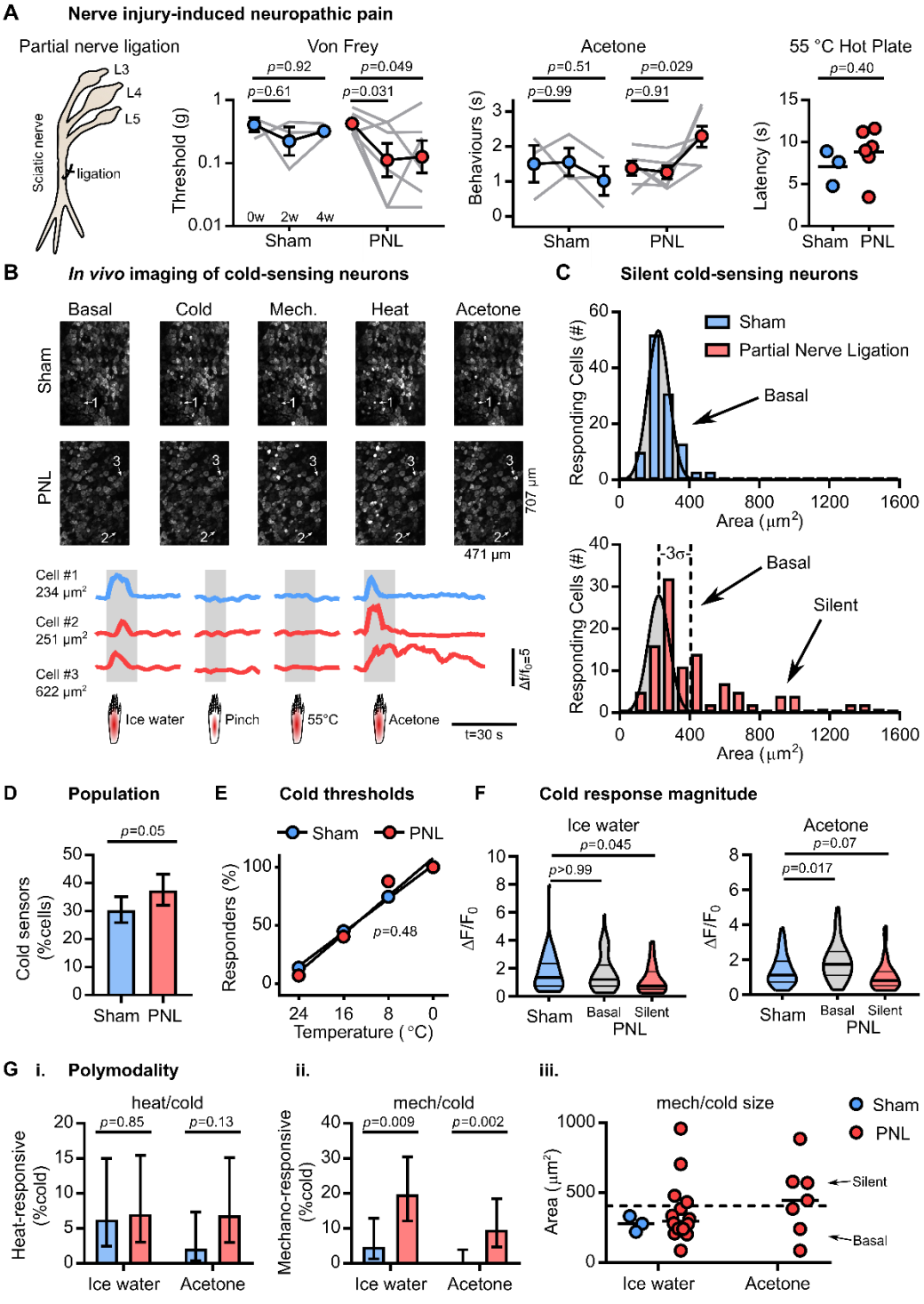
A
Nerve injury-induced neuropathic pain
Partial nerve ligation
L3
L4
L5
Sciatic nerve
ligation
Von Frey
p=0.92
p=0.049
p=0.61
p=0.031
Threshold (g)
0w 2w 4w
Sham
PNL
Acetone
p=0.51
p=0.029
p=0.99
p=0.91
Behaviours (s)
55 °C Hot Plate
p=0.40
Latency (s)
B
In vivo imaging of cold-sensing neurons
Basal
Cold
Mech.
Heat
Acetone
Sham
PNL
707 µm
471 µm
Cell #1
234 µm²
Cell #2
251 µm²
Cell #3
622 µm²
Ice water
Pinch
55°C
Acetone
t=30 s
C
Silent cold-sensing neurons
Sham
Partial Nerve Ligation
Basal
Responding Cells (#)
Area (µm²)
3σ
Silent
D
Population
p=0.05
Cold sensors (%cells)
E
Cold thresholds
Sham
PNL
p=0.48
Responders (%)
Temperature (°C)
F
Cold response magnitude
Ice water
p=0.045
p>0.99
ΔF/F0
Acetone
p=0.07
p=0.017
G
i. Polymodality
heat/cold
p=0.85
p=0.13
Heat-responsive (%cold)
ii.
mech/cold
p=0.009
p=0.002
Mechano-responsive (%cold)
iii.
mech/cold size
Area (µm²)
Silent
Basal

Figure 4.9. Silent cold sensing neurons are activated after partial sciatic nerve ligation.

(A) Behavioural testing of the effect of partial nerve ligation (PNL) on different sensory modalities. n=3 for sham and n=6 for PNL. For Von Frey and Acetone test, means over time were compared using repeated measures 2-way ANOVA followed by post-hoc Sidak's test. Hot Plate latencies at 4 weeks were compared using unpaired t test. Error bars denote 95% confidence interval.

(B) Example images and traces of cold-responding neurons in sham- and PNL-operated animals expressing GCaMP3. Cell #1 is a small-diameter cold-sensing neuron in the sham condition, Cell #2 is a small-diameter basal cold-sensing neuron after PNL and Cell #3 is a large-diameter silent cold-sensing neuron unmasked by PNL.

(C) Histograms of cross-sectional area of all neurons responding to any cold stimulus in sham (top, blue, n=113) and oxaliplatin (bottom, red, n=109) groups. The distribution of areas for sham was fit by non-linear regression (least squares Gaussian; Bin width is 80 μm^2 ; Mean=222.7 μm^2 , Std. Dev. 60.9 μm^2). This model is plotted over the PNL data to aid comparison with the dashed line denoting three standard deviations from the mean. The different in the distribution of areas between groups was assessed by Kolmogorov-Smirnov test ($p<0.001$).

(D) Bar plot of the percentage of responding neurons sensitive to any cold stimulus in sham and PNL groups. Proportions were compared using a χ^2 test, and error bars denote confidence intervals.

(E) Relationship between the number of responding cells and the drop in temperature can be fit by linear regression for both groups. For sham, $y = -3.603 * x + 101.6$, $r^2=0.9979$, n=51. For PNL, $y = -4.079 * x + 107.7$, $r^2=0.9583$, n=57. The slopes are not significantly different.

(F) Violin plots showing the peak responses evoked by cold stimuli in the sham group and separately in the basal and silent cold-sensing neurons for the PNL group. Ice water: n=64 for vehicle, n=46 for basal, and n=25 for silent. Acetone: n=95 for sham, n=42 for basal, and n=31 for silent. Medians were compared by Kruskall-Wallis test followed by Dunn's multiple comparison's test.

(G) Quantification of the proportion of cold-sensing neurons responding to either heat (i.) or mechanical (ii.) stimuli in sham and PNL groups. The proportion of polymodal neurons was compared using χ^2 test, and error bars denote confidence intervals. Ice-water: $n_{sham}=64$, $n_{PNL}=71$. Acetone: $n_{sham}=95$, $n_{PNL}=73$. (iii.) Scatter plots showing mechano-cold neurons have both small and large cross-sectional areas in the PNL group. Mech./ice water: $n_{sham}=3$, $n_{PNL}=14$. Mech./acetone: $n_{sham}=0$, $n_{PNL}=7$.

For this experiment, 373 neurons responding to any stimulus were recorded in 3 sham-operated mice and 291 cells were recorded from 6 PNL-operated animals.

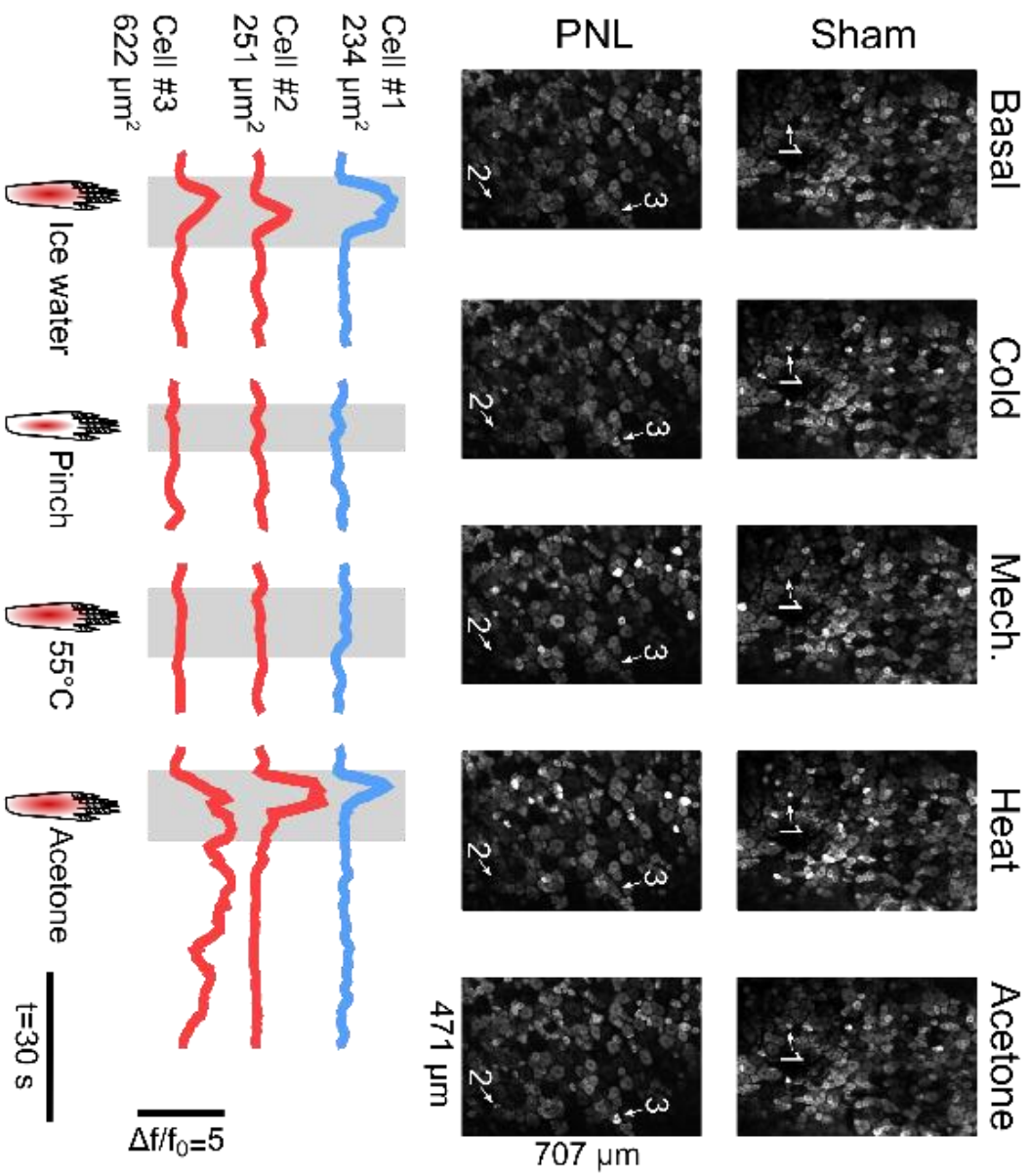

Figure 4.10. ***In vivo*** **imaging of cold-sensing neurons during partial sciatic nerve ligation (enlarged).**

Example images and traces of cold-responding neurons in sham- and PNL-operated animals expressing GCaMP3. Cell #1 is a small-diameter cold-sensing neuron in the sham condition, Cell #2 is a small-diameter basal cold-sensing neuron after PNL and Cell #3 is a large-diameter silent cold-sensing neuron unmasked by PNL.

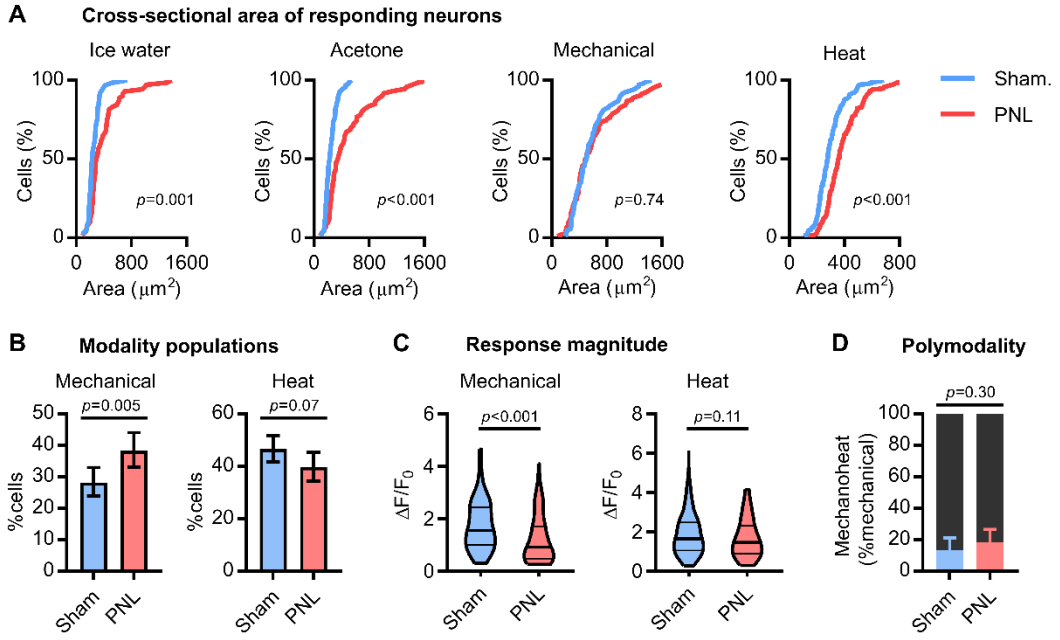

Figure 4.11. Modality-specific effects of partial sciatic nerve ligation on sensory neuron physiology

(A) Cumulative probability plots of cross-sectional areas for cells responding to each stimulus modality, compared using Kolmogorov-Smirnov test.

(B) Bar plots showing the proportion of all responding neurons responding to heat or mechanical stimuli, compared using χ^2 test. Error bars denote 95% confidence interval.

(C) Violin plots showing peak response evoked by each stimulus modality, compared using Mann-Whitney test.

(D) Proportion of mechanically-sensitive neurons also responding to noxious heat, compared using χ^2 test.

Ice-water: n_{sham}=64, n_{PNL}=71. Acetone: n_{sham}=95, n_{PNL}=73. Mechanical: n_{sham}=105, n_{PNL}=114. Heat: n_{sham}=174, n_{PNL}=118.

4.3.4 *In vivo* imaging of cold-sensing neurons during ciguatera poisoning

Both the oxaliplatin and nerve injury model show a delayed onset of cold hypersensitivity. As my imaging preparation is terminal, I could not follow mice longitudinally to determine if silent cold-sensing neurons are truly silent at the naive state. To induce cold allodynia within the same imaging session, I therefore turned to a mouse model of ciguatera poisoning, a chemical-induced neuropathy characterized by cold pain in the extremities.[282]

Intraplantar injection of ciguatoxin-2 (P-CTX-2, 100 nM) into the hindpaw evoked cold pain by 30 minutes, as judged by both the acetone test and the unilateral cold plate at 10°C (**Figure 4.12A**). I therefore imaged the change in sensory neuron cold sensitivity over the same time course (**Figure 4.12B** and enlarged in **Figure 4.13**). After 30 minutes, P-CTX-2 transformed numerous cold-insensitive cells into neurons that showed robust responses to cooling (**Figure 4.12Ci**). As is evident in the heat-map, many basally-active cells actually lost their response to cold, however this was counterbalanced by the large number of cells that were unmasked by P-CTX-2, resulting a net expansion of cold population, especially to ice-water (**Figure 4.12Cii**). The number of neurons responsive to any cold stimulus rose from 91 to 206, and for ice water went from 69 to 174. Compared to vehicle, there was no apparent effect of P-CTX-2 on the number of cells responding to other modalities (**Figure 4.12Cii**). The silent cold-sensing neurons unmasked by P-CTX-2 were generally large diameter, in a manner clearly reminiscent of oxaliplatin and nerve injury, while only a very few large neurons responded before and after vehicle injection (**Figure 4.12D**). The distribution of cell areas for heat was not markedly altered, although more small neurons responded to noxious pinch (**Figure 4.14A**).

How did P-CTX-2 treatment affect the properties of basally-active cold cells? I quantified the change in threshold of these cells after either P-CTX-2 or vehicle, and saw no difference (**Figure 4.12Ei**). Interestingly, P-CTX-2 actually reduced the peak response of these neurons compared to vehicle (**Figure 4.14B**). Silent cold-sensing neurons showed similar thermal activation thresholds to the basal population (**Figure 4.12Eii**), and their activity was not increased (**Figure 4.14C**). P-CTX-2 did not affect the peak response to other modalities (**Figure 4.14D**), however there was an increase in the fraction of polymodal mechano-heat neurons from 12% to 25% (**Figure 4.14E**).

P-CTX-2 increased mechano-cold polymodal neurons responding to ice-water from 4% to 13% (**Figure 4.12Fi**). Heat/cold polymodality was also enhanced, albeit not

significantly (**Figure 4.12ii**). Are polymodal silent cold-sensing neurons basally responsive to other modalities, or are both sensitivities acquired due to neuropathy? Interestingly, the proportion of identified silent cold-sensing neurons that responded to noxious mechanical stimuli was at 16% the same in the naïve state and after P-CTX-2. On the other hand, few mechano-heat cells showed a basal response to heat, indicating heat sensitivity is conferred by P-CTX-2 (**Figure 4.12Fiii**). These results were broadly similar when I looked only at the cold-sensing neurons defined by their response to acetone. (**Figure 4.14F**).

These findings demonstrate cold allodynia induced by P-CTX-2 involves recruitment of silent cold-sensing neurons, some of which are basally sensitive to noxious pinch. Etiologically-distinct neuropathic pain states therefore give rise to cold pain by a similar mechanism of recruiting cold-insensitive sensory neurons to become cold-responsive. Given activation of silent cold-sensing neurons drives pain behaviours in mice and given their sensitivity to noxious mechanical stimulation, silent cold-sensing neurons can likely be classified as nociceptors.

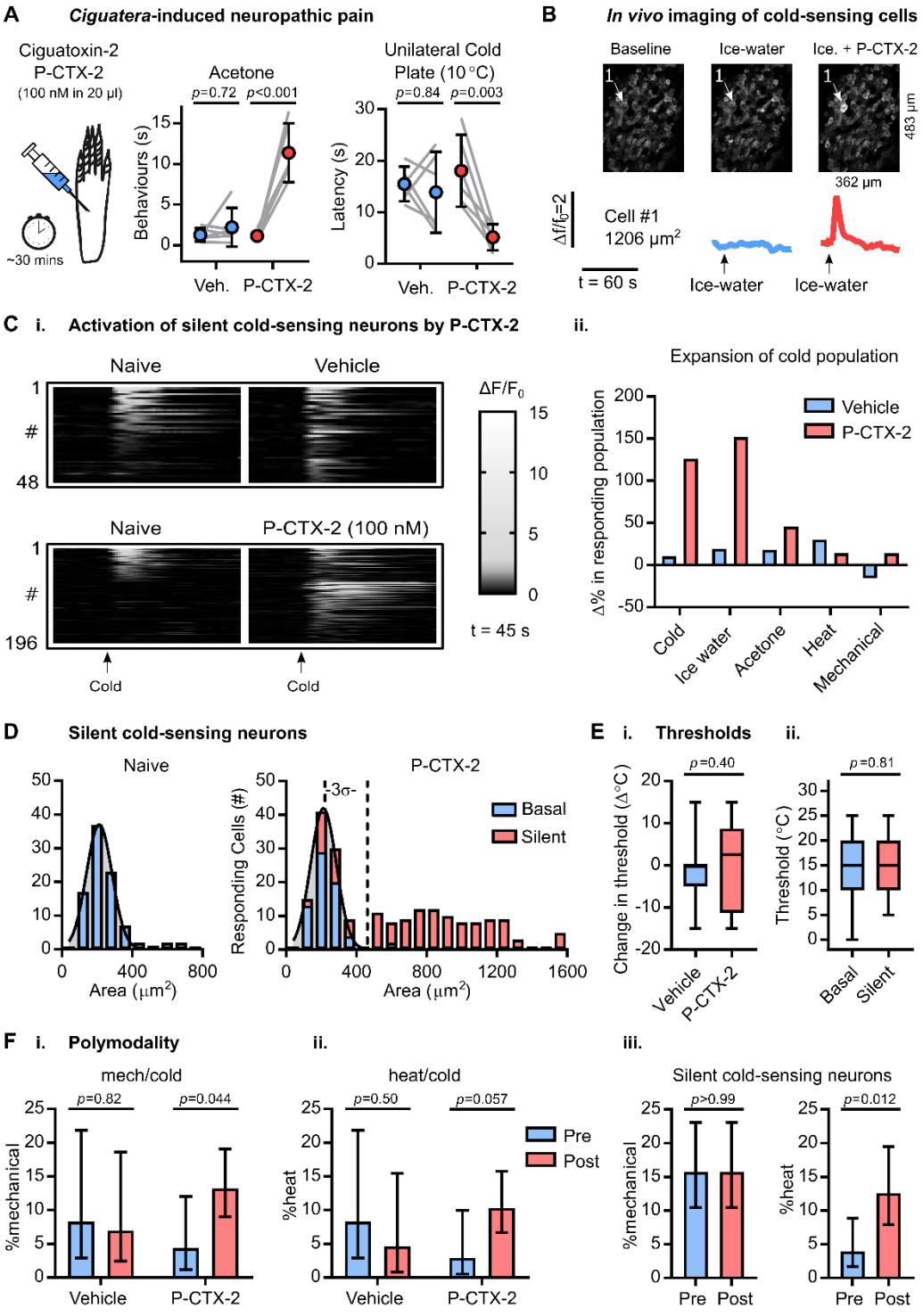
A
Ciguatera-induced neuropathic pain
Ciguatoxin-2
P-CTX-2
(100 nM in 20 µl)
~30 mins
Acetone
p=0.72
p<0.001
Behaviours (s)
Veh.
P-CTX-2
Unilateral Cold Plate (10 °C)
p=0.84
p=0.003
Latency (s)
B
In vivo imaging of cold-sensing cells
Baseline
Ice-water
Ice. + P-CTX-2
483 µm
362 µm
Cell #1
1206 µm2
Δf/f0=2
t = 60 s
C i.
Activation of silent cold-sensing neurons by P-CTX-2
Naive
Vehicle
Naive
P-CTX-2 (100 nM)
ΔF/F0
t = 45 s
Cold
ii.
Expansion of cold population
Vehicle
P-CTX-2
Δ% in responding population
Cold
Ice water
Acetone
Heat
Mechanical
D
Silent cold-sensing neurons
Naive
P-CTX-2
3σ
Basal
Silent
Responding Cells (#)
Area (µm2)
E i.
Thresholds
p=0.40
Change in threshold (Δ°C)
Vehicle
P-CTX-2
ii.
p=0.81
Threshold (°C)
Basal
Silent
F i.
Polymodality
mech/cold
p=0.82
p=0.044
%mechanical
Vehicle
P-CTX-2
ii.
heat/cold
p=0.50
p=0.057
Pre
Post
%heat
iii.
Silent cold-sensing neurons
p>0.99
p=0.012

Figure 4.12. Silent cold-sensing neurons are activated by ciguatoxin-2.

(A) Behavioural testing of the effect of 100 nM ciguatoxin-2 (P-CTX-2) on cold sensitivity n=6 for sham vehicle and n=6 for P-CTX-2. Means were compared by repeated measures 2-way ANOVA followed by post-hoc Sidak's test. Error bars denote 95% confidence interval.

(B) Example images and traces of a large-diameter neuron (Cell #1) that is basally cold-insensitive but begins to respond to cooling after treatment with P-CTX-2.

(C) (i.) Heatmap showing the effect of P-CTX-2 on the number of neurons responding to a cold ice-water stimulus. n=48 for vehicle, and n=196 for P-CTX-2. (ii.) Summary of the change in the number of sensory neurons responding to each modality after treatment with P-CTX-2.

(D) Histograms of cross-sectional area of all neurons responding to any cold stimulus in the naïve state (left, blue, n=91) and after P-CTX-2 (right). For P-CTX-2, blue denotes basally-responsive neurons that maintained their response to cold (n=70) and red denotes the silent cold-sensing neurons that were unmasked after treatment (n=136). The distribution of areas in the naïve state was fit by non-linear regression (least squares Gaussian; Bin width is 80 μm^2; Mean=212.4 μm^2, Std. Dev. 73.33 μm^2). This model is plotted over the P-CTX-2 data to aid comparison with the dashed line denoting three standard deviations from the mean. The different in the distribution of areas between groups was assessed by Kolmogorov-Smirnov test ($p<0.001$).

(E) (i.) Box plot of the change in activation threshold of basally cold-sensitive neurons before and after treatment with vehicle (n=35) or P-CTX (n=8). ii.) Box plot of the thermal activation threshold of all silent cold-sensing neurons unmasked by P-CTX-2 (n=43) compared to all cold-sensing neurons recorded from naïve mice (n=62). Medians were compared by Mann-Whitney test.

(F) Quantification of the proportion of neurons responding to ice-water that were also sensitive to either mechanical (i.) or heat (ii.) before and after treatment. Vehicle: $n_{pre}=36$, $n_{post}=43$. P-CTX-2: $n_{pre}=69$, $n_{post}=174$. (iii.) Comparison of the proportion of silent cold-sensing neurons that were responsive to other modalities before and after the induction of cold-sensitivity by P-CTX-2. n=127. The proportion of polymodal neurons was compared using χ^2 test, and error bars denote 95% confidence intervals.

For this experiment, 615 neurons responding to any stimulus either before or after treatment were recorded in 10 P-CTX-2-injected mice and 193 cells were recorded from 3 vehicle-injected animals.

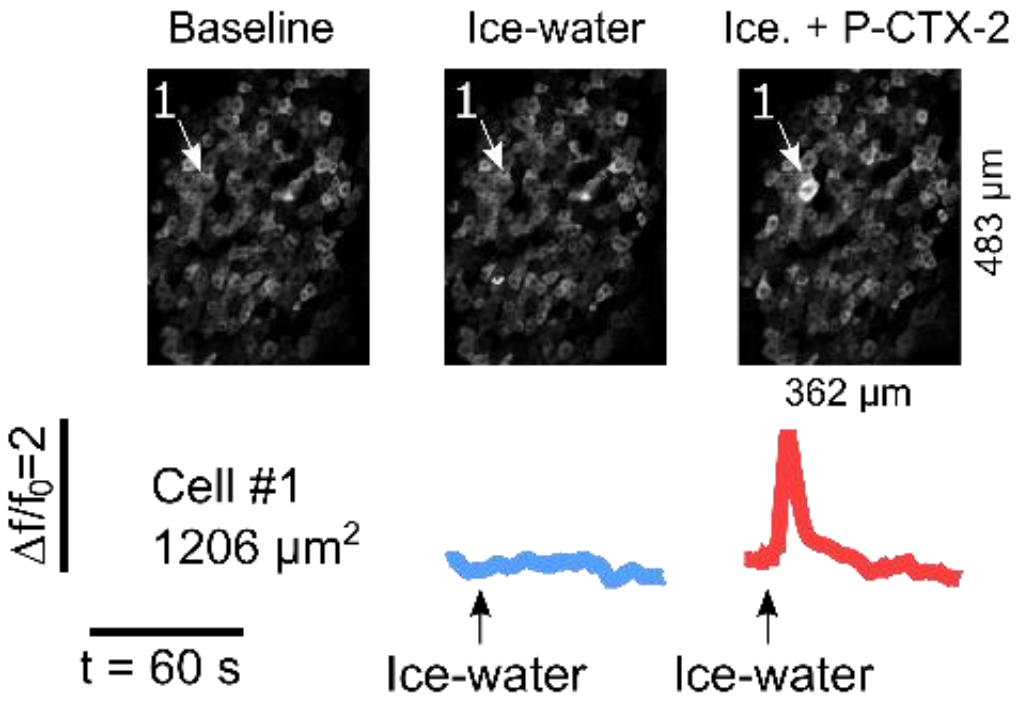

Figure 4.13. ***In vivo*** **imaging of cold-sensing neurons after treatment with ciguatoxin-2 (enlarged).**

Example images and traces of a large-diameter neuron (Cell #1) that is basally cold-insensitive but begins to respond to cooling after treatment with P-CTX-2.

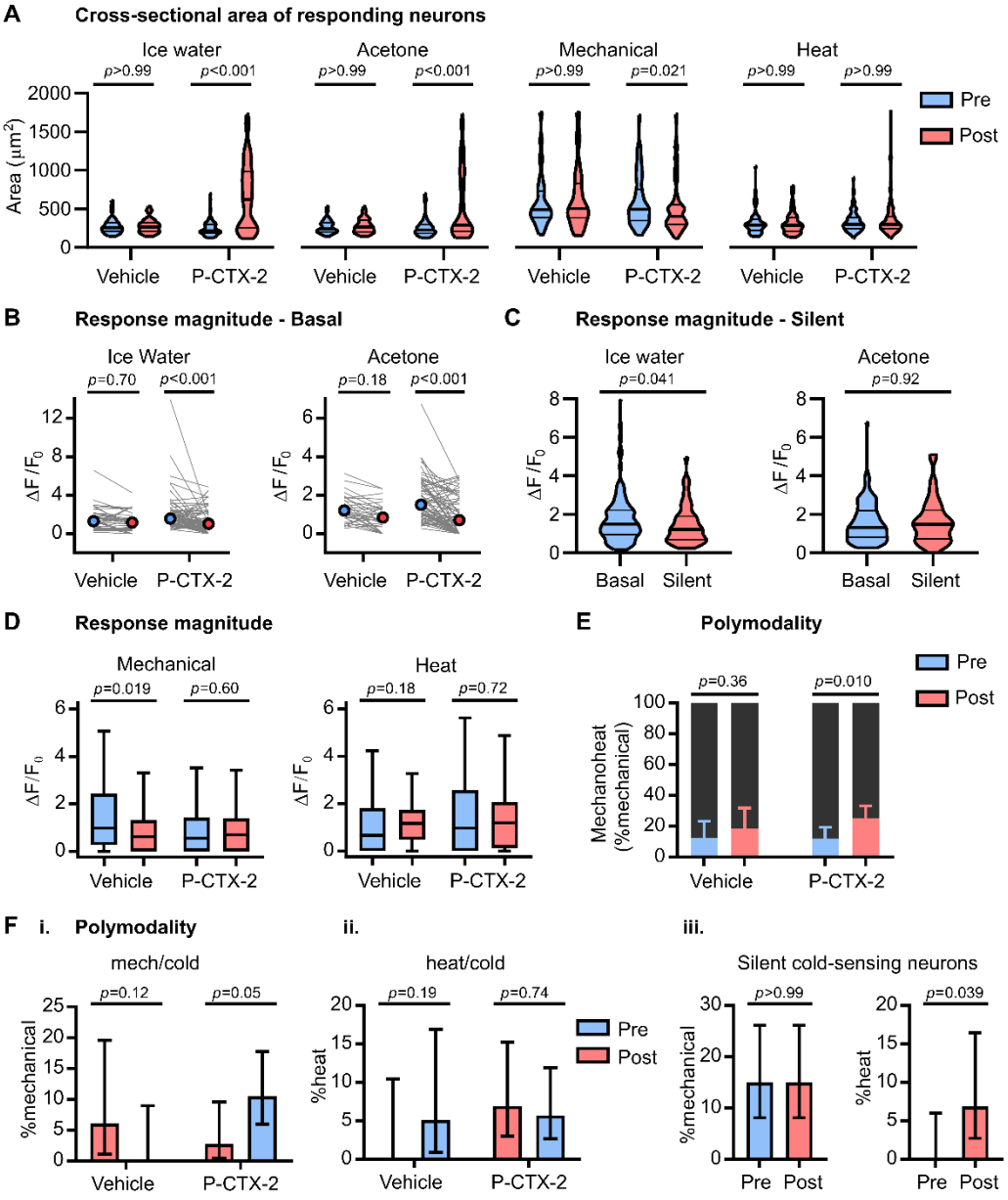
A
Cross-sectional area of responding neurons
Ice water
Acetone
Mechanical
Heat
p>0.99
p<0.001
p=0.021
Area (µm²)
2000
1500
1000
500
0
Pre
Post
Vehicle
P-CTX-2
B
Response magnitude - Basal
Ice Water
p=0.70
p<0.001
p=0.18
ΔF/F0
C
Response magnitude - Silent
Ice water
p=0.041
p=0.92
Basal
Silent
D
Response magnitude
Mechanical
p=0.019
p=0.60
Heat
p=0.18
p=0.72
E
Polymodality
p=0.36
p=0.010
Mechanoheat (%mechanical)
F
i. Polymodality
ii.
iii.
mech/cold
p=0.12
p=0.05
%mechanical
heat/cold
p=0.19
p=0.74
%heat
Silent cold-sensing neurons
p>0.99
p=0.039
Pre
Post

Figure 4.14. Modality-specific effects of ciguatoxin-2 on sensory neuron physiology.

(A) Violin plots of cross-sectional areas for cells responding to each stimulus modality, compared using Kruskall-Wallis test followed by Dunn's multiple comparisons test.

(B) Line plots showing the median response magnitude of basally cold-sensitive neurons before and after treatment, compared using Kruskall-Wallis test followed by Dunn's multiple comparisons test.

(C) Violin plots showing the response magnitude of all silent cold-sensing neurons unmasked by P-CTX-2 (n=127 for ice-water, and n=60 for acetone) compared to all basally-active neurons recorded from naïve mice (n=105 for both). Medians were compared using Mann-Whitney test.

(D) Box plots showing the median response magnitude of all mechanical and heat-responsive neurons before and after treatment.

(E) Proportion of mechanically-sensitive neurons also responding to noxious heat, before and after treatment, compared using χ^2 test. Error bars denote 95% confidence intervals.

(F) Quantification of the proportion of neurons responding acetone that were also sensitive to either mechanical (i.) or heat (ii.) before and after treatment. (iii.) Comparison of the proportion of silent cold-sensing neurons activated by acetone that were responsive to other modalities before and after the induction of cold-sensitivity by P-CTX-2. n=60. The proportion of polymodal neurons was compared using χ^2 test, and error bars denote 95% confidence intervals.

Ice-water: vehicle: n_{pre}=36, n_{post}=43; P-CTX-2: n_{pre}=69, n_{post}=174. Acetone: vehicle: n_{pre}=33, n_{post}=39; P-CTX-2: n_{pre}=72, n_{post}=105. Mechanical: n_{pre}=57, n_{post}=48; P-CTX-2: n_{pre}=115, n_{post}=131. Heat: n_{pre}=59, n_{post}=77; P-CTX-2: n_{pre}=211, n_{post}=241.

4.3.5 Genetic identification of silent cold-sensing neurons that drive cold allodynia in neuropathic pain

What is the molecular identify of silent cold-sensing neurons? Determining which sensory neuron subset(s) they belong to would give me genetic access to them. I crossed subset-specific Cre or CreERT2 mice with animals harbouring a Cre-dependent tdTomato reporter, on a Pirt-GCaMP3 background. The progeny therefore express GCaMP3 in all sensory neurons but tdTomato expression is restricted to the cellular subset of interest (**Figure 4.15A**). Consequently, I was able to ask if functionally-identified silent cold-sensing neurons activated by oxaliplatin express molecular markers labelling major subpopulations of sensory neurons. For this study, I focused on oxaliplatin neuropathy because of its ease, reproducibility and clinical relevance.

The percentage of neurons responding to any cold stimulus in vehicle and oxaliplatin-treated mice expressing each molecular marker is summarized in **Figure 4.15A**, with oxaliplatin split as before into basal and silent populations. Contrary to prior reports that oxaliplatin sensitizes A fibres, the silent cold-sensing neurons showed minimal expression of Aβ-fibre low-threshold mechanoreceptor marker *Calb*1 (Calb1-Cre) with 22% overlap. Expression of Aδ-fibre low-threshold mechanoreceptor marker *Ntrk2* (TrkB-CreERT2) was even less at 4%. To confirm these surprising observations functionally, I systematically challenged these same animals with innocuous tactile stimuli – from 49 large-diameter silent cold-sensing neurons tested, not one responded to stroking the glabrous or hairy skin with a paint-brush or cotton swab. Consistent with expression of *Calb1* in putative cold thermosensors, 57% of the cold-sensing neurons in vehicle-treated mice were marked by Calb1-Cre. Interestingly, silent cold-sensing neurons also showed 30% overlap with *Trpv1* lineage neurons. The Trpv1-Cre line broadly labels a mixture of nociceptors and thermosensors, including basal cold-sensing neurons. This was recapitulated here, where essentially all small-diameter cold cells were marked by Trpv1-Cre, at 100% in vehicle, and 80% in the basal population following oxaliplatin.

Given the fact silent cold cells respond to noxious mechanical stimuli, I wondered if they might express *Scn10a*. $Na_V1.8$-Cre is a nociceptor marker that labels both mechanonociceptors and extreme cold sensors, but does not label the bulk of neurons sensing cold down to 0°C in naïve conditions. Very few small-sized cold-sensing neurons were marked by $Na_V1.8$ in animals treated with either vehicle (14%) or oxaliplatin (19%). In contrast, I found 68% of silent cold-sensing neurons expressed $Na_V1.8$ **(Figure 4.15B** and enlarged in **Figure 4.16**). When I examined animals with cold allodynia evoked by

PNL, 52% of silent cold-sensing neurons were marked by $Na_V1.8$, although 48% of smaller cells also expressed $Na_V1.8$ in this model (**Figure 4.15C**). Similarly, 55% of the silent cold-sensing neurons unmasked by P-CTX-2 were positive for $Na_V1.8$, with only 11% overlap among the cold cells active in the naïve state (**Figure 4.15D**). Thus, in all three neuropathic pain models tested here, a majority of silent cold-sensing neurons express the $Na_V1.8$ molecular marker, consistent with a nociceptive identity.

To determine which nociceptor subset silent cold-sensing neurons belonged to, I used Cre driver lines selective for either *Tmem45b*-expressing non-peptidergic (Tmem45b-Cre) or *Calca*-expressing peptidergic (CGRPα-CreERT2) nociceptors. I saw just 5% overlap of *Tmem45b* with silent cells in oxaliplatin neuropathy (**Figure 4.15A**). CGRP-CreERT2α, however, marked 62% of silent cold cells in oxaliplatin neuropathy (**Figure 4.15E** and enlarged in **Figure 4.17**). The silent cold-sensing neurons also overlapped substantially with *Calca*-expressing cells in mice with cold allodynia evoked by PNL (56%) or P-CTX-2 (54%), identifying silent cold cells as a set of peptidergic nociceptors commonly involved in cold allodynia (**Figure 4.15F&G**). Like *Scn10a*, the smaller basally-active cold cells were rarely positive for *Calca*. Expression of *Scn10a* or *Calca* thereby genetically dissociates silent from basal cold-sensing neurons. It is important to note, however, that *Scn10a* and *Calca* are expressed by a large and heterogenous set of nociceptors neurons; thus, these molecules are not selective markers for silent cold-sensing neurons.

Do silent cold sensing neurons with a nociceptive identity contribute to behavioural cold hypersensitivity in neuropathic pain? Having gained genetic access to silent cold-sensing cells, I used diphtheria toxin to conditionally ablate silent cold-sensing neurons marked by $Na_V1.8$-Cre to test their causal role in cold allodynia (**Figure 4.18A**). Note this ablation encompasses all cells expressing $Na_V1.8$ and is not restricted to silent cold-sensing neurons. Imaging of mice where Scn10a-positive nociceptors are ablated shows very few of the large-diameter silent cold-sensing neurons are unmasked by oxaliplatin compared to $Na_V1.8$-Cre mice lacking DTA (**Figure 4.18B**). Consistent with this, there was a ~50% reduction in oxaliplatin evoked cold hypersensitivity in $Na_V1.8$-Cre DTA animals (**Figure 4.18C**). The genetic identification and subsequent manipulation of silent cold-sensing neurons thus corroborates their causal contribution to cold allodynia in neuropathic pain.

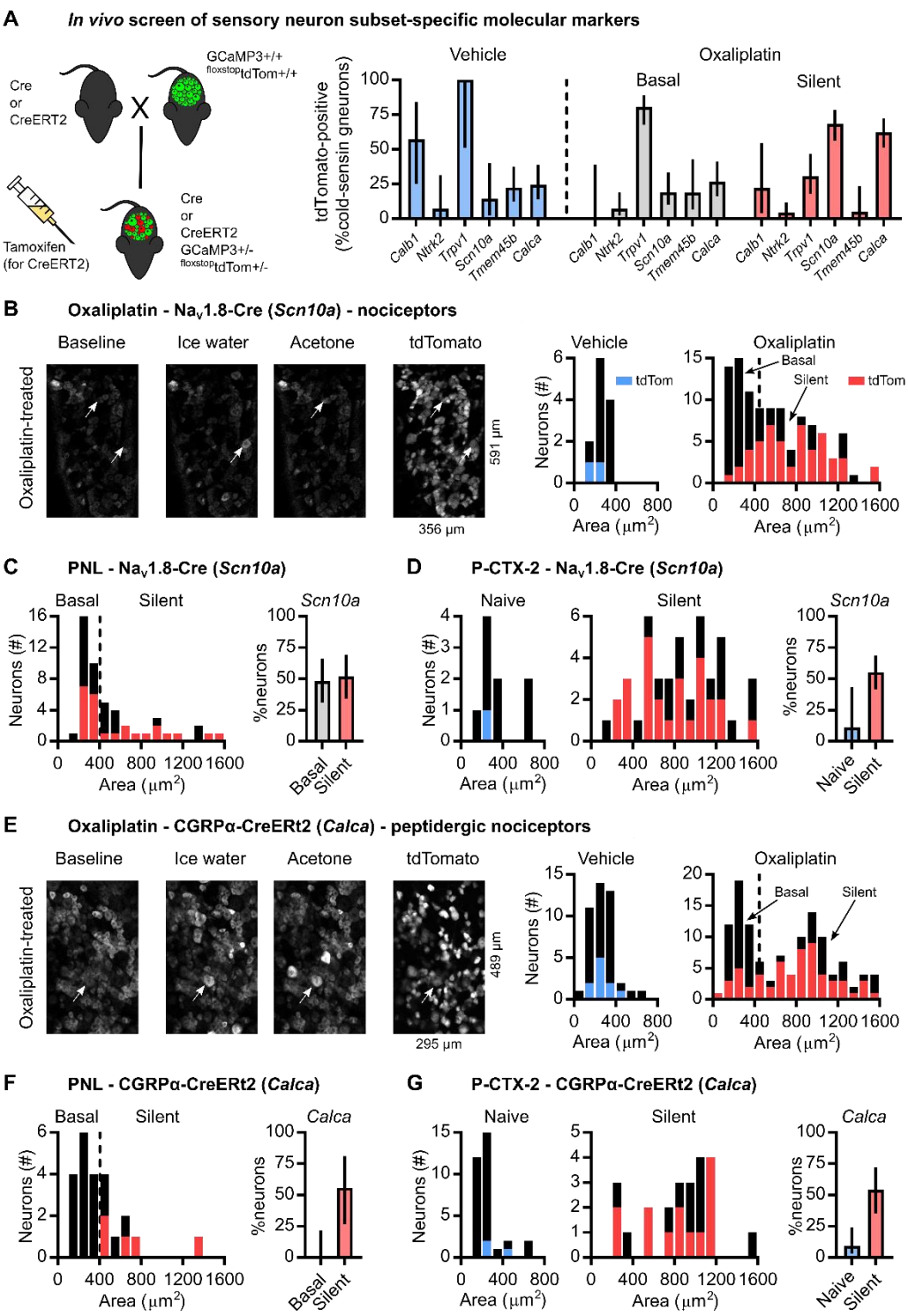
A
In vivo screen of sensory neuron subset-specific molecular markers
Cre
or
CreERT2
GCaMP3+/+
floxstopTdTom+/+
Tamoxifen
(for CreERT2)
Cre
or
CreERT2
GCaMP3+/-
floxstopTdTom+/-
tdTomato-positive
(%cold-sensin gneurons)
Vehicle
Oxaliplatin
Basal
Silent
Calb1
Ntrk2
Trpv1
Scn10a
Tmem45b
Calca
B
Oxaliplatin - Nav1.8-Cre (Scn10a) - nociceptors
Baseline
Ice water
Acetone
tdTomato
Oxaliplatin-treated
591 µm
356 µm
Vehicle
Oxaliplatin
tdTom
Neurons (#)
Area (µm2)
C
PNL - Nav1.8-Cre (Scn10a)
Basal
Silent
Scn10a
%neurons
D
P-CTX-2 - Nav1.8-Cre (Scn10a)
Naive
Silent
E
Oxaliplatin - CGRPα-CreERt2 (Calca) - peptidergic nociceptors
489 µm
295 µm
F
PNL - CGRPα-CreERt2 (Calca)
Calca
G
P-CTX-2 - CGRPα-CreERt2 (Calca)

Figure 4.15. Silent cold-sensing neurons express molecular markers consistent with peptidergic nociceptors.

(A) Cartoon (left) of breeding strategy used to generate GCaMP3 reporter mice for each subset of interest. Bar plot (right) showing overlap of reporter expression for each marker with functionally-defined cold-sensing neurons.

Calb1-Cre (*Calb1*): n_{veh}=7 from 1 mouse, n_{oxa}=15 from 2 mice. TrkB-CreERT2 (*Ntrk2*): n_{veh}=14 from 2 mice, n_{oxa}=112 from 3 mice. Trpv1-Cre (*Trpv1*): n_{veh}=4 from 1 mouse, n_{oxa}=87 from 3 mice. $Na_V1.8$-Cre (*Scn10a*): n_{veh}=14 from 4 mice, n_{oxa}=108 from 6 mice. Tmem45b-Cre (*Tmem45b*): n_{veh}=40 from 1 mouse, n_{oxa}=36 from 3 mice. CGRPα-CreERT2 (*Calca*): n_{veh}=45 from 3 mice, n_{oxa}=122 from 2 mice.

(B) Example images (left) and histograms (right) showing overlap of $Na_V1.8$-Cre-dependent tdTomato expression with cold-sensing neurons of different sizes in vehicle- and oxaliplatin-treated mice. Same data as in (A).

(C) Histogram (left) and bar plot (right) showing overlap of $Na_V1.8$-Cre-dependent tdTomato expression with different types of cold-sensing neurons in PNL-operated mice. n=50 cells from 1 mouse.

(D) Histograms (left) and bar plot (right) showing overlap of $Na_V1.8$-Cre-dependent tdTomato expression with basally-active and silent cold-sensing neurons in mice treated with P-CTX-2. n=56 cells from 4 mice.

(E) Example images (left) and histograms (right) showing overlap of CGRPα-CreERT2-dependent tdTomato expression with cold-sensing neurons of different sizes in vehicle- and oxaliplatin-treated mice. Same data as in (A).

(F) Histogram (left) and bar plot (right) showing overlap of CGRPα-CreERT2-dependent tdTomato expression with different types of cold-sensing neurons in PNL-operated mice. n=23 cells from 2 mice.

(G) Histograms (left) and bar plot (right) showing overlap of CGRPα-CreERT2-dependent tdTomato expression with basally-active and silent cold-sensing neurons in mice treated with P-CTX-2. n=56 cells from 2 mice.

Error bars denote 95% confidence intervals. As these data were obtained as part of a screen, no statistical hypothesis testing was performed.

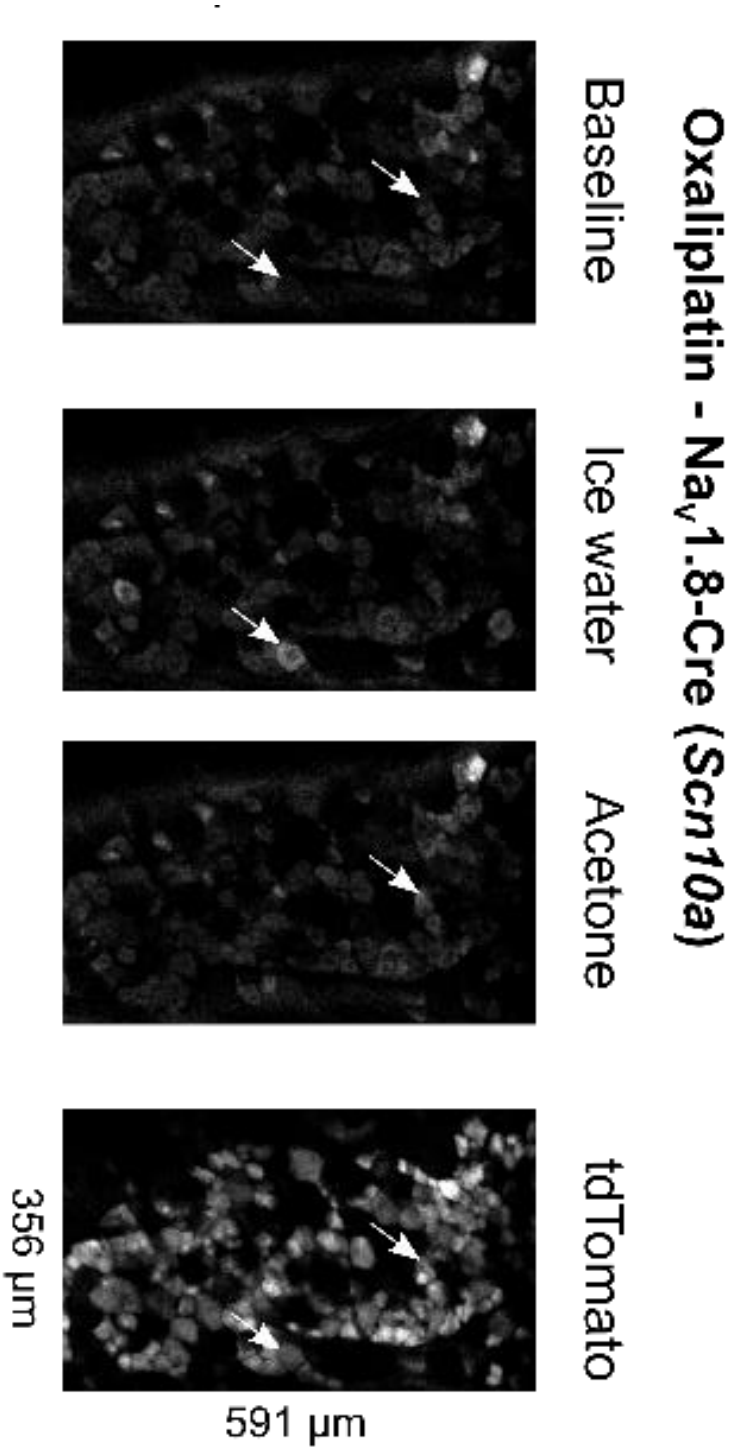

Figure 4.16. Expression of Na$_V$1.8 in silent cold-sensing neurons

Example images showing overlap of Na$_V$1.8-Cre-dependent tdTomato expression with cold-sensing neurons of different sizes in oxaliplatin-treated mice.

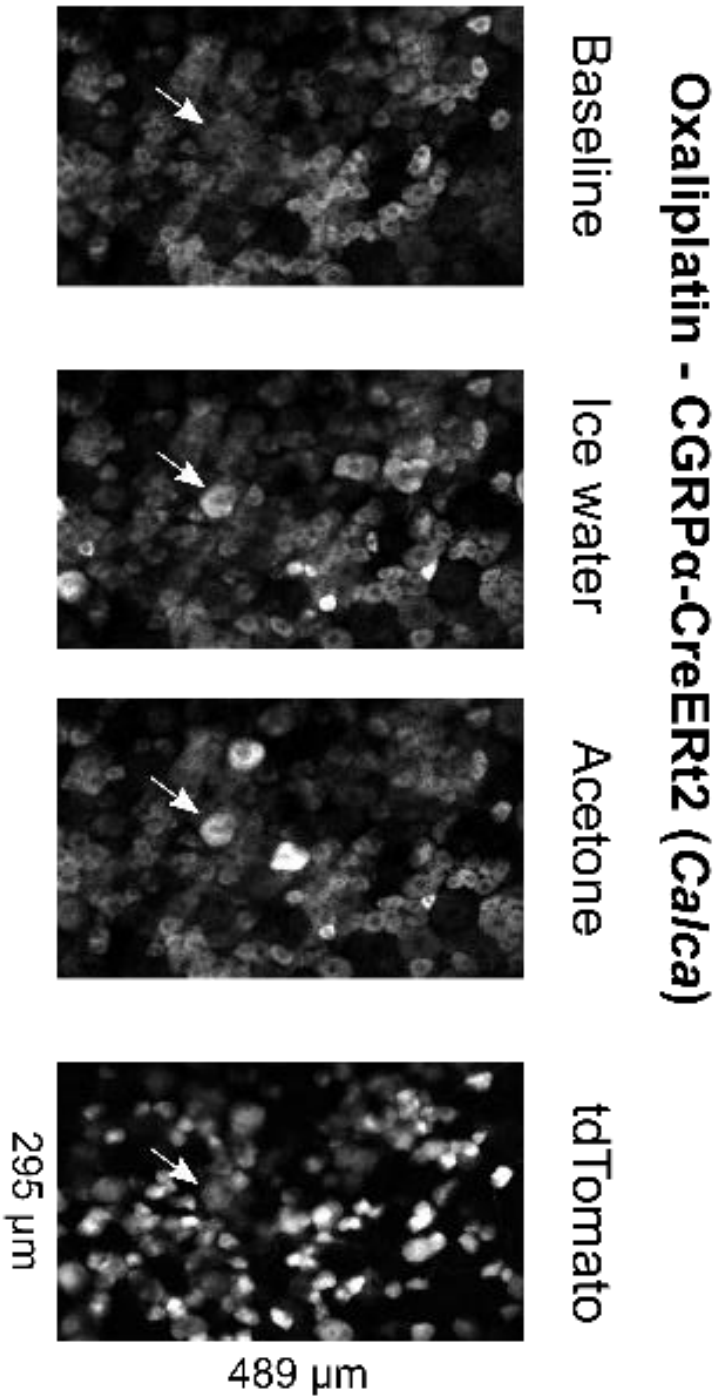

Figure 4.17. Expression of CGRPα in silent cold-sensing neurons

Example images showing overlap of CGRPα-CreERT2-dependent tdTomato expression with cold-sensing neurons of different sizes in oxaliplatin-treated mice.

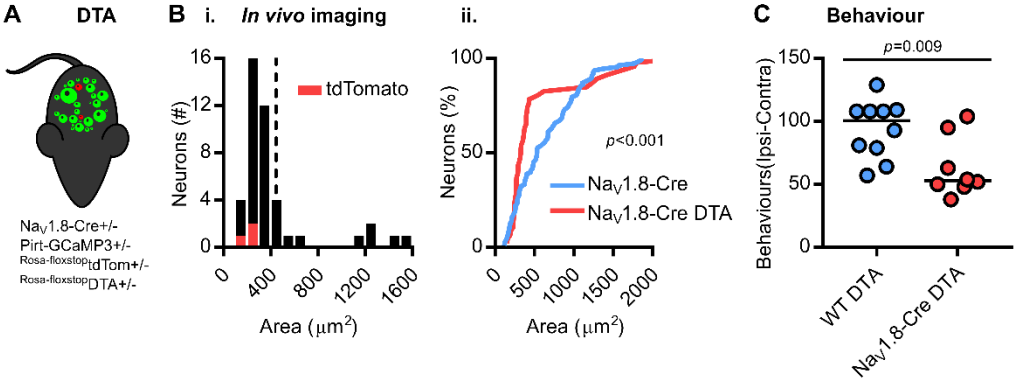

Figure 4.18. Diphtheria toxin-mediated ablation of Na$_V$1.8-positive nociceptors decreases oxaliplatin-induced cold allodynia.

(A) Cartoon of diphtheria toxin-mediated ablation of Na$_V$1.8-positive neurons.

(B) (i.) Histogram of cross-sectional areas of all cold-sensing neurons imaged in Na$_V$1.8-Cre DTA mice treated with oxaliplatin. (ii.) Cumulative probability plot of cell areas in oxaliplatin-treated WT and DTA mice, compared by Kolmogorov-Smirnov test. n=108 cells from 6 WT mice and n=46 cells from 2 DTA mice.

(C) Quantification of the number of pain-like behaviours in 5 minutes on the 5°C Cold Plate in 10 WT and 8 DTA mice treated with oxaliplatin.

4.3.6 Sodium channels controlling silent cold-sensing neuron excitability

Scn10a and *Calca* expression distinguishes basal and silent cold-sensing neurons and therefore offers an inroad to identifying molecules that might underlie pathological cold sensitivity. For molecular characterization studies, I focused on silent cold-sensing neurons responding to ice-water stimuli in the oxaliplatin model. Given the fact silent cold-sensing neurons express $Na_V1.8$ and given oxaliplatin is a known sodium channel activator, I wondered if $Na_V1.8$ might be required for their response to cold. Because Cre is knocked in directly at the $Na_V1.8$ locus, homozygous $Na_V1.8$-Cre mice are $Na_V1.8$ nulls. This was confirmed by my failure to record any TTX-resistant voltage-gated sodium currents in dorsal root ganglia neurons isolated from homozygous $Na_V1.8$-Cre mice (**Figure 4.20A**). I therefore treated homozygous $Na_V1.8$-Cre mice expressing Cre-dependent tdTomato on a Pirt-GCaMP3 background with oxaliplatin. I observed numerous large-diameter silent cold-sensing neurons in null animals, many of which were positive for tdTomato (**Figure 4.19Ai**). There was no difference between oxaliplatin-treated mice heterozygous or homozygous for $Na_V1.8$-Cre in the distribution of cell areas (**Figure 4.19Aii**) or tdTomato-expression of cold-sensing neurons (**Figure 4.19iii**).). I also observed normal development of oxaliplatin-evoked cold allodynia in conventional $Na_V1.8$ KO mice (**Figure 4.20B**). Imaging studies on Advillin-Cre conditional $Na_V1.7$ KO mice also revealed intact recruitment of silent cold-sensing neurons by oxaliplatin (**Figure 4.19B**). Thus, pain-related sodium channels $Na_V1.8$ and $Na_V1.7$ are dispensable for silent cold-sensing neuron activity.

Which sodium isoform then is required for silent cold-sensing neuron excitability? Treatment of oxaliplatin-injected animals with TTX blocked activity in essentially all basal and silent cold-sensing neurons (**Figure 4.19C**). 4,9-anhydrousTTX, reported to preferentially inhibit $Na_V1.6$, reduced the number of silent cold-sensing neurons by 57%. The effect of $Na_V1.6$ blockade on basal cold-sensing neurons was comparable to saline, however (**Figure 4.19D**). Hence, $Na_V1.6$ is likely the predominant sodium channel isoform in silent cold-sensing neurons. However, when I directly activated sodium channels with the pharmacological potentiator veratridine in naïve mice, there was no increase in the number of cold-sensing cells, nor any unmasking of large-sized cells (**Figure 4.19D**). Activation of sodium channels is therefore not sufficient to induce *de novo* cold sensitivity.

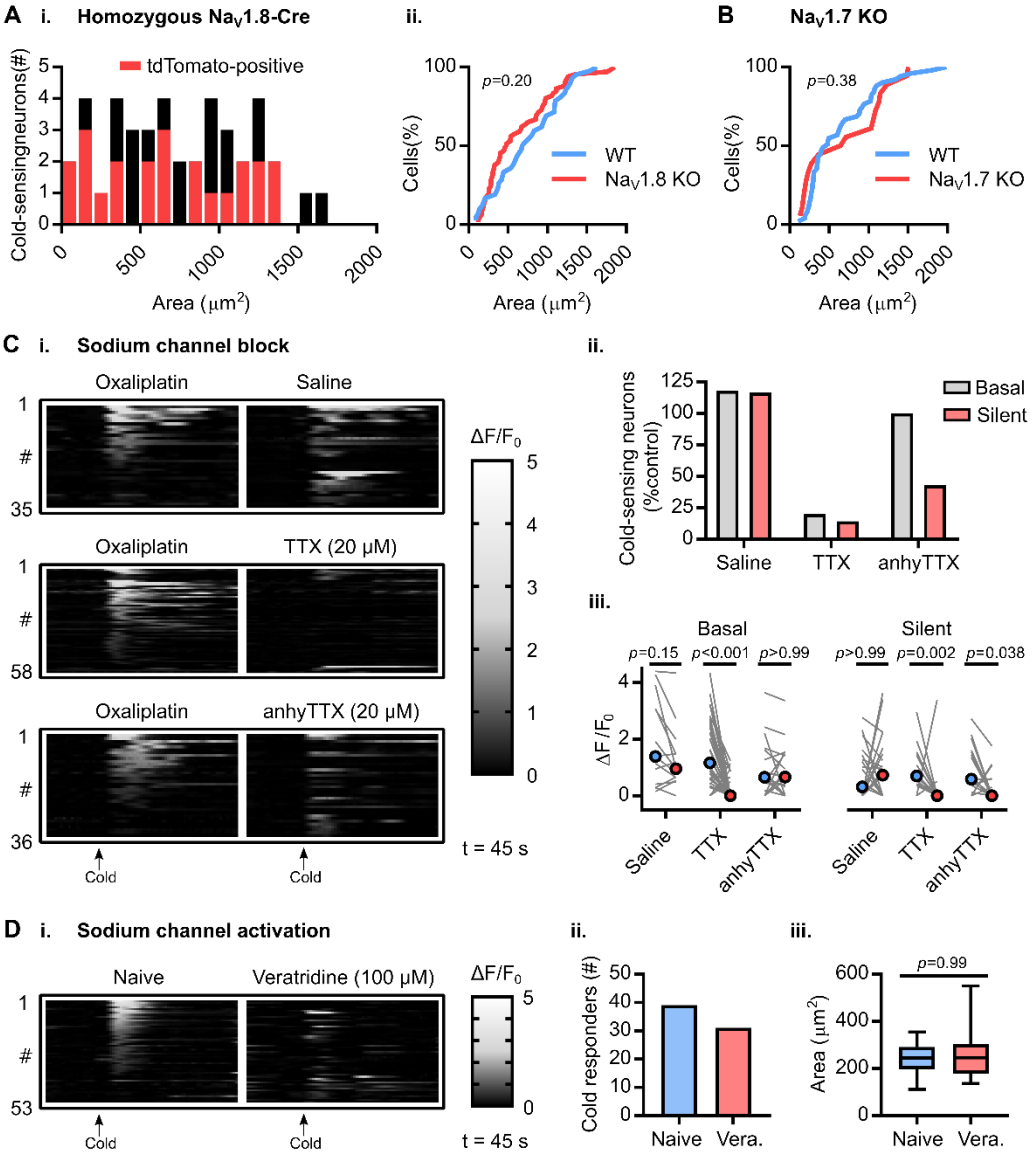

Figure 4.19. TTX-sensitive sodium channel $Na_V1.6$ is required for excitability, but is not sufficient for cold-sensitivity, of silent cold-sensing neurons

(A) (i.) Histogram of cross-sectional areas of all cold-sensing neurons imaged in homozygous $Na_V1.8$-Cre mice with oxaliplatin. (ii.) Cumulative probability plot of cell areas in oxaliplatin-treated heterozygous and homozygous $Na_V1.8$-Cre mice, compared by Kolmogorov-Smirnov test. n=108 cells from 6 heterozygous and n=42 cells from 3 homozygous $Na_V1.8$-Cre mice.

(B) Cumulative probability plot of cell areas in oxaliplatin-treated WT and $Na_V1.7$ KO mice, compared by Kolmogorov-Smirnov test. n=51 cells from 5 WT and n=18 cells from 2 $Na_V1.7$ KO mice.

(C) Heat maps (i.) and quantification (ii.) showing the effect of different sodium channel blockers on the number of basal and silent cold-sensing neurons in mice pre-treated with oxaliplatin. (ii.) Line plot showing the effect of blockers on median peak response, compared using Kruskall-Wallis test followed by Dunn's multiple comparisons test. n=35 cells from 3 mice for saline, n=58 cells from 4 mice for TTX, n=36 cells from 2 mice for 4,9-anhydrous-TTX.

(D) Heat map (i.) and quantification (ii.) of the effect of sodium channel activation with veratridine on the number of cold-sensing neurons. (ii.) Box plot showing no effect of veratridine on the size of cold-sensing cells, compared by Mann-Whitney test. n=53 cells from 3 mice.

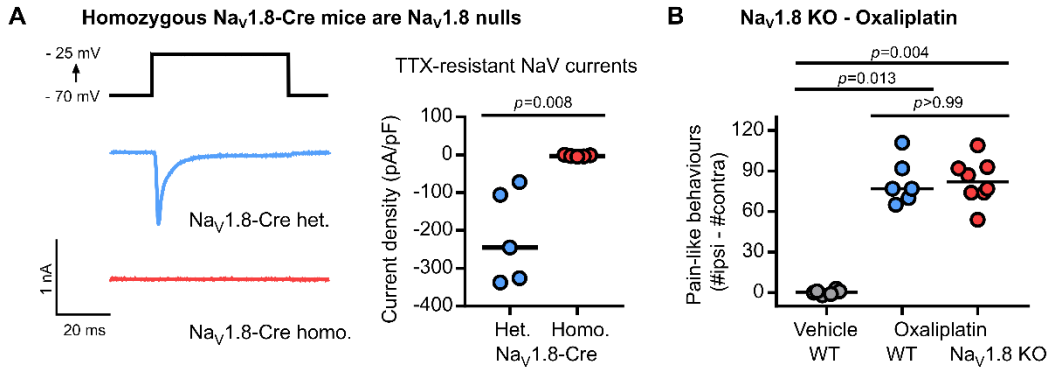

Figure 4.20. Mice lacking $Na_V1.8$ develop oxaliplatin-induced cold allodynia

(A) Example traces and scatter plot of TTX-resistant sodium currents recorded from medium-sized DRG neurons cultured from heterozygous $Na_V1.8$-Cre mice (blue). No TTX-resistant currents were observed in DRGs from homozygous $Na_V1.8$-Cre mice (red). Median (line) current density was compared using the Mann-Whitney test. n=5 cells from 1 heterozygous mouse, and n=5 cells from 1 homozygous mouse.

(B) Scatter plot of the effect of oxaliplatin on pain behaviours evoked by 5°C cold plate in WT and conventional $Na_V1.8$ KO mice. Medians were compared using Kruskall Wallis test followed by Dunn's multiple comparisons test. n=6 for WT treated with vehicle, n=6 for WT treated with oxaliplatin and n=8 for $Na_V1.8$ KO treated with oxaliplatin.

4.3.7 Molecular determinants of cold detection by silent cold-sensing neurons

The genetic dissociation of basal and silent cold sensors based on $Na_V1.8$ expression gave me an entry-point to characterize molecular mechanisms of *de novo* cold sensitivity. To identify ion channels that might control the induction of *de novo* cold sensitivity, my colleague Edward Emery and I asked the question what renders silent cold cells normally cold-insensitive – which ion channels act to suppress their latent cold sensitivity? To identify transcripts differentially expressed between the basally cold-activated $Na_V1.8$-negative neurons and the normally cold-insensitive $Na_V1.8$-positive silent cold-sensing neurons, we combined fluorescence-activated cell sorting (FACS) with microarray analysis. We extracted neurons from $Na_V1.8$ Cre tdTomato Pirt-GCaMP3 mice, dissociated them and separated them by FACS based on GCaMP3 and tdTomato fluorescence in 4°C solution. Sorting in cold solution allowed us to isolate two purified populations of $Na_V1.8$-negative cold-sensitive cells with high GCaMP3 fluorescence and $Na_V1.8$-positive cold-insensitive cells with low GCaMP3 fluorescence (**Figure 6.5A**). While the high GCaMP3 population is relatively specific for basal cold-sensing neurons, the $Na_V1.8$-positive population here encompasses all cold-insensitive $Na_V1.8$-expressing neurons not just the silent cold-sensing cells. Nonetheless, significant transcriptomic differences in RNA samples isolated from the two populations were revealed by microarray analysis (**Figure 6.5B**). We tabulated ion channel transcripts that were differentially expressed between the two populations (**Figure 6.5C**). Importantly, we observed enriched expression of the known cold transducer *Trpm8* in the $Na_V1.8$-negative cold-sensitive neurons, while the $Na_V1.8$-positive, cold-insensitive population showed enhanced levels of *Scn10a*, the gene encoding $Na_V1.8$. Notably, the most and third-most highly expressed ion channels transcripts in the cold-insensitive $Na_V1.8$ population were *Kcna1* and *Kcna2*. The corresponding voltage-gated potassium channel subtypes $K_V1.1$ and $K_V1.2$ are the molecular counterparts to the excitability brake current (I_{KD}) which may act to prevent depolarization in response to cooling.[262]

Do these channels act as switches to control silent cold-sensing neuron sensitivity? I hypothesized that pharmacological block of the I_{KD} current *in vivo* would unmask silent cold-sensing neurons. I imaged sensory neuron responses to cooling in Pirt-GCaMP3 mice at baseline and 30 minutes after intraplantar injection of the non-specific voltage-gated potassium channel blocker 4-aminopyridine (4-AP, 10 mM in 20 μl) (**Figure 4.21A**). 4-AP treatment triggered *de novo* sensitivity to cooling in previously cold-insensitive large diameter neurons (**Figure 4.21A-D**). The effect of 4-AP was occluded by pre-treatment

with oxaliplatin (**Figure 4.21B-D**). Treatment with the selective K_V1 antagonist α-dendrotoxin (100 μM) mimicked the effect of 4-AP (**Figure 4.21B-D**). k-dendrotoxin at 100 μM, purportedly a specific blocker of $K_V1.1$, largely recapitulated the effect of α-dendrotoxin on silent cold-sensing neurons (**Figure 4.21B-D**). The $K_V1.2$ blocker Conotoxin kM-RIIIJ (100 μM) did not, however (**Figure 4.21B-D**).

4-AP and α-dendrotoxin, but not k-dendrotoxin, increased the number of mechano-cold polymodal neurons (**Figure 4.21E**). Interestingly, none of the drug treatments significantly affected the activity of the basally-active population of cold neurons (**Figure 4.21F**). Overall, these data suggest that a functional reduction in $K_V1.1$-containing K_V channels can act a molecular switch that triggers *de novo* cold sensitivity in silent cold-sensing neurons to drive cold allodynia during neuropathic pain.

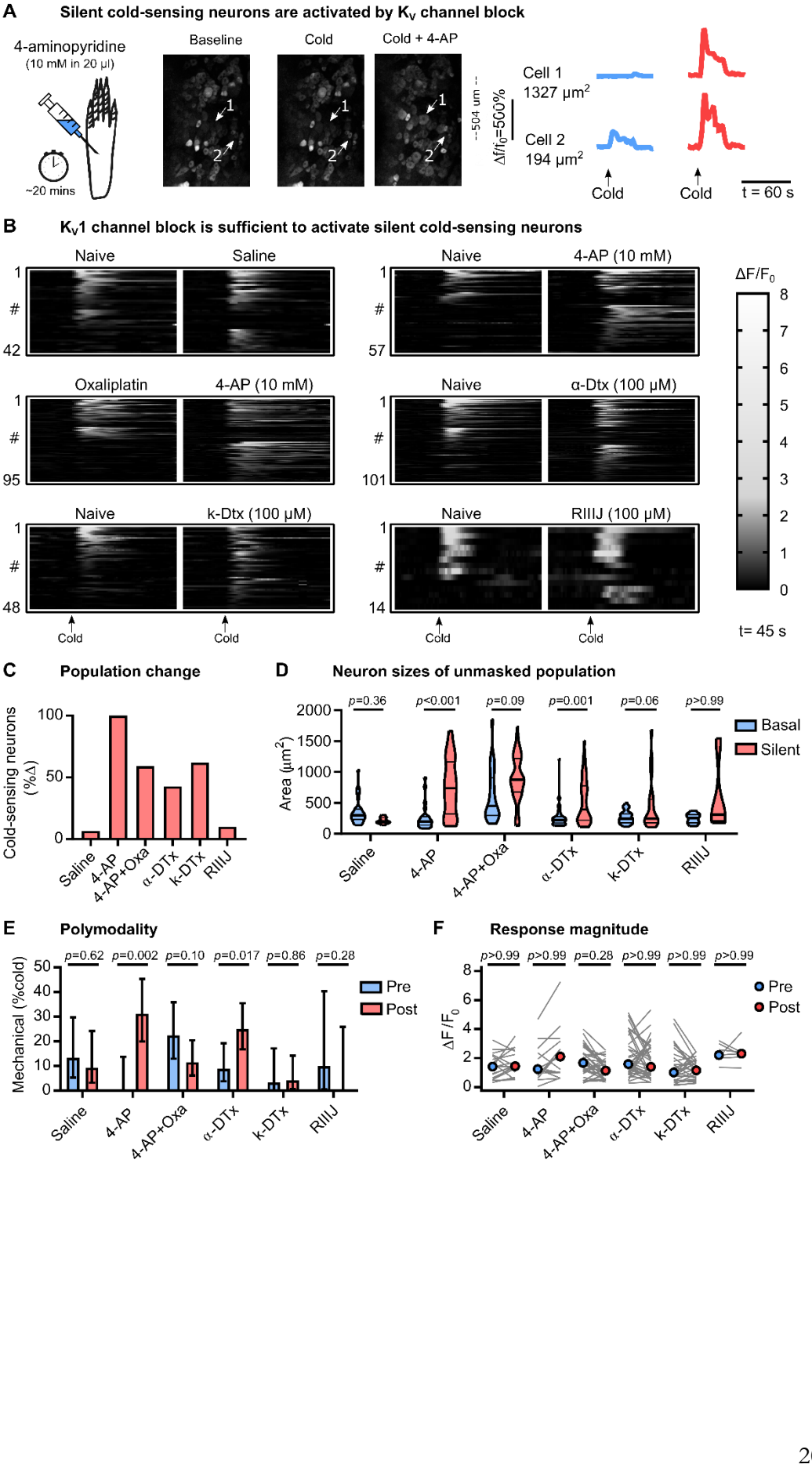
A
Silent cold-sensing neurons are activated by K_V channel block
4-aminopyridine
(10 mM in 20 µl)
~20 mins
Baseline
Cold
Cold + 4-AP
~504 um
Δf/f0=500%
Cell 1
1327 µm2
Cell 2
194 µm2
Cold
Cold
t = 60 s
B
K_V1 channel block is sufficient to activate silent cold-sensing neurons
Naive
Saline
Naive
4-AP (10 mM)
Oxaliplatin
4-AP (10 mM)
Naive
α-Dtx (100 µM)
Naive
k-Dtx (100 µM)
Naive
RIIIJ (100 µM)
ΔF/F0
t= 45 s
C
Population change
Cold-sensing neurons (%Δ)
Saline
4-AP
4-AP+Oxa
α-DTx
k-DTx
RIIIJ
D
Neuron sizes of unmasked population
Area (µm2)
p=0.36
p<0.001
p=0.09
p=0.001
p=0.06
p>0.99
Basal
Silent
E
Polymodality
Mechanical (%cold)
p=0.62
p=0.002
p=0.10
p=0.017
p=0.86
p=0.28
Pre
Post
F
Response magnitude
ΔF/F0
p>0.99
p>0.99
p=0.28
p>0.99
p>0.99
p>0.99
Pre
Post

Figure 4.21. Blocking $K_V1.1$ voltage-gated potassium channels is sufficient to induce de novo cold sensitivity in silent cold-sensing neurons

(A) Examples images and traces showing that peripheral blockade of voltage-gated potassium channels induces novel cold-sensitivity in normally cold-insensitive sensory neurons.

(B) Heat maps showing the effect of different potassium channel blockers on the peripheral representation of cold.

(C) Quantification showing the change in the number of cold-sensing neurons after treatment with different potassium channel blockers.

(D) Violin plots showing the cross-sectional area of basal cold-sensing neurons in the naïve state (blue) and of silent cold-sensing neurons unmasked by potassium channel block (red). Medians were compared using Kruskall-Wallis test followed by Dunn's multiple comparison test.

(E) Bar plot of the percentage of polymodal cold-sensing neurons that also respond to noxious mechanical stimuli before (blue) and after (red) treatment with potassium channel blockers. Proportions were compared using a χ^2 test. Error bars denote 95% confidence intervals.

(F) No change in the median response magnitude of neurons that responded to cold both before (blue) and after (red) treatment with potassium channel blockers, as determined by Kruskall-Wallis test followed by Dunn's multiple comparison test.

n=42 from 3 saline-treated mice, n=57 from 6 4-AP-treated mice, n=95 from 3 4-AP-treated mice pre-injected with oxaliplatin, n=101 from 4 α-dendrotoxin-treated mice, n=48 from 3 k-dendrotoxin-treated mice and n=14 from 3 RIIIJ-treated mice.

4.4 Discussion

In recent years, neuroscience has seen considerable advances in our understanding of the normal physiology underlying cold sensation. Yet the cell and molecular mechanisms driving cold allodynia in neuropathic pain remain unclear. Here I used *in vivo* imaging to investigate changes in the activity of peripheral cold sensing neurons in three different mouse models of neuropathic pain: chemotherapy-induced neuropathy, nerve injury and ciguatera poisoning. These experiments revealed that normally cold-insensitive large-diameter sensory neurons acquire a *de novo* sensitivity to cooling in these three etiologically-distinct neuropathic pain states. Silent cold-sensing neurons were molecularly identified as peptidergic nociceptors; their subsequent genetic ablation confirmed they contribute to behavioural cold hypersensitivity. Voltage-gated potassium channels $K_V1.1$ and $K_V1.2$ – hypothesized to mediate a hyperpolarizing 'brake' current against cooling-induced depolarization – were highly expressed in silent cold-sensing neurons in naïve conditions. Pharmacological inhibition of K_V1 channels consequently induced cold responsiveness in cold-insensitive neurons within minutes *in vivo*, pointing to functional downregulation of K_V1 channels as triggering pathological cold activation. Taken together, these results point to an apparently cell type-specific molecular mechanism that triggers *de novo* cold sensitivity in nociceptors to drive cold allodynia in neuropathic pain.

4.4.1 Chemotherapy-induced neuropathy

Direct investigation of the mechanisms driving cold allodynia *in vivo* has hitherto been difficult, because cold-sensing neurons are comparably rare and difficult to record using classical electrophysiological methods. Compared to traditional electrophysiological techniques, *in vivo* imaging provides a means for unbiased, population-wide measurements of stimulus-evoked single cell activity.[471] Although conscious of its limitations, I believe this method is ideally suited to studying the sparse cold-sensing afferents in health and disease. In the present study, I used *in vivo* imaging to explore the contribution of these cold-responding neurons to cold hypersensitivity in different mouse models of neuropathic pain.

To elicit cold allodynia in mice, I initially used a model of chemotherapy-induced neuropathy where oxaliplatin is delivered at a clinical dose of ~3 mg/kg by intraplantar injection into the hindpaw.[279] I chose this model because peripheral neuropathy associated with cold allodynia is the major dose-limiting side-effect of patients who receive this

chemotherapeutic to treat colorectal cancer.[179,279,472] Cold and tactile hypersensitivity developed rapidly, within 3 hours, but heat thresholds were normal, consistent with a neuropathic phenotype.[178] This is in contrast to other rodent models of oxaliplatin, which use either a single dose intraperitoneal injection where cold allodynia manifests within a week, or a chronic model of several weeks involving twice weekly injections that reportedly elicits prolonged cold hypersensitivity.[473,474] The intraplantar model has several advantages. The rapid onset mimics the human condition where cold allodynia occurs within hours and reverses several days later, and is separable from the more chronic peripheral neuropathy that can also occur.[475] Intraplantar delivery means the direct effects at peripheral nerves can be isolated from the systemic effects of the drug. Unilateral injection facilitates behavioural testing and results in a robust ipsilateral-only cold hypersensitivity that has since been reproduced by others in the lab.

During imaging sessions, I could apply a variety of cooling stimuli to activate cold-sensing neurons specifically at the receptive field affected by oxaliplatin. Cold allodynia properly refers to pain evoked by normally innocuous cooling. Although mice cannot tell us what counts as innocuous, naïve mice do not show a prolonged or overt nocifensive reaction to acetone stimulation, supporting the use of acetone as a mild cooling stimulus, which can also be correlated with behaviour. By using ice-water, nominally 0˚C, I could also ensure that any recruitment of additional cold-sensing neurons I observed really reflected a switch in modality responsiveness, as opposed to a change in thresholds. Finally, the use of the thermode allowed me to directly measure thermal thresholds of individual neurons, *in vivo*.

The *in vivo* imaging experiments revealed a dramatic and qualitative change in the type of neuron that responded to cooling in oxaliplatin-treated mice. Oxaliplatin caused a set of normally cold-insensitive large diameter neurons to respond to cooling. I named these cells 'silent' cold-sensing neurons. They were observed in all oxaliplatin-injected animals in response to ice-water, acetone and thermode stimulation, resulting in a substantial increase in the proportion of cold-sensitive neurons and amplification of the peripheral representation of cold. Importantly, no large cold responders were seen in the vehicle-treated animals, where cold-sensing neurons formed a normally-distributed population of very small cells, consistent with previous studies.[247,248,264] I used cross-sectional area of neuron somata to quantify size as this can easily be measured with confocal imaging. In the oxaliplatin-treated animals, the large cells were spread across a wide range of cross-sectional areas from ~400 to >1600 μm^2. In rat dorsal root ganglia,

this range of cell areas corresponds to the neurofilament-rich neurons that have Aβ and Aδ fibres, which are mainly low-threshold mechanoreceptors, but also comprise many nociceptors.[55] Silent cold-sensing neurons therefore likely represent a mixed population of A fibres that gain ectopic cold sensitivity after oxaliplatin, reflected in the two apparent peaks in the size distribution at ~800 and ~1200 μm^2. It is tempting to speculate that this might map onto separate Aδ and Aβ fibre peaks. The sluggish frame rate used here precludes calculation of conduction velocity, however with video-rate widefield imaging using a camera, a GCaMP with faster on/off kinetics, and controlled electrical stimulation, I could conceivable measure conduction velocity optically.

Both published and unpublished electrophysiological data corroborate my findings. Compound and single action potential recording of rodent nerves exposed to oxaliplatin in *vitro* supports action of the drug at myelinated A fibres.[461,476,477] Skin nerve preparation experiments showed 200-600 μM oxaliplatin applied directly on the receptive fields induced a novel cold sensitivity in half of previously cold insensitive Aβ mechanoreceptors, while a third of Aδ nociceptors also displayed a novel or increased sensitivity to cold.[478] Extending this to humans, recording from donor nerve fascicles showed that 100 μM oxaliplatin induced aberrant burst discharges of action potentials in A but not C fibres during cooling. However, many of these nerves came from patients with polyneuropathy, which may be more excitable to begin with.[461] Notwithstanding this, preferential blockade of A fibres abolishes cold allodynia in patients with oxaliplatin neuropathy, confirming A fibre activity is required for oxaliplatin-evoked cold pain in humans.[469]

Interestingly, oxaliplatin perfused onto dorsal root ganglia somata in culture does not induce novel cold responses.[479] In cultured neurons from mice injected with 6 mg/kg oxaliplatin intraperitoneally, the increase in cold-sensitive neurons was very modest (6.7% vs 4.9%).[480] Anecdotally, in pilot experiments where high concentrations of oxaliplatin (600 μM) was washed directly onto cells or where cells where incubated overnight with the drug, I did not see any novel or unusual cold sensitivity. This may reflect the fact comparatively few large-diameter DRG neurons survive dissociation. On the other hand, unmasking of silent cold-sensing neurons may require oxaliplatin to act directly at the nerve terminal or trunk, where it confers inappropriate cold sensitivity, while the soma is not affected.

Does recruitment of silent cold-sensing neurons entirely account for cold allodynia in oxaliplatin-treated animals? When I quantified the response magnitude of the small, basal cold-sensing neurons to acetone or ice-water, I found no effect of oxaliplatin, suggesting no dramatic change in their excitability. Investigation of the responses of dissociated sensory neurons in culture to cooling of the soma, however, suggests that cold allodynia is associated with a shift in the threshold of cold nociceptors towards milder temperatures.[262,282] The temperature of the soma *in situ* is unlikely ever to deviate far from body temperature, limiting the physiological relevance of such experiments, however. When I examined response thresholds of sensory neurons *in vivo* using the thermode, I saw that oxaliplatin injection did not shift the activation thresholds of cold-sensing neurons to higher temperatures. This argues against the hypothesis that oxaliplatin-induced cold allodynia results from noxious cold sensors becoming responsive to mild cooling. An *in vivo* imaging study which examined cold activity after ultraviolet burn injury did find greater activity with smaller temperature drops, suggesting that threshold shifts may contribute to other forms of cold allodynia.[247]

A fibres comprise both nociceptive and non-nociceptive neurons, including the oft-ignored Aβ nociceptors.[55] Given activation of silent cold-sensing neurons is associated with cold-evoked pain-like behaviours in mice, at least some of these large diameter cells are likely to be A fibre nociceptors. This is supported by my finding that many silent cold-sensing neurons also responded to noxious mechanical stimulation, but rarely to heat or to innocuous touch stimuli. Corroborating my results, application of oxaliplatin (600μM) to receptive fields of intact skin-nerve preparations also makes normally cold-insensitive mechanosensitive afferents highly responsive to cooling.[480] This begs the question: are these mechano-cold silent cold-sensing neurons truly silent at baseline and then acquire both cold- and mechano-sensitivity, or are they mechano-nociceptors that gain cold sensitivity? The effect of oxaliplatin was remarkably quick, occurring within at least three hours, however this was still too slow to watch oxaliplatin-induced cold allodynia unfold in the same animal within one imaging session, precluding direct testing of this question. The recent development of *in vivo* imaging of dorsal root ganglia in awake mice means the effect of oxaliplatin on afferent activity could now be followed in real time, however.[255]

It is important to note that most silent cold-sensing neurons are not mechano-cold polymodal nociceptors. The percentage of silent cold-sensing neurons found to be pinch-sensitive is likely to be an under-estimate due to the differing receptive field areas of these two stimuli.[245] Nonetheless, even with this caveat in mind, the bulk (>60%) of

silent cold-sensing neurons did not respond to pinch stimuli, or to any other non-cold stimulus. Thus, silent cold-sensing neurons seem to encompass both polymodal mechano-cold cells and a set of modality-specific neurons responding to cooling, after treatment with oxaliplatin.

Overall, my results demonstrate that chemotherapy-induced neuropathy is associated with profound plasticity in the peripheral representation of cold. Normally cold-insensitive, large-diameter neurons acquire a *de novo* sensitivity to cooling after intraplantar injection of oxaliplatin. The basal cold-sensing population is little altered. What is the relevance of this finding to humans? Intravenous oxaliplatin does not penetrate the blood brain barrier, but it does reach the dorsal root ganglia and peripheral nerves, supporting a peripheral mechanism of action.[481,482] While we cannot rule out an additional contribution of central sensitization of cold input, my data strongly suggest that it is the activation of these silent cold-sensing neurons in the periphery that drives cold allodynia in oxaliplatin-induced neuropathy.

4.4.2 Peripheral nerve injury

Is the unmasking of silent cold-sensing neurons particular to the acute oxaliplatin model? Cold allodynia is also a feature of more prolonged pain conditions. Nerve injury, particularly in the upper body, is often associated with cold hypersensitivity that develops some time after injury and persists long after (**Figure 4.2**). To mimic this chronic neuropathic pain state in mice, I used a modified version of the Seltzer or partial nerve ligation (PNL) model, where about a third of the sciatic nerve trunk is tightly ligated, resulting in significant nerve injury.[281] As expected, injured animals developed mechanical hypersensitivity by 2 weeks, and at 4 weeks a modest cold allodynia was apparent. This is in contrast to spared nerve injury (SNI), where cold allodynia supposedly precedes tactile allodynia.[186] In fact, the choice of PNL was dictated by the fact I observed absent or altogether too variable cold allodynia in the other models I tested (SNI, CCI). Nerve injury models were developed for rats, however, and do not necessarily always translate well to the robust strains of mice used here.[178] Nonetheless, the emergence of delayed cold allodynia, combined with the persistent effects of injury, render PNL an acceptable model of chronic, injury-associated neuropathy. Unfortunately, I could not test how long cold allodynia lasts beyond 4 weeks due to the ethical requirement to cull animals at 40 days.

I performed *in vivo* imaging from sham and PNL mice between 4 and 5 weeks. I chose to image the L4 dorsal root ganglion as this provides the bulk of the sciatic nerve

axons in mice.[483] The effect of axotomy was apparent in the reduced number of responding cells observed on a per animal basis. To my surprise, I saw little if any spontaneous activity after injury; this lack of spontaneous firing has been attributed to anesthesia.[255] Indeed, ketamine is known to act peripherally to inhibit sensory neuron activity.[484] Nonetheless, when I applied cold stimuli I saw a greater fraction of cells respond due to the recruitment of additional large-diameter neurons. Compared to oxaliplatin, there were fewer unmasked, consistent with milder cold hypersensitivity. As with oxaliplatin, no change in thresholds was evident, contrasting with the impact of chronic constriction injury on cold thresholds *in vitro*.[262] My findings are consistent with previous electrophysiological studies that showed that spinal nerve ligation caused a marked increase in the number of cold-sensitive Aδ fibres.[485] *In vitro* calcium imaging experiments also support the observation that nerve injury increases the fraction of cold-sensitive cutaneous sensory neurons.[262,486,487] I also noted an increase in the number of polymodal neurons following PNL. Interestingly, recent single nucleus RNA sequencing data suggest that sensory neurons lose their subtype-specific gene expression after nerve injury, which may account for enhanced polymodality after injury.[488,489] However, like with oxaliplatin, most of the large-diameter silent cold-sensing neurons unmasked by PNL were modality-specific for cold. Overall, despite the difference in time to onset, the effects of oxaliplatin and nerve injury on cold-evoked activity appeared qualitatively similar.

4.4.3 Ciguatera poisoning

A critical caveat of both oxaliplatin and PNL experiments is that I compared separate groups of animals and so cannot know if silent cold sensing neurons are truly silent at baseline. I thus needed a model where cold allodynia could be elicited in the same animal within a single imaging session. Others groups have used burn injury, however I am skeptical of the relevance of this to cold allodynia, as cold typically alleviates burn-related pain.[247,417] I therefore induced cold allodynia using ciguatoxin-2 (P-CTX-2), a toxin from dinoflagellate algae which accumulates in the food chain to cause ciguatera poisoning and associated cold allodynia in humans who eat contaminated sea-food.[407] Ciguatoxin-1 is the more potent toxin and has been successful exploited before to study cold allodynia in mice through intraplantar injection, thereby avoiding gastrointestinal side-effects, and isolating effects on peripheral neurons.[282,490] Unfortunately, the world stock – purified from Moray eel in 1991 by Richard Lewis – has been used up.[491] Nonetheless, intraplantar injection of P-CTX-2 has been reported to increase spinal cord wide dynamic range

neuron firing in response to cold within 20 minutes in the rat.[492] I therefore made intraplantar injections of 100 nM P-CTX-2 into mice and observed marked cold hypersensitivity arise after 20-30 minutes. This mimics the acute effects in human volunteers, where very low doses of ciguatoxin also elicit localized cold allodynia with flare.[490]

I injected mice undergoing *in vivo* imaging with P-CTX-2 intraplantar – after 30 minutes, I observed that many previously cold-insensitive large-diameter neurons began to respond to cooling. This echoed *in vitro* findings using P-CTX-1 where novel cold-responses emerged in culture.[282] Some, but not all, of these cells responded to noxious pinch at baseline. Pinch activates a smaller receptive field than cold so this is likely an under-estimate. Nonetheless, most unmasked neurons were silent to begin with and gained modality-specific responses to cooling. Compared to oxaliplatin, P-CTX-2 recruited more ice-water than acetone responsive neurons, reflected in its less effective sensitization of acetone-evoked behaviour. Importantly, many small diameter neurons actually lost sensitivity with P-CTX-2, with newly-unmasked small cells replenishing the pool of active neurons. This mirrors the finding that oral burn injury silences cold thermosensors.[417] Others have reported that there is generally little stability in the representations of sensory stimuli before and after treatment with pro-algesics.[193] In my view, this is partly explained by the way swelling and edema associated with inflammation changes the geometry of the paw and consequently the receptive fields of the imaged neurons. Of the cold cells that responded before treatment, their response was dampened by P-CTX-2, emphasizing that unmasking of silent cold-sensing neurons is not the only effect of P-CTX-2.

Silent cold-sensing neurons are thus unmasked in all three neuropathic pain states tested here, but to varying degrees, and within the context of multifarious other changes in the peripheral representation of cold. In all three models, some silent cold-sensing neurons also responded to noxious pinch, however the bulk were modality-specific. There is a gradation in the magnitude of both behavioural and cellular sensitization. Fewer cells are unmasked in PNL animals which show the least cold allodynia, while more are activated by oxaliplatin and P-CTX-2 which correspondingly cause more pain. This apparent relationship between nociceptive behaviour and silent cold-sensing neuron activity supports similar core pathophysiology operating in all three models. This work therefore identifies a common cellular mechanism underlying cold allodynia in chemotherapy-, nerve injury- and ciguatera-induced neuropathy, which would have been

impossible to identify using conventional behavioural methods alone. In so doing, I have defined a new group of cold-sensitive afferents, which I term silent cold-sensing neurons, that are engaged in etiologically-distinct neuropathic pain states to drive cold allodynia.

4.4.4 Molecular identity of silent cold-sensing neurons

Single cell RNA sequencing has created an increasingly detailed classification of sensory neurons subtypes.[76–78] These studies confirm and extend traditional taxonomies based on electrophysiological, morphological and molecular markers.[47,55] But to which of these subtypes do silent cold-sensing neurons belong? I designed an *in vivo* genetic screen to investigate the molecular identity of silent cold-sensing neurons. Animals homozygous for both Pirt-GCaMP3 and Cre-dependent tdTomato were crossed onto different subset specific Cre lines, thus generating mice where GCaMP3 is expressed by all sensory neurons but the tdTomato reporter is restricted in a Cre-dependent manner to the subset of interest. Because of its reproducibility and clinical importance, I focused on the oxaliplatin model to investigate whether functionally-identified silent cold-sensing neurons expressed genetically-defined markers of particular afferent subsets.

Cre lines were chosen based on the subtype marker genes originally identified by Usoskin *et al.*[76] Silent cold-sensing neurons did not express Calb1, a marker of rapidly-adapting Aβ low-threshold mechanoreceptors.[493] Nor did silent cold-sensing neurons express TrkB, which labels Aδ low-threshold mechanoreceptors.[270] This was surprising given prior findings that oxaliplatin preferentially modulates A fibre activity.[461,469,476,477] However, even using a wide-range of light touch stimuli, applied to both hairy and glabrous skin, I was unable to evoke activity in silent cold-sensing neurons, so they are unlikely to be low-threshold mechanoreceptors. My findings are consistent with data which suggests TrkB-positive neurons are essential to tactile but not cold allodynia in the spared nerve injury model.[194] Having ruled out the touch neurons, I turned to the Trpv1 lineage, which marks diverse C fibre-type afferents.[462] There was little overlap, despite the finding that Trpv1-DTA mice do not develop cold allodynia.[186] This may reflect the fact Trpv1 lineage marked the basal cold-sensing neurons, which may play a larger role driving cold hypersensitivity in the SNI model.[67,248]

The majority of silent cold-sensing neurons did express $Na_V1.8$, however, a classic marker of nociceptors, in all three tested models.[72,73,265] Consistent with our previous observations, very few of the small diameter, basal cold-sensing cells expressed $Na_V1.8$.[264] I saw $Na_V1.8$-Cre-dependent tdTomato expression in numerous small, medium and large

diameter neurons, most of which were not silent cold-sensing neurons, agreeing with recent observations that $Na_V1.8$, as well as being expressed by ~90% of nociceptors, is also expressed by ~40% of A fibre neurons, encompassing both nociceptors and touch sensors.[494] $Na_V1.8$-lineage neurons are required for noxious mechanosensation, inflammatory pain, and the response to subzero cold stimuli, but are dispensable for physiological cold-sensing down to 1°C.[73,264] A previous study using $Na_V1.8$-Cre DTA mice suggested $Na_V1.8$-positive neurons were not required for cold allodynia induced by intravenous oxaliplatin injection, however.[307] Using the distinct intraplantar injection model, I however saw a reduction of cold hypersensitivity by 50%, supporting a substantial contribution of $Na_V1.8$-positive silent cold-sensing to cold allodynia. The imperfect overlap of $Na_V1.8$ expression with silent cold sensors and the less than 100% effectiveness of DTA ablation likely explains why I did not see a greater loss of pain behaviour. Indeed, $Na_V1.8$-DTA mice expressing GCaMP3 did show residual large-diameter cold-sensing neurons. Although the $Na_V1.8$-Cre DTA mouse does not develop neuropathic mechanical hypersensitivity, prolonged optogenetic silencing of $Na_V1.8$-lineage neurons was analgesic for this modality.[73,495] Finally, HCN2 channels – which control action potential firing – were shown to contribute to cold allodynia in chronic constriction injury by conditional deletion of HCN2 using $Na_V1.8$-Cre.[197] Interestingly, $Na_V1.8$ is found in normally cold-insensitive cells that become responsive to cold after a 5 minute exposure to 1°C, hinting at a physiological role for silent cold-sensing neurons.[264]

Having identified silent cold-sensing neurons as putative nociceptors, I then investigated Cre lines with more restricted patterns of expression to identify which nociceptor subset they belong to. Most did not express Tmem45b, believed to be a marker of non-peptidergic nociceptors based on single cell RNA sequencing data.[76] However, using the CGRPα-CreERT2 mouse line, I discovered that the majority of silent cold-sensing neurons in all three models are positive for CGRPα. They are thus likely to be peptidergic nociceptors, which comprise both A and C fibres. The bulk of CGRPα-positive sensory neurons also express $Na_V1.8$.[495,496] The silent cold-sensing neurons awakened after heat injury were identified as CGRPα-positive peptidergic nociceptors, suggesting they are also engaged in this model.[417] Tellingly, optogenetic inhibition of these neurons transiently and reversibly relieves cold allodynia after spared nerve injury.[465] These CGRPα-positive neurons have been identified as a mixture of small diameter heat sensors and large diameter mechanonociceptors using *in vivo* imaging of the trigeminal ganglion, in tune with our finding that large-diameter silent cold-sensing neurons often

also respond to noxious pinch.[67] P-CTX-2 has also been reported to increase CGRP release and produces flare when injected into humans.[490,497] I wanted to use CGRPα-CreERT2 Advillin-DTA mice to ablate these cells and test their behavioural role as this approach avoids the developmental ablation seen in the $Na_V1.8$-Cre line. Unfortunately, trial experiments failed to recapitulate the expected acute pain phenotype of peptidergic nociceptor loss, casting doubt on the efficacy of the ablation, and precluding the use of this line here. Nonetheless, the imaging data strongly suggest the majority of silent cold-sensing neurons are petidergic nociceptors that become activated by cooling to drive pain during neuropathy.

Neither $Na_V1.8$ nor CGRPα perfectly labelled all silent cold-sensing neurons and certainly neither was specific for silent cold cells alone. We must bear in mind that evolution did not make marker genes for the convenience of scientists. Many markers change expression with injury, such as galanin – indeed, Galanin-Cre proved futile as a marker in early experiments due to variable expression.[82] However, the fact both $Na_V1.8$ and CGRPα genetically dissociate basal and silent cold-sensing neurons makes them useful tools for targeted manipulation of the pathologically active cold-responsive neurons. In the future, I envisage further experiments using DTA lines with behaviour to test the requirement of these cells for different forms of cold allodynia. Increasing the tamoxifen dose and waiting longer before testing might circumvent the issues with the CGRPα-CreERT2 Avil-DTA mouse. GCaMP imaging of the $Na_V1.8$-Cre DTA mouse was very difficult due to the small size of the ganglion, illustrating the problematic side-effects of permanent ablation experiments. Moreover, this mouse expressed GFP constitutively.[73] The deployment of Cre-dependent chemogenetic and optogenetic technology should provide an alternative approach that would allow for transient silencing of the subset of interest.[238,465,495,498]

4.4.5 Ionic mechanisms of *de novo* cold sensitivity

By genetically identifying the silent cold-sensing neurons, I hoped to characterize specific molecules involved in driving *de novo* cold sensitivity. Both oxaliplatin and P-CTX-2 are reported to directly activate voltage-gated sodium channels.[461,499] Sodium channels are also upregulated and redistributed after nerve injury.[130,195] Which sodium channel isoforms are required for silent cold-sensing excitability? $Na_V1.8$ is expressed by silent cold-sensing neurons, however my imaging and behavioural data confirm that $Na_V1.8$ is not essential for activity in these cells. These experiments do not rule out a role for $Na_V1.9$, however.[432]

Nonetheless, TTX injection was sufficient to block cold evoked activity in both small and large cold-sensing cells. Consistent with this, skin-nerve recordings of cold-sensitive afferents from $Na_V1.8$ knockout mice showed application of TTX to the peripheral terminal could block discharge triggered by cooling to 10°C.[431] Deletion of $Na_V1.7$ had no effect on the activation of silent colds-sensing neurons, however.

Given the fact that oxaliplatin has been shown to directly activate $Na_V1.6$ and inhibition of $Na_V1.6$ prevents oxaliplatin-evoked cold allodynia, $Na_V1.6$ is the most probable candidate sodium channel subtype mediating cooling-evoked excitability in silent cold-sensing neurons.[279,461] I used intraplantar injection of 4,9-anhyTTX to test the role of $Na_V1.6$, and saw a marked reduction in silent, but not basal, cold-sensing neuron activity, although complete isoform selectivity at the high doses used *in vivo* is doubtful.[360,500,501] Interestingly, local knockdown of $Na_V1.6$ in rats had only a minor effect on cold allodynia induced by spinal nerve ligation.[502] A conditional knockout of $Na_V1.6$ was recently described, with AAV-Cre mediated deletion of floxed $Na_V1.6$ partially impairing mechanical hypersensitivity in the spared nerve injury mouse model. Cold allodynia was apparently not tested in these experiments, however.[127] In the future, I would like to conclusively examine the contribution of $Na_V1.6$ to silent cold-sensing neuron excitability by using a different blocker or by conditional knockout of the coding gene.[127,279]

Using fluorescence activated cell sorting followed by microarray analysis, we found that the voltage-gated potassium channels $K_V1.1$ and $K_V1.2$ were enriched in cold-insensitive, $Na_V1.8$-positive neurons compared to basally cold-insensitive neurons. Thus, at basal conditions, presumptive silent cold-sensing neurons express high levels of K_V1 channels which pass a voltage-dependent excitability brake current (I_{KD}) that normally opposes cold-induced depolarization.[81,262,464] Broad-spectrum inhibition of voltage-gated potassium channels with 4-aminopyridine induced *de novo* cold sensitivity in many large-diameter neurons, indicating that functional loss of the I_{KD} current is sufficient to unmask silent cold-sensing neurons. Silent cold-sensing neurons were also activated by selective antagonism of K_V1 channels with α-dendrotoxin, and this effect was at least partially recapitulated by specific block of $K_V1.1$, but not $K_V1.2$. Interestingly, activation of sodium channels was not sufficient to drive *de novo* cold-sensitivity, indicating that ectopic cold activation is not merely a consequence of a general increase in excitability, but particular to the downregulation of the K_V1 channels that mediate the brake current.

Does neuropathic pain actually lead to functional downregulation of K_V1 channels? In dissociated cultures, 4-AP induces *de novo* cold sensitivity in neurons from control but not from mice with chronic constriction injury.[262] This is paralleled by behavioural results which show 4-AP evoked cold hypersensitivity is suppressed in injured animals, indicating that chronic constriction injury-induced cold allodynia operates via the same pathway as 4-AP to drive *de novo* cold sensitivity.[262] Similarly, both oxaliplatin and 4-AP cold allodynia can be blocked by inhibition of $Na_V1.6$, highly suggestive of a common cellular pathway.[279] Consequently, I predicted that 4-AP would unmask fewer silent cold neurons in mice pre-treated with oxaliplatin, as the brake current would already be inhibited – this was indeed the case, although the effect of 4-AP was not entirely abolished.

By what mechanism could K_V1 channels be downregulated in neuropathy? Quantitative PCR of samples from oxaliplatin-treated mice reveal that there is a decrease in $K_V1.1$ but not $K_V1.2$ RNA, suggesting that transcriptional downregulation may be responsible for loss of the brake current.[460] Numerous reports have also found a decrease in both $K_V1.1$ and $K_V1.2$ expression following nerve injury.[503–509] On the other hand, *in vitro* studies support a direct antagonist effect of both oxaliplatin and ciguatoxin on voltage-gated potassium channels.[461,477,510] It would have therefore been useful to perform voltage-clamp recordings of large-diameter $Na_V1.8$-expressing neurons in culture to determine if there is a direct action of oxaliplatin or ciguatoxin on K_V1 in these cells. Likewise, RNAscope, microarray, RNA sequencing and qPCR studies could be used to determine if there is a change in K_V1 channel gene expression. Detailed characterization of changes in K_V1 function and expression in each model of neuropathic pain would have been a Herculean endeavor, however. The focus of this work was the silent cold-sensing neurons not the peculiarities of each model. My data convincingly show that silent cold-sensing neurons express $K_V1.1$, inhibition of which leads to their activation by cooling, thereby strongly implicating these channels in mediating pathological cold sensitivity during neuropathy.

4.4.6 Molecular transduction of cooling by silent cold-sensing neurons

K_V1 channels are not intrinsically modulated by the cold so cannot provide the initial cold-induced depolarization in the peripheral nerve endings of silent cold-sensing neurons. Which transducer molecules might mediate the cold-induced generator potential in these cells? The silent thermosensors uncovered by burn injury co-express both Trpm8

and CGRP, however Trpm8-Cre used to drive GCaMP6 in the burn injury experiments is a lineage Cre, therefore does not definitely reveal if Cre-positive neurons express Trpm8 in adulthood.[417] Indeed, knockout and pharmacological data suggests both Trpm8 and Trpa1 are dispensable for the model of oxaliplatin neuropathy used in my thesis, although Trpa1 is important to cold allodynia in ciguatera.[279,282] Trpm8 is however reportedly required for cold allodynia induced by chronic constriction injury.[420,422]

How could I test if canonical Trp channels contribute to cold detection by silent cold-sensing neurons? The Trpm8-Cre and Trpa1-Cre line could be used to identify afferents expressing these transducers, while Trpm8-DTR and Trpa1-DTR mice could be used to explore their contribution to behaviour.[74,417,420] While there is a Trpm8-GFP knock-in line, the overlap in emission wavelength between GFP and GCaMP precludes its use for labelling Trpm8 neurons in my experiments.[436] As I did not have access to these mouse lines or to Trp channel KOs, I had to take an alternative approach. Pharmacological identification of Trpm8 neurons by menthol sensitivity *in vivo* was a possibility, but intraplantar injection failed to elicit any response in my hands, while direct DRG injection was technically daunting.[152] Because Calb1 shows considerable overlap with Trpm8 according to single-cell RNA sequencing studies, we can use Calb1 expression as a surrogate for Trpm8.[76,77] Indeed, Calb1 marked the small diameter basal cold neurons, but was mostly absent in the large cells. This is consistent with our microarray data which suggests that Trpm8 is highly enriched in the $Na_V1.8$-negative basally cold sensitive neurons, but has low expression in $Na_V1.8$-positive normally cold-insensitive neurons. It therefore seems unlikely that Trpm8 is usually expressed in silent cold-sensing neurons, although this does not preclude its upregulation by neuropathy.

What other cold transducers are present in sensory neurons and could mediate cold detection in silent cold-sensing neurons? ENaC is directly gated by cold *in vitro* while ASICs are strongly modulated by cooling, however their role in cold-sensing has not been explicitly tested *in vivo*.[511] Recombinant Trpc5 homomers are cold-sensitive in the innocuous range but no deficit is seen in the KO animal.[427] A recent *C. elegans* screen identified a cold-gated metabotropic glutamate receptor GLR-3. The vertebrate homolog GluK2 is cold-sensitive and its knockdown impaired the response of mouse DRG neurons to cooling down to 10°C, *in vitro*.[512] Testing the role of these channels would require me to develop an *in vitro* screen of silent cold-sensing neurons. This was foiled by the fact they do not seem to be active in culture, at least in the presence of oxaliplatin.[479]

Closure of background potassium channels that maintain the hyperpolarized resting membrane potential is also proposed to mediate depolarization evoked by cooling.[513] In identified cold-responsive neurons voltage-clamped at -60 mV, a cold-induced inward current with negative reversal potential was accompanied by decreasing membrane conductance, and no increase in intracellular calcium, consistent with shutting of background potassium channels.[514] Molecular identification of these potassium channels has proved challenging. Transcriptomic characterization of basal cold-sensing or Trpm8-positive neurons isolated by FACS shows an enrichment of TASK-3, a pH-sensitive two-pore domain leak potassium (K2P) channel.[264,419] Selective block of this channel alters the thermal threshold of cold-sensing neurons, and the mouse KO shows a moderate behavioural hypersensitivity to cold.[419] Given its expression in basal cold-sensing neurons, however, this channel in unlikely to mediate cold transduction in silent cold-sensing neurons.

Candidate K2P channels that are intrinsically cold-sensitive abound, however. TREK1, TREK2 and TRAAK all undergo loss-of-function at low temperatures and are expressed in peripheral sensory neurons.[515–517] Double KO of TREK1 and TRAAK results in increased numbers of cold-sensitive neurons in culture and cold-activated fibres in the skin, matched by increased sensitivity to noxious cold temperatures and enhanced chronic constriction injury-evoked cold allodynia.[98] TREK2-deficient mice have increased responses to innocuous cooling, but acute cold pain is unchanged.[429] Importantly, oxaliplatin-induced cold allodynia does not develop in TREK2 KOs, TREKS KOs and TRAAK/TREK1 double KOs, and TRAAK/TREK1/TREK2 triple KOs.[429,430,460] As all these KO lines are basally hypersensitive to cold, the blunting of cold allodynia suggests oxaliplatin-induced neuropathy could act via a common molecular target to drive cold pain.

K2P channels play at least a modulatory role in the control of the sensory neuron response to cold. Testing whether closure of a given channel is necessary for cold-induced excitation in silent cold-sensing neurons would require selective agonists or dynamic clamp experiments, however. A complex and changing complement of these channels may be present at the afferent terminals of silent cold-sensing neurons, in both homomeric and heteromeric forms, and whose closure can together trigger cold-induced action potentials in the absence of Trpm8 or Trpa1.[518] As multiple potassium channels are expressed by cold-sensing neurons, a single channel isoform is unlikely to be the sole transducer in cold allodynia.[264]

4.4.7 Analgesic treatment of cold allodynia

How do my results inform the treatment of cold allodynia? Analgesic treatment of cold allodynia is typically symptomatic. For neuropathic pain patients, cold allodynia is one sensory abnormality among many, and may not even be the primary complaint. Despite advances in defining the mechanistic basis of cold allodynia, patients are treated using standard analgesics that do not rationally target specific pain modalities. This is compounded by clinical trials of analgesics where pain is assessed in a manner blind to modality using patient self-report rather than using quantitative sensory testing which could discriminate cold pain effects.[256]

Given the vast number of molecules implicated in cold allodynia, rational therapy must be informed by a detailed understanding of what drives cold allodynia in that particular pain condition in that specific patient. As such personalized medicine currently lies out of reach, a promising alternative is to identify core pathophysiology that is agnostic to the particular molecular changes involved and that is in principle druggable. The unmasking of silent cold-sensing neurons is just such an example. There is a clear mechanistic link between the induction of *de novo* cold-sensitivity and the excitability state of a neuron. My data suggests this is primarily driven by downregulation of the excitability brake current passed by K_V1 potassium channels, however the literature also supports the involvement of other potassium and sodium channels.[279,282,519,520]

An attractive therapeutic strategy would therefore be to reduce afferent terminal excitability by enhancing or restoring hyperpolarizing voltage-gated potassium channel activity. For instance, the KCNQ voltage-gated potassium channel activators retigabine and flupirtine have been shown to reduce cold allodynia evoked by oxaliplatin and nerve injury, presumably by shifting hyperexcitable afferents into a quiescent state through increased potassium efflux.[519,521] Clinical trials that include diabetic neuropathy patients suffering from cold pain show efficacy for sodium channel inhibitors.[522] Unfortunately, ensuring selectivity of such drugs remains a challenge.

This could be overcome using gene therapy. For example, AAV-mediated over-expression of $K_V1.2$ RNA impaired the development of cold allodynia induced by nerve injury in rats.[523] In preclinical studies, a virally-delivered chemogenetic system which selectively silences sensory neurons has been used to treat neuropathic cold allodynia.[238] A recent study used CRISPR activation to increase expression of *Kcna1* – which encodes the K_V1 channel here implicated in cold allodynia – in excitatory neurons in the

hippocampus, diminishing their excitability, and decreasing seizures in a rodent model of epilepsy.[524] Targeted over-expression of *Kcna1* in silent cold-sensing neurons using this technology could strongly ameliorate cold allodynia and thus represent a rational gene therapy for neuropathic pain. Although many hurdles remain, I believe my discovery of silent cold-sensing neurons and the K_V1 channels they express as key players in the induction of cold allodynia identifies a new molecular target for novel analgesic therapies to combat neuropathic pain.

4.5 Conclusions

Taken together, these data provide evidence that cold allodynia results from a set of normally silent cold-sensing neurons gaining *de novo* cold sensitivity in neuropathic pain. Cold allodynia is therefore a profound form of peripheral sensitization. Silent cold-sensing neurons were identified as putative A fibre peptidergic nociceptors based on their large diameter, response to noxious mechanical stimulation, and expression of molecular markers $Na_V1.8$ and CGRPα. Silent cold-sensing neurons have basally high expression of $K_V1.1$ and $K_V1.2$ voltage-gated potassium channels that mediate an excitability brake current that opposes cooling-induced depolarization. Block of K_V1 channels is sufficient to induce *de novo* cold sensitivity, pointing to downregulation of these channels during disease as a likely driver of cold allodynia. By defining the cells and molecules triggering cold allodynia, these findings will, I hope, inform the development of better targeted therapeutics for neuropathic pain. The *in vivo* imaging data collected here provides a unique insight into the cellular mechanisms underpinning cold allodynia, for the first time identifying silent cold-sensing neurons as critical drivers of cold-evoked neuropathic pain.

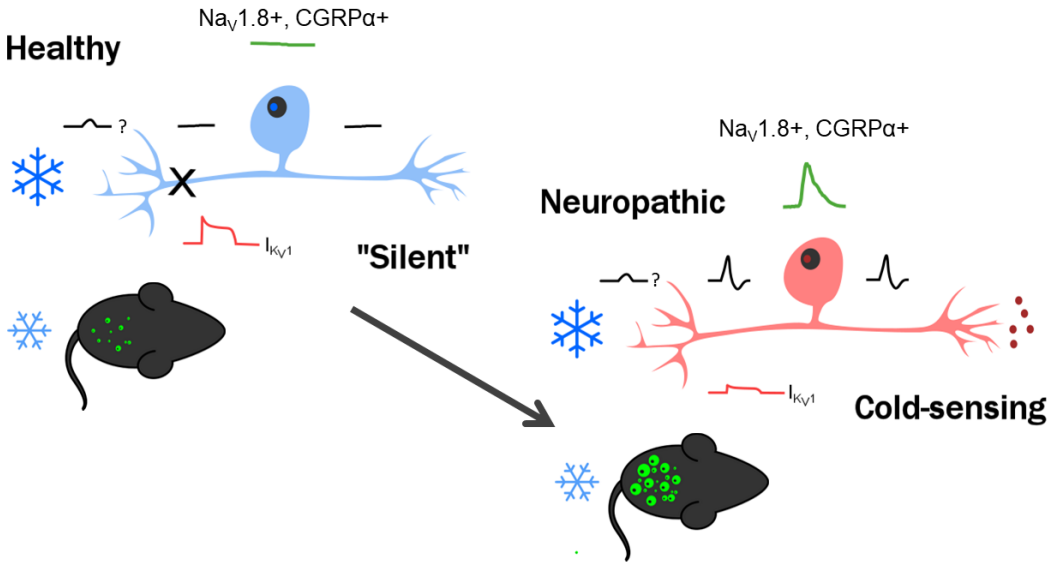

Figure 4.22. Proposed model of silent cold-sensing neuron activation during neuropathy to cause cold allodynia

In healthy mice, only small neurons respond to cold. The large-diameter silent cold-sensing neurons have high K_V1 activity, thus any cold-induced depolarization does not trigger action potential firing and there is no subsequent GCaMP signal at the level of the dorsal root ganglion.

In neuropathic animals, we hypothesize that a functional reduction in K_V1 activity means that silent cold-sensing neurons are now sensitive to cold, increasing the nociceptive input to the brain in response to cooling. Thus both small and large neurons now show GCaMP signals to cold stimuli.

The molecules mediating the initial generator potential to cold in silent cold-sensing neurons are currently unknown.

5 General Conclusion

When Antonie van Leeuwenhoek first looked down the microscope he built and saw tiny "animalcules" swimming around, he changed biology forever. Human eyes evolved to see a coarse world of food and water, predators and prey – to see only what we need to survive. But with the development of optical microscopy, science illuminated a hidden and bustling universe of cells, tissues and molecules. We can now watch biological processes unfold in real-time that were previously invisible or evidenced only circumstantially. In particular, the combination of optical imaging and genetically-encoded fluorescent indicators of neural activity has revolutionized neuroscience by allowing researchers to record activity in unprecedented numbers of neurons, *in situ*.

In the last five years, *in vivo* GCaMP imaging has been exploited to monitor calcium activity in peripheral sensory neurons as a surrogate for action potential firing.[67,185,245–248] This technique forms the core of the research presented in this thesis. The peripheral sensory neurons of the dorsal root ganglia form modality-specific subsets that detect environmental stimuli such as force, heat or cold.[245] The focus here were the nociceptors: afferents specialized to detect damage and whose activation typically drives the perception of pain. Both nociception and pain are essential for survival, but can go awry. A handful of individuals in the world today are born with an unusual genetic condition that abolishes their sense of nociception leading to congenital insensitivity to pain (CIP). Millions more are burdened by persistent pain states such as neuropathic pain. Among the worst symptoms of chronic neuropathic pain is allodynia when normally innocuous stimuli are experienced as painful. While CIP patients fail to experience pain in response to dangerous stimuli, patients with allodynia maladaptively experience pain in response to harmless stimuli.

In this thesis, I used imaging techniques to investigate the contribution of peripheral sensory neurons to these two unusual pain states. In Chapter Three, I characterized the mechanism of analgesia in knockout mice and CIP individuals lacking the gene *SCN10A* that encodes the nociceptor-enriched sodium channel $Na_V1.7$. In Chapter Four, I identified and characterized a novel population of nociceptors that are engaged in different neuropathic pain conditions to drive cold allodynia – pain in response to innocuous cooling. Crucial to the success of these studies was the ability afforded by *in vivo* imaging to monitor peripheral sensory neuron activity in an objective, global

fashion, meaning hypotheses could be rapidly generated, tested and explored by recording large numbers of cells.

Early findings from imaging studies that were at odds with the traditional understanding of afferent nerve response characteristics led many investigators to question the value of this technique. Specifically, imaging revealed the number of polymodal nociceptors was far fewer than classical electrophysiological studies attested. The experiments presented here have consistently reproduced these two key observations that polymodal nociceptors are comparatively rare, but that polymodality is enhanced after damage or inflammation. Reappraisal of historical *in vivo* intracellular recording data from dorsal root ganglia has corroborated this.[55] *In vivo* imaging has also been validated by studying genetically-modified animals with known pain deficits that ought to cause a predictable impairment in peripheral activity. Thus, I contributed to studies that showed $Na_V1.8$ KO animals showed fewer mechano- and extreme cold nociceptors, in line with their loss of mechanical and cold, but not heat nociception, as judged by behaviour.[264]

When I turned to the $Na_V1.7$ KO mouse which shows a dramatic loss of mechanical, heat and inflammatory pain, I was however very surprised to find essentially unchanged nociceptor activity during the acute and sensitized states. The findings in Chapter Three challenge the prevailing view that $Na_V1.7$ loss-of-function abolishes pain by silencing nociceptors through reduced peripheral excitability. I hypothesized that nociceptive input to the CNS was instead lost at the central terminal in the spinal cord through a decrease in presynaptic release. To test this hypothesis, I developed a glutamate imaging method to study neurotransmitter release from the afferent central terminal in spinal cord slices, but could in future be extended *in vivo*. Using imaging, electrophysiological and biochemical assays of transmitter release, I found pronounced deficits in synaptic transmission between nociceptors and the CNS in $Na_V1.7$ null animals. In agreement with previous findings from the lab, these deficits were dependent on opioid receptors, although the underlying signalling pathways remains unclear. Behavioural pharmacology experiments demonstrated that central – but not peripheral – opioid receptors are essential for the maintenance of analgesia in $Na_V1.7$ null mutants. This work thus defines a novel central mechanism of analgesia in $Na_V1.7$ nulls that depends on opioid receptors and therefore provide an explanation for the failure of peripherally-targeted inhibitors of $Na_V1.7$ to relieve pain.

Can *in vivo* imaging shed new light on potential peripheral mechanisms of chronic pain? Cold allodynia is among the most mysterious and inexplicable of pain states, having

apparently little evolutionary value. In Chapter Four, I wondered whether cold allodynia is peripheral in origin and whether it might depend on plasticity in cold-sensing neurons or nociceptors. After a great deal of trial and error, I settled on the intraplantar model of oxaliplatin neuropathy as a mouse model that reliably elicits cold allodynia. There was a stark change in the peripheral representation of cold after induction of cold allodynia, with a subset of normally 'silent' cold-sensing neurons becoming responsive to cooling. This population was observed in two further mouse models of neuropathic pain displaying cold allodynia: ciguatera poisoning and nerve injury. Silent cold-sensing neurons were functionally and molecularly identified as peptidergic nociceptors, and their genetic ablation diminished behavioural cold allodynia. Unmasking of a latent cold-sensitivity in nociceptors during neuropathic pain presumably provides enhanced nociceptive drive during exposure to the cold thereby causing pain. Molecular characterization of these neurons identified K_V1 voltage-gated potassium channels as controlling cold sensitivity, pointing to an underlying molecular mechanism for cold allodynia. The molecules subserving cold transduction in the nerve endings of silent cold-sensing neurons remain unknown, however. Overall, this study showed that silent cold-sensing neurons contribute to cold allodynia in etiologically-distinct neuropathic pain states and that their sensitivity to cold depends on K_V1 channels. Activation of silent cold-sensing neurons thus represents a general mechanism of cold allodynia in neuropathic pain.

What do the two studies described in this thesis tell us about the molecular mechanisms of nociception and pain? By pairing imaging of afferent activity in live animals with genetic manipulation, we can gain insights at the molecular level, *in vivo*. This combination of systems neuroscience and molecular genetic techniques may yet prove useful for identifying improved clinical targets. Here I provide a rationale for the failure of $Na_V1.7$ blockers as analgesics and point to manipulations of $Na_V1.7$ that affect the opioid system as a better translational approach. For cold allodynia, I identify a cellular population and associated molecules specific for the induction of cold-evoked neuropathic pain, hinting at targets that might rationally target this form of pain in a modality-specific manner.

In conclusion, these data stress the importance of the nociceptor to the experience of pain. This work demonstrates that $Na_V1.7$ at the central terminal of peripheral neurons is critical to congenital analgesia, while peripheral plasticity accounts for the development of cold allodynia in neuropathic pain. Crucially, the insights into unusual pain states

gleaned here would likely have been missed had an *in vivo* approach not been used. By putting pain under the microscope, I believe this thesis makes a small, but important, contribution to our understanding of the molecular mechanisms of nociception and pain.

6 Supplementary Data

Figures where the majority of the data were collected by colleagues and collaborators are presented in the following pages. In some cases, I contributed to the analysis of the data, and this is highlighted in the legends. The narrative results pertaining to each figure can be found in the appropriate results chapter.

I would like to take this opportunity again to thank everyone whose experimental work contributed to the science presented in this thesis. Acknowledgements for each figure can be found in the corresponding legend.

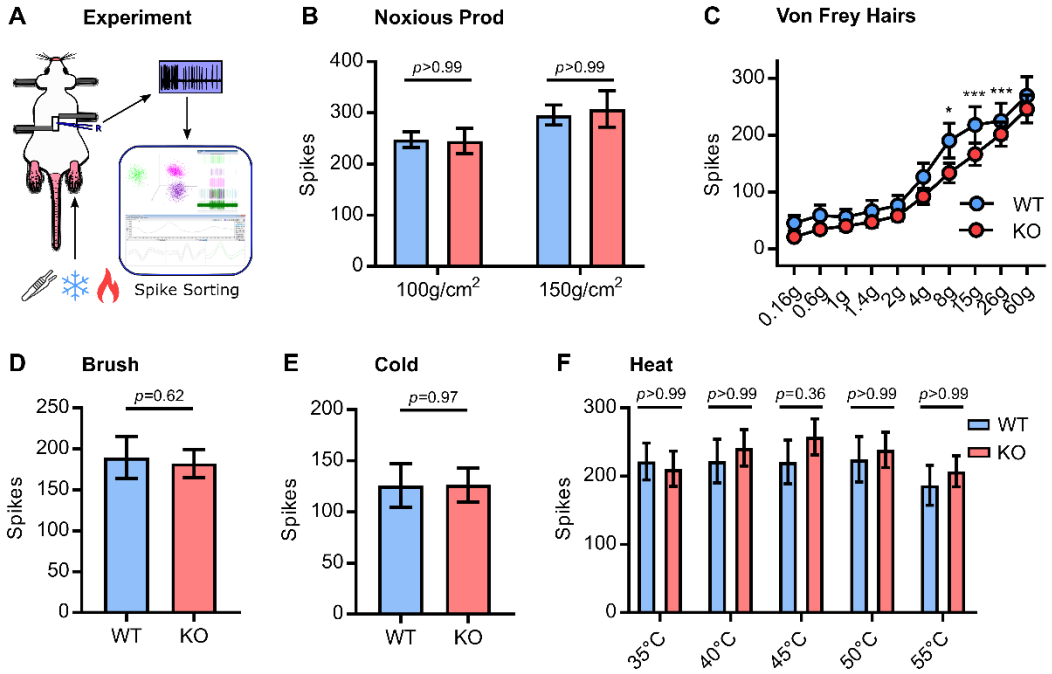

Figure 6.1. Excitability of $Na_V1.7$-deficient sensory neurons, *in vivo*

(A) Schematic of *in vivo* dorsal root ganglion extracellular recording setup.

(B) Quantification of spikes fired in response to noxious prodding in WT (blue) and $Na_V1.7$ KO (red). Data from both Advillin-Cre and Wnt1-Cre $Na_V1.7$ KO mice were pooled for these experiments.

(C) Quantification of spikes fired in response to Von Frey Hair stimulation. For 8g, p=0.014. For 15g, p<0.001. For 26g, p<0.001.

(D) Quantification of spikes fired in response to brushing.

(E) Quantification of spikes fired in response to cooling.

(F) Quantification of spikes fired in response to heating.

For (B), (C) and (F) mean number of spikes fired in 10 s were compared using repeated measures Two-Way ANOVA followed by post-hoc Bonferroni test. For (D) and (E), means were compared using Student's *t* test. Error bars represent 95% confidence interval around the mean. n=90 cells from 10 WT animals and n=146 cells from 13 $KO^{Adv/Wnt}$ animals.

(The data in this figure were collected and analysed by Dr Shafaq Sikandar, with Dr Ana Luiz.)

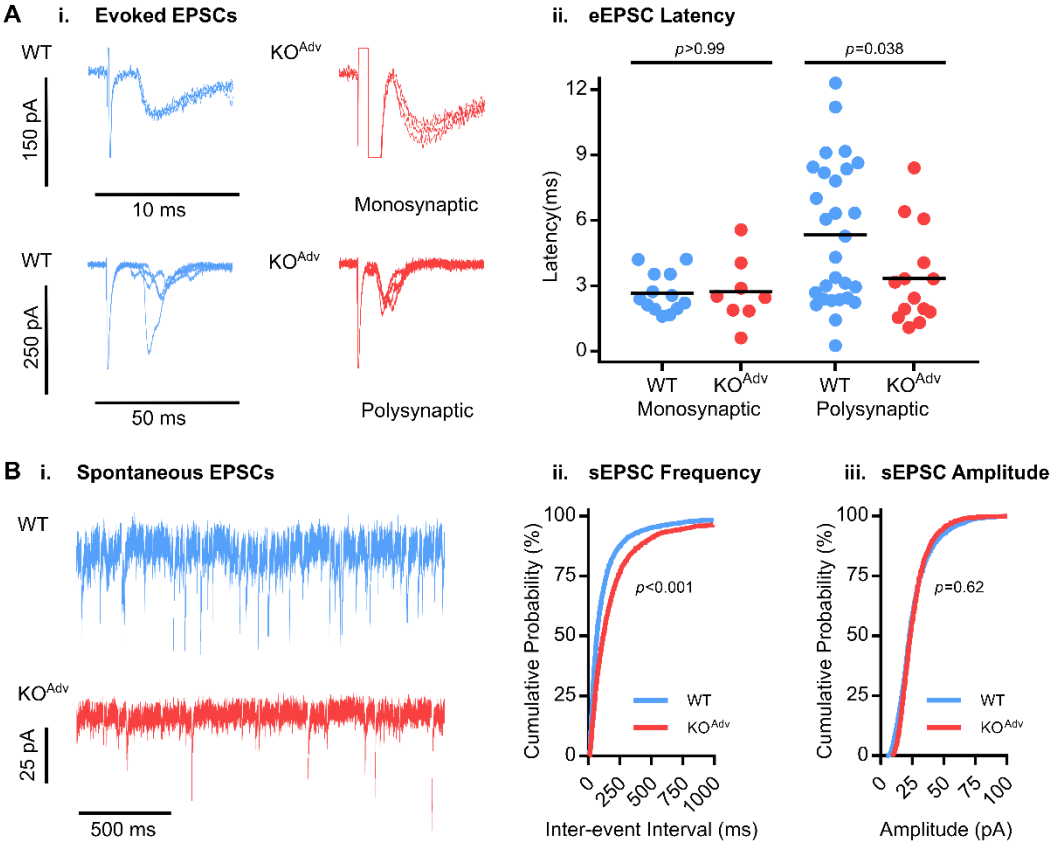

Figure 6.2. Impaired synaptic transmission between $Na_V1.7$-deficient sensory neurons and post-synaptic dorsal horn neurons

(A) (i.) Example traces showing dorsal root stimulation evoked monosynaptic and polysynaptic EPSCs recorded from lamina II neurons in WT and $Na_V1.7$ KO^{Adv} mice. The onset of stimulation is apparent by the stimulus artefact. (ii.) Dot plot of EPSC latency shows the slower polysynaptic events are absent in KO^{Adv} slices. Means were compared using One-way ANOVA followed by post-hoc Sidak's test for multiple comparisons. WT: n=13 monosynaptic and n=28 polysynaptic. KO^{Adv}: n=8 monosynaptic and n=14 polysynaptic.

(B) (i.) Example traces showing spontaneous EPSCs recorded from lamina II neurons in WT and KO^{Adv} mice. Cumulative probability plots showing frequency (ii.) but not amplitude (iii.) is reduced in KO^{Adv} animals. Means were compared using unpaired t tests. n=6972 events from 40 WT slices, and n=2406 events from 23 KO^{Adv} slices.

(The data in this figure were collected by Dr Sascha Alles, Dr Filipe Nascimento and Prof. Marco Beato. I performed the analyses.)

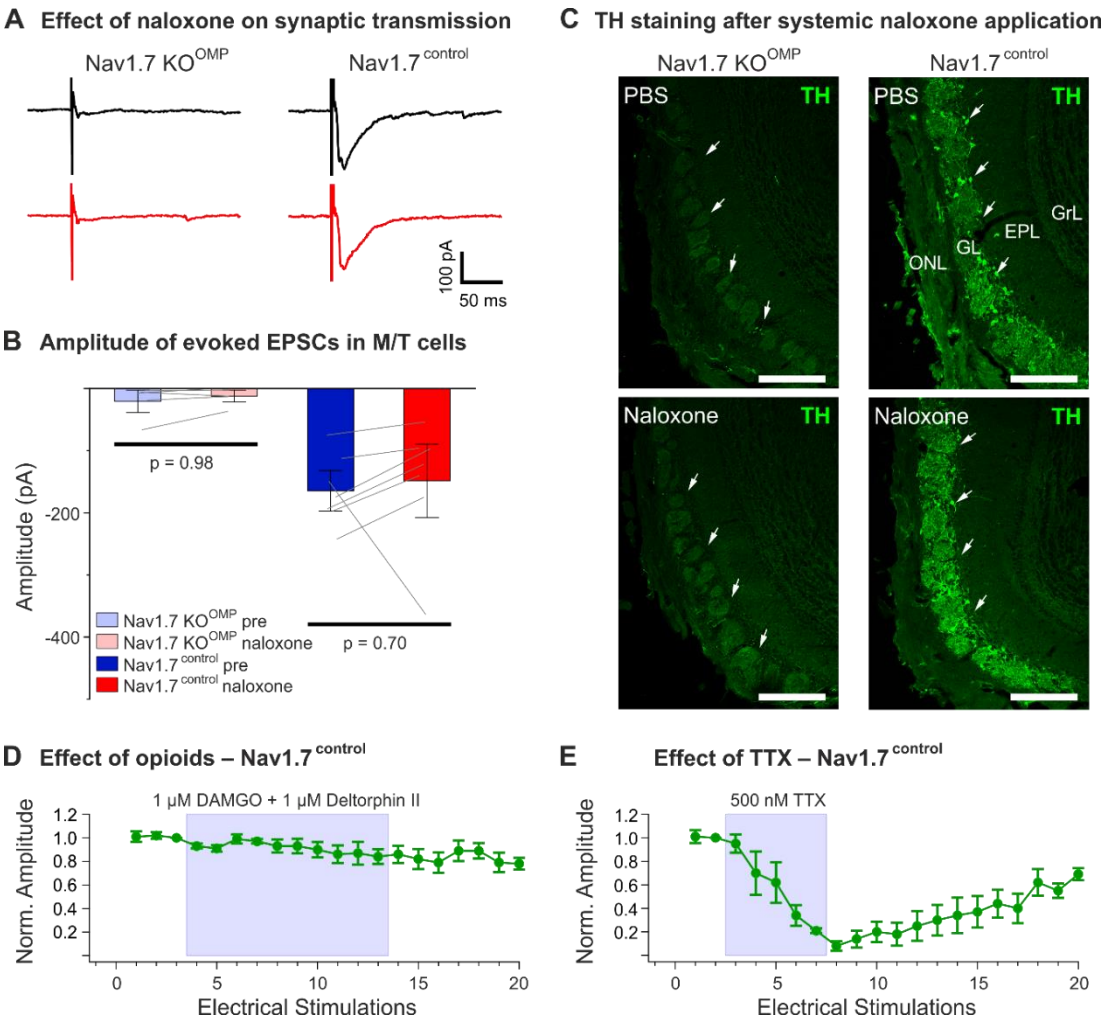

Figure 6.3. Opioid receptor block does not rescue synaptic transmission in mice lacking $Na_V1.7$ in olfactory sensory neurons

(A) Loss of synaptic transmission onto M/T cells in olfactory bulb slices of $Na_V1.7$ KO^{OMP} mice after olfactory sensory neuron nerve stimulation cannot be rescued by 300 µM naloxone (left, red trace). Naloxone does not affect M/T EPSCs to presynaptic nerve stimulation in control mice (right, red trace).

(B) Summary plot showing naloxone does not affect EPSC amplitudes in M/T cells after presynaptic nerve stimulation in KO^{OMP} (n=17 from 5 animals) and control mice (n=7 from 4 animals). Error bars represent SEM. Means were compared using paired t test.

(C) Confocal images of tyrosine hydroxylase (TH) immunostaining (green) in coronal cryosections of the major olfactory bulb following systemic administration of PBS or naloxone of KO^{OMP} (left) and control (right) mice. TH staining is absent in the glomerular layer (GL) of KO^{OMP} mice independent of treatment (arrows), while the olfactory bulb of control mice shows robust TH labeling of neuronal processes and periglomerular cell somata (arrows) in both PBS vs naloxone conditions. ONL (olfactory nerve layer), EPL (external plexiform layer), GrL (granule cell layer). Scale bars, 200 µm.

(D) Time course showing treatment with 1 µM DAMGO and 1 µM Deltorphin II does not affect M/T cell EPSCs evoked by olfactory nerve stimulation (n=4). Normalized EPCS peak amplitudes are plotted as a function of the number of electrical ONL stimulation (1-min intervals). Error bars represent SEM.

(E) Time course showing treatment with 500 nM TTX completely and reversibly abolishes M/T cell EPSCs evoked by ONL stimulation (n=4). Error bars represent standard error of the mean.

(The data in this figure were collected by Dr Jan Weiss, Dr Martina Pyrski and Prof Frank Zufall)

PARTICIPANT	MUTATION	CHARACTERIZATION
Male 1	c.377+5C>T (intronic) – point mutation in splice donor site in intron 3 resulting in the use of a cryptic splice donor site, leading to a frameshift and premature stop codon in exon 4.[284,525]	Pathogenic.[525]
	c.2686C>T (R896W) – amino acid change in exon 16.[284]	No $Na_V1.7$ current when expressed in HEK293T cells.[284]
Male 2	c.2488C>T (R830X) – premature stop codon in exon 16.[285]	No $Na_V1.7$ current when expressed in HEK293T cells.[284]
	c.5318delA (FS1773) – 1 bp deletion in exon 27, that induces a frameshift at position 1773 in the C terminal domain.[285]	8-fold reduction in $Na_V1.7$ current density versus WT when expressed in HEK293T cells.[284]

Table 6-1. Mutations in SCN9A of human participants.

(The mutations were identified and characterized by the authors of the highlighted references.)

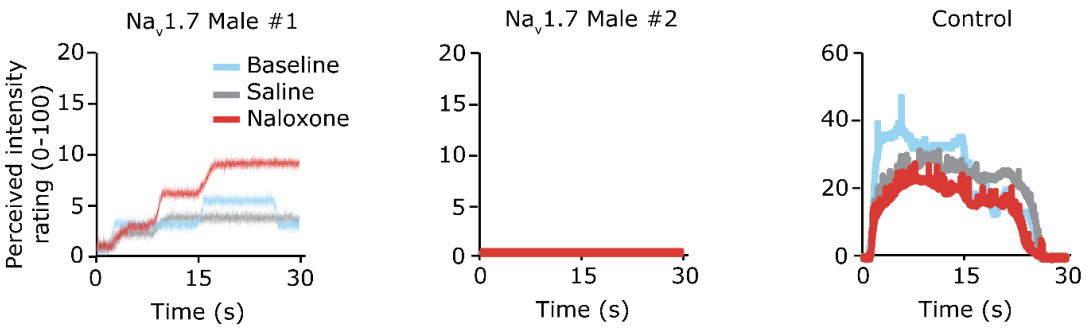

Figure 6.4. Opioid receptor antagonism restores nociception in a second human Na$_V$1.7 null mutant

Line plots showing the reported, perceived intensity of tonic, radiant heat stimuli (45-48ºC) in two newly-reported male Na$_V$1.7 null individuals and one control participant, at baseline, during saline administration and after treatment with naloxone (12 mg). Naloxone appears to increase heat sensitivity in one Na$_V$1.7 null participant ("male 1"), replicating previous observations in a single female null participant.[261] Naloxone had no effect in a second Na$_V$1.7 null participant ("male 2"). The control participant shows higher perceived pain intensity, which is not enhanced by naloxone.

(The data in this figure were collected by Dr Flavia Mancini and Prof. Gian D. Iannetti.)

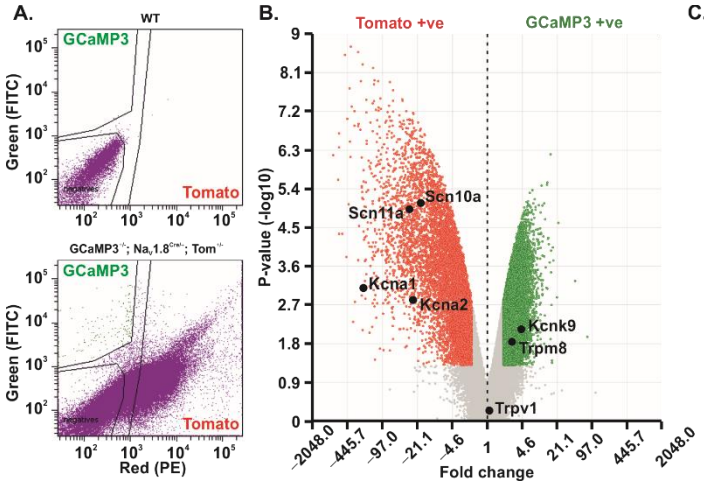

C.i. GCaMP3 +ve

Gene	Fold change	P-value
Kcnk9	4.11	7.60E-03
Cnga3	3.55	4.00E-04
Trpm8	2.96	1.50E-02
Kcnj15	2.7	3.20E-03
Kcne1	2.69	3.10E-03
Hvcn1	2.67	9.00E-04
Kcnc2	2.53	4.10E-03
Cnga4	2.52	1.28E-02
Kcnj5	2.52	6.00E-04
Kcnj11	2.44	9.00E-04
Kcng1	2.43	4.70E-03
Trpm6	2.42	1.30E-03
Kcnj4	2.36	2.88E-02
Kcnh4	2.31	1.90E-03
Asic5	2.3	2.60E-03
Kcnu1	2.24	1.80E-03
P2rx2	2.22	5.20E-03
Cacna1f	2.14	1.50E-03
Tmc1	2.12	7.00E-03
Kcnj8	2.12	1.52E-02
P2rx1	2.04	3.20E-03
Trpv5	2	3.80E-03

ii. Tomato +ve

Gene	Fold change	P-value
Kcna1	221.06	8.00E-04
Scn11a	29.62	1.00E-05
Kcna2	25.3	1.60E-03
Vdac3	24.98	6.00E-04
Kcnj10	24.01	1.87E-07
Scn7a	22.9	8.00E-04
Clic4	21.64	8.28E-06
P2rx7	19.18	7.37E-07
Trpm3	18.54	3.10E-06
Scn10a	18.08	8.75E-06
Kcnip3	10.77	6.80E-03
Kcna6	8.94	3.06E-05
Tpcn1	8.4	7.12E-05
Kcnh8	6.4	1.09E-05
Trpm7	5.65	1.00E-04
Clcn6	5.43	6.39E-05
Vdac1	5.41	1.50E-03
Tmc7	4.77	1.63E-05
Ano1	4.58	8.90E-03
Trpc4ap	4.12	3.00E-04
Kctd1	3.78	1.10E-03
Piezo2	3.78	4.82E-02

Figure 6.5. Isolation and transcriptomic analysis of cold-sensitive and cold-insensitive sensory neurons.

(A) Fluorescent-activated cell sorting (FACS) of non-fluorescent WT neurons (*top*) and GCaMP3-tdTomato expressing neurons (*bottom*). Gating was performed to isolate GCaMP3 and tdTomato fluorescence, as well as to remove non-fluorescent cells.

(B) Volcano plot showing the average fold difference in gene expression versus the P-value between GCaMP3-positive (*green*) and tdTomato-positive (*red*) populations. Results are filtered for genes that show at least a two-fold change in expression with $p<0.05$.

(C) Summary of ion channel genes showing the greatest fold change in expression between GCaMP3-positive and Tomato-positive populations, respectively.

In (B) and (C), gene expression was compared by repeated measures 2-Way ANOVA with Bonferroni correction of post-hoc *t* test.

(These data were collected by Dr Edward Emery. I contributed to the analyses.)

List of references

1. Duncan, G. The Meanings of 'Pain' in Historical, Social, and Political Context. *Monist* **100**, 514–531 (2017).
2. Unto the woman he said, "I will greatly multiply thy sorrow and thy conception; in sorrow thou shalt bring forth children. in *King James Bible* Gen. 3.16a
3. Pain terms: a list with definitions and notes on usage. Recommended by the IASP Subcommittee on Taxonomy. *Pain* **6**, 249 (1979).
4. Wright, A. A Criticism of the IASP's Definition of Pain. *J. Conscious. Stud.* **18**, 19–44 (2011).
5. Cox, J. J. *et al.* An SCN9A channelopathy causes congenital inability to experience pain. *Nature* **444**, 894–898 (2006).
6. Sherrington, C. S. *The integrative action of the nervous system.* (Yale University Press, 2012).
7. IASP Terminology - IASP. Available at: https://www.iasp-pain.org/Education/Content.aspx?ItemNumber=1698. (Accessed: 1st April 2019)
8. Henry, J. L., Lalloo, C. & Yashpal, K. Central poststroke pain: an abstruse outcome. *Pain Res. Manag.* **13**, 41–9 (2008).
9. Corder, G. *et al.* Loss of μ opioid receptor signaling in nociceptors, but not microglia, abrogates morphine tolerance without disrupting analgesia. *Nat. Med.* **23**, 164–173 (2017).
10. Scarry, E. *The Body in Pain*. (Oxford University Press, 1985).
11. Levina, N. *et al.* Protection of Escherichia coli cells against extreme turgor by activation of MscS and MscL mechanosensitive channels: identification of genes required for MscS activity. *EMBO J.* **18**, 1730–1737 (1999).
12. Sneddon, L. U. Comparative Physiology of Nociception and Pain. *Physiology* **33**, 63–73 (2018).
13. Puri, S. & Faulkes, Z. Can crayfish take the heat? Procambarus clarkii show nociceptive behaviour to high temperature stimuli, but not low temperature or chemical stimuli. *Biol. Open* **4**, 441–448 (2015).
14. Smith, E. S. J. & Lewin, G. R. Nociceptors: a phylogenetic view. *J. Comp. Physiol. A. Neuroethol. Sens. Neural. Behav. Physiol.* **195**, 1089–106 (2009).
15. Smith, E. S. J. *et al.* The molecular basis of acid insensitivity in the African naked mole-rat. *Science* **334**, 1557–60 (2011).
16. Gold, M. S. & Gebhart, G. F. Nociceptor sensitization in pain pathogenesis. *Nat. Med.* **16**, 1248–57 (2010).
17. Crook, R. J., Dickson, K., Hanlon, R. T. & Walters, E. T. Nociceptive Sensitization Reduces Predation Risk. *Curr. Biol.* **24**, 1121–1125 (2014).
18. Breivik, H., Collett, B., Ventafridda, V., Cohen, R. & Gallacher, D. Survey of chronic pain in Europe: Prevalence, impact on daily life, and treatment. *Eur. J. Pain* **10**, 287–287 (2006).
19. Freburger, J. K. *et al.* The rising prevalence of chronic low back pain. *Arch. Intern. Med.* **169**, 251–8 (2009).
20. Tompkins, D. A., Hobelmann, J. G. & Compton, P. Providing chronic pain management in the "Fifth Vital Sign" Era: Historical and treatment perspectives on a modern-day medical dilemma. *Drug Alcohol Depend.* **173 Suppl 1**, S11–S21 (2017).
21. Sheather-Reid, R. B. & Cohen, M. Efficacy of analgesics in chronic pain: a series of N-of-1 studies. *J. Pain Symptom Manage.* **15**, 244–52 (1998).
22. Classification of chronic pain. Descriptions of chronic pain syndromes and definitions of pain terms. Prepared by the International Association for the Study of Pain, Subcommittee on Taxonomy. *Pain. Suppl.* **3**, S1-226 (1986).
23. Fayaz, A., Croft, P., Langford, R. M., Donaldson, L. J. & Jones, G. T. Prevalence of chronic pain in the UK: a systematic review and meta-analysis of population studies. *BMJ Open* **6**, e010364 (2016).

24. van Hecke, O., Torrance, N. & Smith, B. H. Chronic pain epidemiology - where do lifestyle factors fit in? *Br. J. pain* **7**, 209–17 (2013).

25. Johannes, C. B., Le, T. K., Zhou, X., Johnston, J. A. & Dworkin, R. H. The Prevalence of Chronic Pain in United States Adults: Results of an Internet-Based Survey. *J. Pain* **11**, 1230–1239 (2010).

26. McWilliams, L. A., Cox, B. J. & Enns, M. W. Mood and anxiety disorders associated with chronic pain: an examination in a nationally representative sample. *Pain* **106**, 127–33 (2003).

27. Gaskin, D. J. & Richard, P. The Economic Costs of Pain in the United States. *J. Pain* **13**, 715–724 (2012).

28. Derry, S. *et al.* Pregabalin for neuropathic pain in adults. *Cochrane Database Syst. Rev.* (2019). doi:10.1002/14651858.CD007076.pub3

29. Saragiotto, B. T. *et al.* Paracetamol for low back pain. *Cochrane Database Syst. Rev.* (2016). doi:10.1002/14651858.CD012230

30. Stannard, C. Where now for opioids in chronic pain? *Drug Ther. Bull.* **56**, 118–122 (2018).

31. Overdose Death Rates | National Institute on Drug Abuse (NIDA). Available at: https://www.drugabuse.gov/related-topics/trends-statistics/overdose-death-rates. (Accessed: 5th April 2019)

32. Marcum, Z. A. & Hanlon, J. T. Recognizing the risks of chronic nonsteroidal anti-inflammatory drug use in older adults. *Annals of Long-Term Care* **18**, 24–27 (2010).

33. Pain, I. P. S. of the I. A. for the S. of. Declaration of montréal: Declaration that access to pain management is a fundamental human right. *J. Pain Palliat. Care Pharmacother.* **25**, 29–31 (2011).

34. Squire, L. R. & Society for Neuroscience. *The history of neuroscience in autobiography*. (Society for Neuroscience, 1996).

35. Ochs, S. *A History of Nerve Functions*. (Cambridge University Press, 2004). doi:10.1017/cbo9780511546358

36. Cervero, F. & Wood, J. N. A History of Pain Research. in *The Oxford Handbook of the Neurobiology of Pain* (Oxford University Press, 2019). doi:10.1093/oxfordhb/9780190860509.013.26

37. Perl, E. R. Ideas about pain, a historical view. *Nat. Rev. Neurosci.* **8**, 71–80 (2007).

38. Moayedi, M. & Davis, K. D. Theories of pain: from specificity to gate control. *J. Neurophysiol.* **109**, 5–12 (2013).

39. Bell, C. & Shaw, A. Reprint of the 'Idea of a New Anatomy of the Brain,' with Letters, &c. *J. Anat. Physiol.* **3**, 147–82 (1868).

40. Bessou, P. & Perl, E. R. Response of cutaneous sensory units with unmyelinated fibers to noxious stimuli. *J. Neurophysiol.* **32**, 1025–43 (1969).

41. Burgess, P. R. & Perl, E. R. Myelinated afferent fibres responding specifically to noxious stimulation of the skin. *J. Physiol.* **190**, 541–62 (1967).

42. Nafe, J. P. A quantitative theory of feeling. *J. Gen. Psychol.* **2**, 199–211 (1929).

43. Mendell, L. M. Physiological properties of unmyelinated fiber projection to the spinal cord. *Exp. Neurol.* **16**, 316–332 (1966).

44. Melzack, R. & Wall, P. D. Pain mechanisms: a new theory. *Science* **150**, 971–9 (1965).

45. Specificity Versus Patterning Theory: Continuing the Debate | Pain Research Forum. Available at: https://www.painresearchforum.org/forums/discussion/7347-specificity-versus-patterning-theory-continuing-debate. (Accessed: 1st April 2019)

46. Emery, E. C. & Wood, J. N. Somatosensation a la mode: plasticity and polymodality in sensory neurons. *Current Opinion in Physiology* **11**, 29–34 (2019).

47. Le Pichon, C. E. & Chesler, A. T. The functional and anatomical dissection of somatosensory subpopulations using mouse genetics. *Front. Neuroanat.* **8**, 21 (2014).

48. Dennett, D. C. *Consciousness Explained*. (Little, Brown and Co, 1991).

49. Gross, C. G. Genealogy of the 'grandmother cell'. *Neuroscientist* **8**, 512–518 (2002).

50. Casey, K. *Chasing Pain: The search for a neurobiological mechanism (implications for practice and theory) View project*. (Oxford University Press, 1968).

51. Fields;, H. How expectations influence pain. *Pain* **159**, (2018).

52. Seymour, B. Pain: A Precision Signal for Reinforcement Learning and Control. *Neuron* **101**, 1029–1041 (2019).

53. Adrian, E. D. & Zotterman, Y. The impulses produced by sensory nerve-endings: Part II. The response of a Single End-Organ. *J. Physiol.* **61**, 151–71 (1926).

54. Gasser, H. S. The classification of nerve fibers. *Ohio J. Sci.* **41**, 145–159 (1941).

55. Lawson, S. N., Fang, X. & Djouhri, L. Nociceptor subtypes and their incidence in rat lumbar dorsal root ganglia (DRGs): focussing on C-polymodal nociceptors, Aβ-nociceptors, moderate pressure receptors and their receptive field depths. *Current Opinion in Physiology* **11**, 125–146 (2019).

56. Thomas, L. & Pochin, E. E. *The double pain response of the human skin to a single stimulus*. (1937).

57. Zotterman, Y. Specific action potentials in the lingual nerve of cat. *Skand. Arch. Physiol.* **75**, 105–119 (1936).

58. Zotterman, Y. Touch, pain and tickling: an electro-physiological investigation on cutaneous sensory nerves. *J. Physiol.* **95**, 1–28 (1939).

59. Torebjörk, H. E. Afferent G Units Responding to Mechanical, Thermal and Chemical Stimuli in Human Non-Glabrous Skin. *Acta Physiol. Scand.* **92**, 374–390 (1974).

60. Konietzny, F., Perl, E. R., Trevino, D., Light, A. & Hensel, H. Sensory experiences in man evoked by intraneural electrical stimulation of intact cutaneous afferent fibers. *Exp. Brain Res.* **42**, 219–222 (1981).

61. Wall, P. D. & McMahon, S. B. Microneuronography and its relation to perceived sensation. a critical review. *Pain* **21**, 209–229 (1985).

62. Lawson, S. N. & Waddell, P. J. Soma neurofilament immunoreactivity is related to cell size and fibre conduction velocity in rat primary sensory neurons. *J. Physiol.* **435**, 41–63 (1991).

63. Goldstein, M. E., House, S. B. & Gainer, H. NF-L and peripherin immunoreactivities define distinct classes of rat sensory ganglion cells. *J. Neurosci. Res.* **30**, 92–104 (1991).

64. Emery, E. C. & Ernfors, P. Dorsal Root Ganglion Neuron Types and Their Functional Specialization. in *The Oxford Handbook of the Neurobiology of Pain* (Oxford University Press, 2018). doi:10.1093/oxfordhb/9780190860509.013.4

65. Lawson, S. N., McCarthy, P. W. & Prabhakar, E. Electrophysiological properties of neurones with CGRP-like immunoreactivity in rat dorsal root ganglia. *J. Comp. Neurol.* **365**, 355–366 (1996).

66. Lawson, S. N., Crepps, B. & Perl, E. R. Calcitonin gene-related peptide immunoreactivity and afferent receptive properties of dorsal root ganglion neurones in guinea-pigs. *J. Physiol.* **540**, 989–1002 (2002).

67. Ghitani, N. *et al.* Specialized Mechanosensory Nociceptors Mediating Rapid Responses to Hair Pull. *Neuron* **95**, 944-954.e4 (2017).

68. Wende, H. *et al.* The transcription factor c-Maf controls touch receptor development and function. *Science* **335**, 1373–6 (2012).

69. Abdo, H. *et al.* Dependence on the transcription factor Shox2 for specification of sensory neurons conveying discriminative touch. *Eur. J. Neurosci.* **34**, 1529–1541 (2011).

70. Li, L. *et al.* The functional organization of cutaneous low-threshold mechanosensory neurons. *Cell* **147**, 1615–27 (2011).

71. Bai, L. *et al.* Genetic Identification of an Expansive Mechanoreceptor Sensitive to Skin Stroking. *Cell* **163**, 1783–1795 (2015).

72. Stirling, L. C. *et al.* Nociceptor-specific gene deletion using heterozygous NaV1.8-Cre recombinase mice. *Pain* **113**, 27–36 (2005).

73. Abrahamsen, B. *et al.* The cell and molecular basis of mechanical, cold, and inflammatory pain. *Science* **321**, 702–5 (2008).

74. Pogorzala, L. A., Mishra, S. K. & Hoon, M. A. The cellular code for mammalian thermosensation. *J. Neurosci.* **33**, 5533–41 (2013).

75. Teichert, R. W., Memon, T., Aman, J. W. & Olivera, B. M. Using constellation pharmacology to define comprehensively a somatosensory neuronal subclass. *Proc. Natl. Acad. Sci.* **111**, 2319–2324 (2014).

76. Usoskin, D. *et al.* Unbiased classification of sensory neuron types by large-scale single-cell RNA sequencing. *Nat. Publ. Gr.* **18**, (2014).

77. Zeisel, A. *et al.* Molecular Architecture of the Mouse Nervous System. *Cell* **174**, 999-1014.e22 (2018).

78. Li, C.-L. *et al.* Somatosensory neuron types identified by high-coverage single-cell RNA-sequencing and functional heterogeneity. *Cell Res.* **26**, 83–102 (2016).

79. Li, C., Wang, S., Chen, Y. & Zhang, X. Somatosensory Neuron Typing with High-Coverage Single-Cell RNA Sequencing and Functional Analysis. *Neurosci. Bull.* **34**, 200–207 (2018).

80. Hull, D. L. The Effect of Essentialism on Taxonomy--Two Thousand Years of Stasis (I). *The British Journal for the Philosophy of Science* **15**, 314–326

81. Madrid, R., de la Pena, E., Donovan-Rodriguez, T., Belmonte, C. & Viana, F. Variable Threshold of Trigeminal Cold-Thermosensitive Neurons Is Determined by a Balance between TRPM8 and Kv1 Potassium Channels. *J. Neurosci.* **29**, 3120–3131 (2009).

82. Bangash, M. A. *et al.* Distinct transcriptional responses of mouse sensory neurons in models of human chronic pain conditions. *Wellcome Open Res.* **3**, 78 (2018).

83. Guzmán, I. & Bosland, P. W. Sensory properties of chile pepper heat – and its importance to food quality and cultural preference. *Appetite* **117**, 186–190 (2017).

84. Julius, D. *et al.* The capsaicin receptor: a heat-activated ion channel in the pain pathway. *Nature* **389**, 816–824 (1997).

85. Cavanaugh, D. J. *et al.* Trpv1 Reporter Mice Reveal Highly Restricted Brain Distribution and Functional Expression in Arteriolar Smooth Muscle Cells. *J. Neurosci.* **31**, 5067–5077 (2011).

86. Caterina, M. J. *et al.* Impaired nociception and pain sensation in mice lacking the capsaicin receptor. *Science* **288**, 306–13 (2000).

87. Davis, J. B. *et al.* Vanilloid receptor-1 is essential for inflammatory thermal hyperalgesia. *Nature* **405**, 183–187 (2000).

88. Vandewauw, I. *et al.* A TRP channel trio mediates acute noxious heat sensing. *Nature* **555**, 662–666 (2018).

89. Viana, F. & Voets, T. Heat Pain and Cold Pain. in *The Oxford Handbook of the Neurobiology of Pain* (Oxford University Press, 2019). doi:10.1093/oxfordhb/9780190860509.013.13

90. Dhaka, A. *et al.* TRPM8 is required for cold sensation in mice. *Neuron* **54**, 371–8 (2007).

91. Bautista, D. M. *et al.* The menthol receptor TRPM8 is the principal detector of environmental cold. *Nature* **448**, 204–208 (2007).

92. Tan, C.-H. & McNaughton, P. A. The TRPM2 ion channel is required for sensitivity to warmth. *Nature* **536**, 460–3 (2016).

93. Karashima, Y. *et al.* TRPA1 acts as a cold sensor in vitro and in vivo. *Proc. Natl. Acad. Sci. U. S. A.* **106**, 1273–8 (2009).

94. Brierley, S. M. *et al.* The Ion Channel TRPA1 Is Required for Normal Mechanosensation and Is Modulated by Algesic Stimuli. *Gastroenterology* **137**, 2084-2095.e3 (2009).

95. Bautista, D. M., Pellegrino, M. & Tsunozaki, M. TRPA1: A Gatekeeper for Inflammation. *Annu. Rev. Physiol.* **75**, 181–200 (2013).

96. Bele, T. & Fabbretti, E. P2X receptors, sensory neurons and pain. *Curr. Med. Chem.* **22**, 845–50 (2015).

97. Wemmie, J. A., Taugher, R. J. & Kreple, C. J. Acid-sensing ion channels in pain and disease. *Nat. Rev. Neurosci.* **14**, 461–71 (2013).

98. Noël, J. *et al.* The mechano-activated K+ channels TRAAK and TREK-1 control both warm and

cold perception. *EMBO J.* **28**, 1308–18 (2009).

99. Coste, B. *et al.* Piezo1 and Piezo2 are essential components of distinct mechanically activated cation channels. *Science* **330**, 55–60 (2010).

100. Ranade, S. S. *et al.* Piezo2 is the major transducer of mechanical forces for touch sensation in mice. *Nature* **516**, 121–5 (2014).

101. Woo, S.-H. *et al.* Piezo2 is the principal mechanotransduction channel for proprioception. *Nat. Neurosci.* **18**, 1756–1762 (2015).

102. Chesler, A. T. *et al.* The Role of *PIEZO2* in Human Mechanosensation. *N. Engl. J. Med.* **375**, 1355–1364 (2016).

103. Szczot, M. *et al.* Cell-Type-Specific Splicing of Piezo2 Regulates Mechanotransduction. *Cell Rep.* **21**, 2760–2771 (2017).

104. Beaulieu-Laroche, L. *et al.* TACAN Is an Ion Channel Involved in Sensing Mechanical Pain. *Cell* **180**, 956-967.e17 (2020).

105. Moehring, F. *et al.* Keratinocytes mediate innocuous and noxious touch via ATP-P2X4 signaling. *Elife* **7**, (2018).

106. Abdo, H. *et al.* Specialized cutaneous schwann cells initiate pain sensation. *Science (80-.).* **365**, 695–699 (2019).

107. Paricio-Montesinos, R. *et al.* The Sensory Coding of Warm Perception. *Neuron* (2020). doi:10.1016/j.neuron.2020.02.035

108. Wedel, M. J. A monument of inefficiency: The presumed course of the recurrent laryngeal nerve in sauropod dinosaurs. *Acta Palaeontol. Pol* **57**, 251–256 (2012).

109. Devor, M. Unexplained peculiarities of the dorsal root ganglion. *Pain* **Suppl 6**, S27-35 (1999).

110. Schuetze, S. M. The discovery of the action potential. *Trends Neurosci.* **6**, 164–168 (1983).

111. Hodgkin, A. L. & Huxley, A. F. Action Potentials Recorded from Inside a Nerve Fibre. *Nature* **144**, 710–711 (1939).

112. Hodgkin, A. L. & Huxley, A. F. A quantitative description of membrane current and its application to conduction and excitation in nerve. *J. Physiol.* **117**, 500–44 (1952).

113. Narahashi, T., Moore, J. W. & Scott, W. R. Tetrodotoxin blockage of sodium conductance increase in lobster giant axons. *J. Gen. Physiol.* **47**, 965–74 (1964).

114. Hamill, O. P., Marty, A., Neher, E., Sakmann, B. & Sigworth, F. J. Improved patch-clamp techniques for high-resolution current recording from cells and cell-free membrane patches. *Pflügers Arch. - Eur. J. Physiol.* **391**, 85–100 (1981).

115. Neher, E. & Sakmann, B. Single-channel currents recorded from membrane of denervated frog muscle fibres. *Nature* **260**, 799–802 (1976).

116. Catterall, W. A. Voltage-gated sodium channels at 60: structure, function and pathophysiology. *J. Physiol.* **590**, 2577–89 (2012).

117. Akopian, A. N., Sivilotti, L. & Wood, J. N. A tetrodotoxin-resistant voltage-gated sodium channel expressed by sensory neurons. *Nature* **379**, 257–262 (1996).

118. Goldin, A. L. Resurgence of Sodium Channel Research. *Annu. Rev. Physiol.* **63**, 871–894 (2001).

119. Bennett, D. L., Clark, A. J., Huang, J., Waxman, S. G. & Dib-Hajj, S. D. The Role of Voltage-Gated Sodium Channels in Pain Signaling. *Physiol. Rev.* **99**, 1079–1151 (2019).

120. Akopian, A. N. *et al.* The tetrodotoxin-resistant sodium channel SNS has a specialized function in pain pathways. *Nat. Neurosci.* **2**, 541–548 (1999).

121. Priest, B. T. *et al.* Contribution of the tetrodotoxin-resistant voltage-gated sodium channel NaV1.9 to sensory transmission and nociceptive behavior. *Proc. Natl. Acad. Sci.* **102**, 9382–9387 (2005).

122. Renganathan, M., Cummins, T. R. & Waxman, S. G. Contribution of Na_v 1.8 Sodium Channels to Action Potential Electrogenesis in DRG Neurons. *J. Neurophysiol.* **86**, 629–640 (2001).

123. Huang, J. *et al.* Small-fiber neuropathy Nav1.8 mutation shifts activation to hyperpolarized

potentials and increases excitability of dorsal root ganglion neurons. *J. Neurosci.* **33**, 14087–97 (2013).

124. Cummins, T. R. *et al.* A novel persistent tetrodotoxin-resistant sodium current in SNS-null and wild-type small primary sensory neurons. *J. Neurosci.* **19**, RC43 (1999).

125. Leipold, E. *et al.* A de novo gain-of-function mutation in SCN11A causes loss of pain perception. *Nat. Genet.* **45**, 1399–1404 (2013).

126. Touska, F. *et al.* Heat-resistant action potentials require TTX-resistant sodium channels NaV1.8 and NaV1.9. *J. Gen. Physiol.* **150**, 1125–1144 (2018).

127. Chen, L. *et al.* Conditional knockout of NaV1.6 in adult mice ameliorates neuropathic pain. *Sci. Rep.* **8**, 3845 (2018).

128. Caldwell, J. H., Schaller, K. L., Lasher, R. S., Peles, E. & Levinson, S. R. Sodium channel Na(v)1.6 is localized at nodes of ranvier, dendrites, and synapses. *Proc. Natl. Acad. Sci. U. S. A.* **97**, 5616–20 (2000).

129. Osteen, J. D. *et al.* Selective spider toxins reveal a role for the Nav1.1 channel in mechanical pain. *Nature* **534**, 494–499 (2016).

130. Waxman, S. G., Kocsis, J. D. & Black, J. A. Type III sodium channel mRNA is expressed in embryonic but not adult spinal sensory neurons, and is reexpressed following axotomy. *J. Neurophysiol.* **72**, 466–470 (1994).

131. Cummins, T. R. *et al.* Nav1.3 sodium channels: rapid repriming and slow closed-state inactivation display quantitative differences after expression in a mammalian cell line and in spinal sensory neurons. *J. Neurosci.* **21**, 5952–61 (2001).

132. Nassar, M. A. *et al.* Nerve Injury Induces Robust Allodynia and Ectopic Discharges in Na_v 1.3 Null Mutant Mice. *Mol. Pain* **2**, 1744-8069-2–33 (2006).

133. Tsantoulas, C. & McMahon, S. B. Opening paths to novel analgesics: the role of potassium channels in chronic pain. *Trends Neurosci.* **37**, 146–58 (2014).

134. Jan, L. Y. & Jan, Y. N. Voltage-gated potassium channels and the diversity of electrical signalling. *J. Physiol.* **590**, 2591–9 (2012).

135. Chi, X. X. & Nicol, G. D. Manipulation of the Potassium Channel Kv1.1 and Its Effect on Neuronal Excitability in Rat Sensory Neurons. *J. Neurophysiol.* **98**, 2683–2692 (2007).

136. Clark, J. D. & Tempel, B. L. Hyperalgesia in mice lacking the Kv1.1 potassium channel gene. *Neurosci. Lett.* **251**, 121–4 (1998).

137. Hao, J. *et al.* Kv1.1 Channels Act as Mechanical Brake in the Senses of Touch and Pain. *Neuron* **77**, 899–914 (2013).

138. Smart, S. L. *et al.* Deletion of the K(V)1.1 potassium channel causes epilepsy in mice. *Neuron* **20**, 809–19 (1998).

139. Manole, A. *et al.* De novo *KCNA2* mutations cause hereditary spastic paraplegia. *Ann. Neurol.* **81**, 326–328 (2017).

140. Sachdev, M. *et al.* Novel clinical manifestations in patients with KCNA2 mutations. *Seizure* **51**, 74–76 (2017).

141. Klein, A. H. *et al.* Sodium Channel Na_v 1.8 Underlies TTX-Resistant Axonal Action Potential Conduction in Somatosensory C-Fibers of Distal Cutaneous Nerves. *J. Neurosci.* **37**, 5204–5214 (2017).

142. Du, X. *et al.* Local GABAergic signaling within sensory ganglia controls peripheral nociceptive transmission. *J. Clin. Invest.* **127**, 1741–1756 (2017).

143. Clark, A. J. *et al.* Functional imaging in microfluidic chambers reveals sensory neuron sensitivity is differentially regulated between neuronal regions. *Pain* **159**, 1413–1425 (2018).

144. Todd, A. J. Neuronal circuitry for pain processing in the dorsal horn. *Nat. Rev. Neurosci.* **11**, 823–36 (2010).

145. Fatt, P. & Katz, B. Spontaneous subthreshold activity at motor nerve endings. *J. Physiol.* **117**, 109–28 (1952).

146. Del Castillo, J. & Katz, B. Quantal components of the end-plate potential. *J. Physiol.* **124**, 560–73 (1954).

147. Brunger, A. T., Choi, U. B., Lai, Y., Leitz, J. & Zhou, Q. Molecular Mechanisms of Fast Neurotransmitter Release. *Annu. Rev. Biophys.* **47**, 469–497 (2018).

148. Dolphin, A. C. Voltage-gated calcium channels and their auxiliary subunits: physiology and pathophysiology and pharmacology. *J. Physiol.* **594**, 5369–5390 (2016).

149. Nieto-Rostro, M., Ramgoolam, K., Pratt, W. S., Kulik, A. & Dolphin, A. C. Ablation of $\alpha_2\delta$-1 inhibits cell-surface trafficking of endogenous N-type calcium channels in the pain pathway in vivo. *Proc. Natl. Acad. Sci.* **115**, E12043–E12052 (2018).

150. Lagerström, M. C. *et al.* A sensory subpopulation depends on vesicular glutamate transporter 2 for mechanical pain, and together with substance P, inflammatory pain. *Proc. Natl. Acad. Sci. U. S. A.* **108**, 5789–5794 (2011).

151. Olson, W. *et al.* Sparse genetic tracing reveals regionally specific functional organization of mammalian nociceptors. *Elife* **6**, (2017).

152. Vrontou, S., Wong, A. M., Rau, K. K., Koerber, H. R. & Anderson, D. J. Genetic identification of C fibres that detect massage-like stroking of hairy skin in vivo. *Nature* **493**, 669–73 (2013).

153. Abraira, V. E. *et al.* The Cellular and Synaptic Architecture of the Mechanosensory Dorsal Horn. *Cell* **168**, 295-310.e19 (2017).

154. Todd, A. J., Wang, F., Todd, A. J. & Wang, F. Central Nervous System Pain Pathways. in *The Oxford Handbook of the Neurobiology of Pain* (Oxford University Press, 2018). doi:10.1093/oxfordhb/9780190860509.013.5

155. Grudt, T. J. & Perl, E. R. Correlations between neuronal morphology and electrophysiological features in the rodent superficial dorsal horn. *J. Physiol.* **540**, 189–207 (2002).

156. Todd, A. J. Identifying functional populations among the interneurons in laminae I-III of the spinal dorsal horn. *Mol. Pain* **13**, 1744806917693003 (2017).

157. Duan, B. *et al.* Identification of spinal circuits transmitting and gating mechanical pain. *Cell* **159**, 1417–1432 (2014).

158. Bráz, J. M. *et al.* Forebrain GABAergic Neuron Precursors Integrate into Adult Spinal Cord and Reduce Injury-Induced Neuropathic Pain. *Neuron* **74**, 663–675 (2012).

159. Barik, A., Thompson, J. H., Seltzer, M., Ghitani, N. & Chesler, A. T. A Brainstem-Spinal Circuit Controlling Nocifensive Behavior. *Neuron* **100**, 1491-1503.e3 (2018).

160. Rodriguez, E. *et al.* A craniofacial-specific monosynaptic circuit enables heightened affective pain. *Nat. Neurosci.* **20**, 1734–1743 (2017).

161. Burma, N. E., Leduc-Pessah, H., Fan, C. Y. & Trang, T. Animal models of chronic pain: Advances and challenges for clinical translation. *J. Neurosci. Res.* **95**, 1242–1256 (2017).

162. Gregory, N. S. *et al.* An overview of animal models of pain: disease models and outcome measures. *J. Pain* **14**, 1255–69 (2013).

163. Jensen, T. S. & Finnerup, N. B. Allodynia and hyperalgesia in neuropathic pain: clinical manifestations and mechanisms. *Lancet Neurol.* **13**, 924–935 (2014).

164. Hargreaves, K., Dubner, R., Brown, F., Flores, C. & Joris, J. A new and sensitive method for measuring thermal nociception in cutaneous hyperalgesia. *Pain* **32**, 77–88 (1988).

165. Randall, L. O. & Selitto, J. J. A method for measurement of analgesic activity on inflamed tissue. *Arch. Int. Pharmacodyn. Ther.* **111**, 409–19 (1957).

166. Deuis, J. R., Dvorakova, L. S. & Vetter, I. Methods Used to Evaluate Pain Behaviors in Rodents. *Front. Mol. Neurosci.* **10**, 284 (2017).

167. Woolf, C. J. Long term alterations in the excitability of the flexion reflex produced by peripheral tissue injury in the chronic decerebrate rat. *Pain* **18**, 325–43 (1984).

168. Balayssac, D. *et al.* Assessment of thermal sensitivity in rats using the thermal place preference test. *Behav. Pharmacol.* **25**, 99–111 (2014).

169. Langford, D. J. *et al.* Coding of facial expressions of pain in the laboratory mouse. *Nat. Methods* **7**, 447–449 (2010).

170. Tuttle, A. H. *et al.* A deep neural network to assess spontaneous pain from mouse facial expressions. *Mol. Pain* **14**, 1744806918763658 (2018).

171. Chakrabarti, S. *et al.* Acute inflammation sensitizes knee-innervating sensory neurons and decreases mouse digging behavior in a TRPV1-dependent manner. *Neuropharmacology* **143**, 49–62 (2018).

172. Sorge, R. E. *et al.* Olfactory exposure to males, including men, causes stress and related analgesia in rodents. *Nat. Methods* **11**, 629–632 (2014).

173. Smith, M. L., Hostetler, C. M., Heinricher, M. M. & Ryabinin, A. E. Social transfer of pain in mice. *Sci. Adv.* **2**, e1600855 (2016).

174. Abdus-Saboor, I. *et al.* Development of a Mouse Pain Scale Using Sub-second Behavioral Mapping and Statistical Modeling. *Cell Rep.* **28**, 1623-1634.e4 (2019).

175. Mathis, A. *et al.* DeepLabCut: markerless pose estimation of user-defined body parts with deep learning. *Nat. Neurosci.* **21**, 1281–1289 (2018).

176. Dubuisson, D. & Dennis, S. G. The formalin test: a quantitative study of the analgesic effects of morphine, meperidine, and brain stem stimulation in rats and cats. *Pain* **4**, 161–74 (1977).

177. Sikandar, S. *et al.* Brain-derived neurotrophic factor derived from sensory neurons plays a critical role in chronic pain. *Brain* **141**, 1028–1039 (2018).

178. Jaggi, A. S., Jain, V. & Singh, N. Animal models of neuropathic pain. *Fundam. Clin. Pharmacol.* **25**, 1–28 (2011).

179. Flatters, S. J. L., Dougherty, P. M. & Colvin, L. A. Clinical and preclinical perspectives on Chemotherapy-Induced Peripheral Neuropathy (CIPN): a narrative review. *Br. J. Anaesth.* **119**, 737–749 (2017).

180. Pitcher, T., Sousa-Valente, J. & Malcangio, M. The Monoiodoacetate Model of Osteoarthritis Pain in the Mouse. *J. Vis. Exp.* (2016). doi:10.3791/53746

181. ter Heegde, F. *et al.* Noninvasive Mechanical Joint Loading as an Alternative Model for Osteoarthritic Pain. *Arthritis Rheumatol.* **71**, 1078–1088 (2019).

182. Meents, J. E. *et al.* The role of Nav1.7 in human nociceptors: Insights from human induced pluripotent stem cell-derived sensory neurons of erythromelalgia patients. *Pain* **160**, 1327–1341 (2019).

183. Dawes, J. M. *et al.* Immune or Genetic-Mediated Disruption of CASPR2 Causes Pain Hypersensitivity Due to Enhanced Primary Afferent Excitability. *Neuron* **97**, 806-822.e10 (2018).

184. Aguirre, J., Del Moral, A., Cobo, I., Borgeat, A. & Blumenthal, S. The Role of Continuous Peripheral Nerve Blocks. *Anesthesiol. Res. Pract.* **2012**, 1–20 (2012).

185. Smith-Edwards, K. M., DeBerry, J. J., Saloman, J. L., Davis, B. M. & Woodbury, C. J. Profound alteration in cutaneous primary afferent activity produced by inflammatory mediators. *Elife* **5**, (2016).

186. Cobos, E. J. *et al.* Mechanistic Differences in Neuropathic Pain Modalities Revealed by Correlating Behavior with Global Expression Profiling. *Cell Rep.* **22**, 1301–1312 (2018).

187. Tominaga, M. *et al.* The Cloned Capsaicin Receptor Integrates Multiple Pain-Producing Stimuli. *Neuron* **21**, 531–543 (1998).

188. Petty, B. G. *et al.* The effect of systemically administered recombinant human nerve growth factor in healthy human subjects. *Ann. Neurol.* **36**, 244–246 (1994).

189. Denk, F., Bennett, D. L. & McMahon, S. B. Nerve Growth Factor and Pain Mechanisms. *Annu. Rev. Neurosci.* **40**, 307–325 (2017).

190. Kan, S.-L. *et al.* Tanezumab for Patients with Osteoarthritis of the Knee: A Meta-Analysis. *PLoS One* **11**, e0157105 (2016).

191. Nocchi, L. *et al.* NGF-mediated photoablation of nociceptors reduces pain behavior in mice. *bioRxiv* 575274 (2019). doi:10.1101/575274

192. Murthy, S. E. *et al.* The mechanosensitive ion channel Piezo2 mediates sensitivity to mechanical pain in mice. *Sci. Transl. Med.* **10**, eaat9897 (2018).

193. Szczot, M. *et al.* PIEZO2 mediates injury-induced tactile pain in mice and humans. *Sci. Transl. Med.* **10**, eaat9892 (2018).

194. Dhandapani, R. *et al.* Control of mechanical pain hypersensitivity in mice through ligand-targeted photoablation of TrkB-positive sensory neurons. *Nat. Commun.* **9**, 1640 (2018).

195. Gold, M. S. *et al.* Redistribution of Na(V)1.8 in uninjured axons enables neuropathic pain. *J. Neurosci.* **23**, 158–66 (2003).

196. Roza, C., Laird, J. M. A., Souslova, V., Wood, J. N. & Cervero, F. The tetrodotoxin-resistant Na+ channel Nav1.8 is essential for the expression of spontaneous activity in damaged sensory axons of mice. *J. Physiol.* **550**, 921–6 (2003).

197. Emery, E. C., Young, G. T., Berrocoso, E. M., Chen, L. & McNaughton, P. A. HCN2 ion channels play a central role in inflammatory and neuropathic pain. *Science* **333**, 1462–6 (2011).

198. Ramírez, D., Zúñiga, R., Concha, G. & Zúñiga, L. HCN Channels: New Therapeutic Targets for Pain Treatment. *Molecules* **23**, 2094 (2018).

199. Lamont, L. A., Tranquilli, W. J. & Grimm, K. A. Physiology of pain. *Vet. Clin. North Am. - Small Anim. Pract.* **30**, 703–728 (2000).

200. Woolf, C. J. Evidence for a central component of post-injury pain hypersensitivity. *Nature* **306**, 686–688 (1983).

201. Woolf, C. J. & Thompson, S. W. N. The induction and maintenance of central sensitization is dependent on N-methyl-d-aspartic acid receptor activation; implications for the treatment of post-injury pain hypersensitivity states. *Pain* **44**, 293–299 (1991).

202. Woolf, C. J. Pain amplification-A perspective on the how, why, when, and where of central sensitization. *J. Appl. Biobehav. Res.* **23**, e12124 (2018).

203. Woolf, C. J. Windup and central sensitization are not equivalent. *Pain* **66**, 105–8 (1996).

204. Reuben, S. S. & Buvanendran, A. Preventing the Development of Chronic Pain After Orthopaedic Surgery with Preventive Multimodal Analgesic Techniques. *J. Bone Jt. Surg.* **89**, 1343–1358 (2007).

205. Tsuda, M. *et al.* P2X4 receptors induced in spinal microglia gate tactile allodynia after nerve injury. *Nature* **424**, 778–783 (2003).

206. Sorge, R. E. *et al.* Different immune cells mediate mechanical pain hypersensitivity in male and female mice. *Nat. Neurosci.* **18**, 1081–1083 (2015).

207. Ratté, S., Zhu, Y., Lee, K. Y. & Prescott, S. A. Criticality and degeneracy in injury-induced changes in primary afferent excitability and the implications for neuropathic pain. *Elife* **3**, (2014).

208. Wasner, G. Central Pain Syndromes. *Curr. Pain Headache Rep.* **14**, 489–496 (2010).

209. Woo, C.-W. *et al.* Quantifying cerebral contributions to pain beyond nociception. *Nat. Commun.* **8**, 14211 (2017).

210. Salomons, T. V., Iannetti, G. D., Liang, M. & Wood, J. N. The "Pain Matrix" in Pain-Free Individuals. *JAMA Neurol.* **73**, 755 (2016).

211. Hebben, N., Corkin, S., Eichenbaum, H. & Shedlack, K. Diminished ability to interpret and report internal states after bilateral medial temporal resection: case H.M. *Behav. Neurosci.* **99**, 1031–9 (1985).

212. Corder, G. *et al.* An amygdalar neural ensemble that encodes the unpleasantness of pain. *Science* **363**, 276–281 (2019).

213. Alhadeff, A. L. *et al.* A Neural Circuit for the Suppression of Pain by a Competing Need State. *Cell* **173**, 140-152.e15 (2018).

214. Browne, L. E. *et al.* Time-Resolved Fast Mammalian Behavior Reveals the Complexity of Protective Pain Responses. *Cell Rep.* **20**, 89–98 (2017).

215. Becker, B. & McGregor, A. J. Article Commentary: Men, Women, and Pain. *Gend. Genome* **1**, 46–50 (2017).

216. Martin, L. J., Acland, E. L., Carlson, E. N., Schweinhardt, P. & Mogil Correspondence, J. S. Male-

Specific Conditioned Pain Hypersensitivity in Mice and Humans In Brief. *Curr. Biol.* **29**, 192-201.e4 (2019).

217. Macfarlane, G. J., Norrie, G., Atherton, K., Power, C. & Jones, G. T. The influence of socioeconomic status on the reporting of regional and widespread musculoskeletal pain: results from the 1958 British Birth Cohort Study. *Ann. Rheum. Dis.* **68**, 1591–1595 (2009).

218. Connolly, V., Unwin, N., Sherriff, P., Bilous, R. & Kelly, W. Diabetes prevalence and socioeconomic status: a population based study showing increased prevalence of type 2 diabetes mellitus in deprived areas. *J. Epidemiol. Community Health* **54**, 173–7 (2000).

219. Hannibal, K. E. & Bishop, M. D. Chronic stress, cortisol dysfunction, and pain: a psychoneuroendocrine rationale for stress management in pain rehabilitation. *Phys. Ther.* **94**, 1816–25 (2014).

220. Lévesque, H. & Lafont, O. L'aspirine à travers les siècles: Rappel historique. *Rev. Med. Interne* **21**, 8–17 (2000).

221. Wood, J. N. From plant extract to molecular panacea: a commentary on Stone (1763) 'An account of the success of the bark of the willow in the cure of the agues'. *Philos. Trans. R. Soc. Lond. B. Biol. Sci.* **370**, (2015).

222. Ferreira, S. H., Moncada, S. & Vane, J. R. Indomethacin and Aspirin abolish Prostaglandin Release from the Spleen. *Nat. New Biol.* **231**, 237–239 (1971).

223. Andersson, D. A. *et al.* TRPA1 mediates spinal antinociception induced by acetaminophen and the cannabinoid Δ9-tetrahydrocannabiorcol. *Nat. Commun.* **2**, 551 (2011).

224. Klinger-Gratz, P. P. *et al.* Acetaminophen Relieves Inflammatory Pain through CB $_1$ Cannabinoid Receptors in the Rostral Ventromedial Medulla. *J. Neurosci.* **38**, 322–334 (2018).

225. Brownstein, M. J. *Review A brief history of opiates, opioid peptides, and opioid receptors*. *Proc. Natl. Acad. Sci. USA* **90**, (1993).

226. Hughes, J. *et al.* Identification of two related pentapeptides from the brain with potent opiate agonist activity. *Nature* **258**, 577–579 (1975).

227. Corder, G., Castro, D. C., Bruchas, M. R. & Scherrer, G. Endogenous and Exogenous Opioids in Pain. *Annu. Rev. Neurosci.* **41**, 453–473 (2018).

228. Levine, J. D., Gordon, N. C. & Fields, H. L. The mechanism of placebo analgesia. *Lancet (London, England)* **2**, 654–7 (1978).

229. Pert, C. B. & Snyder, S. H. Properties of opiate-receptor binding in rat brain. *Proc. Natl. Acad. Sci. U. S. A.* **70**, 2243–7 (1973).

230. Madariaga-Mazón, A. *et al.* Mu-Opioid receptor biased ligands: A safer and painless discovery of analgesics? *Drug Discov. Today* **22**, 1719–1729 (2017).

231. Wang, D. *et al.* Functional Divergence of Delta and Mu Opioid Receptor Organization in CNS Pain Circuits. (2018). doi:10.1016/j.neuron.2018.03.002

232. The prescription opioid addiction and abuse epidemic: how it happened and what we can do about it. *Pharm. J.* (2015). doi:10.1211/PJ.2015.20068579

233. Emery, E. C., Luiz, A. P. & Wood, J. N. Nav1.7 and other voltage-gated sodium channels as drug targets for pain relief. *Expert Opin. Ther. Targets* **20**, 975–83 (2016).

234. Tso, A. R. & Goadsby, P. J. Anti-CGRP Monoclonal Antibodies: the Next Era of Migraine Prevention? *Curr. Treat. Options Neurol.* **19**, 27 (2017).

235. Habib, A. M. *et al.* Microdeletion in a FAAH pseudogene identified in a patient with high anandamide concentrationsand pain insensitivity. *Br. J. Anaesth.* **0**, (2019).

236. Falowski, S. M. Deep Brain Stimulation for Chronic Pain. *Curr. Pain Headache Rep.* **19**, 27 (2015).

237. Samineni, V. K. *et al.* Optogenetic silencing of nociceptive primary afferents reduces evoked and ongoing bladder pain. *Sci. Rep.* **7**, 15865 (2017).

238. Weir, G. A. *et al.* Using an engineered glutamate-gated chloride channel to silence sensory neurons and treat neuropathic pain at the source. *Brain* **140**, 2570–2585 (2017).

239. Tuttle, A. H. *et al.* Increasing placebo responses over time in U.S. clinical trials of neuropathic pain. *Pain* **156**, 2616–2626 (2015).

240. Selman, C. & Swindell, W. R. Putting a strain on diversity. *EMBO J.* **37**, (2018).

241. Button, K. S. *et al.* Power failure: why small sample size undermines the reliability of neuroscience. *Nat. Rev. Neurosci.* **14**, 365–376 (2013).

242. Nieuwenhuis, S., Forstmann, B. U. & Wagenmakers, E.-J. Erroneous analyses of interactions in neuroscience: a problem of significance. *Nat. Neurosci.* **14**, 1105–1107 (2011).

243. Ioannidis, J. P. A. Why Most Published Research Findings Are False. *PLoS Med.* **2**, e124 (2005).

244. Lin, M. Z. & Schnitzer, M. J. Genetically encoded indicators of neuronal activity. *Nat. Neurosci.* **19**, 1142–1153 (2016).

245. Emery, E. C. *et al.* In vivo characterization of distinct modality-specific subsets of somatosensory neurons using GCaMP. *Sci. Adv.* **2**, e1600990 (2016).

246. Kim, Y. S. *et al.* Coupled Activation of Primary Sensory Neurons Contributes to Chronic Pain. *Neuron* **91**, 1085–1096 (2016).

247. Chisholm, K. I., Khovanov, N., Lopes, D. M., La Russa, F. & McMahon, S. B. Large Scale In Vivo Recording of Sensory Neuron Activity with GCaMP6. *eNeuro* **5**, (2018).

248. Wang, F. *et al.* Sensory Afferents Use Different Coding Strategies for Heat and Cold. *Cell Rep.* **23**, 2001–2013 (2018).

249. Meyer, R. A., Davis, K. D., Cohen, R. H., Treede, R. D. & Campbell, J. N. Mechanically insensitive afferents (MIAs) in cutaneous nerves of monkey. *Brain Res.* **561**, 252–61 (1991).

250. Prato, V. *et al.* Functional and Molecular Characterization of Mechanoinsensitive "Silent" Nociceptors. *Cell Rep.* **21**, 3102–3115 (2017).

251. Kucharczyk, M. W. *et al.* Novel mechanisms of bone cancer pain revealed with in vivo GCaMP6s imaging. *bioRxiv* 498980 (2018). doi:10.1101/498980

252. Miller, R. E. *et al.* Visualization of Peripheral Neuron Sensitization in a Surgical Mouse Model of Osteoarthritis by In Vivo Calcium Imaging. *Arthritis Rheumatol.* **70**, 88–97 (2018).

253. Kim, Y. S. *et al.* Central terminal sensitization of TRPV1 by descending serotonergic facilitation modulates chronic pain. *Neuron* **81**, 873–87 (2014).

254. Chen, T.-W. *et al.* Ultrasensitive fluorescent proteins for imaging neuronal activity. *Nature* **499**, 295–300 (2013).

255. Chen, C. *et al.* Long-term imaging of dorsal root ganglia in awake behaving mice. *Nat. Commun.* **10**, (2019).

256. Yin, K., Zimmermann, K., Vetter, I. & Lewis, R. J. Therapeutic opportunities for targeting cold pain pathways. *Biochem. Pharmacol.* **93**, 125–140 (2015).

257. Minett, M. S. *et al.* Distinct Nav1.7-dependent pain sensations require different sets of sensory and sympathetic neurons. *Nat. Commun.* **3**, 791 (2012).

258. Kingwell, K. Nav1.7 withholds its pain potential. *Nat. Rev. Drug Discov.* (2019). doi:10.1038/d41573-019-00065-0

259. Vetter, I. *et al.* NaV1.7 as a pain target – From gene to pharmacology. *Pharmacol. Ther.* **172**, 73–100 (2017).

260. Marvin, J. S. *et al.* An optimized fluorescent probe for visualizing glutamate neurotransmission. *Nat. Methods* **10**, 162–70 (2013).

261. Minett, M. S. *et al.* Endogenous opioids contribute to insensitivity to pain in humans and mice lacking sodium channel Nav1.7. *Nat. Commun.* **6**, 8967 (2015).

262. González, A. *et al.* Role of the Excitability Brake Potassium Current I_{KD} in Cold Allodynia Induced by Chronic Peripheral Nerve Injury. *J. Neurosci.* **37**, 3109–3126 (2017).

263. Weiss, J. *et al.* Loss-of-function mutations in sodium channel Na v 1.7 cause anosmia. *Nature* **472**, 186–192 (2011).

264. Luiz, A. P. *et al.* Cold sensing by NaV1.8-positive and NaV1.8-negative sensory neurons. *Proc. Natl. Acad. Sci. U. S. A.* **116**, 3811–3816 (2019).

265. Nassar, M. A. *et al.* Nociceptor-specific gene deletion reveals a major role for Nav1.7 (PN1) in acute and inflammatory pain. *Proc. Natl. Acad. Sci. U. S. A.* **101**, 12706–11 (2004).

266. Zhou, X. *et al.* Deletion of PIK3C3/Vps34 in sensory neurons causes rapid neurodegeneration by disrupting the endosomal but not the autophagic pathway. *Proc. Natl. Acad. Sci. U. S. A.* **107**, 9424–9429 (2010).

267. Danielian, P. S., Muccino, D., Rowitch, D. H., Michael, S. K. & McMahon, A. P. Modification of gene activity in mouse embryos in utero by a tamoxifen-inducible form of Cre recombinase. *Curr. Biol.* **8**, 1323–1326 (1998).

268. Madisen, L. *et al.* A robust and high-throughput Cre reporting and characterization system for the whole mouse brain. *Nat. Neurosci.* **13**, 133–140 (2010).

269. Nigro, M. J., Hashikawa-Yamasaki, Y. & Rudy, B. Diversity and connectivity of layer 5 somatostatin-expressing interneurons in the mouse barrel cortex. *J. Neurosci.* **38**, 1622–1633 (2018).

270. Rutlin, M. *et al.* The cellular and molecular basis of direction selectivity of Aδ-LTMRs. *Cell* **159**, 1640–51 (2014).

271. Song, H. *et al.* Functional characterization of pulmonary neuroendocrine cells in lung development, injury,and tumorigenesis. *Proc. Natl. Acad. Sci. U. S. A.* **109**, 17531–17536 (2012).

272. Ivanova, A. *et al.* In vivo genetic ablation by Cre-mediated expression of diphtheria toxin fragment A. *Genesis* **43**, 129–135 (2005).

273. Metzger, D. & Feil, R. Engineering the mouse genome by site-specific recombination. *Current Opinion in Biotechnology* **10**, 470–476 (1999).

274. Feil, S., Valtcheva, N. & Feil, R. Inducible cre mice. *Methods Mol. Biol.* **530**, 343–363 (2009).

275. Chaplan, S. R., Bach, F. W., Pogrel, J. W., Chung, J. M. & Yaksh, T. L. Quantitative assessment of tactile allodynia in the rat paw. *J. Neurosci. Methods* **53**, 55–63 (1994).

276. Woolfe, G. & MacDonald, A. D. The evaluation of the analgesic action of pethidine hydrochloride (Demerol). *J. Pharmacol. Exp. Ther.* **80**, (1944).

277. Brenner, D. S., Golden, J. P. & Gereau IV, R. W. A novel behavioral assay for measuring cold sensation in mice. *PLoS One* **7**, (2012).

278. Allchorne, A. J., Broom, D. C. & Woolf, C. J. Detection of cold pain, cold allodynia and cold hyperalgesia in freely behaving rats. *Mol. Pain* **1**, (2005).

279. Deuis, J. R. *et al.* An animal model of oxaliplatin-induced cold allodynia reveals a crucial role for Nav1.6 in peripheral pain pathways. *Pain* **154**, 1749–57 (2013).

280. Yoon, C., Young Wook, Y., Heung Sik, N., Sun Ho, K. & Jin Mo, C. Behavioral signs of ongoing pain and cold allodynia in a rat model of neuropathic pain. *Pain* **59**, 369–376 (1994).

281. Seltzer, Z., Dubner, R. & Shir, Y. A novel behavioral model of neuropathic pain disorders produced in rats by partial sciatic nerve injury. *Pain* **43**, 205–218 (1990).

282. Vetter, I. *et al.* Ciguatoxins activate specific cold pain pathways to elicit burning pain from cooling. *EMBO J.* **31**, 3795–808 (2012).

283. Bolz, F., Kasper, S., Bufe, B., Zufall, F. & Pyrski, M. Organization and plasticity of sodium channel expression in the mouse olfactory and vomeronasal epithelia. *Front. Neuroanat.* **11**, (2017).

284. McDermott, L. A. *et al.* Defining the Functional Role of Na V 1.7 in Human Nociception. *Neuron* **101**, 905-919.e8 (2019).

285. Ramirez, J. D. *et al.* Null mutation in scn9a in which noxious stimuli can be detected in the absence of pain. *Neurology* **83**, 1577–1580 (2014).

286. Legrain, V., Iannetti, G. D., Plaghki, L. & Mouraux, A. The pain matrix reloaded: A salience detection system for the body. *Progress in Neurobiology* **93**, 111–124 (2011).

287. Churyukanov, M., Plaghki, L., Legrain, V. & Mouraux, A. Thermal Detection Thresholds of Aδ- and C-Fibre Afferents Activated by Brief CO2 Laser Pulses Applied onto the Human Hairy Skin.

PLoS One **7**, e35817 (2012).

288. Yang, Y. Mutations in SCN9A, encoding a sodium channel alpha subunit, in patients with primary erythermalgia. *J. Med. Genet.* **41**, 171–174 (2004).

289. Fertleman, C. R. *et al.* SCN9A Mutations in Paroxysmal Extreme Pain Disorder: Allelic Variants Underlie Distinct Channel Defects and Phenotypes. *Neuron* **52**, 767–774 (2006).

290. Faber, C. G. *et al.* Gain of Function Na V 1.7 Mutations in Idiopathic Small Fiber Neuropathy. *Ann Neurol* **71**, 26–39 (2012).

291. How a Single Gene Could Become a Volume Knob for Pain—and End America's Opioid Epidemic | WIRED. Available at: https://www.wired.com/2017/04/the-cure-for-pain/. (Accessed: 18th November 2019)

292. Vetter, I. *et al.* NaV1.7 as a pain target – From gene to pharmacology. *Pharmacology and Therapeutics* **172**, 73–100 (2017).

293. Emery, E. C. *et al.* Novel SCN9A mutations underlying extreme pain phenotypes: Unexpected electrophysiological and clinical phenotype correlations. *J. Neurosci.* **35**, 7674–7681 (2015).

294. Yuan, J. *et al.* Hereditary sensory and autonomic neuropathy type IID caused by an SCN9A mutation. *Neurology* **80**, 1641–1649 (2013).

295. Cummins, T. R., Dib-Hajj, S. D. & Waxman, S. G. Electrophysiological properties of mutant Nav1.7 sodium channels in a painful inherited neuropathy. *J. Neurosci.* **24**, 8232–8236 (2004).

296. Dib-Hajj, S. D., Yang, Y., Black, J. A. & Waxman, S. G. The Na(V)1.7 sodium channel: from molecule to man. *Nat. Rev. Neurosci.* **14**, 49–62 (2013).

297. Wu, M. T., Huang, P. Y., Yen, C. T., Chen, C. C. & Lee, M. J. A Novel SCN9A Mutation Responsible for Primary Erythromelalgia and Is Resistant to the Treatment of Sodium Channel Blockers. *PLoS One* **8**, (2013).

298. Blesneac, I. *et al.* Rare NaV1.7 variants associated with painful diabetic peripheral neuropathy. *Pain* **159**, 469–480 (2018).

299. Toledo-Aral, J. J. *et al.* Identification of PN1, a predominant voltage-dependent sodium channel expressed principally in peripheral neurons. *Proc. Natl. Acad. Sci. U. S. A.* **94**, 1527–1532 (1997).

300. Djouhri, L. *et al.* Sensory and electrophysiological properties of guinea-pig sensory neurones expressing Nav 1.7 (PN1) Na+ channel α subunit protein. *Journal of Physiology* **546**, 565–576 (2003).

301. Black, J. A., Frézel, N., Dib-Hajj, S. D. & Waxman, S. G. Expression of Nav1.7 in DRG neurons extends from peripheral terminals in the skin to central preterminal branches and terminals in the dorsal horn. *Mol. Pain* **8**, 82 (2012).

302. Alles, S. R. A. *et al.* Sensory neuron–derived NaV1.7 contributes to dorsal horn neuron excitability. *Sci. Adv.* **6**, eaax4568 (2020).

303. Ahn, H. S. *et al.* Nav1.7 is the predominant sodium channel in rodent olfactory sensory neurons. *Mol. Pain* **7**, (2011).

304. Morinville, A. *et al.* Distribution of the voltage-gated sodium channel NaV1.7 in the rat: Expression in the autonomic and endocrine systems. *J. Comp. Neurol.* **504**, 680–689 (2007).

305. Branco, T. *et al.* Near-Perfect Synaptic Integration by Nav1.7 in Hypothalamic Neurons Regulates Body Weight. *Cell* **165**, 1749–1761 (2016).

306. Ahmad, S. *et al.* A stop codon mutation in SCN9A causes lack of pain sensation. *Hum. Mol. Genet.* **16**, 2114–2121 (2007).

307. Minett, M. S. *et al.* Pain without Nociceptors? Nav1.7-Independent Pain Mechanisms. *Cell Rep.* **6**, 301–312 (2014).

308. Wheeler, D. W., Lee, M. C. H., Harrison, E. K., Menon, D. K. & Woods, C. G. Case Report: Neuropathic pain in a patient with congenital insensitivity to pain. *F1000Research* **3**, 135 (2015).

309. Minett, M. S., Eijkelkamp, N. & Wood, J. N. Significant determinants of mouse pain behaviour. *PLoS One* **9**, e104458 (2014).

310. Minett, M. S. The role of sensory and sympathetic neurons in distinct pain sensations. (University

College London, 2013).

311. Pereira, V. *et al.* Analgesia linked to nav1.7 loss of function requires μ-and δ-opioid receptors [version 1; referees: 2 approved]. *Wellcome Open Res.* **3**, (2018).

312. Gingras, J. *et al.* Global Nav1.7 knockout mice recapitulate the phenotype of human congenital indifference to pain. *PLoS One* **9**, e105895 (2014).

313. Shields, S. D. *et al.* Insensitivity to Pain upon Adult-Onset Deletion of Nav1.7 or Its Blockade with Selective Inhibitors. *J. Neurosci.* **38**, 10180–10201 (2018).

314. Grubinska, B. *et al.* Rat Na v 1.7 loss-of-function genetic model: Deficient nociceptive and neuropathic pain behavior with retained olfactory function and intra-epidermal nerve fibers. *Mol. Pain* **15**, 174480691988184 (2019).

315. Noda, M. *et al.* Expression of functional sodium channels from cloned cDNA. *Nature* **322**, 826–828 (1986).

316. Guy, H. R. & Seetharamulu, P. Molecular model of the action potential sodium channel. *Proc. Natl. Acad. Sci. U. S. A.* **83**, 508–512 (1986).

317. Payandeh, J., Scheuer, T., Zheng, N. & Catterall, W. A. The crystal structure of a voltage-gated sodium channel. *Nature* **475**, 353–359 (2011).

318. Yan, Z. *et al.* Structure of the Nav1.4-β1 Complex from Electric Eel. *Cell* **170**, 470-482.e11 (2017).

319. Shen, H. *et al.* Structure of a eukaryotic voltage-gated sodium channel at near-atomic resolution. *Science (80-.).* **355**, (2017).

320. Xu, H. *et al.* Structural Basis of Nav1.7 Inhibition by a Gating-Modifier Spider Toxin. *Cell* **176**, 702–715 (2019).

321. Shen, H., Liu, D., Wu, K., Lei, J. & Yan, N. Structures of human Na v 1.7 channel in complex with auxiliary subunits and animal toxins. *Science (80-.).* **363**, 1303–1308 (2019).

322. Cummins, T. R., Waxman, S. G. & Wood, J. N. Sodium Channels and Pain. in *The Oxford Handbook of the Neurobiology of Pain* (ed. Wood, J. N.) (Oxford University Press, 2019). doi:10.1093/oxfordhb/9780190860509.013.3

323. Challapalli, V., Tremont-Lukats, I. W., Mcnicol, E. D., Lau, J. & Carr, D. B. Systemic administration of local anesthetic agents to relieve neuropathic pain. *Cochrane Database of Systematic Reviews* (2005). doi:10.1002/14651858.CD003345.pub2

324. Zakrzewska, J. M. *et al.* Safety and efficacy of a Nav1.7 selective sodium channel blocker in patients with trigeminal neuralgia: a double-blind, placebo-controlled, randomised withdrawal phase 2a trial. *Lancet Neurol.* **16**, 291–300 (2017).

325. Schmalhofer, W. A. *et al.* ProTx-II, a selective inhibitor of NaV1.7 sodium channels, blocks action potential propagation in nociceptors. *Mol. Pharmacol.* **74**, 1476–1484 (2008).

326. Deuis, J. R. *et al.* Pharmacological characterisation of the highly NaV1.7 selective spider venom peptide Pn3a. *Sci. Rep.* **7**, 40883 (2017).

327. Mueller, A. *et al.* Antiallodynic effects of the selective NaV1.7 inhibitor Pn3a in a mouse model of acute postsurgical pain. *Pain* **160**, 1766–1780 (2019).

328. Ahuja, S. *et al.* Structural basis of Nav1.7 inhibition by an isoform-selective small-molecule antagonist. *Science (80-.).* **350**, (2015).

329. Alexandrou, A. J. *et al.* Subtype-selective small molecule inhibitors reveal a fundamental role for Nav1.7 in nociceptor electrogenesis, axonal conduction and presynaptic release. *PLoS One* **11**, (2016).

330. Cao, L. *et al.* Pharmacological reversal of a pain phenotype in iPSC-derived sensory neurons and patients with inherited erythromelalgia. *Sci. Transl. Med.* **8**, 335ra56-335ra56 (2016).

331. Mc Donnell, A. *et al.* Efficacy of the Na v 1.7 blocker PF-05089771 in a randomised, placebo-controlled, double- blind clinical study in subjects with painful diabetic peripheral neuropathy. (2018). doi:10.1097/j.pain.0000000000001227

332. Siebenga, P. *et al.* Lack of detection of the analgesic properties of PF-05089771, a selective Nav1.7 inhibitor, using a battery of pain models in healthy subjects. *Clin. Transl. Sci.* (2019).

doi:10.1111/cts.12712

333. Deuis, J. R. *et al.* Analgesic effects of GpTx-1, PF-04856264 and CNV1014802 in a mouse model of NaV1.7-Mediated pain. *Toxins (Basel).* **8**, (2016).

334. Bankar, G. *et al.* Selective Na V 1.7 Antagonists with Long Residence Time Show Improved Efficacy against Inflammatory and Neuropathic Pain Correspondence Article Selective Na V 1.7 Antagonists with Long Residence Time Show Improved Efficacy against Inflammatory and Neuropathic Pain. *Cell Rep.* **24**, 3133–3145 (2018).

335. Cummins, T. R., Howe, J. R. & Waxman, S. G. Slow closed-state inactivation: a novel mechanism underlying ramp currents in cells expressing the hNE/PN1 sodium channel. *J. Neurosci.* **18**, 9607–19 (1998).

336. Raouf, R. *et al.* Sodium channels and mammalian sensory mechanotransduction. *Mol. Pain* **8**, (2012).

337. Yang, L. *et al.* FGF13 Selectively Regulates Heat Nociception by Interacting with Na v 1.7. *Neuron* **93**, 806-821.e9 (2017).

338. Hoffmann, T. *et al.* NaV1.7 and pain: contribution of peripheral nerves. *Pain* **159**, 496–506 (2018).

339. Marchi, M. *et al.* A novel SCN9A splicing mutation in a compound heterozygous girl with congenital insensitivity to pain, hyposmia and hypogeusia. *J. Peripher. Nerv. Syst.* **23**, 202–206 (2018).

340. Nilsen, K. B. *et al.* Two novel SCN9A mutations causing insensitivity to pain. *Pain* **143**, 155–158 (2009).

341. Klein, C. J. *et al.* Infrequent SCN9A mutations in congenital insensitivity to pain and erythromelalgia. *J. Neurol. Neurosurg. Psychiatry* **84**, 386–391 (2013).

342. Isensee, J. *et al.* Synergistic regulation of serotonin and opioid signaling contribute to pain insensitivity in Nav1.7 knockout mice. *Sci. Signal.* **10**, (2017).

343. Dehen, H., Willer, J. C., Boureau, F. & Cambier, J. Congenital insensitivity to pain, and endogenous morphine-like substances. *The Lancet* **310**, 293–294 (1977).

344. Kolesnikov, Y. A., Chereshnev, I. & Pasternak, G. W. Analgesic synergy between topical lidocaine and topical opioids. *J. Pharmacol. Exp. Ther.* **295**, 546–51 (2000).

345. Moreno, A. M. *et al.* Long-lasting Analgesia via Targeted in vivo Epigenetic Repression of Nav1.7. *bio*R*xiv* 711812 (2019). doi:10.1101/711812

346. Dana, H. *et al.* High-performance calcium sensors for imaging activity in neuronal populations and microcompartments. *Nat. Methods* **16**, 649–657 (2019).

347. Kanellopoulos, A. H. *et al.* Mapping protein interactions of sodium channel NaV1.7 using epitope-tagged gene-targeted mice. *EMBO J.* **37**, 427–445 (2018).

348. Manfredi, M. *et al.* Congenital Absence of Pain. *Arch. Neurol.* **38**, 507–511 (1981).

349. Kato, G. *et al.* Electrophysiological mapping of the nociceptive inputs to the substantia gelatinosa in rat horizontal spinal cord slices. *J. Physiol.* **560**, 303–315 (2004).

350. Yang, K., Kumamoto, E., Furue, H. & Yoshimura, M. Capsaicin facilitates excitatory but not inhibitory synaptic transmission in substantia gelatinosa of the rat spinal cord. *Neurosci. Lett.* **255**, 135–8 (1998).

351. Baccei, M. L., Bardoni, R. & Fitzgerald, M. Development of nociceptive synaptic inputs to the neonatal rat dorsal horn: glutamate release by capsaicin and menthol. *J. Physiol.* **549**, 231–242 (2003).

352. Kato, G. *et al.* Electrophysiological mapping of the nociceptive inputs to the substantia gelatinosa in rat horizontal spinal cord slices. *J. Physiol.* **560**, 303–315 (2004).

353. Helassa, N. *et al.* Ultrafast glutamate sensors resolve high-frequency release at Schaffer collateral synapses. *Proc. Natl. Acad. Sci. U. S. A.* **115**, 5594–5599 (2018).

354. Li, Z. *et al.* Membrane protein Nav1.7 contributes to the persistent post-surgical pain regulated by p-p65 in dorsal root ganglion (DRG) of SMIR rats model. *BMC Anesthesiol.* **17**, 150 (2017).

355. Flinspach, M. *et al.* Insensitivity to pain induced by a potent selective closed-state Nav1.7 inhibitor. *Sci. Rep.* **7**, (2017).

356. Yaksh, T. L., Jessell, T. M., Gamse, R., Mudge, A. W. & Leeman, S. E. Intrathecal morphine inhibits

substance P release from mammalian spinal cord in vivo. *Nature* **286**, 155–157 (1980).

357. Heinke, B., Gingl, E. & Sandkühler, J. Multiple Targets of-Opioid Receptor-Mediated Presynaptic Inhibition at Primary Afferent A-and C-Fibers. *J. Neurosci.* **31**, 1313–1322 (2011).

358. Scherrer, G. *et al.* Dissociation of the Opioid Receptor Mechanisms that Control Mechanical and Heat Pain. *Cell* **137**, 1148–1159 (2009).

359. Saraiva, L. R. *et al.* Hierarchical deconstruction of mouse olfactory sensory neurons: From whole mucosa to single-cell RNA-seq. *Sci. Rep.* **5**, (2015).

360. Vysokov, N., McMahon, S. B. & Raouf, R. The role of NaV channels in synaptic transmission after axotomy in a microfluidic culture platform. *Sci. Rep.* **9**, (2019).

361. Medvedeva, Y. V., Kim, M. S., Schnizler, K. & Usachev, Y. M. Functional tetrodotoxin-resistant Na+ channels are expressed presynaptically in rat dorsal root ganglia neurons. *Neuroscience* **159**, 559–569 (2009).

362. Nassar, M. A., Levato, A., Stirling, L. C. & Wood, J. N. Neuropathic Pain Develops Normally in Mice Lacking both $Na_v1.7$ and $Na_v1.8$. *Mol. Pain* **1**, 1744-8069-1–24 (2005).

363. Ferrari, L. F. *et al.* Inflammatory sensitization of nociceptors depends on activation of NMDA receptors in DRG satellite cells. *Proc. Natl. Acad. Sci. U. S. A.* **111**, 18363–18368 (2014).

364. Melo, H. *et al.* Itch induced by peripheral mu opioid receptors is dependent on TRPV1-expressing neurons and alleviated by channel activation. *Sci. Rep.* **8**, (2018).

365. Fabbri, A. *et al.* Intracerebroventricular injection of cerebrospinal fluid (CSF) from a patient with congenital indifference to pain induces analgesia in rats. *Experientia* **40**, 1365–1366 (1984).

366. Vythilingam, M. *et al.* Cerebrospinal Fluid Corticotropin-Releasing Hormone in Healthy Humans: Effects of Yohimbine and Naloxone 1 . *J. Clin. Endocrinol. Metab.* **85**, 4138–4145 (2000).

367. Gordon, R. J. *et al.* Effects of Opioid Antagonism on Cerebrospinal Fluid Melanocortin Peptides and Cortisol Levels in Humans. *J. Endocr. Soc.* **1**, 1235–1246 (2017).

368. Cesselin, F. *et al.* Normal CSF levels of met-enkephalin-like material in a case of naloxone-Reversible congenital insensitivity to pain. *Neuropeptides* **4**, 217–225 (1984).

369. Fitzgerald, E. M., Okuse, K., Wood, J. N., Dolphin, A. C. & Moss, S. J. cAMP-dependent phosphorylation of the tetrodotoxin-resistant voltage-dependent sodium channel SNS. *J. Physiol.* **516**, 433–446 (1999).

370. Kanellopoulos, A. H., Zhao, J., Emery, E. C. & Wood, J. N. Intracellular Sodium Regulates Opioid Signalling in Peripheral Neurons. *bioRxiv* 117952 (2017). doi:10.1101/117952

371. Pert, C. B. & Snyder, S. H. Opiate Receptor Binding of Agonists and Antagonists Affected Differentially by Sodium. *Mol. Pharmacol.* **10**, (1974).

372. Fenalti, G. *et al.* Molecular control of δ-opioid receptor signalling. *Nature* **506**, 191–196 (2014).

373. Chen, C. *et al.* GpTx-1 and [Ala^{5}, Phe^{6}, Leu^{26}, Arg^{28}]GpTx-1, two peptide $Na_v1.7$ inhibitors: analgesic and tolerance properties at the spinal level. *Br. J. Pharmacol.* **175**, 3911–3927 (2018).

374. Scherer, P. C. *et al.* TRPV1 is a physiological regulator of μ-opioid receptors. *Proc. Natl. Acad. Sci. U. S. A.* **114**, 13561–13566 (2017).

375. Basso, L. *et al.* TRPV1 promotes opioid analgesia during inflammation. *Sci. Signal.* **12**, (2019).

376. Semizoglou, E., Gentry, C., Bevan, S. & Andersson, D. Kappa opioid receptors mediate TRPA1 analgesia. in *Society for Neuroscience* 484.07 (2019).

377. Pajouhesh, H. *et al.* Discovery of a Selective, State-Independent Inhibitor of NaV1.7 by Modification of Guanidinium Toxins. *bioRxiv* 869206 (2019). doi:10.1101/869206

378. Chew, L. A., Bellampalli, S. S., Dustrude, E. T. & Khanna, R. Mining the Na v 1.7 interactome: Opportunities for chronic pain therapeutics. *Biochemical Pharmacology* **163**, 9–20 (2019).

379. Dustrude, E. T., Wilson, S. M., Ju, W., Xiao, Y. & Khanna, R. CRMP2 protein SUMOylation modulates NaV1.7 channel trafficking. *J. Biol. Chem.* **288**, 24316–24331 (2013).

380. Dustrude, E. T. *et al.* Hierarchical CRMP2 posttranslational modifications control NaV1.7 function. *Proc. Natl. Acad. Sci. U. S. A.* **113**, E8443–E8452 (2016).

381. Moutal, A. *et al.* Blocking CRMP2 SUMOylation reverses neuropathic pain. *Molecular Psychiatry* **23**, 2119–2121 (2018).

382. Francois-Moutal, L. *et al.* Inhibition of the Ubc9 E2 SUMO-conjugating enzyme-CRMP2 interaction decreases NaV1.7 currents and reverses experimental neuropathic pain. *Pain* **159**, 2115–2127 (2018).

383. Khanna, R. Unlocking NaV1.7's pain potential: Discovery and initial characterization of a novel class of compounds selectively targeting NaV1.7 through inhibition of a protein-protein interaction. in *Society for Neuroscience* 543.07 (2019).

384. Foulkes, T. & Wood, J. Mechanisms of Cold Pain. *Channels* **1**, 154–160 (2007).

385. Palkar, R., Lippoldt, E. K. & McKemy, D. D. The molecular and cellular basis of thermosensation in mammals. *Curr. Opin. Neurobiol.* **34**, 14–9 (2015).

386. Lolignier, S. *et al.* New Insight in Cold Pain: Role of Ion Channels, Modulation, and Clinical Perspectives. *J. Neurosci.* **36**, 11435–11439 (2016).

387. MacDonald, D. I., Wood, J. N. & Emery, E. C. Molecular mechanisms of cold pain. *Neurobiology of Pain* **7**, 100044 (2020).

388. Machover, D. *et al.* Two consecutive phase II studies of oxaliplatin (L-OHP) for treatment of patients with advanced colorectal carcinoma who were resistant to previous treatment with fluoropyrimidines. *Ann. Oncol.* **7**, 95–98 (1996).

389. Bécouarn, Y. *et al.* Phase II trial of oxaliplatin as first-line chemotherapy in metastatic colorectal cancer patients. *J. Clin. Oncol.* **16**, 2739–2744 (1998).

390. Craigen, M., Kleinert, J. M., Crain, G. M. & McCabe, S. J. Patient and injury characteristics in the development of cold sensitivity of the hand: A prospective cohort study. *J. Hand Surg. Am.* **24**, 8–15 (1999).

391. Irwin, M. S., Gilbert, S. E. A., Terenghi, G., Smith, R. W. & Green, C. J. Cold intolerance following peripheral nerve injury: Natural history and factors predicting severity of symptoms. *J. Hand Surg. Eur. Vol.* **22**, 308–316 (1997).

392. Lithell, M., Backman, C. & Nyström, A. Cold intolerance is not more common or disabling after digital replantation than after other treatment of compound digital injuries. *Ann. Plast. Surg.* **40**, 256–9 (1998).

393. Ruijs, A. C. J., Jaquet, J. B., van Riel, W. G., Daanen, H. A. M. & Hovius, S. E. R. Cold intolerance following median and ulnar nerve injuries: prognosis and predictors. *J. Hand Surg. Eur. Vol.* **32**, 434–439 (2007).

394. Nijhuis, T. H. J. *et al.* Prevalence and severity of cold intolerance in patients after hand fracture. *J. Hand Surg. Eur. Vol.* **35**, 306–311 (2010).

395. Nurmikko, T., Bowsher, D., Hospital, W., Nurmikko, L. T. & Bowsher, D. Somatosensory findings in postherpetic neuralgia Pain Relief Foundation and Centre for Pain Relief. *Neurosurgery, and Psychiatry* **53**, 135–141 (1990).

396. Baron, R., Tölle, T. R., Gockel, U., Brosz, M. & Freynhagen, R. A cross-sectional cohort survey in 2100 patients with painful diabetic neuropathy and postherpetic neuralgia: Differences in demographic data and sensory symptoms. *Pain* **146**, 34–40 (2009).

397. Vestergaard, K. *et al.* Sensory abnormalities in consecutive, unselected patients with central post-stroke pain. *Pain* **61**, 177–186 (1995).

398. Kim, J. S. & Choi-Kwon, S. Sensory Sequelae of Medullary Infarction. *Stroke* **30**, 2697–2703 (1999).

399. Bowsher, D. Allodynia in Relation to Lesion Site in Central Post-Stroke Pain. *J. Pain* **6**, 736–740 (2005).

400. Díaz-Rubio, E. *et al.* Oxaliplatin as single agent in previously untreated colorectal carcinoma patients: A phase II multicentric study. *Ann. Oncol.* **9**, 105–108 (1998).

401. Toth, C., Lander, J. & Wiebe, S. The Prevalence and Impact of Chronic Pain with Neuropathic Pain Symptoms in the General Population. *Pain Med.* **10**, 918–929 (2009).

402. Bengtsson, A. *et al.* Primary Fibromyalgia. *Scand. J. Rheumatol.* **15**, 340–347 (1986).

403. Koroschetz, J. *et al.* Fibromyalgia and neuropathic pain--differences and similarities. A comparison of 3057 patients with diabetic painful neuropathy and fibromyalgia. *BMC Neurol.* **11**, 55 (2011).

404. Halawa, M. R. *et al.* Prevalence of painful diabetic peripheral neuropathy among patients suffering from diabetes mellitus in Saudi Arabia. *Curr. Med. Res. Opin.* **26**, 337–343 (2010).

405. Cersosimo, R. J. Oxaliplatin-Associated Neuropathy: A Review. *Ann. Pharmacother.* **39**, 128–135 (2005).

406. de Gramont, A. *et al.* Leucovorin and Fluorouracil With or Without Oxaliplatin as First-Line Treatment in Advanced Colorectal Cancer. *J. Clin. Oncol.* **18**, 2938–2947 (2000).

407. Laugier, S., Kuberski, T. & Bagnis, R. Clinical Observations on 3,009 Cases of Ciguatera (Fish Poisoning) in the South Pacific. *Am. J. Trop. Med. Hyg.* **28**, 1067–1073 (1979).

408. Lange, W. R., Snyder, F. R. & Fudala, P. J. Travel and ciguatera fish poisoning. *Arch. Intern. Med.* **152**, 2049–53 (1992).

409. Lawrence, D. N., Enriquez, M. B., Lumish, R. M. & Maceo, A. Ciguatera fish poisoning in Miami. *JAMA* **244**, 254–8 (1980).

410. Forsyth, P. A. *et al.* Prospective study of paclitaxel-induced peripheral neuropathy with quantitative sensory testing. *J. Neurooncol.* **35**, 47–53 (1997).

411. Dougherty, P. M., Cata, J. P., Cordella, J. V, Burton, A. & Weng, H.-R. Taxol-induced sensory disturbance is characterized by preferential impairment of myelinated fiber function in cancer patients. *Pain* **109**, 132–142 (2004).

412. Campero, M., Baumann, T. K., Bostock, H. & Ochoa, J. L. Human cutaneous C fibres activated by cooling, heating and menthol. *J. Physiol.* **587**, 5633–52 (2009).

413. Dubner, R., Sumino, R. & Wood, W. I. A peripheral cold fiber population responsive to innocuous and noxious thermal stimuli applied to monkey's face. *J. Neurophysiol.* **38**, 1373–89 (1975).

414. Simone, D. A. & Kajander, K. C. Excitation of rat cutaneous nociceptors by noxious cold. *Neurosci. Lett.* **213**, 53–6 (1996).

415. Milenkovic, N. *et al.* A somatosensory circuit for cooling perception in mice. *Nat. Neurosci.* **17**, 1560–1566 (2014).

416. Mckemy, D. D. Therapeutic potential of Trpm8 modulators. *Open Drug Discov. J.* **2**, 81–88 (2010).

417. Yarmolinsky, D. A. *et al.* Coding and Plasticity in the Mammalian Thermosensory System. *Neuron* **92**, 1079–1092 (2016).

418. Leijon, S. C. M. *et al.* Oral thermosensing by murine trigeminal neurons: modulation by capsaicin, menthol and mustard oil. *J. Physiol.* **597**, 2045–2061 (2019).

419. Morenilla-Palao, C. *et al.* Ion Channel Profile of TRPM8 Cold Receptors Reveals a Role of TASK-3 Potassium Channels in Thermosensation. *Cell Rep.* **8**, 1571–1582 (2014).

420. Knowlton, W. M. *et al.* A sensory-labeled line for cold: TRPM8-expressing sensory neurons define the cellular basis for cold, cold pain, and cooling-mediated analgesia. *J. Neurosci.* **33**, 2837–48 (2013).

421. Knowlton, W. M., Bifolck-Fisher, A., Bautista, D. M. & McKemy, D. D. TRPM8, but not TRPA1, is required for neural and behavioral responses to acute noxious cold temperatures and cold-mimetics in vivo. *Pain* **150**, 340–50 (2010).

422. Colburn, R. W. *et al.* Attenuated cold sensitivity in TRPM8 null mice. *Neuron* **54**, 379–86 (2007).

423. Gentry, C., Stoakley, N., Andersson, D. A. & Bevan, S. The roles of iPLA2, TRPM8 and TRPA1 in chemically induced cold hypersensitivity. *Mol. Pain* **6**, 4 (2010).

424. Bautista, D. M. *et al.* TRPA1 Mediates the Inflammatory Actions of Environmental Irritants and Proalgesic Agents. *Cell* **124**, 1269–1282 (2006).

425. Kwan, K. Y. *et al.* TRPA1 Contributes to Cold, Mechanical, and Chemical Nociception but Is Not Essential for Hair-Cell Transduction. *Neuron* **50**, 277–289 (2006).

426. Winter, Z., Gruschwitz, P., Eger, S., Touska, F. & Zimmermann, K. Cold Temperature Encoding by Cutaneous TRPA1 and TRPM8-Carrying Fibers in the Mouse. *Front. Mol. Neurosci.* **10**, 209 (2017).

427. Zimmermann, K. *et al.* Transient receptor potential cation channel, subfamily C, member 5 (TRPC5) is a cold-transducer in the peripheral nervous system. *Proc. Natl. Acad. Sci. U. S. A.* **108**, 18114–9 (2011).

428. Alloui, A. *et al.* TREK-1, a K+ channel involved in polymodal pain perception. *EMBO J.* **25**, 2368–76 (2006).

429. Pereira, V. *et al.* Role of the TREK2 potassium channel in cold and warm thermosensation and in pain perception. *PAIN*® **155**, 2534–2544 (2014).

430. Castellanos, A. *et al.* TRESK background K+ channel deletion selectively uncovers enhanced mechanical and cold sensitivity. *J. Physiol.* **598**, 1017–1038 (2020).

431. Zimmermann, K. *et al.* Sensory neuron sodium channel Nav1.8 is essential for pain at low temperatures. *Nature* **447**, 855–8 (2007).

432. Lolignier, S. *et al.* The Nav1.9 Channel Is a Key Determinant of Cold Pain Sensation and Cold Allodynia. *Cell Rep.* **11**, 1067–1078 (2015).

433. Amaya, F. *et al.* The Voltage-Gated Sodium Channel Nav1.9 Is an Effector of Peripheral Inflammatory Pain Hypersensitivity. *J. Neurosci.* **26**, 12852–12860 (2006).

434. Peier, A. M. *et al.* A TRP channel that senses cold stimuli and menthol. *Cell* **108**, 705–15 (2002).

435. McKemy, D. D., Neuhausser, W. M. & Julius, D. Identification of a cold receptor reveals a general role for TRP channels in thermosensation. *Nature* **416**, 52–8 (2002).

436. Dhaka, A., Earley, T. J., Watson, J. & Patapoutian, A. Visualizing Cold Spots: TRPM8-Expressing Sensory Neurons and Their Projections. *J. Neurosci.* **28**, 566–575 (2008).

437. Reimúndez, A. *et al.* Deletion of the Cold Thermoreceptor TRPM8 Increases Heat Loss and Food Intake Leading to Reduced Body Temperature and Obesity in Mice. *J. Neurosci.* **38**, 3643–3656 (2018).

438. Ran, C., Hoon, M. A. & Chen, X. The coding of cutaneous temperature in the spinal cord. *Nat. Neurosci.* **19**, 1201–9 (2016).

439. Jankowski, M. P., Rau, K. K. & Koerber, H. R. Cutaneous TRPM8-expressing sensory afferents are a small population of neurons with unique firing properties. *Physiol. Rep.* **5**, (2017).

440. Story, G. M. *et al.* ANKTM1, a TRP-like channel expressed in nociceptive neurons, is activated by cold temperatures. *Cell* **112**, 819–29 (2003).

441. Munns, C., AlQatari, M. & Koltzenburg, M. Many cold sensitive peripheral neurons of the mouse do not express TRPM8 or TRPA1. *Cell Calcium* **41**, 331–342 (2007).

442. Michot, B., Lee, C. S. & Gibbs, J. L. TRPM8 and TRPA1 do not contribute to dental pulp sensitivity to cold. *Sci. Rep.* **8**, 13198 (2018).

443. Bandell, M. *et al.* High-throughput random mutagenesis screen reveals TRPM8 residues specifically required for activation by menthol. *Nat. Neurosci.* **9**, 493–500 (2006).

444. Yin, Y. *et al.* Structure of the cold- and menthol-sensing ion channel TRPM8. *Science* **359**, 237–241 (2018).

445. Yin, Y. *et al.* Structural basis of cooling agent and lipid sensing by the cold-activated TRPM8 channel. *Science* **363**, eaav9334 (2019).

446. Zakharian, E., Cao, C. & Rohacs, T. Gating of transient receptor potential melastatin 8 (TRPM8) channels activated by cold and chemical agonists in planar lipid bilayers. *J. Neurosci.* **30**, 12526–34 (2010).

447. Voets, T., Owsianik, G., Janssens, A., Talavera, K. & Nilius, B. TRPM8 voltage sensor mutants reveal a mechanism for integrating thermal and chemical stimuli. *Nat. Chem. Biol.* **3**, 174–182 (2007).

448. Matos-Cruz, V. *et al.* Molecular Prerequisites for Diminished Cold Sensitivity in Ground Squirrels and Hamsters. *Cell Rep.* **21**, 3329–3337 (2017).

449. Chigurapati, S., Sulak, M., Miller, W. & Lynch, V. J. Relaxed constraint and thermal desensitization of the cold-sensing ion channel TRPM8 in mammoths. *bioRxiv* 397356 (2018). doi:10.1101/397356

450. Gormley, P. *et al.* Meta-analysis of 375,000 individuals identifies 38 susceptibility loci for migraine.

Nat. Genet. **48**, 856–866 (2016).

451. Dussor, G. & Cao, Y. Q. TRPM8 and Migraine. *Headache* **56**, 1406–1417 (2016).

452. Key, F. M. *et al.* Human local adaptation of the TRPM8 cold receptor along a latitudinal cline. *PLOS Genet.* **14**, e1007298 (2018).

453. Leipold, E. *et al.* Cold-aggravated pain in humans caused by a hyperactive NaV1.9 channel mutant. *Nat. Commun.* **6**, 10049 (2015).

454. Griffith, T. N., Docter, T. A. & Lumpkin, E. A. Tetrodotoxin-Sensitive Sodium Channels Mediate Action Potential Firing and Excitability in Menthol-Sensitive Vglut3-Lineage Sensory Neurons. *J. Neurosci.* **39**, 7086–7101 (2019).

455. Goldstein, R. H. *et al.* Location and Plasticity of the Sodium Spike Initiation Zone in Nociceptive Terminals In Vivo. *Neuron* **102**, 801-812.e5 (2019).

456. Memon, T., Chase, K., Leavitt, L. S., Olivera, B. M. & Teichert, R. W. TRPA1 expression levels and excitability brake by K V channels influence cold sensitivity of TRPA1-expressing neurons. *Neuroscience* **353**, 76–86 (2017).

457. Gong, K. & Jasmin, L. Sustained Morphine Administration Induces TRPM8-Dependent Cold Hyperalgesia. *J. Pain* **18**, 212–221 (2017).

458. Lippoldt, E. K., Elmes, R. R., McCoy, D. D., Knowlton, W. M. & McKemy, D. D. Artemin, a Glial Cell Line-Derived Neurotrophic Factor Family Member, Induces TRPM8-Dependent Cold Pain. *J. Neurosci.* **33**, 12543–12552 (2013).

459. Nassini, R. *et al.* Oxaliplatin elicits mechanical and cold allodynia in rodents via TRPA1 receptor stimulation. *PAIN®* **152**, 1621–1631 (2011).

460. Descoeur, J. *et al.* Oxaliplatin-induced cold hypersensitivity is due to remodelling of ion channel expression in nociceptors. *EMBO Mol. Med.* **3**, 266–78 (2011).

461. Sittl, R. *et al.* Anticancer drug oxaliplatin induces acute cooling-aggravated neuropathy via sodium channel subtype Na(V)1.6-resurgent and persistent current. *Proc. Natl. Acad. Sci. U. S. A.* **109**, 6704–9 (2012).

462. Cavanaugh, D. J. *et al.* Restriction of transient receptor potential vanilloid-1 to the peptidergic subset of primary afferent neurons follows its developmental downregulation in nonpeptidergic neurons. *J. Neurosci.* **31**, 10119–27 (2011).

463. Leo, S., D'Hooge, R. & Meert, T. Exploring the role of nociceptor-specific sodium channels in pain transmission using Nav1.8 and Nav1.9 knockout mice. *Behav. Brain Res.* **208**, 149–157 (2010).

464. Pertusa, M. & Madrid, R. The I_{KD} current in cold detection and pathological cold pain. *Temperature* **4**, 346–349 (2017).

465. Cowie, A. M., Moehring, F., O'Hara, C. & Stucky, C. L. Optogenetic Inhibition of CGRPα Sensory Neurons Reveals Their Distinct Roles in Neuropathic and Incisional Pain. *J. Neurosci.* **38**, 5807–5825 (2018).

466. Serra, J. *et al.* C-nociceptors sensitized to cold in a patient with small-fiber neuropathy and cold allodynia. *Pain* **147**, 46–53 (2009).

467. Ongun, S., Sarkisian, A. & McKemy, D. D. Selective cold pain inhibition by targeted block of TRPM8-expressing neurons with quaternary lidocaine derivative QX-314. *Commun. Biol.* **1**, 53 (2018).

468. Jørum, E. & Opstad, P.-K. A 4-year follow-up of non-freezing cold injury with cold allodynia and neuropathy in 26 naval soldiers. *Scand. J. Pain* **0**, (2019).

469. Forstenpointner, J. *et al.* A-Fibers Mediate Cold Hyperalgesia in Patients with Oxaliplatin-Induced Neuropathy. *Pain Pract.* **18**, 758–767 (2018).

470. Tang, Z. *et al.* Pirt functions as an endogenous regulator of TRPM8. *Nat. Commun.* **4**, (2013).

471. Anderson, M., Zheng, Q. & Dong, X. Investigation of Pain Mechanisms by Calcium Imaging Approaches. *Neurosci. Bull.* **34**, 194–199 (2018).

472. Starobova, H. & Vetter, I. Pathophysiology of Chemotherapy-Induced Peripheral Neuropathy. *Front. Mol. Neurosci.* **10**, 174 (2017).

473. Ling, B., Authier, N., Balayssac, D., Eschalier, A. & Coudore, F. Behavioral and pharmacological description of oxaliplatin-induced painful neuropathy in rat. *Pain* **128**, 225–234 (2007).

474. Ling, B. *et al.* Behavioral and immunohistological assessment of painful neuropathy induced by a single oxaliplatin injection in the rat. *Toxicology* **234**, 176–184 (2007).

475. Argyriou, A. A., Polychronopoulos, P., Iconomou, G., Chroni, E. & Kalofonos, H. P. A review on oxaliplatin-induced peripheral nerve damage. *Cancer Treat. Rev.* **34**, 368–377 (2008).

476. Kagiava, A., Tsingotjidou, A., Emmanouilides, C. & Theophilidis, G. The effects of oxaliplatin, an anticancer drug, on potassium channels of the peripheral myelinated nerve fibres of the adult rat. *Neurotoxicology* **29**, 1100–1106 (2008).

477. Sittl, R., Carr, R. W., Fleckenstein, J. & Grafe, P. Enhancement of axonal potassium conductance reduces nerve hyperexcitability in an in vitro model of oxaliplatin-induced acute neuropathy. *Neurotoxicology* **31**, 694–700 (2010).

478. Vastani, N. Mechanisms of thermal sensitivity in rodent primary afferent neurons innervating the skin. (University College London, 2009).

479. Munns, C. H. Mechanisms and plasticity of cold sensitivity in peripheral neurons. (University College London, 2008).

480. Nurjahan Saleque, Clive Gentry, Nisha Vastani, S. B. and D. A. Sensitization of nociceptive sensory neurons by oxaliplatin. in *The Challenge of Chronic Pain* (2019).

481. Jacobs, S. S. *et al.* Plasma and cerebrospinal fluid pharmacokinetics of intravenous oxaliplatin, cisplatin, and carboplatin in nonhuman primates. *Clin. Cancer Res.* **11**, 1669–1674 (2005).

482. Screnci, D. *et al.* Relationships between hydrophobicity, reactivity, accumulation and peripheral nerve toxicity of a series of platinum drugs. *Br. J. Cancer* **82**, 966–972 (2000).

483. Rigaud, M. *et al.* Species and strain differences in rodent sciatic nerve anatomy: Implications for studies of neuropathic pain. *Pain* **136**, 188–201 (2008).

484. Petrocchi, J. A. *et al.* Peripheral antinociception induced by ketamine is mediated by the endogenous opioid system. *Eur. J. Pharmacol.* **865**, (2019).

485. Ji, G., Zhou, S., Kochukov, M. Y., Westlund, K. N. & Carlton, S. M. Plasticity in intact Aδ- and C-fibers contributes to cold hypersensitivity in neuropathic rats. *Neuroscience* **150**, 182–193 (2007).

486. Djouhri, L., Wrigley, D., Thut, P. D. & Gold, M. S. Spinal nerve injury increases the percentage of cold-responsive DRG neurons. *Neuroreport* **15**, 457–60 (2004).

487. Xing, H., Chen, M., Ling, J., Tan, W. & Gu, J. G. TRPM8 Mechanism of Cold Allodynia after Chronic Nerve Injury. *J. Neurosci.* **27**, 13680–13690 (2007).

488. Nguyen, M. Q., Le Pichon, C. E. & Ryba, N. Stereotyped transcriptomic transformation of somatosensory neurons in response to injury. *Elife* **8**, (2019).

489. Renthal, W. *et al.* Transcriptional reprogramming of distinct peripheral sensory neuron subtypes after axonal injury. *bioRxiv* 838854 (2019). doi:10.1101/838854

490. Zimmermann, K. *et al.* Analgesic treatment of ciguatoxin-induced cold allodynia. *PAIN*® **154**, 1999–2006 (2013).

491. Lewis, R. J. *et al.* Purification and characterization of ciguatoxins from moray eel (Lycodontis javanicus, Muraenidae). *Toxicon* **29**, 1115–1127 (1991).

492. Patel, R., Brice, N. L., Lewis, R. J. & Dickenson, A. H. Ionic mechanisms of spinal neuronal cold hypersensitivity in ciguatera. *Eur. J. Neurosci.* **42**, 3004–3011 (2015).

493. Zheng, Y. *et al.* Deep Sequencing of Somatosensory Neurons Reveals Molecular Determinants of Intrinsic Physiological Properties. *Neuron* **103**, 598-616.e7 (2019).

494. Shields, S. D. *et al.* Na v1.8 expression is not restricted to nociceptors in mouse peripheral nervous system. *Pain* **153**, 2017–2030 (2012).

495. Daou, I. *et al.* Optogenetic silencing of Nav1.8-positive afferents alleviates inflammatory and neuropathic pain. *eNeuro* **3**, 702–705 (2016).

496. Patil, M. J., Hovhannisyan, A. H. & Akopian, A. N. Characteristics of sensory neuronal groups in

CGRP-cre-ER reporter mice: Comparison to Nav1.8-cre, TRPV1-cre and TRPV1-GFP mouse lines. *PLoS One* **13**, e0198601 (2018).

497. Touska, F. *et al.* Ciguatoxins Evoke Potent CGRP Release by Activation of Voltage-Gated Sodium Channel Subtypes NaV1.9, NaV1.7 and NaV1.1. *Mar. Drugs* **15**, 269 (2017).

498. Roth, B. L. *et al.* DREADDs for Neuroscientists. *Neuron* **89**, 683–694 (2016).

499. Inserra, M. C. *et al.* Multiple sodium channel isoforms mediate the pathological effects of Pacific ciguatoxin-1. *Sci. Rep.* **7**, 42810 (2017).

500. Rosker, C. *et al.* The TTX metabolite 4,9-anhydro-TTX is a highly specific blocker of the Nav1.6 voltage-dependent sodium channel. *Am. J. Physiol. - Cell Physiol.* **293**, (2007).

501. Teramoto, N. & Yotsu-Yamashita, M. Selective blocking effects of 4,9-anhydrotetrodotoxin, purified from a crude mixture of tetrodotoxin analogues, on NaV1.6 channels and its chemical aspects. *Marine Drugs* **13**, 984–995 (2015).

502. Xie, W., Strong, J. A. & Zhang, J.-M. Local knockdown of the NaV1.6 sodium channel reduces pain behaviors, sensory neuron excitability, and sympathetic sprouting in rat models of neuropathic pain. *Neuroscience* **291**, 317–330 (2015).

503. Ishikawa, K., Tanaka, M., Black, J. A. & Waxman, S. G. Changes in expression of voltage-gated potassium channels in dorsal root ganglion neurons following axotomy. *Muscle and Nerve* **22**, 502–507 (1999).

504. Kim, D. S., Choi, J. O., Rim, H. D. & Cho, H. J. Downregulation of voltage-gated potassium channel alpha gene expression in dorsal root ganglia following chronic constriction injury of the rat sciatic nerve. *Brain Res. Mol. Brain Res.* **105**, 146–52 (2002).

505. Park, S. Y. *et al.* Downregulation of voltage-gated potassium channel α gene expression by axotomy and neurotrophins in rat dorsal root ganglia. *Mol. Cells* **16**, 256–259 (2003).

506. Rasband, M. N. *et al.* Distinct potassium channels on pain-sensing neurons. *Proc. Natl. Acad. Sci. U. S. A.* **98**, 13373–13378 (2001).

507. Yang, E. K., Takimoto, K., Hayashi, Y., De Groat, W. C. & Yoshimura, N. Altered expression of potassium channel subunit mRNA and α-dendrotoxin sensitivity of potassium currents in rat dorsal root ganglion neurons after axotomy. *Neuroscience* **123**, 867–874 (2004).

508. Calvo, M. *et al.* Altered potassium channel distribution and composition in myelinated axons suppresses hyperexcitability following injury. *Elife* **5**, (2016).

509. Zhao, X. *et al.* A long noncoding RNA contributes to neuropathic pain by silencing Kcna2 in primary afferent neurons. *Nat. Neurosci.* **16**, 1024–1031 (2013).

510. Birinyi-Strachan, L. C., Gunning, S. J., Lewis, R. J. & Nicholson, G. M. Block of voltage-gated potassium channels by Pacific ciguatoxin-1 contributes to increased neuronal excitability in rat sensory neurons. *Toxicol. Appl. Pharmacol.* **204**, 175–186 (2005).

511. Askwith, C. C., Benson, C. J., Welsh, M. J. & Snyder, P. M. DEG/ENaC ion channels involved in sensory transduction are modulated by cold temperature. *Proc. Natl. Acad. Sci. U. S. A.* **98**, 6459–63 (2001).

512. Gong, J. *et al.* A Cold-Sensing Receptor Encoded by a Glutamate Receptor Gene. *Cell* **178**, 1375-1386.e11 (2019).

513. Reid, G. & Flonta, M.-L. Cold transduction by inhibition of a background potassium conductance in rat primary sensory neurones. *Neurosci. Lett.* **297**, 171–174 (2001).

514. Viana, F., de la Peña, E. & Belmonte, C. Specificity of cold thermotransduction is determined by differential ionic channel expression. *Nat. Neurosci.* **5**, 254–260 (2002).

515. Patel, A. J. *et al.* A mammalian two pore domain mechano-gated S-like K+ channel. *EMBO J.* **17**, 4283–4290 (1998).

516. Kang, D., Choe, C. & Kim, D. Thermosensitivity of the two-pore domain K $^{+}$ channels TREK-2 and TRAAK. *J. Physiol.* **564**, 103–116 (2005).

517. Viatchenko-Karpinski, V., Ling, J. & Gu, J. G. Characterization of temperature-sensitive leak K+ currents and expression of TRAAK, TREK-1, and TREK2 channels in dorsal root ganglion neurons of rats. *Mol. Brain* **11**, 40 (2018).

518. Blin, S. *et al.* Mixing and matching TREK/TRAAK subunits generate heterodimeric K2P channels with unique properties. *Proc. Natl. Acad. Sci. U. S. A.* **113**, 4200–5 (2016).

519. Abd-Elsayed, A. A. *et al.* KCNQ channels in nociceptive cold-sensing trigeminal ganglion neurons as therapeutic targets for treating orofacial cold hyperalgesia. *Mol. Pain* **11**, 45 (2015).

520. Ling, J., Erol, F. & Gu, J. G. Role of KCNQ2 channels in orofacial cold sensitivity: KCNQ2 upregulation in trigeminal ganglion neurons after infraorbital nerve chronic constrictive injury. *Neurosci. Lett.* **664**, 84–90 (2018).

521. Deuis, J. R. *et al.* Analgesic effects of clinically used compounds in novel mouse models of polyneuropathy induced by oxaliplatin and cisplatin. *Neuro. Oncol.* **16**, 1324–32 (2014).

522. Eisenberg, E., Lurie, Y., Braker, C., Daoud, D. & Ishay, A. Lamotrigine reduces painful diabetic neuropathy: a randomized, controlled study. *Neurology* **57**, 505–9 (2001).

523. Fan, L. *et al.* Impaired neuropathic pain and preserved acute pain in rats overexpressing voltage-gated potassium channel subunit Kv1.2 in primary afferent neurons. *Mol. Pain* **10**, (2014).

524. Colasante, G. *et al.* CRISPRa-mediated Kcna1 upregulation decreases neuronal excitability and suppresses seizures in a rodent model of temporal lobe epilepsy. *bioRxiv* 431015 (2018). doi:10.1101/431015

525. Shaikh, S. S., Nahorski, M. S., Rai, H. & Woods, C. G. Before progressing from "exomes" to "genomes"… don't forget splicing variants. *Eur. J. Hum. Genet.* **26**, 1559–1562 (2018).